AN ABSTRACT OF THE DISSERTATION OF

Kaleb C. Scarberry for the degree of Doctor of Philosophy in Geology presented on August 22, 2007.

Title: Extension and Volcanism: Tectonic Development of the Northwestern Margin of the Basin and Range Province in Southern Oregon

Abstract approved:

Anita L. Grunder

The northwestern corner of the Basin and Range Province (NWBR) lies in southeast Oregon where extensive Late Miocene, mafic to bimodal basalt-rhyolite volcanism and extensional faults dominate a stark and arid landscape. Near Lake Abert, the Late Miocene volcanic section abuts Early Miocene, dominantly intermediate composition volcanoes at the Coleman Hills and Rabbit Hills. Such exposures are few in the NWBR and shed light on the volcanic and structural development of the region and significantly extend the known distribution of Early Miocene magmatism.

New ^{40}Ar-^{39}Ar ages indicate that magmatism occurred at the Coleman Hills between 21.4 and 22.3 Ma and at the Rabbit Hills between 20.2 and 23.4 Ma. Magmatism at the Coleman Hills initiated with an episode of silicic volcanism that was rapidly followed by the intrusion and emplacement of dacite and andesite dikes and lavas. Early Miocene rhyolite of the Coleman Hills exhibits high $^{87}Sr/^{86}Sr_i$ relative to most Late Miocene rocks in the region (0.7051 vs. 0.7037) suggesting that crustal melting was important in their genesis. A notable lack of a Nb-trough, characteristic of subduction zone settings, and high $^{207}Pb/^{204}Pb$, and $^{206}Pb/^{204}Pb$ suggests that these rocks were not generated within a volcanic arc setting and instead likely formed in a back-arc region that had been metasomatized by prior subduction. Crystal fractionation readily accounts for

the generation of andesite and dacite compositions from basaltic andesite however a gap in the data between ~66 to 70% SiO_2, isotopic variability and disequilibrium textures indicate that crustal anatexis, magma mixing and/or crustal assimilation may also be important processes in the evolutionary history of the Coleman Hills.

Dike orientations within Early Miocene volcanoes often mimic the trend of faults that cut Late Miocene volcanic strata, suggesting that the faults may have utilized an existing structural fabric. Contact relations suggest as much as 500 m of volcanic paleo-topography existed near Lake Abert prior to deposition of the Middle Miocene Steens flood basalts at ~16 Ma. Late Miocene structural development of the Abert Rim fault is chronologically linked to the formation and northward propagation of the Walker Lane transform fault system in Nevada between 9 and 3 Ma. At Lake Abert, bimodal basalt-rhyolite volcansim from 8.8 to 7.7 Ma occurred within a zone of active NW-striking faulting. Volcanism during this interval was related to the initiation of faulting at Abert Rim fault. On the basis of morphology and geochemical correlation, Juniper Mountain and Venator Buttes are the source of silicic and mafic volcanism, respectively, between 8.8 to 7.7 Ma. Partial restorations demonstrate that the Abert Rim fault south of 42º40’ N latitude had >250 m of stratigraphic separation prior to deposition of the Rattlesnake Tuff at 7 Ma. The topography north of latitude 42º40’ N was gently sloping at 7 Ma, much like the High Lava Plains are today. Thus, faulting along the NNE-striking Abert Rim initiated between 7.7 and 7 Ma and after the formation of NW-striking fault systems.

Extension and Volcanism: Tectonic Development of the Northwestern Margin of the Basin and Range Province in Southern Oregon

By

Kaleb C. Scarberry

A DISSERTATION

Submitted to

Oregon State University

in partial fulfillment of
the requirements for the
degree of

Doctor of Philosophy

Presented August 22, 2007
Commencement June 2008

Doctor of Philosophy dissertation of Kaleb C. Scarberry

Presented on August 22, 2007

APPROVED:

Anita L. Grunder

Major Professor, representing Geology

Chair of the Department of Geosciences

Dean of the Graduate School

I understand that my dissertation will become part of the permanent collection of Oregon State University libraries. My signature below authorizes release of my dissertation to any reader upon request.

Kaleb Scarberry

Kaleb C. Scarberry, Author

ACKNOWLEDGMENTS

I would like to thank Anita Grunder for her assistance with all aspects of this work. Anita provided financial, intellectual and sometimes emotional support for field, lab and office work. Most importantly, Anita gave me a lot of leeway with respect to defining my own research project and, in general, on my own terms. She spent her 50th birthday with me in the field. Without her help this project would not have developed and expanded as it has. Significant help from Anita and Andrew Meigs with the development of research proposals has led to success in funding the bulk of my work through NSF Tectonics and USGS EdMap programs. Not only have these grants supported my project, they now provide funding for additional students and for that I am proud.

Many people have helped me with fieldwork during the three summers that I spent exploring southern Oregon and others helped with my understanding of the problems associated with tectonism in the Pacific Northwest. Field assistants include (in chronological order): Anita Grunder, Andy Uhrig, Tom Wagner, Chris Johnson, Shawn Majors (SMPM), Mark Ford, Barry Walker, Emelda Zuschlag, and Jamie (The Runaway). Tom Wagner deserves a special note of recognition for his high level of interest and invariable dedication to this project- even when there was no money to pay him. Conversations with Matt Coble, Nancye Dawers, John Dilles, Bob Duncan, Jim Faulds, Mark Ford, Anita Grunder, Chris Henry, Gene Humphreys, Mike Iademarco, Jenda Johnson, Jeff Lee, Bob Lillie, Andrew Meigs, Jeremiah Oxford, Silvio Pezzopane, Dave Sherrod and Tom Wagner have made me think in detail about my research

questions. Denise Giles and Isabelle Chambefort are great friends and I thank them for helping me to prepare for my defense and final dissertation submission.

My family has been exceptionally supportive of my pursuits. Without their interest in what I do it would be meaningless in a lot of ways. I dedicate this thesis to my dad, Jim Scarberry, who would have been fascinated by what I have learned and proud of the challenges that I have successfully faced. My beautiful wife, Nicole and baby daughter Mia Noelle keep me motivated to do good. I look forward to taking Mia to see the Abert Rim when she is old enough to walk.

CONTRIBUTION OF AUTHORS

Anita Grunder and Andrew Meigs are listed as co-authors for the manuscripts submitted as chapters 2 and 3 of this dissertation. Grunder assisted with sample collection and selection of samples for geochemical and geochronologic analysis. Meigs helped to develop cross-sections and structural restorations presented in chapter 3. Grunder and Meigs provided critical reviews of the two manuscripts constituting chapters 2 and 3, respectively, and suggested substantive revisions.

TABLE OF CONTENTS

	Page
Chapter 1: Introduction to problems regarding tectonism of the northwestern Basin and Range Province	1
Geophysical characterization	1
The NWBR: a locus of volcanism	3
The NWBR: a young extensional province	4
Research questions	7
References Cited	8
Chapter 2: Transition from intermediate to bimodal volcanism in the northwestern Basin and Range Province: compositional evolution and tectonic implications	11
Abstract	12
Introduction	12
Structural and stratigraphic setting of the Abert Rim, Coleman Hills and adjacent lake basins	16
Methods	20
Results	22
Early Miocene Coleman Hills volcanic complex	23
Rhyolite	35
Dacite	36
Basaltic andesite to andesite	39
Middle to Late Miocene volcanic rocks	39
Steens Basalt	41
Mafic tholeiitic lavas of the bimodal suite	42
Tholeiitic basaltic andesite	42
HAOT	43
Silicic units of the bimodal suite	44
Vent complexes north of Lake Abert	44
Rattlesnake Tuff	45

TABLE OF CONTENTS (CONTINUED)

Page

Eruptive sources of Late Miocene bimodal volcanic units 45

Compositional Variation 46

The Coleman Hills suite 46
The Late Miocene bimodal suite 47
Isotopic composition 47

Discussion 50

Petrologic modeling 50
Crystal fractionation 52
Crustal contamination and magma mixing 55
Petrogenetic model 56

Generation of mafic parent 58

Episodes of volcanism 58

Conclusions 62

References Cited 64

Chapter 3: Inception and style of faulting at the edge of a propagating continental rift system: insight from the structural development of the Abert Rim fault, southern Oregon 68

Abstract 69

Introduction 69

Regional constraints on Basin and Range opening 74

Opening of the Oregon Basin and Range 75

Major structures 75
Timing of extension 76
The Abert Rim fault 78

Methods 78

TABLE OF CONTENTS (CONTINUED)

Page

Results 80

Geologic mapping and ^{40}Ar-^{39}Ar geochronology 80
Stratigraphy of the Early Miocene Coleman Hills 82
Stratigraphy of Middle to Late Miocene rock units 88

Structural Geology 90

NW-striking faults 90
Southern segment: Abert Rim fault 95
Northern segment: Abert Rim fault 95

Timing of deformation 96

Oligocene magmatism 96
Late Cenozoic faulting: 16-7 Ma 97
Late Cenozoic faulting: post-7 Ma 100

Magnitude of deformation 100

Geologic rates of deformation 101

Discussion 102

Regional model for NW-propagation of the Basin and Range 103

Implications for the kinematic nature of the Brothers Fault Zone 105

Conclusions 106

References Cited 108

Chapter 4: Early Miocene volcanoes in southern Oregon: long-term extension In an evolving backarc 113

Abstract 114

Introduction 114

Pre-Steens volcanoes of southern Oregon 114

TABLE OF CONTENTS (CONTINUED)

Page

Methods 115

Results 117

Beatys Butte 117
The Rabbit Hills 120

Chemical Composition 120

Isotopic Composition 126

Discussion 126

Conclusions 131

References Cited 132

Chapter 5: Summary 134

Re-visit research questions 134

Bibliography 138

Appendices 147

Appendix 1: Comparison of XRF and ICP-MS analytical totals 147

Appendix 2: CIPW normative mineral compositions for rock analyses 148

Appendix 3: Detailed data for ^{40}Ar-^{39}Ar analyses conducted at Oregon State University 152

LIST OF FIGURES

CHAPTER 1

Figure		Page
1.	Physiographic and geophysical setting of the NWBR	2
2.	Model reconstructions of the tectonic setting of the western U.S. and DEM of the Lake Abert fault system	5

CHAPTER 2

Figure		Page
1.	Volcano-tectonic setting of the Basin and Range margin	13
2.	Simplified geologic map of the Coleman Hills	17
3.	Stratigraphic section of the Coleman Hills	18
4.	Photographs of rocks from the Coleman Hills	19
5.	Regional volcanic centers associated with Abert Rim	21
6.	TAS classification diagram for volcanic rocks near Lake Abert	24
7.	Elemental variation diagrams for volcanic rocks near Lake Abert	37
8.	Chondrite normailized spider diagrams for volcanic rocks near Lake Abert	38
9.	REE diagrams for volcanic rocks near Lake Abert	40
10.	$^{87}Sr/^{86}Sr$-εNd covariation diagram	49
11.	Pb isotope correlation diagrams	51
12.	X-Y plots of petrologic model results	54
13.	Cartoon illustrating model for petrogenesis at the Coleman Hills	57
14.	Isotope composition through time	59

LIST OF FIGURES (CONTINUED)

CHAPTER 3

Figure		Page
1.	Tectonic setting of the Basin and Range Province	70
2.	DEM of NWBR showing regional Basin and Range faults	72
3.	Map showing structural fabric of the NWBR, distribution of Quaternary lavas, and distribution of the Steens basalts in Oregon	73
4.	Map of Lake Abert and Alkali Lake basins showing faults and locations of eruptive centers	79
5.	Sketch geologic map of the Coleman Hills and north end of Lake Abert	81
6.	Composite stratigraphic section for volcanic units within the mapped area	83
7.	^{40}Ar-^{39}Ar spectra for samples collected near the north end of Lake Abert	85
8.	Photograph of Oligocene andesite dike and comparison of Oligocene dike orientations to Late Cenozoic fault trends	87
9.	Morphology of the principal NW- and NNE-striking fault sets along-strike of the Abert Rim fault	91
10.	Photographs, maps and cross-section of system of NW-striking faults near Sawed Horn	93
11.	Photographs, maps and cross-section of system of NW-striking faults near Table Top	94
12.	Cross-sections perpendicular to the Abert Rim fault	98
13.	Restored cross-sections for the Abert Rim fault	99
14.	Summary of Miocene tectonic development	104

LIST OF FIGURES (CONTINUED)

CHAPTER 4

Figure		Page
1.	Location map of Oligocene-Early Miocene volcanic centers of the NWBR	116
2.	Sketch geologic maps and sample locations for Beatys Butte and the Rabbit Hills	118
3.	^{40}Ar-^{39}Ar spectra for samples collected from the Rabbit Hills and Beatys Butte	119
4.	TAS classification diagrams for rock suites of Oligocene-Late Miocene volcanic centers of the NWBR	125
5.	Chondrite-normalized spider diagrams for rock suites of Oligocene-Late Miocene volcanic centers of the NWBR	127
6.	$^{87}Sr/^{86}Sr$-εNd covariation diagram for isotopic compositions of the Rabbit Hills	129
7.	Age contour map for Oligocene-Late Miocene volcanic centers of the NWBR	130

LIST OF TABLES

CHAPTER 2

Table Page

1. Major and Trace element geochemical analysis of Lake Abert samples 25

2. Isotopic composition of volcanic rocks from the Lake Abert region 48

3. Composition data for minerals used in major element models and summary of major element model results 53

CHAPTER 3

Table Page

1. Summary of ^{40}Ar-^{39}Ar age results from samples collected north of Lake Abert 84

CHAPTER 4

Table Page

1. Major and Trace element geochemical analysis of Rabbit Hills and Beatys Butte samples 121

2. Isotopic composition of volcanic units from the Rabbit Hills 128

LIST OF PLATES

Plate Page

1. 1:24,000 Geologic Map of the north end of Lake Abert, OR……(back cover)

EXTENSION AND VOLCANISM: TECTONIC DEVELOPMENT OF THE NORTHWESTERN MARGIN OF THE BASIN AND RANGE PROVINCE IN SOUTHERN OREGON

CHAPTER 1: INTRODUCTION TO PROBLEMS REGARDING TECTONISM OF THE NORTHWESTERN BASIN AND RANGE PROVINCE

This chapter summarizes principal research questions pertaining to the tectonic development of the northwestern corner of the Basin and Range Province in Oregon (NWBR) (Figure 1). This thesis takes a two-pronged approach to addressing these questions and is organized accordingly: (1) Assessment of the volcanic history of the NWBR through analysis of the style and composition of the products of magmatism in time and space within the province; and (2) Assessment of the deformational history of the NWBR through analysis of the structural development of the province. The primary goal of this thesis is to synthesis the results of these approaches, in hope that in doing so, a coherent model of the tectonic development of the NWBR will emerge.

Geophysical Characterization

The Basin and Range Province of the western United States has undergone a complex magmatic and structural history that reflects prolonged continental rifting since the early Tertiary. Seismic observations of the crust and uppermost mantle (Donath, 1962; Catchings and Mooney, 1988; Mooney and Braile, 1989; Allmendinger et al., 1987; Hearn et al., 1991) confirm this complexity and provide many of the physical constraints used to reconstruct the tectonic history of the region (Figure 1). Historic earthquakes (e.g., Qamar and Meagher, 1993) provide information about actively

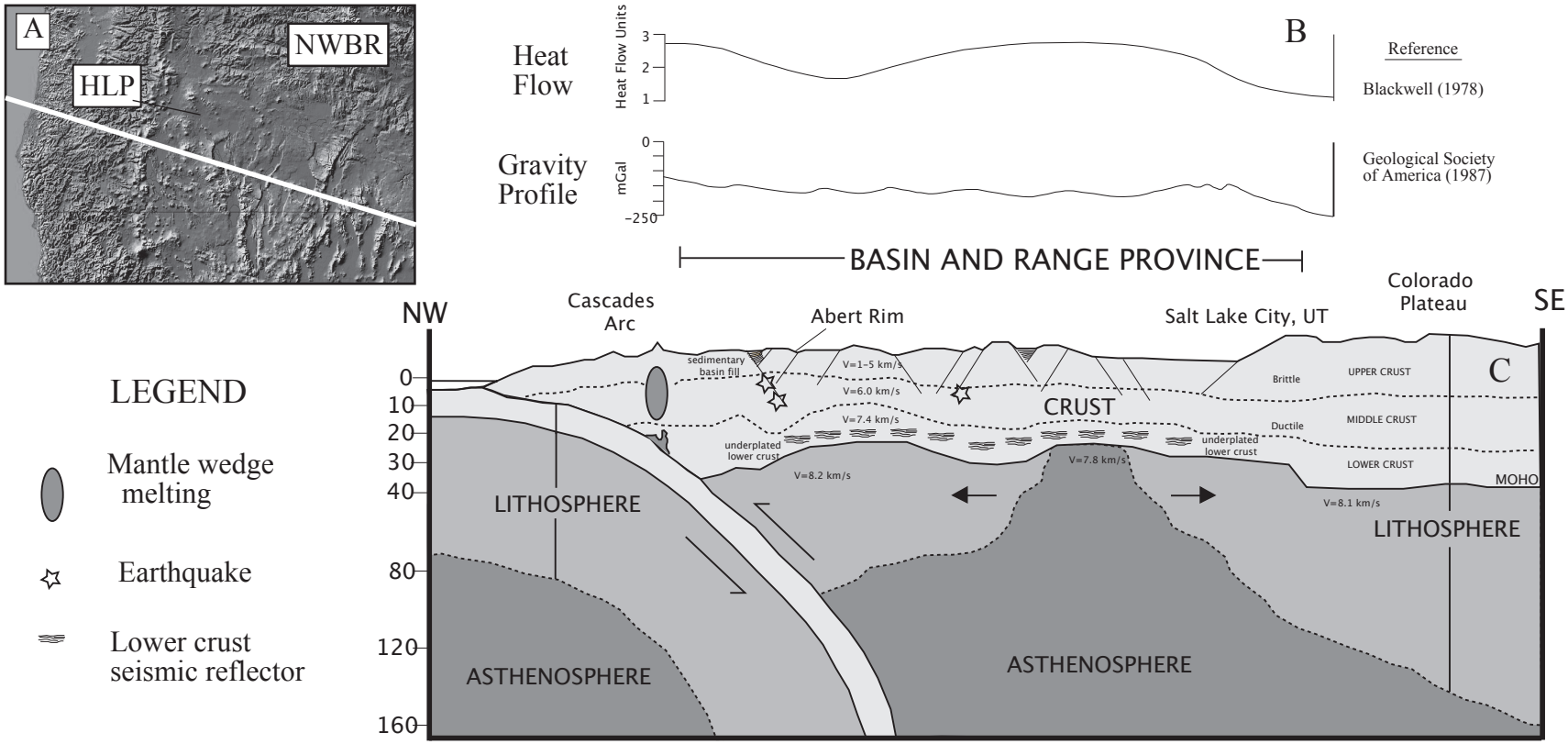

Figure 1. Physiographic and geophysical setting of the northwestern Basin and Range Province (NWBR) of southern Oregon. (A) DEM of NWBR illustrates declining relief of Basin and Range faults along-strike to the north and into the High Lava Plains (HLP). (B) Heat flow and gravity profiles accross the Basin and Range Province. (C) Schematic cross-section through the Basin and Range. Orientation of section shown by white line in panel A although entire section line not shown. 1.5x vertical exagerration for the uppermost 40 km of the section. Earthquake data from Qamar and Meagher (1993).

operating tectonic forces and the brittle-ductile transition within the crust. The addition of gravity and heat flow profiles provides a complimentary set of constraints, which collectively produce an image of the crust and uppermost mantle that displays these qualities: (1) a fairly uniform crustal thickness of 30-35 km, with an upper brittle part that is at most 16 km thick and a transition to ductile lower crust at ~20 km depth (2) asymmetrical rift grabens that are filled with 1.5-6 km of sedimentary and volcanic strata, (3) dense layering within the middle and lower crust thought to reflect ductile stretching and gabbroic underplating, (4) low-angle normal faults that extend to mid-crustal levels, (5) hot asthenosphere at depths ranging between 42-44 km, which lead to an elevated thermal state throughout the region, (6) a contemporary tectonic stress oriented ~N60˚W ± 20˚ that produces normal to right-oblique slip of as much as 6 mm/yr along faults (Pezzopanne and Weldon, 1993), (7) a bouguer gravity anomaly that lies between -150 to -200 mGals, and (8) high heat flow (2-2.5 HFU) particularly focused within the center and eastern margin of the province. These observations indicate the NWBR is a region of active continental rifting and that crust has been modified due to past episodes of extension and magmatism.

The NWBR: A Locus of Volcanism

Belts of intermediate composition magmatism within the interior of the Basin and Range Province broadly correlate with intervals of extreme Tertiary rifting (Armstrong and Ward, 1991). During the Quaternary magmatism has focused outward towards the margins of the Basin and Range province relative to a more central locus during the Tertiary (Christiansen and McKee, 1978). For these reasons, most volcanic rocks

exposed within the NWBR are younger than Middle Miocene Steens flood basalt volcanism that essentially buried Early Tertiary and older rocks within a vast portion of southeastern Oregon (e.g., Johnson et al., 1998; Walker and MacLeod, 1991). Late Miocene mafic to bimodal basalt-rhyolite volcanism of the High Lava Plains (HLP) (Jordan et al., 2004) has obscured the older geology even more.

Isolated Early Miocene volcanoes of intermediate composition (andesite-dacite) are identified within the NWBR (e.g., Mathis, 1993; Thomas, 1981) and are intriguing targets for study because they possess promise for understanding the post-Laramide transition from Cretaceous subduction and calc-alkaline volcanism and plutonism to Late Miocene extension and primarily mafic volcanism within the Basin and Range Province. This transition is clear elsewhere in the Basin and Range but is not well established within the NWBR where the Late Miocene geologic history is complicated. For example, the region is likely affected by the Yellowstone hotspot (e.g., Jordan et al., 2004) or mantle flow produced by the northward motion of the Menodcino Triple Junction with respect to North America (Christiansen et al., 2002). Therefore, the coincidence of the High Lava Plains with the NWBR (Figure 1) is not well understood.

The NWBR: A Young Extensional Province

Continental deformation of the western margin of North America, due to Post-Laramide reorganization of the plate boundary (e.g., Christiansen and Yeats, 1991), is recorded by the formation of the vast Basin and Range extensional province (e.g., Wernicke, 1992) and the development and growth of intracontinental transform fault systems such as the San Andreas and Walker Lane fault systems (Figure 2) (Atwater and

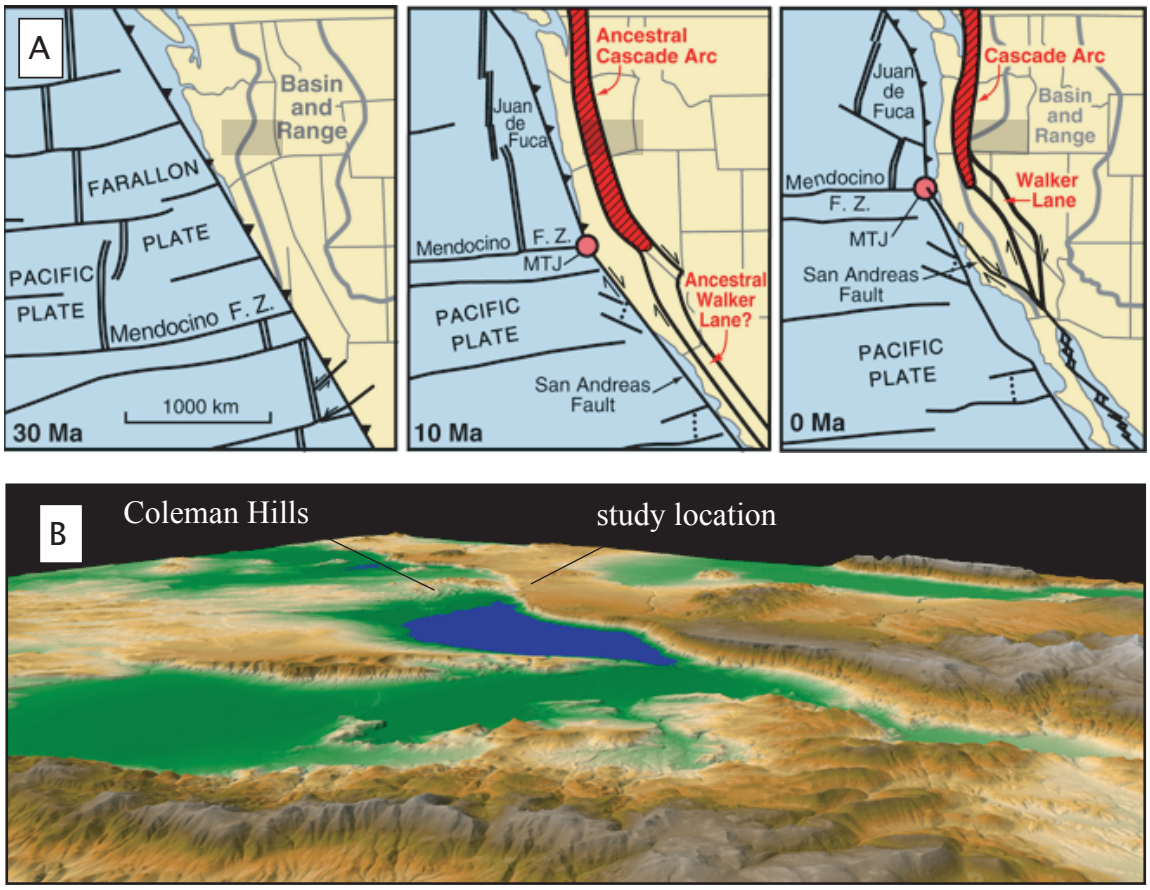

Figure 2. (A) Model reconstruction of the tectonic development of the western margin of the U.S. since ~30 Ma. Box indicates position of the NWBR and the ocus of this study. Based on work of Atwater and Stock (1998) and modified from Faulds et al. (2005). (B) Oblique DEM of the Lake Abert Basin and Abert Rim fault. View to NE. 2x vertical exaggeration. The junction of the Coleman Hills with Abert Rim is primary region of sampling and geologic mapping.

Stock, 1998; Faulds et al., 2005). Numerous models describe driving forces that facilitate expansion of the Basin and Range Province. These include: Subduction zone roll-back (Humphreys, 1994), clock-wise rotation of the Cascadia forearc (Wells and Heller, 1998), northward propagation of intracontinental transform faults (Faulds et al., 2005), and collapse of the overthickened Laramide crust due to excess gravitational potential energy (Humphreys and Coblentz, 2007).

Active Basin and Range extension was established in the NWBR sometime after 12 Ma based on previous work in the area (Dilles and Gans, 1995; Surpless et al., 2002; Colgan et al., 2004). Along-strike propagation of the Walker Lane transfers extensional strain to the north, which may correlate with the arrival of extension in southern Oregon. The NWBR is characterized by two principal sets of faults that strike NW and NNE and cut Late Cenozoic volcanic units. The temporal development of these faults has not been established.

The Abert Rim fault (Figure 2B) is the type of structure where questions about timing and style of Basin and Range faulting can be addressed. The Abert Rim fault is one of the major structures in Oregon (the trace is > 100 km) and systems of NW-striking faults interact with the NNE-striking Basin and Range fault at the north end of Lake Abert, a large playa that lies in the hanging wall of the fault. Topographic and presumably stratigraphic separation on the fault declines along-strike to the north and the area is characterized by a protracted Miocene volcanic history.

RESEARCH QUESTIONS

1. What are causes for a change form calc-alkaline to mafic/bimodal magmatism within the NWBR?
2. Are intermediate Early Miocene volcanoes within the NWBR part of the ancestral Cascades volcanic arc?
3. When did extension arrive in southern Oregon, and what were the tectonic controls on its arrival?
4. How did extension expand into the NWBR? Along-strike propagation from the south? Across-strike propagation from the east? Both?
5. What is the relative temporal development of NW- vs. NNE-striking faults of the NWBR?
6. Are the patterns of Late Miocene faults of the NWBR formed solely in response to regional stress or are their orientations affected by an older tectonic fabric?

REFERENCES CITED

Armstrong, R.L., and Ward, P., 1991, Evolving geographic patterns of Cenozoic magmatism in the North American Cordillera: The temporal and spatial association of magmatism and metamorphic core complexes, Journal of Geophysical Research, v. 96, p. 13,201-13,224.

Allmendinger, R.W., Hauge, T.A., Huaser, E.C., Potter, C.J., Klemperer, S.L., Nelson, K.D., Knuepfer, P., and Oliver, J., 1987, Overview of the COCORP 40˚ N transect, western United States: The fabric of an orogenic belt, Geological Society of America Bulletin, v. 98, p. 308-319

Atwater, T., and Stock, J., 1998, Pacific-North America plate tectonics of the Neogene southwestern United States-An update, in Ernst, W.G., ed, International Geological Review, Clarence Hall Symposium volume, v. 40, p. 375-402.

Blackwell, D.D., 1978, Heat flow and energy loss in the Western United States, Geological Society of America Memoir 152, p. 175-208.

Catchings, R.D., and Mooney, W.D., 1988, Crustal structure of east central Oregon: Relation between Newberry volcano and regional crustal structure, Journal of Geophsical Research, v. 93, p. 10,081-10,094.

Christiansen, R.L., and McKee, E.H., 1978, Late Cenozoic volcanic and tectonic evolution of the Great Basin and Columbia Intermontane regions, Geological Society of America Memoir 152, p. 283-311.

Christiansen, R.L., Yeats, R.S., 1992, Post-Laramide geology of the U.S. Cordilleran region, in Geological Society of America Special Publication, The geology of North America: The Cordilleran Orogen; conterminous U.S., Burchfiel, B.C., Lipman, P.W., and Zoback, M.L. (eds.), p. 261-406.

Christiansen, R.L., Foulger, G.R., and Evans, J.R., 2002, Upper-mantle origin of the Yellowstone hotspot, Geological Society of America Bulletin, v. 114, p. 1,245-1,256.

Colgan, J.P., Dumitru, T.A., and Miller, E.L., 2004, Diachroneity of Basin and Range extension and Yellowstone hotspot volcanism in northwestern Nevada, Geological Society of America Bulletin, v. 32, p. 121-124.

Dilles, J.H., and Gans, P.B., 1995, The chronology of Cenozoic volcanism and deformation in the Yerringtion area, western Basin and Range and Walker Lane, Geological Society of America Bulletin, v. 107, p. 474-486.

Donath, F.A., 1962, Analysis of Basin-Range structure, south-central Oregon, Geological Society of America Bulletin, v. 73, p. 1-16.

Faulds, J.E., Henry, C.D., and Hinz, N.H., 2005, Kinematics of the northern Walker Lane: An incipient transform fault along the Pacific-North American plate boundary, Geology, v. 33, p. 505-508.

Geological Society of America, 1987, Gravity Anomaly Map of North America, GSA Decade of North American Geology, scale: 1:5,000,000.

Hearn, T., Beghoul, N., and Barazangi, M., 1991, Tomography of the Western UnitedStates from regional arrival times, Journal of Geophysical Research, v. 96, p. 16,369-16,381.

Humphreys, E.D., 1994, post-Laramide removal of the Farallon slab, western United States, Geology, v. 23, p. 987-990.

Humphreys, E.D., and Coblentz, D.D., 2007, North American dynamics and western U.S. tectonics, Reviews of Geophysics, v. 45, 30 p.

Johnson, J.A., Hawkesworth, C.J., Hooper, P.R., and Binger, G.B., 1998, Major- and trace-element analyses of Steens basalt, southeastern Oregon, U.S. Geological Survey Open-File Report 98-482, 30 p.

Jordan, B.T., Grunder, A.L., Duncan, R.A., and Deino, A.L., 2004, Geochronology of Oregon High Lava Plains volcanism: Mirror image of the Yellowstone hotspot?, Journal of Geophysical Research, 19 pp.

Mathis, A.C., 1993, Geology and petrology of a 26-Ma trachybasalt to peralkaline rhyolite suite exposed at Hart Mountain, southern OR [M.S. thesis]: Corvallis, Oregon, Oregon State University, 141 p.

Mooney, W.D., and Braile, L.W., 1989, The seismic structure of the continental crust and upper mantle of North America, *in* The geology of North America-An overview, Bally, A.W., and Palmer, A.R. *eds.*, Boulder, Colorado: Geological Society of America, Decade of North American Geology, v. 1 p. 437-462.

Pezzopane, S.K., and Weldon, R.J., 1993, Tectonic role of active faulting in central Oregon, Tectonics, v. 12, p. 1,140-1,169.

Qamar, A., and Meagher, K.L., 1993, Precisely locating the Klamath Falls, Oregon, earthquakes, Earthquakes and Volcanoes, v. 24, p. 129-139.

Surpless, B.E., Stockli, D.F., Dumitru, T.A., Miller, E.L., and Farley, K.A., 2002, Progressive westward encroachment of Basin and Range extension into the stable northern Sierra Nevada block, Tectonics, v. 21, no. 1, 2-1 – 2-13.

Thomas, T.H., 1981, Geology and Mineral Deposits of the Coyote Hills Mining District, Lake County, Oregon, [M.S. Thesis] Oregon State University, Corvallis, OR 137 p.

Walker, G.W., and MacLeod, N.S., 1991, Geologic map of Oregon, U.S. Geological Survey, Reston, VA.

Wells, R.E., and Heller, P.H., 1988, The relative contribution of accretion, shear, and extension to Cenozoic tectonic rotation in the Pacific Northwest, Geological Society of America Bulletin, v. 100, p. 325-338.

Wernicke, B.P., 1992, Cenozoic extensional tectonics of the U.S. Cordillera, in Burchfiel, B.C., et al., eds., The Cordilleran orogen: Conterminous U.S.: Boulder, Colorado, Geological Society of America, Geology of North America, v. G-3, p. 553-581.

CHAPTER 2

TRANSITION FROM INTERMEDIATE TO BIMODAL VOLCANISM IN THE NORTHWESTERN BASIN AND RANGE PROVINCE: COMPOSITIONAL EVOLUTION AND TECTONIC IMPLICATIONS

Kaleb C. Scarberry[1]

Anita L. Grunder[1]

[1]Department of Geosciences,
Oregon State University, Corvallis, OR 97331

For submission to Geological Society of America Bulletin

ABSTRACT

Volcanic rocks exposed at the north end of Lake Abert in southern Oregon preserve an Early Miocene volcano incompletely buried by Late Miocene volcanic units. Exposure of Early Miocene volcanic centers in southern Oregon are uncommon and chemical and geologic description of them adds to an understanding of the transition from subduction-related to rift-related volcanism along the western margin of North America. Early Miocene volcanic units of the Coleman Hills consist primarily of intermediate rocks (SiO_2 = 55-65 wt. %) that intrude and overlie a core of rhyolite domes and associated pyroclastic deposits (SiO_2 = 70-72 wt. %).

Trace element concentrations suggest that the Early Miocene rocks were not generated within an active arc but instead formed in a back-arc region that had been metasomatized by prior subduction. Volcanic rocks of the Coleman Hills exhibit isotopic ratios that indicate generation in a crustal environment, such as elevated $^{208}Pb/^{204}Pb$, $^{207}Pb/^{204}Pb$, and $^{206}Pb/^{204}Pb$ and lower $^{143}Nd/^{144}Nd$ and $^{176}Hf/^{177}Hf$, relative to the onlapped Late Miocene volcanic section. $^{87}Sr/^{86}Sr$ ratios are the same for intermediate compositions of the Coleman Hills and Late Miocene lavas although rhyolite of the Coleman Hills has much higher values (0.7051 vs. 0.7037) suggesting that they are the product of crustal anatexis

INTRODUCTION

The geologic history of the Basin and Range Province in southeastern Oregon (Figure 1A) is difficult to unravel because exposures older than 16.6-15.3 Ma (Hooper et al., 2002) are largely covered by flood basalts associated with Steens Mountain (e.g., Johnson et al., 1998) and by post-10 Ma bimodal basalt-rhyolite volcanism of the High

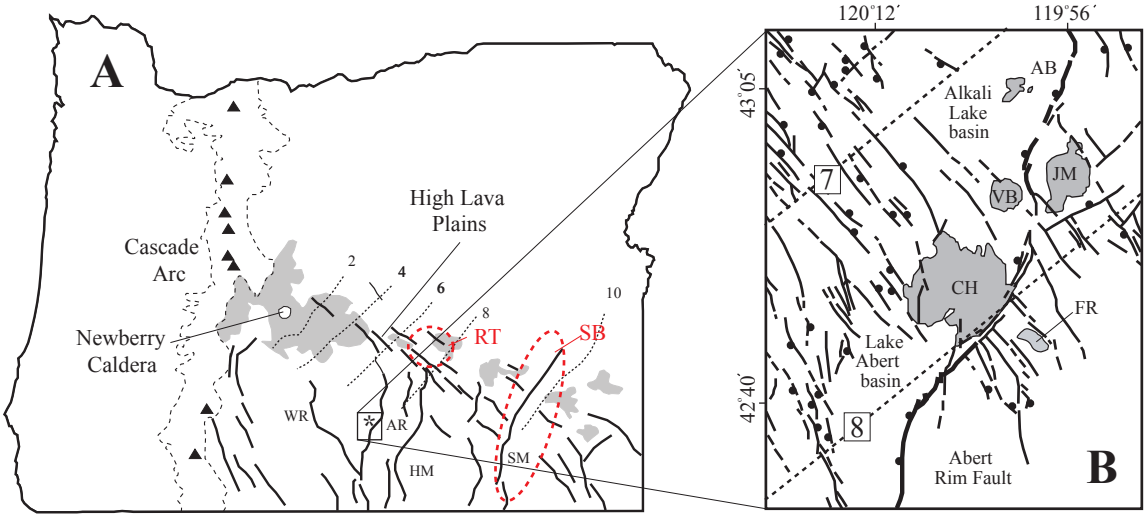

Figure 1. (A) regional volcano-tectonic setting of the Basin and Range margin in southern Oregon and (B) detailed structral fabric of the study area. (A) Quaternary mafic volcanism of the Cascade Arc to the west and the High Lava Plains (HLP) to the north border Basin and Range extension accross southern Oregon. Primary source of Middle Miocene Steens Basalts (SB) and Late Miocene Rattlesnake Tuff (RT) are shown in red. Prominent regional escarpments are labeled: WR-Winter Rim; AR-Abert Rim; HM-Hart Mountain; SM-Steens Mountain. The HLP is defined by a track of Quaternary basalts (shade) where isochrons (thin stippled line) show an age-progressive westward trend for the onset of silicic volcanism (in Ma) after Jordan et al., 2004. (B) The Coleman Hills (CH) are one of many volcanic centers (shaded polygons) associated with the convergence of NW-striking structures and the NE-striking Abert Rim Fault. AB- Alkali Butte; VB- Venator Butte; JM- Juniper Mountain; FR=Flint Ridge.

Lava Plains (HLP) (e.g., Walker and Nolf, 1981; Jordan et al., 2004). Prior to ~16 m.y., much of the Basin and Range Province was characterized by sweeping belts of intermediate composition magmatism, broadly related to extreme extension (e.g., Stewart and Carlson, 1974; Armstrong and Ward, 1991). Since then volcanism has focused to the margins of the extensional province (Christiansen and McKee, 1978). The widely distributed Middle Tertiary calcalkaline magmatism of the Basin and Range Province has been principally attributed to (a) shallow subduction followed by delamination of the slab from the base of the lithosphere with attendant mantle upwelling (Coney and Reynolds, 1977) and (b) extreme extension of thickened Laramide crust via low-angle detachment faulting (e.g., Armstrong and Ward, 1991; Wernicke, 1992).

The transition from Middle Tertiary calcalkaline magmatism to Late Tertiary and Quaternary, bimodal basalt-rhyolite magmatism is not well established in the northwestern corner of the Basin and Range Province, in southeastern Oregon. This region has seen little geologic study compared with much of the Basin and Range Province despite a complex tectonic setting and protracted post-Laramide volcanic history (e.g., Christiansen and Yeats). The Late Cenozoic geologic history of southeastern Oregon is complex with respect to tectonic influences. On the one hand, part of the transition from intermediate calc-alkaline to basaltic volcanism is similar to what is observed during evolution of the margins of the Basin and Range Province in general (e.g., Christiansen and McKee, 1978). On the other hand, the region is potentially influenced by the Yellowstone hotspot (e.g., Jordan et al., 2004) or mantle flow related to northward migration of the Mendocino Triple Junction (e.g., Christiansen et al., 2002). The Cascade Arc and High Lava Plains form the western and northern

borders, respectively, to the extensional province in Oregon (Figure 1). The HLP has been interpreted as part of the Yellowstone hotspot system due to a westward age-progression in younger rhyolite volcanism (e.g., Draper, 1991; Jordan et al., 2004) that mirrors the eastward trend observed on the Snake River Plain (e.g., Pierce and Morgan, 1992).

This paper addresses the Coleman Hills, an Early Miocene volcanic complex associated with the Abert Rim, a major Basin and Range escarpment in southern Oregon (Figure 1B). Magmatism of the Coleman Hills volcanic complex provides important information about the tectonic transition from Middle Tertiary volcanism to Late Cenozoic extension within a young margin of the Basin and Range Province. The occurrence of the volcanic center at the intersection of NW- and NE-striking faults, characteristic of the Late Cenozoic structural fabric of the region, brings to question the role of older episodes of deformation in the evolution of younger extensional fault systems within the Basin and Range Province. The Coleman Hills provide insight into crustal processes that controlled the composition of magmas prior to Late Miocene block-style faulting of the Basin and Range Province. We here present new compositional and isotopic (Nd, Sr, Pb, and Hf) data from the Early Miocene section of the Coleman Hills and Late Miocene volcanic strata exposed in the vicinity of Lake Abert, OR. We consider the compositional and structural development of the Coleman Hills and environs with respect to the crustal development of the Basin and Range extensional province.

STRUCTURAL AND STRATIGRAPHIC SETTING OF THE ABERT RIM, COLEMAN HILLS AND ADJACENT LAKE BASINS

The Abert Rim Fault is a NNE-striking Basin and Range fault that can be traced for >100 km in southern Oregon. It has maximum relief of ~400 m near Lake Abert and declines to the north where it disappears into the High Lava Plains (Figure 1). The Abert Rim fault forms a half-graben that has controlled sedimentation and hosts Lake Abert and Alkali Lake. The 8-10 km wide valley is capped by a broad swath of Quaternary alluvium, dune sands and playa deposits parallel to the NNE-strike of the Abert Rim Fault (Figure 2). Structural studies of the region indicate that stratigraphic separation along the Abert Rim Fault, as well as activity along NW-striking extensional faults, had initiated prior to ~7 Ma (see Chapter 3). The post-Coleman Hills volcanic section is generally conformable in the footwall of the Abert Rim Fault but an angular discordance of ~20° occurs between 8.6 Ma and 7.7 Ma basaltic lavas in the hanging wall of the fault. This discordance indicates that the primarily NW-striking structures within the hanging wall (Figure 1 and 2) were active by ~8.6 Ma and that formation of the NE-striking Abert Rim Fault is largely younger. Segments of these NNE- and NW-striking fault systems have remained active into the Holocene (Pezzopane and Weldon, 1993).

The west-dipping Abert Rim fault exposes a volcanic section >500 m thick (Figure 3). Volcanic units exposed by and near the Abert Rim and north of Lake Abert record punctuated episodes of volcanism during the Early, Middle and Late Miocene. Early Miocene volcanic rocks of the Coleman Hills range in composition from silicic to mafic through time (Figure 4) and possess ^{40}Ar-^{39}Ar ages that are ~22 Ma. The Early Miocene Coleman Hills lie within the hanging wall of the Abert Rim Fault (Figure 1).

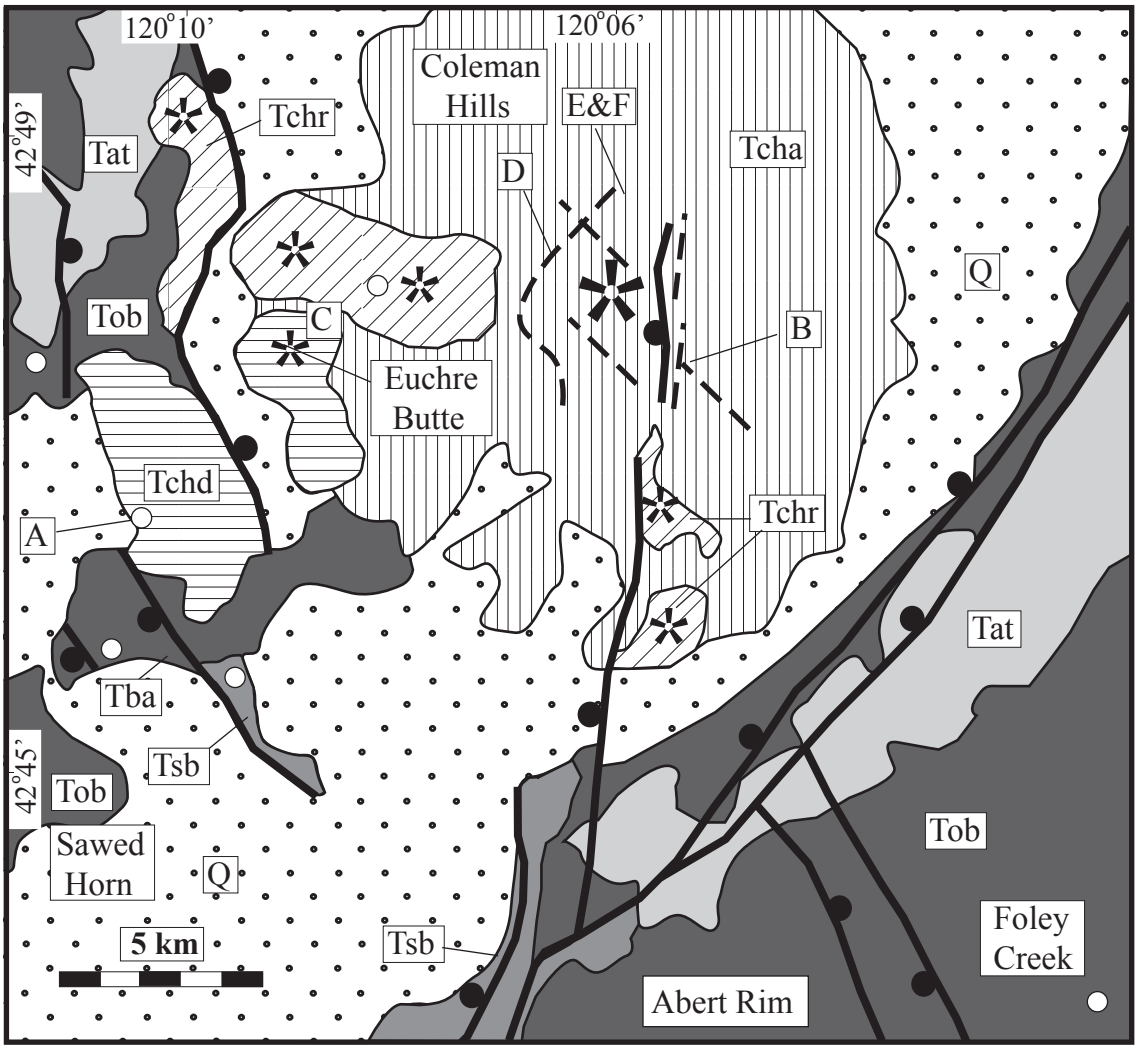

Figure 2. Simplified geologic map of the Coleman Hills volcanic complex. Tchr- Coleman Hills rhyolite; Tchd- Coleman Hills dacite; Tcha- Coleman Hills bsaltic andesite to andesite; Tsb- Steens basalt; Tba- basaltic andesite; Tob- olivine basalt; Tat- Rattlesnake Tuff; Q- undifferentiated pediment, playa and sand dune deposits. Faults shown with ball on side down. Prominent dike trends are illustrated dashed line. ✻ = infered volcanic vents. White circles indicate locations of samples that were dated. Letters A-F are in reference to photographs shown in Figure 4.

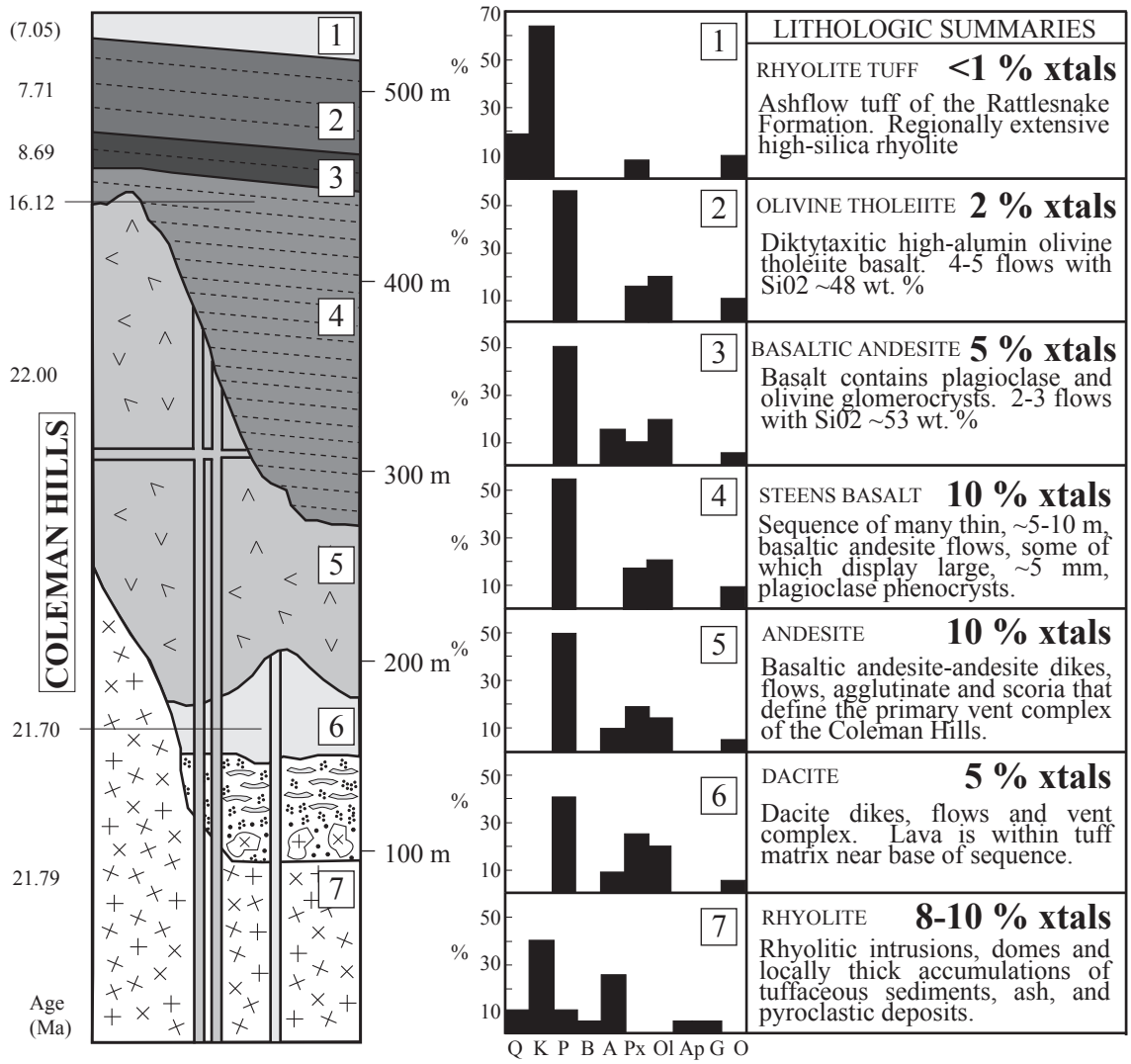

Figure 3. Composite stratigraphic section of the Coleman Hills shows mineral modes and estimate of crystallinity for the primary rock units of the study region. Estimates determined from thin-sections and hand samples except for the Rattlensake tuff, which is obtained from the average of four pumice groups reported by Streck and Grunder (1997). Ages are reported in Scarberry (in prep) except for the Rattlesnake Tuff in parentheses (Streck and Grunder, 1995). Minerals shown on histograms: Q=quartz, K=potassium feldspar, P=plagioclase, B=biotitie, A=amphibole, Px=pyroxene, Ol=olivine, Ap=apatite, G=garnet, O=oxides (magnetite and ilmenite).

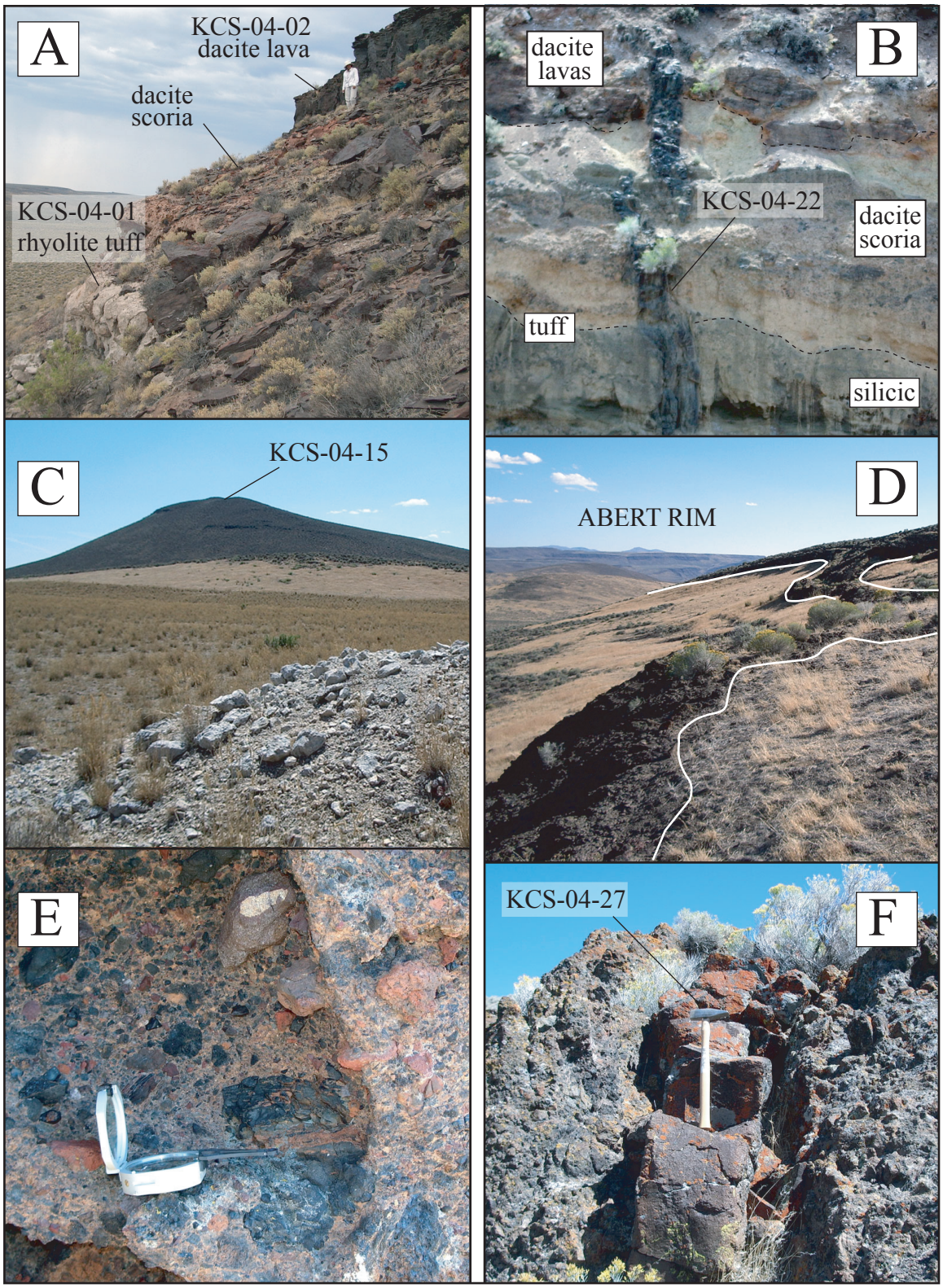

Figure 4. Coleman Hills volcanic rocks: (A) rhyolite volcaniclastic deposit overlain by dacite lavas; (B) basaltic andesite dike in road-cut; (C) Euchre Butte with rhyolite exposed in prospect pit; (D) large dike; (E) mafic pyroclastic deposit; (F) basaltic andesite dike.

Walker (1963) described rocks of the Coleman Hills (Figures 1 and 2) as remnants of composite volcanoes consisting largely of intermediate composition lavas and intrusive rhyolite and dacite plugs, dikes and domes. The Coleman Hills volcanic complex crops out over an area of ~80 km^2 and has an estimated total volume of ~150 km^3. It divides the Alkali Lake Basin to the north from the Lake Abert Basin to the south (Figure 1) and many dikes (Figure 4) within the volcano strike, in general, parallel to the structural fabric of both NW- and NNE-striking faults in the area. Numerous volcanic vents are located north of Lake Abert (Figure 5) and are separated from one another by Abert Rim. The average topographic relief along the Abert Rim Fault abruptly declines by >100 m north of the Coleman Hills. Near Lake Abert, the Coleman Hills formed a paleotopographic high against which Middle and Late Miocene volcanic units were banked, consistent with the model of Mankinen et al. (1987) that illustrates that local relief of as much as 1000 m existed prior to Middle Miocene eruption of Steens basalts.

METHODS

Detailed 1:24,000 geologic mapping of a ~625 km^2 area north of Lake Abert (Figure 2) was conducted over the course of three field seasons. Volcanic centers in the immediate vicinity of the map area (Figures 1 and 5) were sampled for the purpose of acquiring a broader understanding of the regional stratigraphy. Representative samples of Early, Middle and Late Miocene volcanic units were sampled for the purpose of compositional and petrographic analysis. Samples were crushed using an alumina jaw crusher and clean, pea-sized fragments were hand picked and soaked in dilute HCl to remove traces of $CaCO_3$. Samples were washed thoroughly with de-ionized H_2O, dried

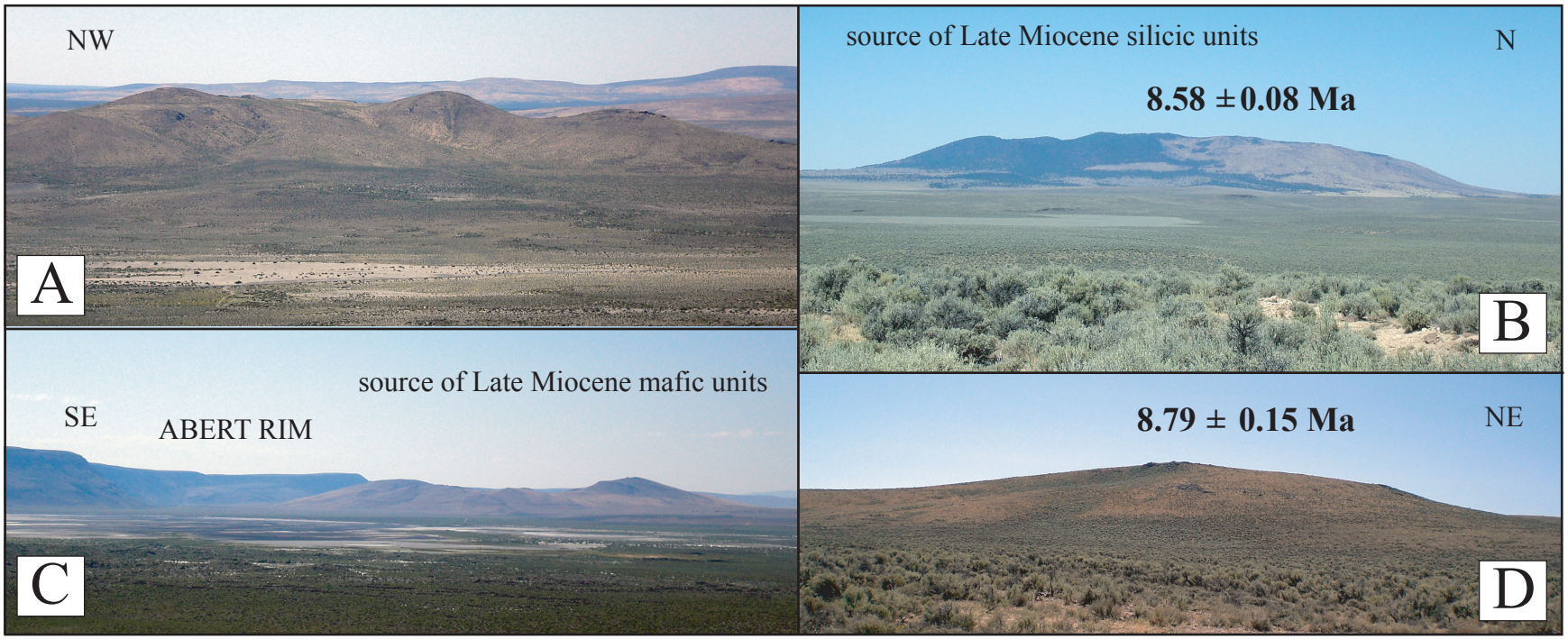

Figure 5. Regional volcanic centers associated with the Abert Rim Fault. New ages are shown for rhyolite at Juniper Mountain and dacite at Flint Ridge. Location of volcanic centers with respect to the Abert Rim Fault is shown on Figure 1. (A) Alkali Buttes; (B) Juniper Mountain; (C) Venator Butte; and (D) Flint Ridge.

at low temperature prior to shipment to the Washington State University GeoAnalytical Laboratory for XRF (Johnson et al., 1999) ICP-MS analysis. For the twelve elements that were analyzed by both XRF and ICP-MS there is generally good agreement, particularly for the Early Miocene rocks (Appendix I). XRF analysis of HAOT samples produced 3-fold overestimates for Pb relative to ICP-MS analysis of the same rock while slightly overestimating (< 1-fold) La and Ce and underestimating Th. XRF analysis of Steens basalts slightly overestimated Pb concentrations relative to ICP-MS analysis. For elements duplicated by XRF and ICP-MS we use ICP-MS values due to increased precision for a wider range of elements.

Sr, Nd, Pb and Hf isotopic analysis was performed at the Carnegie Institution of Washington (Department of Terrestrial Magnetism) in Washington, D.C. over a two-week period. Isotope dilutions and standard corrections were performed according to the procedure and values described in Carlson et al. (2006). ^{40}Ar-^{39}Ar ages are reported with 2-σ errors (Appendix 3). See Chapter 3 for ^{40}Ar-^{39}Ar age determination methods.

RESULTS

Mapping focused on the Coleman Hills (Plate 1) and was complemented by reconnaissance of other nearby volcanic centers distributed along Abert Rim. Stratigraphic and geochronologic data summarized below yield the compiled stratigraphic column in Figure 3. ^{40}Ar-^{39}Ar ages discussed here are presented in Chapter 3 unless otherwise noted.

Early Miocene Coleman Hills Volcanic Complex

The Coleman Hills lie within the hanging wall of the Abert Rim fault. They define a volcanic complex that extends over 80 km^2 with an estimated total volume of ~4.2 km^3. Compositions of the volcanic rock range from basaltic andesite through andesite to dacite (~55 to ~65 wt. % SiO_2), which are separated from rhyolites by a compositional gap of ~7 wt. % SiO_2 (Figure 6; Table 1). Analyses of the Coleman Hills presented here are complimented by unpublished data provided by V. Camp (Figure 6), that are from lavas, dikes, and tuff blocks exposed in three road-cuts (e.g., Figure 4B) that traverse the principal vent location in the Coleman Hills (Figure 2). The Coleman Hills makes a continuous suite from basaltic andesite to trachydacite (~55 to ~65 wt. % SiO_2) with inflections in Al_2O_3 and P_2O_5 wt. % occurring at 60 and 57 wt. % SiO_2, respectively. This suite of alkaline intermediate rocks fills a compositional gap that is characteristic of the products of Middle and Late Miocene volcanism.

The ages of rhyolite, dacite and basaltic andesite of the Coleman Hills are ~22 Ma and indistinguishable (Figure 5). Stratigraphic and intrusive relationships indicate that rhyolites were emplaced first, followed by dacite and then andesite to basaltic andesite (Figure 4). Rhyolite and dacite define N-W vent alignments and occur as small, distributed vents (Figure 3). Later andesite and basaltic andesite volcanism centered at the tip of an extension of the Abert Rim Fault and dike orientations strike both NW and NNE, paralleling the strike of faults that cut Middle and Late Miocene volcanic units.

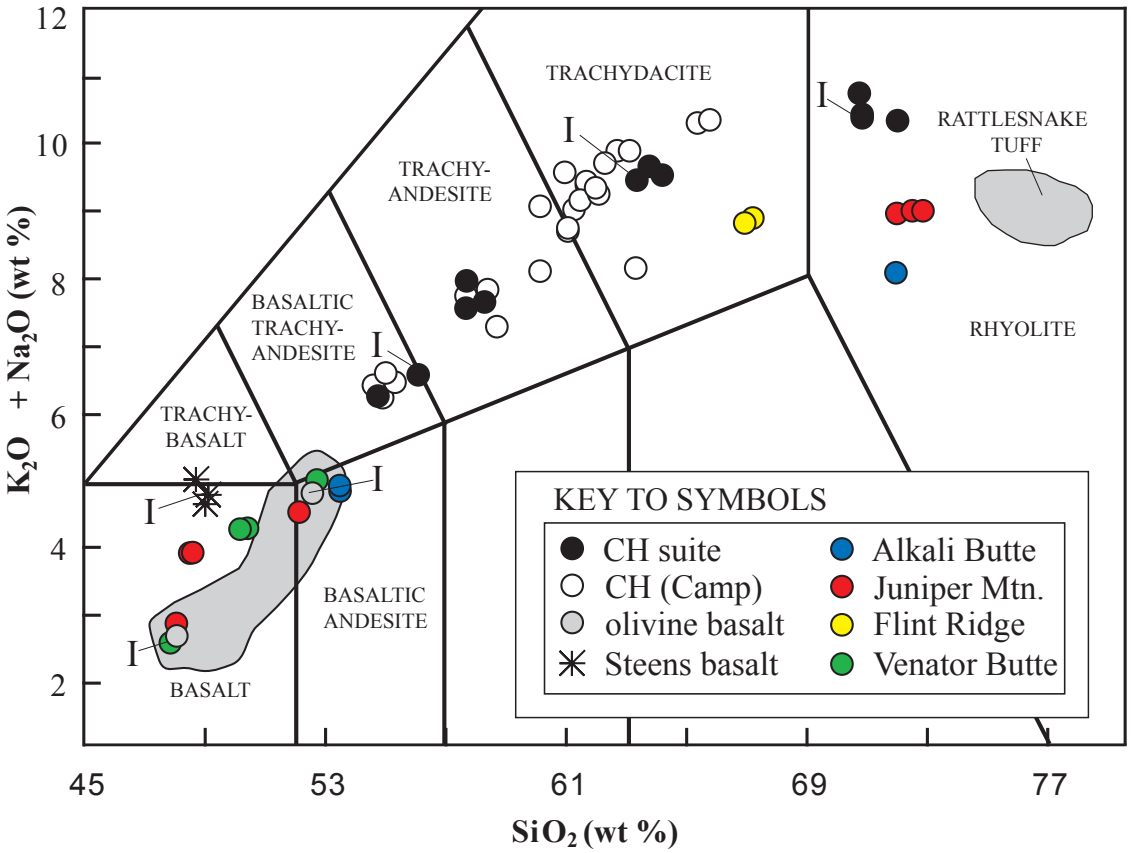

Figure 6. Total alkali-silica classification of chemical analyses from northern Lake Abert and regional volcanic centers, after LeBas et al., 1986. "Trachy" prefix is not used in the text. The plot shows a shift from dominantly intermediiate compositions at ~22 Ma: this study (filled circles) and unpublished data from Camp (open circles) to more mafic during eruption of the Steens basalt at ~16 Ma, to bimodal, basalt-ryolite (shade) by ~9-7 Ma. Regional volcanic centers are color-coded. Rattlesnake Tuff analyses are plotted from Streck and Grunder (1995). Samples with "I" label are analyzed for Sr, Nd, Hf, and Pb isotopic composition. Symbols within shaded basalt field denote end-member analyzed for isotopinc composition.

Table 1. Chemical composition of volcanic rocks from northern Lake Abert normalized to 100% volatile free.

sample ID	**KCS-04-22**	**KCS-04-21**	**KCS-04-28**	**KCS-04-23**	**KCS-04-27**	**KCS-04-14**	**KCS-04-02**	**KCS-04-15**	**KCS-04-01**
location	Coleman Hills	Coleman Hills	Coleman Hills	Coleman Hills	Coleman Hills	Coleman Hills	Coleman Hills	Coleman Hills	Coleman Hills
rock type	bas-ands-dike	bas-ands-dike	andesite-flow	andesite-flow	andesite-dike	dacite-dike	dacite flow	dacite-scoria	rhy-block/ash
lat. (N)	42.7928	42.7931	42.8219	42.7742	42.8142	42.7736	42.7869	42.7975	42.7856
long. (W)	120.0853	120.0847	120.0764	120.1083	120.0814	120.1444	120.1750	120.1464	120.1750
XRF (wt. %)									
SiO_2	54.75	56.04	58.33	57.69	57.66	64.19	63.33	63.76	70.69
TiO_2	2.15	2.33	1.70	1.72	1.76	0.70	0.73	0.71	0.14
Al_2O_3	16.01	16.28	17.15	16.73	16.39	16.15	16.40	16.08	15.01
FeO*	10.09	9.51	8.12	8.21	8.45	5.93	6.53	5.96	2.45
MnO	0.15	0.16	0.12	0.13	0.13	0.14	0.16	0.16	0.08
MgO	3.19	2.31	1.54	1.99	1.64	0.70	0.59	0.73	0.08
CaO	6.74	6.01	4.77	5.30	5.18	2.31	2.45	2.64	0.83
Na_2O	3.56	3.69	4.19	4.14	3.95	4.95	4.98	4.10	4.73
K_2O	2.72	2.90	3.44	3.39	4.00	4.67	4.55	5.61	5.97
P_2O_5	0.64	0.77	0.64	0.70	0.84	0.26	0.28	0.25	0.02
a.t.	97.41	96.52	97.13	97.62	96.81	97.54	97.65	94.63	95.62
Trace elements (ppm) (XRF)									
Ni	41	16	19	21	16	9	6	7	7
Cr	36	8	6	4	3	4	2	1	1
Sc	18	18	12	13	13	13	15	13	2
V	156	143	83	93	85	25	19	5	0
Ba	590	730	868	820	911	1511	1587	1384	30
Rb	81	73	79	82	98	110	108	114	186
Sr	417	458	467	462	415	287	319	249	4
Zr	392	381	467	449	511	590	561	576	401
Y	40	41	36	40	46	42	38	42	60
Nb	35	33	41	40	44	42	39	41	62
Ga	23	26	25	25	25	24	23	23	27
Cu	69	51	51	61	64	23	11	8	10
Zn	121	140	119	117	127	144	124	124	133
Pb	8	9	11	8	10	12	11	14	20
La	38	39	46	43	52	50	47	49	72
Ce	83	84	93	91	112	98	100	99	149
Th	6	7	7	6	8	10	10	10	19
Nd	47	47	52	51	58	51	49	46	65

Table 1. Continued.

	KCS-04-22	KCS-04-21	KCS-04-28	KCS-04-23	KCS-04-27	KCS-04-14	KCS-04-02	KCS-04-15	KCS-04-01
Trace elements (ppm) (ICP-MS)									
La		39.3	44.4	46.4	52.7	51.4	47.7		
Ce		80.8	86.1	93.5	107.8	96.8	94.6		
Pr		10.3	10.9	11.4	13.2	12.1	11.3		
Nd		45.6	46.9	49.1	57.0	50.2	47.4		
Sm		11.5	11.1	11.8	13.8	11.9	11.2		
Eu		3.3	3.1	3.1	3.4	3.3	3.4		
Gd		10.8	9.9	10.7	12.5	10.6	9.9		
Tb		1.6	1.5	1.6	1.9	1.7	1.5		
Dy		9.3	8.2	9.1	10.6	9.6	8.8		
Ho		1.8	1.5	1.7	2.0	1.9	1.7		
Er		4.4	3.9	4.4	5.0	4.9	4.4		
Tm		0.6	0.5	0.6	0.7	0.7	0.6		
Yb		3.7	3.2	3.6	4.1	4.3	3.9		
Lu		0.6	0.5	0.6	0.6	0.7	0.6		
Ba		730.8	875.9	832.8	901.1	1523.5	1584.7		
Th		7.0	8.1	7.7	8.5	10.6	10.0		
Nb		34.6	42.5	41.2	46.4	43.8	40.8		
Y		45.6	39.7	45.3	52.4	49.1	43.0		
Hf		9.2	11.3	10.8	12.3	13.8	13.3		
Ta		2.4	3.1	2.9	3.3	2.9	2.7		
U		2.3	2.7	2.6	2.9	3.5	3.0		
Pb		7.2	8.6	8.7	9.2	11.4	10.4		
Rb		70.6	75.4	79.3	94.1	105.9	103.3		
Cs		1.9	1.6	1.8	2.2	2.2	2.1		
Sr		459.3	455.2	463.4	414.9	281.6	313.5		
Sc		19.6	12.9	13.2	14.5	15.9	16.4		
Zr		371.1	445.8	433.7	497.1	579.0	543.3		

a.t.- prenormalization totals. XRF and ICP-MS nalyses performed at Washington State University. See Johnson et al (2000) for procedural information.

Table 1. Continued.

sample ID	**KCS-04-10**	**KCS-05-19**	**KCS-04-33**	**KCS-05-20**	**KCS-04-38**	**KCS-04-07**	**KCS-05-21**	**KCS-04-40**	**KCS-04-41**
location	Coleman Hills	Coleman Hills	Coleman Hills	Steens	Steens	Steens	HAOT	HAOT	HAOT
rock type	rhy-intrus.	rhy-flow	rhy-intrus.	basalt	basalt	basalt	bas-andesite	basalt	basalt
lat. (N)	42.8108	42.8114	42.7664	42.7733	42.7392	42.5811	42.7731	42.6761	42.6761
long. (W)	120.1394	120.1467	120.0825	120.1714	120.1147	120.3031	120.1761	120.0111	120.0111
XRF (wt. %)									
SiO_2	70.83	70.87	71.96	49.14	49.00	48.68	52.55	48.22	48.61
TiO_2	0.18	0.18	0.22	2.94	2.79	3.61	0.96	0.96	0.99
Al_2O_3	15.22	15.19	14.68	15.06	15.50	15.59	17.73	17.54	17.73
FeO*	2.51	2.53	2.10	13.53	12.95	14.17	8.50	9.40	9.33
MnO	0.03	0.02	0.03	0.22	0.21	0.21	0.16	0.18	0.18
MgO	0.09	0.05	0.16	5.13	5.25	3.89	6.32	9.06	8.34
CaO	0.75	0.78	0.49	8.67	9.13	8.31	8.65	11.70	11.74
Na_2O	4.63	4.61	4.93	3.45	3.42	3.67	3.48	2.59	2.68
K_2O	5.74	5.74	5.38	1.33	1.26	1.34	1.41	0.23	0.27
P_2O_5	0.03	0.04	0.05	0.53	0.49	0.54	0.23	0.13	0.13
a.t.	98.45	98.53	97.93	98.10	97.33	96.97	98.46	98.10	98.39
Trace elements (ppm) (XRF)									
Ni	7	6	8	66	75	33	107	183	145
Cr	1	1	1	56	63	4	26	224	207
Sc	4	6	4	34	31	28	26	37	38
V	11	6	8	432	418	355	185	263	268
Ba	124	128	106	711	463	464	545	167	171
Rb	208	207	147	22	21	19	13	0	2
Sr	26	30	14	452	438	522	354	300	321
Zr	361	367	718	211	198	212	112	44	47
Y	47	70	46	38	37	28	22	21	21
Nb	57	57	49	13	13	27	6	2	1
Ga	23	25	25	24	24	24	17	18	18
Cu	18	17	8	279	291	96	103	122	115
Zn	89	63	64	130	125	133	73	69	67
Pb	17	13	14	8	7	5	5	0	2
La	67	68	55	20	19	21	12	5	5
Ce	130	123	99	50	52	52	26	16	17
Th	23	22	13	2	3	3	0	0	0
Nd	55	58	56	32	35	31	16	11	10

Table 1. Continued.

	KCS-04-10	KCS-05-19	KCS-04-33	KCS-05-20	KCS-04-38	KCS-04-07	KCS-05-21	KCS-04-40	KCS-04-41
Trace elements (ppm) (ICP-MS)									
La		68.6	53.5	22.9	21.0	24.1	12.8	3.8	
Ce		120.9	98.4	50.4	46.8	49.5	24.1	8.4	
Pr		14.6	13.6	6.7	6.3	6.3	2.9	1.3	
Nd		55.7	55.4	31.4	29.3	28.2	13.0	7.4	
Sm		12.9	13.4	8.6	8.1	7.2	3.5	2.6	
Eu		0.9	1.5	2.7	2.5	2.6	1.2	1.1	
Gd		11.9	11.7	8.7	8.3	7.1	3.8	3.3	
Tb		2.1	1.9	1.4	1.3	1.1	0.7	0.6	
Dy		12.8	10.8	8.4	7.9	6.2	4.1	4.1	
Ho		2.7	2.1	1.7	1.5	1.2	0.9	0.9	
Er		7.5	5.5	4.3	4.0	3.0	2.4	2.4	
Tm		1.1	0.8	0.6	0.6	0.4	0.4	0.4	
Yb		7.2	5.1	3.6	3.4	2.4	2.3	2.3	
Lu		1.2	0.8	0.6	0.5	0.4	0.4	0.4	
Ba		129.1	104.9	686.7	448.4	440.6	532.5	167.4	
Th		22.4	12.9	2.5	2.3	2.6	1.0	0.1	
Nb		60.3	52.9	13.5	12.4	28.8	5.4	1.0	
Y		80.3	53.3	43.6	40.1	30.7	23.5	23.9	
Hf		11.6	17.7	5.6	5.2	5.1	2.6	1.3	
Ta		4.5	3.3	0.9	0.8	1.9	0.3	0.1	
U		6.8	4.1	0.7	0.7	0.8	0.4	0.1	
Pb		12.6	12.8	5.3	4.9	2.8	3.7	0.7	
Rb		195.7	140.3	22.3	21.5	18.9	12.8	1.5	
Cs		2.5	1.7	0.3	0.4	0.2	0.2	0.0	
Sr		29.8	14.6	460.0	454.2	534.6	352.7	308.9	
Sc		6.3	5.1	36.9	34.5	29.7	26.5	41.7	
Zr		347.1	697.3	207.4	192.4	205.2	105.2	39.9	

Table 1. Continued.

sample ID	**KCS-04-42**	**KCS-04-43**	**KCS-04-19**	**KCS-04-04**	**KCS-04-08**	**KCS-04-17**	**KCS-04-34**	**KCS-06-34**	**KCS-06-36**
location	HAOT	HAOT	HAOT	HAOT	HAOT	HAOT	HAOT	Juniper Mtn.	Juniper Mtn.
rock type	basalt	basalt	basalt	basalt	basalt	basalt	basalt	basalt	basalt
lat. (N)	42.6764	42.6764	42.6939	42.6942	42.7517	42.7933	42.7483	42.94012	42.92793
long. (W)	120.0125	120.0125	120.1467	120.1481	120.1903	120.1967	120.0717	119.9248	119.93625
XRF (wt. %)									
SiO_2	48.62	48.26	48.03	48.03	49.02	48.07	48.53	48.48	48.60
TiO_2	1.05	0.90	0.95	0.95	0.68	0.89	1.03	1.71	1.72
Al_2O_3	17.31	17.43	17.24	17.25	17.69	17.32	17.65	16.50	16.56
FeO*	9.71	9.19	9.68	9.69	8.17	9.33	9.58	12.84	12.75
MnO	0.18	0.17	0.18	0.18	0.16	0.18	0.18	0.23	0.23
MgO	8.34	9.36	9.51	9.63	9.86	9.75	8.00	6.54	6.37
CaO	11.64	11.79	11.50	11.37	11.78	11.66	11.90	9.43	9.52
Na_2O	2.71	2.49	2.56	2.52	2.34	2.48	2.65	3.43	3.41
K_2O	0.29	0.27	0.24	0.26	0.22	0.21	0.30	0.61	0.60
P_2O_5	0.14	0.14	0.11	0.11	0.07	0.12	0.17	0.23	0.24
a.t.	99.45	99.08	98.84	97.56	99.43	98.86	98.29	99.32	99.31
Trace elements (ppm)									
Ni	140	180	193	193	205	206	145	57	58
Cr	209	226	261	257	267	269	173	30	33
Sc	40	42	39	39	37	41	39	41	41
V	285	261	262	253	219	252	293	368	374
Ba	179	145	132	153	135	119	321	313	325
Rb	0	2	1	3	1	1	2	4	5
Sr	316	280	283	277	213	270	309	419	427
Zr	51	44	46	46	38	45	50	81	78
Y	23	22	22	20	19	23	23	27	29
Nb	2	1	2	2	2	2	2	6	5
Ga	17	16	16	16	14	15	16	19	20
Cu	119	122	122	110	113	121	136	117	167
Zn	72	64	68	66	57	66	71	107	105
Pb	2	3	2	1	2	2	1	3	2
La	7	5	2	1	4	0	1	5	11
Ce	10	12	9	13	3	15	14	14	19
Th	0	0	0	0	0	0	0	1	0
Nd	8	9	6	8	6	9	10	13	15

Table 1. Continued.

	KCS-04-42	KCS-04-43	KCS-04-19	KCS-04-04	KCS-04-08	KCS-04-17	KCS-04-34	KCS-06-36
Trace elements (ppm) (ICP-MS)								
La		3.6	3.2		2.8	3.2	4.7	7.0	8.9
Ce		8.8	8.0		6.2	7.9	10.6	16.5	16.6
Pr		1.4	1.3		0.9	1.3	1.7	2.5	2.9
Nd		7.4	6.9		5.1	6.9	8.9	12.4	14.3
Sm		2.6	2.5		1.9	2.5	3.1	3.7	4.1
Eu		1.0	1.0		0.8	1.0	1.2	1.6	1.7
Gd		3.2	3.1		2.5	3.2	3.8	4.4	4.9
Tb		0.6	0.6		0.5	0.6	0.7	0.8	0.8
Dy		4.1	4.0		3.4	4.0	4.5	4.9	5.5
Ho		0.9	0.9		0.7	0.9	1.0	1.1	1.2
Er		2.5	2.4		2.2	2.6	2.8	3.0	3.2
Tm		0.4	0.4		0.3	0.4	0.4	0.4	0.5
Yb		2.3	2.3		2.0	2.4	2.4	2.8	3.0
Lu		0.4	0.4		0.3	0.4	0.4	0.4	0.5
Ba		139.3	127.4		129.7	116.8	312.9	303.0	312.2
Th		0.2	0.1		0.2	0.1	0.1	0.4	0.4
Nb		1.3	1.1		0.9	1.1	1.3	5.5	5.2
Y		23.0	22.7		20.1	23.8	25.9	26.3	28.6
Hf		1.3	1.3		1.1	1.3	1.5	2.4	2.3
Ta		0.1	0.1		0.1	0.1	0.1	0.3	0.3
U		0.1	0.0		0.1	0.0	0.1	0.1	0.2
Pb		0.7	0.8		0.9	0.5	1.0	1.8	1.8
Rb		2.3	1.2		2.0	1.3	2.1	4.7	4.6
Cs		0.0	0.0		0.0	0.0	0.0	0.0	0.0
Sr		284.5	283.4		214.4	274.9	313.2	426.6	417.9
Sc		42.2	41.3		39.9	45.5	40.0	43.7	40.7
Zr		39.8	40.1		34.0	40.7	45.2	77.2	72.9

Table 1. Continued.

sample ID	**KCS-06-18**	**KCS-06-38**	**KCS-06-35B**	**KCS-06-35A**	**KCS-06-37**	**KCS-06-09**	**KCS-06-11**	**KCS-06-10**	**KCS-06-13**
location	Juniper Mtn.	Juniper Mtn.	Juniper Mtn.	Juniper Mtn.	Juniper Mtn.	Venator Butte	Venator Butte	Venator Butte	Venator Butte
rock type	basalt	basaalt	rhyolite	rhyolite	rhyolite	basalt	basalt	basalt	basalt
lat. (N)	42.93608333	42.93854	42.93858	42.93858	42.93259	42.91835	42.91146	42.90553	42.90848
long. (W)	119.9126	119.92448	119.92584	119.92584	119.92724	120.1035833	120.0366	120.040116	120.01973
XRF (wt. %)									
SiO_2	48.22	52.29	71.88	72.71	73.15	47.83	50.44	50.21	52.79
TiO_2	0.77	1.40	0.21	0.19	0.17	0.86	1.48	1.45	1.26
Al_2O_3	18.76	16.48	14.99	14.42	14.25	17.84	17.07	16.94	17.35
FeO*	8.84	10.25	2.39	2.19	1.97	9.86	11.01	10.95	8.91
MnO	0.17	0.19	0.09	0.08	0.08	0.18	0.20	0.20	0.17
MgO	8.66	5.38	0.18	0.17	0.16	8.94	5.93	6.41	5.75
CaO	11.62	9.07	1.13	1.05	1.00	11.77	9.31	9.23	8.09
Na_2O	2.60	3.41	4.25	3.90	4.21	2.46	3.40	3.42	3.60
K_2O	0.23	1.21	4.84	5.25	4.97	0.18	0.86	0.89	1.61
P_2O_5	0.13	0.31	0.04	0.04	0.03	0.07	0.29	0.31	0.47
a.t.	98.13	99.31	94.70	95.16	95.89	98.95	98.25	98.88	98.06
Trace elements (ppm)									
Ni	174	44	4	2	1	157	75	73	78
Cr	45	105	2	1	2	115	112	112	103
Sc	37	36	6	6	5	41	35	34	24
V	245	296	2	2	6	273	296	284	209
Ba	129	497	1152	1101	1119	109	504	454	691
Rb	2	15	97	104	110	1	9	9	19
Sr	316	375	111	104	94	228	429	428	493
Zr	37	104	210	202	200	40	92	92	130
Y	22	29	38	37	37	22	25	25	23
Nb	2	7	14	13	14	1	7	6	9
Ga	15	20	17	16	18	15	20	19	16
Cu	64	123	7	8	7	122	114	130	60
Zn	61	93	59	57	54	69	99	98	85
Pb	0	5	18	17	17	2	3	4	6
La	2	13	28	25	25	5	9	12	14
Ce	6	31	56	51	46	3	23	22	40
Th	0	1	10	8	8	0	1	0	1
Nd	6	16	27	25	23	10	15	16	20

Table 1. Continued.

	KCS-06-18	KCS-06-38	KCS-06-35B	KCS-06-35A	KCS-06-37	KCS-06-09	KCS-06-11	KCS-06-10	KCS-06-13
Trace elements (ppm) (ICP-MS)									
La	4.0	13.4	29.6	26.9	26.7	4.2	9.9	10.2	18.2
Ce	7.9	28.2	52.0	50.0	48.9	5.9	21.9	22.5	37.6
Pr	1.4	3.8	6.9	6.4	6.3	1.2	3.1	3.2	4.9
Nd	7.4	16.9	26.6	24.8	24.2	6.3	14.1	14.6	20.3
Sm	2.3	4.4	6.0	5.6	5.5	2.1	4.0	4.0	4.6
Eu	0.9	1.6	1.1	0.9	1.0	0.9	1.6	1.6	1.6
Gd	3.0	4.9	5.5	5.3	5.2	2.8	4.3	4.3	4.3
Tb	0.6	0.8	1.0	1.0	0.9	0.5	0.7	0.7	0.7
Dy	3.7	5.3	6.2	6.1	6.1	3.6	4.7	4.7	4.3
Ho	0.8	1.2	1.3	1.3	1.3	0.8	1.0	1.0	0.9
Er	2.4	3.2	3.9	3.9	3.9	2.2	2.7	2.7	2.4
Tm	0.3	0.5	0.6	0.6	0.6	0.3	0.4	0.4	0.3
Yb	2.2	2.9	4.1	4.1	4.0	2.1	2.5	2.5	2.2
Lu	0.4	0.5	0.7	0.7	0.7	0.3	0.4	0.4	0.3
Ba	129.2	492.4	1170.8	1114.5	1132.9	112.2	490.3	441.7	684.5
Th	0.2	1.1	6.3	6.5	6.8	0.2	0.6	0.6	1.2
Nb	1.6	6.5	14.2	13.9	13.9	0.9	6.4	6.3	8.9
Y	21.3	29.1	37.4	36.4	35.8	21.1	24.3	24.5	21.9
Hf	1.1	2.8	5.9	5.6	5.8	1.1	2.5	2.5	3.2
Ta	0.1	0.4	1.4	1.4	1.5	0.1	0.4	0.4	0.5
U	0.1	0.4	2.6	2.8	3.0	0.1	0.2	0.2	0.4
Pb	0.7	4.4	15.9	15.9	17.0	0.7	2.8	2.9	5.5
Rb	1.5	15.4	94.1	101.5	102.8	1.6	8.8	8.6	18.8
Cs	0.0	0.3	2.6	3.2	3.0	0.0	0.1	0.1	0.2
Sr	311.8	375.4	110.4	104.7	91.7	234.1	426.9	422.5	488.7
Sc	39.5	40.3	7.2	6.9	6.1	44.5	37.2	36.4	26.7
Zr	34.6	99.6	197.1	184.5	189.1	38.3	87.1	86.1	122.7

Table 1. Continued.

sample ID	**KCS-06-07**	**KCS-06-08**	**KCS-06-06**	**KCS-06-15**	**KCS-06-16**
location	Alkali Buttes	Alkali Buttes	Alkali Buttes	Flint Ridge	Flint Ridge
rock type	basalt	basalt	rhyolite	dacite	obsidian
lat. (N)	43.01433	43.01981	43.02018	43.01981	43.01981
long. (W)	120.02966	120.01991	120.05618	120.01991	120.01991
XRF (wt. %)					
SiO_2	53.36	53.40	71.83	67.39	67.24
TiO_2	1.09	1.08	0.28	0.47	0.51
Al_2O_3	17.34	17.30	14.12	16.40	16.49
FeO*	8.71	8.62	2.54	3.35	3.47
MnO	0.17	0.17	0.10	0.09	0.09
MgO	5.45	5.69	0.55	0.73	0.74
CaO	8.71	8.58	2.25	2.56	2.56
Na_2O	3.49	3.44	4.05	4.60	4.63
K_2O	1.35	1.42	4.20	4.21	4.06
P_2O_5	0.33	0.31	0.09	0.19	0.19
a.t.	98.99	99.49	98.32	96.55	96.78
Trace elements (ppm)					
Ni	67	69	6	2	1
Cr	116	118	9	1	2
Sc	29	29	6	7	8
V	229	223	24	12	18
Ba	611	615	713	1979	1828
Rb	15	19	77	78	78
Sr	434	429	146	293	303
Zr	119	119	96	235	224
Y	23	22	20	28	26
Nb	7	6	9	10	11
Ga	17	18	14	18	18
Cu	81	93	23	12	11
Zn	84	82	47	65	63
Pb	5	5	14	12	12
La	12	13	13	29	26
Ce	31	30	24	56	54
Th	1	1	5	5	5
Nd	16	17	10	24	25

Table 1. Continued.

	KCS-06-07	KCS-06-08	KCS-06-06	KCS-06-15	
Trace elements (ppm) (ICP-MS)					
La	15.2	14.9	14.2	30.5	30.2
Ce	30.8	30.5	27.8	57.1	56.9
Pr	4.0	3.9	3.1	6.8	6.7
Nd	16.7	16.4	11.8	25.7	25.8
Sm	4.0	3.9	2.9	5.3	5.4
Eu	1.4	1.4	0.7	1.6	1.6
Gd	4.0	3.9	2.8	4.8	4.8
Tb	0.7	0.7	0.5	0.8	0.8
Dy	4.3	4.3	3.4	4.8	4.8
Ho	0.9	0.9	0.7	1.0	1.0
Er	2.4	2.4	2.2	2.9	2.8
Tm	0.3	0.4	0.3	0.4	0.4
Yb	2.3	2.3	2.3	2.8	2.8
Lu	0.4	0.4	0.4	0.5	0.5
Ba	602.0	606.1	720.0	2012.7	1880.2
Th	1.2	1.3	4.0	4.8	4.8
Nb	7.4	7.4	10.3	11.4	11.3
Y	22.8	22.6	20.0	26.7	26.4
Hf	3.0	3.0	3.4	5.8	5.7
Ta	0.4	0.4	0.9	0.9	0.9
U	0.5	0.5	1.5	1.8	1.8
Pb	4.9	4.9	13.8	12.4	12.2
Rb	15.9	17.5	73.8	75.0	75.1
Cs	0.2	0.3	1.0	1.6	1.6
Sr	431.4	426.8	143.5	287.5	300.3
Sc	31.9	31.2	7.6	7.4	8.5
Zr	113.2	113.7	93.4	228.4	221.2

***Coleman Hills Rhyolite: 21*.79 ± 0.66 Ma**

Rhyolite (70.7-72.0 SiO_2 wt. %) crops out over a ~30 km^2 area (Figure 2) and occurs as large domes, and localized flows and volcaniclastic and pyroclastic deposits (Figure 3). Rhyolite intrusions typically form domes that are ~4-12 km^2 and have 8-10% crystals. Exposures of silicic volcaniclastic and pyroclastic deposits (4A,B, and C) are locally ~15-50 m thick and either underlie or are intruded by dacite lavas or dikes. The thinner accumulations consist of ~3-5 m of unsorted rhyolite blocks supported in an ash matrix. These are overlain by ~10 m of clast supported mafic scoria and thin layers of interstratified volcanic ash (Figure 4A). Thicker exposures consist of poorly sorted pyroclastic material of homogeneous composition that ranges from ash to ~10 cm diameter in size. The top of the pyroclastic unit is exposed in a road-cut where it transitions to more mafic compositions (Figure 4B) and contains volcaniclastic tuffaceous material. These beds are laminar, strike ~N75°E and dip ~25° to the southeast, and are characterized by 0.5-1.0 cm subrounded to angular fragments within a sand-ash matrix.

Potassium feldspar, hornblende, quartz and plagioclase are the dominant phenocrysts observed in hand-samples and thin-sections (Figure 3). Sanidine that exhibits rapikivi texture, and 1-2 mm hornblende crystals are the most common phenocrysts and diagnostic minerals for the rhyolite intrusions. In thin section hornblende commonly displays clinopyroxene reaction rims that are ~100-200 μm. Hornblende crystals from rhyolite flows exhibit strong alignments in thin-sections. Intergrowths of euhedral to subhedral sanidine, plagioclase and quartz crystals are common. Chemical data (Table 1) demonstrate that rhyolites of the Coleman Hills are dominantly metaluminous, although one sample (KCS-04-10; Table 1) is mildly

peraluminous, with aluminum saturation index values that range from 0.953 to 1.002. TiO_2, FeO, CaO, and MgO wt. % decrease and K_2O and Na_2O wt. % and Nb, Y, and La concentrations (ppm) increase with increasing SiO_2 wt. % (Figure 7). Rhyolites are distinct from the intermediate compositions of the suite in departing from the trend to low K, Ba, Na and Zr (Figures 6 and 7) indicating fractionation of alkali feldspar and zircon.

Coleman Hills Dacite: 21.70 ± 0.56 Ma

Dacite dikes, lavas, and scoria from Euchre Butte (63.3-64.2 SiO_2 wt. %), located ~10 km due west from the principal vent of the Coleman Hills volcanic complex (Figures 2 and 4C), intrude and overlie rhyolite deposits of the Coleman Hills volcanic complex (Figures 3 and 4). Dacite is exposed over a ~25 km^2 area. Agglutinate at the summit of Euchre Butte contains plagioclase-rich, flattened, dense glassy pyroclasts within a pink scoracious matrix. The glass was separated from the matrix and analyzed (Table 1; KCS-04-15). Dacite lava flows are platy and have a maximum thickness of ~60 m near the vent and thin to ~10 m where the flows extend ~5 km southwest of the vent (Figures 2 and 4A). Plagioclase laths as long as 2-3 mm and equant ~0.5 mm pyroxene phenocrysts occur together with sparse plagioclase-olivine glomerocrysts within an aphanitic, devitrified groundmass. The larger plagioclase laths commonly exhibit sieve textures. Groundmass plagioclase and olivine microlites are euhedral to subhedral crystal forms. Trace-element patterns in dacite of the Coleman Hills (Figure 8) are transitional to rhyolite in that they exhibit decreased P and increased Hf and Zr relative to basaltic andesite to dacite.

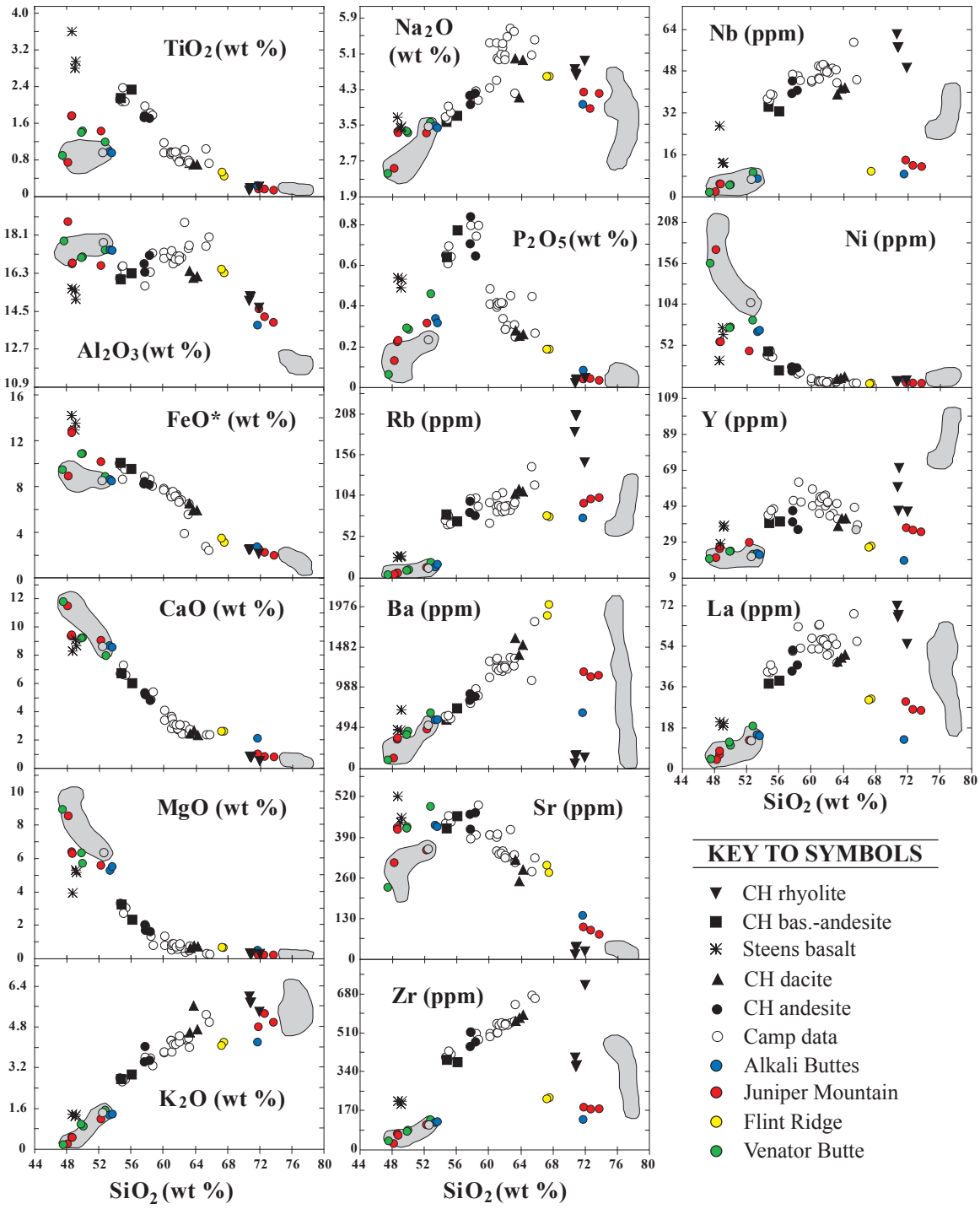

Figure 7. Elemental variation diagrams, plotted as normalized to 100% volatile free, for samples from the Coleman Hills (CH) and northern Lake Abert. Data from Table 1 and additional analyses of the Coleman Hills from Camp (unpublished data). Shaded fields highlight the compositional range for basalt and rhyolite (Ratlesnake Tuff) assemblage from Lake Abert. 8.6 Ma basaltic andesite marked with gray circle. Rhyolite field shows analyses of high silica rhyolite pumices and glass shards of the 7.05 Ma Rattlesnake Tuff; data from Streck and Grunder (1997).

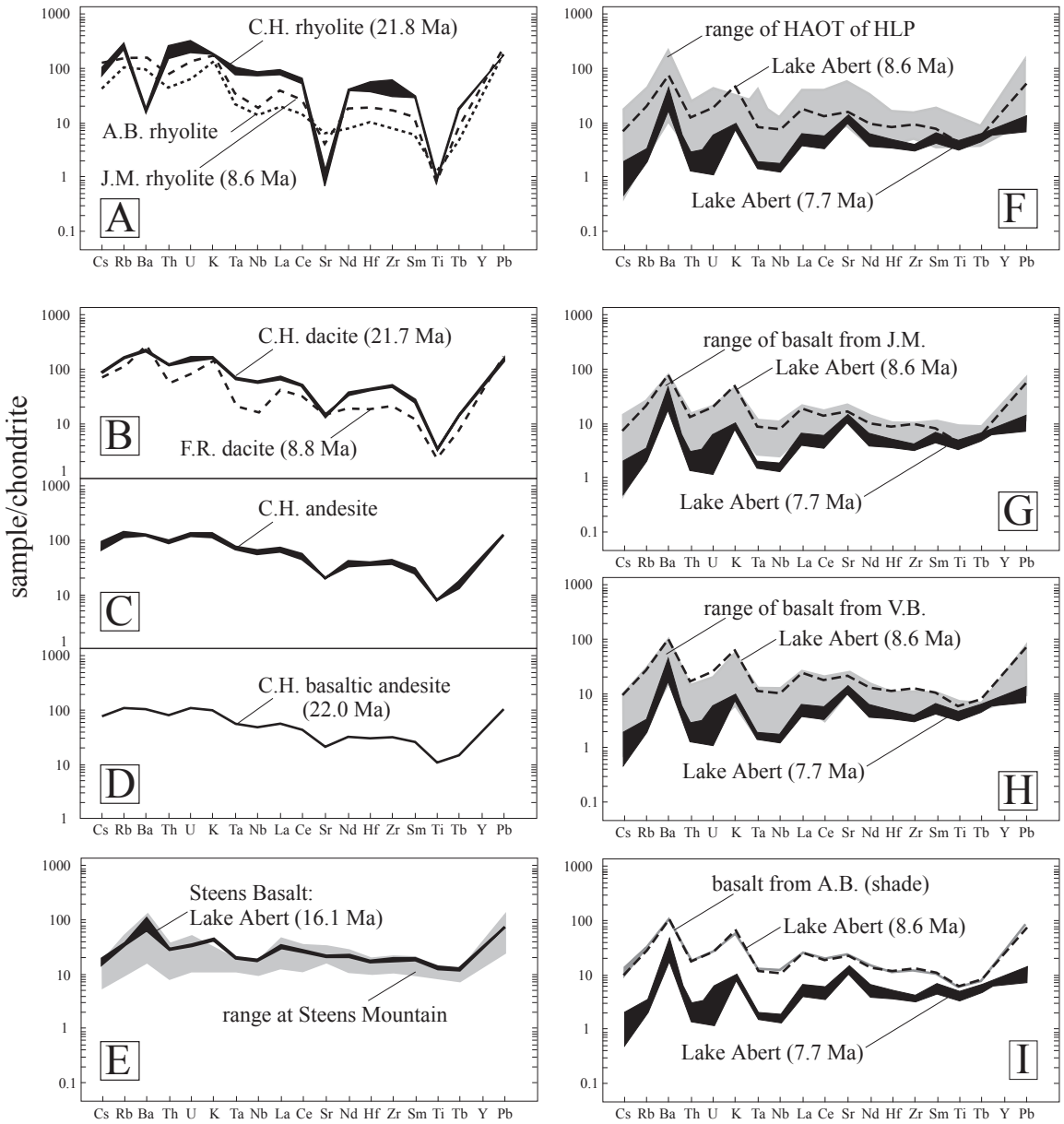

Figure 8. Chondrite-normalized spider diagrams (A-I) for igneous rocks exposed near Lake Abert. Normalization values from McDonough et al. (1992). Ages shown are from chapter 3. (E) Steens basalt with compositional range of section exposed at Steens Mountain from Johnson et al. (1998) shown with shaded field; (F-H) compositional range of High Lava Plains (HLP) basalts from Jordan (2001) shown as light shade; range of Lake Abert basalt shown as dark shade; 8.6 Ma olivine tholeite from Lake Abert shown as stippled line.

Basaltic andesite to andesite: 22.00 ± 0.54 Ma

Basaltic andesite (54.8-56.0 SiO_2 wt. %) to andesite (57.7-58.3 SiO_2 wt. %) dikes and lavas are exposed over a ~80 km^2 area and are the dominant composition of the Coleman Hills (Figures 2 and 4B, D, E and F). Dikes cut, and lavas overlie, silicic volcaniclastic deposits (Figure 4A) defining a ~20 km^2 vent within the center of the complex (Figure 2). The vent is characterized by thick accumulations of scoria (Figure 4E) and a N-S dike that is >5 m wide in places and can be traced for ~10 km (Figure 4F). A N-striking splay of the Abert Rim Fault (Figure 2) produces a ~150 m escarpment in the center of the complex and a number of small faults associated with this structure trend N5-10°W and dip 40-55° SW.

Some of the basaltic andesites and andesites are particularly crystal-rich (25-30%) and contain plagioclase, pyroxene, olivine, and amphibole phenocrysts set in a glassy to devitrified aphanitic matrix. In thin section plagioclase laths are generally longer than 3 mm with the largest commonly exhibiting skeletal form and sieve textures. Olivine and plagioclase laths smaller than 3 mm have mostly euhedral forms and amphibole exhibits thin clinopyroxene reaction rims. Basaltic andesite and andesite of the Coleman Hills have similar spider and REE patterns (Figures 8 and 9).

Middle to Late Miocene Volcanic Rocks

An unconformity reflecting ~6 m.y. separates volcanism of the Coleman Hills from Middle Miocene Steens Basalt volcanism. Steens Basalts erupted from a source near Steens Mountain (e.g., Johnson et al., 1998), ~100 km to the east (Figure 1), between 16.7-15.3 Ma and deposited a thick lava section contemporaneous with the

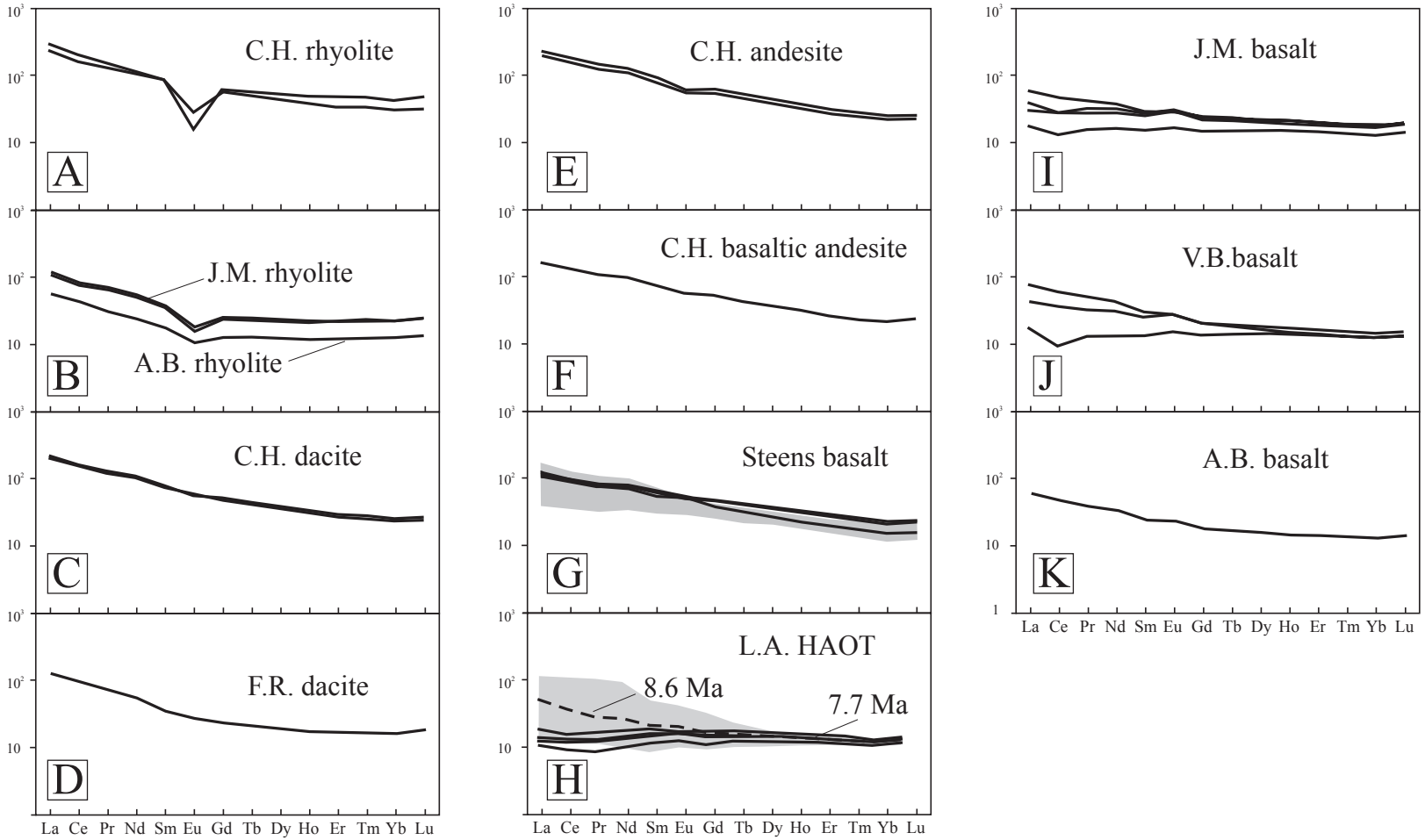

Figure 9. Rare-earth element (REE) diagrams (A-K) for igneous rocks exposed near Lake Abert. (C.H.)=Coleman Hills; (J.M.)=Juniper Mountain; (A.B.)=Alkali Buttes; (F.R.)=Flint Ridge; (L.A.)=Lake Abert; (HAOT)=high aluminum olivine tholeiite; (V.B.)= Venator Butte. (G) Steens basalt with compositional range of section exposed at Steens Mountain from Johnson et al. (1998) shown with shaded field; (H) compositional range of High Lava Plains (HLP) basalts from Jordan (2001) shown as light shade.

earliest stages of Columbia River flood basalt volcanism across most of southeastern Oregon (Hooper et al., 2002; Duncan and Johnson pers. com. 2007). Basalt and rhyolite volcanic activity picked up again near Lake Abert during the Late Miocene between ~ 8.6 and 7.7 Ma and correlates, in terms of age and composition, with regional volcanism of the High Lava Plains (e.g., Jordan et al., 2004). Near Abert Rim these units consist dominantly of mafic and silicic lava flows and eruptive centers (Figures 3 and 5) and dacite of Flint Ridge (Figure 5D) exhibits the only intermediate composition within this suite (Figure 6). The Rattlesnake Tuff, erupted at ~7 Ma and sourced ~130 km to the northwest within the Harney Basin (Streck and Grunder, 1995), caps the volcanic section (Figure 3).

Steens Basalt: 16.12 ± 0.30 Ma

At Abert Rim (Figure 1) the greatest thickness of Steens Basalt is a ~500 m section that occurs ~15 km south of the study area, where it has been correlated with the earliest flows at Steens Mountain on the basis of similarities in magnetic polarity and isotopic composition (Mankinen et al., 1987; Carlson and Hart, 1987). Exposure of the section declines northward to a thickness of ~150 m within the study area, consistent with along-strike decline of stratigraphic separation on the Abert Rim fault (see Chapter 1; Figure 1). Baked sedimentary horizons within individual flows of the Steens basalts attest to periods of prolonged volcanic quiescence separation individual eruptions.

Like elsewhere, the Middle Miocene Steens Basalt within the study area contain flows that are 1-10 m thick (avg. 5 m) with ~5 cm plagioclase laths (Johnson et al., 1998). Steens Basalt is enriched in TiO_2, FeO, Na_2O, and P_2O_5 (wt. %) and Sr, Zr, Nb

and La and depleted in Al_2O_3, CaO and MgO (wt. %) and Ni relative to Late Miocene basalts (Figure 7). Relative to primordial mantle compositions the Steens basalt exhibits a higher degree of enrichment for most incompatible trace elements, most notably Th and U, and REE compared to the younger mafic lavas (Figures 7 and 8). Steens Basalt at Abert Rim is elevated in incompatible elements relative to other Steens Basalts. Such incompatible element enrichments are characteristic of the top of the Steens basalt section (Johnson et al., 1988) (Figures 8 and 9) at Steens Mountain (Figure 1), suggesting that the lavas near Abert Rim are from high in the section, consistent with their age.

Mafic Tholeiitic Lavas of the Bimodal Suite: ~8.7 to 7.7 Ma

MORB-like, olivine thoeliites equivalent to HAOT of Hart (1984) and basaltic andesites found within the High Lava Plains (e.g., Jordan et al., 2004) occur at Alkali Buttes, Juniper Mountain and Venator Butte (Figures 1 and 5) and throughout the map area (Figure 2). ^{40}Ar-^{39}Ar ages indicate that an earlier episode of mafic volcanism began at ~8.7 Ma and was followed by a more voluminous episode of basaltic volcanism at ~7.7 Ma.

Tholeiitic Basaltic Andesite: 8.69 ± 0.42 Ma

Two to three tholeiitic basaltic andesite (SiO_2 of 52.6 wt.%) (KCS-05-21; Table 1) outcrop over an area of ~10 km^2 < 1 km northwest of the Sawed Horn (Figure 2). The unit is relatively coarse grained, porphyrytic, diktytaxitic and contains 1-2 mm zoned plagioclase laths that exhibit sieve textures. Plagioclase and olivine glomerocrysts are common. This basalt is not unlike older HAOT lavas associated with High Lava Plain

volcanism, which exhibit higher K_2O, Na_2O, and P_2O_5 (wt. %) and Ba, Sr, Zr, and La (ppm) and lower CaO and MgO (wt. %) and Cr and Ni (ppm) than younger HAOT lavas (e.g., Jordan, 2001) (Figures 6, 7 and 8). This point is further illustrated by enrichments in chondrite-normalized incompatible elements within the basaltic andesite, notably U, Th, K, Nb, Ta, La, Ce, Hf, Zr, (Figure 8) and light REE's relative to other HAOT near Lake Abert. (Figure 9).

HAOT: 7.71 ± 0.42 Ma

HAOT (SiO_2 of 48.0 to 49.0 wt. %) is the typical mafic member of the bimodal basalt-rhyolite suite that is characteristic of High Lava Plains volcanism since ~10 Ma (Jordan et al., 2004). HAOT outcrops over a >100 km^2 area (Figure 2) and identical ages were obtained from samples located on either side of the Coleman Hills (Table 1; KCS-04-17; KCS-04-43). A flow sampled from the Sawed Horn (Figure 3; KCS-04-08) exhibits the highest SiO_2 at 49.0 wt. %. The best exposures of this unit occur near Foley Creek in the eastern part of the map area (Figure 2) where the unit consists of four flows and is a total thickness of ~60 m; from bottom to top, these are samples KCS-04-40 through KCS-04-43 in Table 1. There is very little chemical variability within this lava succession and sedimentary units separating flows are absent. Subophitic texture is common in these fine-grained basalts and they are generally diktytaxitic, microcrystalline and contain 50-70% plagioclase and olivine phenocrysts that occasionally occur together as glomerocrysts. The younger HAOT at Lake Abert lie at the low end of incompatible element and REE enrichment compared with similar compositions of the HLP (Figures 8 and 9). Mafic tholeiitic lavas sampled from Juniper Mountain, Alkali Butte and Venator

Butte (Figure 5) exhibit chemical similarities (Figures 6, 7, 8, and 9) to both the ~8.6 Ma tholeiitic basaltic andesite and the ~7.7 Ma HAOT sampled near the Coleman Hills (Figure 3). Two samples (KCS-04-19; KCS-04-04) collected from a lava flow located directly at the base of the Abert Rim fault ~5 km south of the map area (Figure 1) were dated by Hart and Mertzman (1982) who report a K-Ar age of 6.1 ± 0.7 Ma. In contrast to the interpretation of Hart and Mertzman (1982), who suggest that the flow banked against the escarpment, we believe that these lavas sample the top of the HAOT section within a large landslide block, thus explaining their position at the base of the escarpment.

Silicic Units of the Bimodal Suite (~8.8 to 7.0 Ma)

Biotite-rich silicic dome complexes, ranging in size from ~7 to 20 km^2, crop out north of the map area (Figures 1 and 5). These are Alkali Buttes (~0.7 km^3), Juniper Mountain (~1.5 km^3) and Flint Ridge (~0.5 km^3). Although silicic, Flint Ridge is a dacite lava flow rather than a high-silica rhyolite dome, typical of the bimodal High Lava Plains suite (Streck and Grunder, 2006). The ages of rhyolite from Juniper Mountain and Flint Ridge are 8.58 ± 0.16 Ma and 8.79 ± 0.30 Ma, respectively. These ages are in general agreement with those predicted by regional isochrons that show a westward decrease in the onset of volcanism among Late Tertiary rhyolites (Figure 1).

Late Miocene silicic compositions of the bimodal suite are depleted in the most incompatible trace elements relative to the Early Miocene Coleman Hills suite except for Ba, K, and Sr (Figures 8 and 9). Silicic compositions at Juniper Mountain, Flint Ridge and Alkali Buttes (Figure 5) all have similar trace element and REE patterns, yet rhyolite

of Juniper Mountain shows the strongest incompatible element enrichment (Figures 8 and 9).

Rattlesnake Tuff

Exposure of the 7.05 Ma Rattlesnake Tuff near Lake Abert defines the southwestern most known extent of the tuff outcrop. The tuff is an important regional stratigraphic and structural marker that is known for a remarkably uniform thickness of ~15-30 m exposed over a ~9000 km^2 area of eastern Oregon (Streck and Grunder, 1995). At Abert Rim the Rattlesnake Tuff is mainly densely welded and has a maximum thickness of ~15 m.

Eruptive sources of Late Miocene Bimodal Volcanic Units

Basalts from Juniper Mountain and Venator Butte are chemically correlated with basalt types at Lake Abert (Figuree 8G and 8H) whereas basalts at Alkali Butte correlate only with the ~8.6 Ma unit at Lake Abert (Figure 8I). We interpret Venator Buttes to be the primary source of both ~8.6 Ma and ~7.7 Ma basalts due to its central location (Figure 1) and vent morphology (Figure 5C). Rhyolite of Alkali Buttes and dacite of Flint Ridge exhibit similar trace element enrichments to Rhyolite of Juniper Mountain (Figure 8A and B). Juniper Mountain (Figures 1 and 5B) is the likely source of silicic volcanism at Alkali Buttes (Figures 1 and 5A) and Flint Ridge (Figures 1 and 5D) beginning ~ 8.8 Ma. Thus, Late Miocene volcanic activity centered at Abert Rim between ~8.8 and 7.7 Ma began with an episode of silicic volcanism followed by widespread basaltic volcanism.

COMPOSITIONAL VARIATION

In addition to the vast age difference, the Early Miocene Coleman Hills suite and the Late Miocene bimodal suite differ in two main ways. First, the Early Miocene suite is dominantly intermediate in composition with only a small gap of ~5 to 7 % SiO_2 (Figure 6) separating dacites and rhyolites. In contrast, the Late Miocene suite is dominated by a gap in SiO_2 spanning from ~53 to 68 wt. % SiO_2. Second, the Early Miocene suite is more alkalic than the Late Miocene suite. Among basaltic andesites, those of the Coleman Hills have higher K_2O concentrations and among silicic compositions the suite has higher K_2O + Na_2O. Zr concentrations are also higher within the Early Miocene suite at comparable wt. % SiO_2, reflecting the greater solubility of zircon (Figure 7). Late Miocene rhyolites cluster at lower values for most elements except Ba (Figures 7) with respect to Early Miocene rhyolites.

The Coleman Hills Suite

The general variation trend of K_2O + Na_2O vs. SiO_2 wt. % projects to Steens Basalts rather than the field of Late Miocene bimodal volcanics (Figure 6). Ti, Ca, Fe, Sr and Sc decrease and K and Rb increase systematically within the suite (Figures 7 and 8). Mg and Ni have convex-downward patterns of decrease with SiO_2 wt. % (Figure 7) suggesting a role for fractionation of olivine and pyroxene. P_2O_5 has a strong peak in trend at ~56 wt. % SiO_2 reflecting apatite saturation and fractionation. Al broadly increases among basaltic andesites to andesite and decreasing at higher wt. % SiO_2 (Figure 7). Zr and Ba drops sharply among rhyolites, suggesting a role for fractionation

of zircon and alkali feldspar, respectively. Nb, La, and Y have fan shaped distributions and are more scattered and in higher concentration among the rhyolites (Figure 7).

The Late Miocene bimodal suite

The Late Miocene basalts form trends and clusters in composition that generally coincide with the range of HLP basalts (Figures 6, 7, 8 and 9). Within the suite, there are two compositional groupings that conform to age differences. The older ~8.6 Ma basalts, found at Lake Abert, Venator Butte, Juniper Mountain and Alkali Butte, are characterized by higher Na, Fe, Ti, P, and Sr (Figure 7) relative to the ~7.7 Ma basalts found at Lake Abert, Juniper Mountain, and Venator Butte.

Late Miocene silicic compositions cluster at lower values for most elements, except Ba, relative to the Early Miocene Coleman Hills suite. Dacite of Flint Ridge defines a trend with Late Miocene rhyolite and is separated by a similar SiO_2 gap as for Early Miocene Coleman Hills dacite to rhyolite.

Isotopic composition

The isotopic composition of rocks from the Coleman Hills volcanic center and onlapping volcanic units span a narrow range in $^{87}Sr/^{86}Sr$ and $^{143}Nd/^{144}Nd$, 0.70352-0.70515 and 0.51284-0.51292, respectively (Table 2). The range of isotope data falls within the range published for Early Tertiary calc-alkaline volcanic rocks of the Clarno Formation and of basalts of the northwestern Great Basin (Figure 10). Only the Coleman Hills rhyolite differs in that it has elevated $^{87}Sr/^{86}Sr$ (at 26 ppm Sr). Miocene volcanic rocks of central and southern Oregon, east of the Cascade arc (Figure 1) follow an

Table 2. Isotopic composition of rocks from northern Lake Abert

Sample	KCS-04-10	KCS-04-02	KCS-04-21	KCS-05-20	KCS-06-16	KCS-05-21	KCS-06-37	KCS-04-17
Age	(1) 21.79	(1) 21.7	(1) 22.01	(1) 16.12	8.79	(1) 8.69	8.58	(1) 7.71
location	Coleman Hills	Coleman Hills	Coleman Hills	Lake Abert	Flint Ridge	Lake Abert	Juniper Mtn.	Lake Abert
rock type	rhyolite	dacite	bas-and	basalt	dacite	bas-and	rhyolite	basalt
SiO_2(wt. %)	70.8	63.3	56.0	49.1	67.24	52.6	73.15	48.1
$^{87/86}Sr_m$	0.71099	0.70388	0.70366	0.70374	0.704247	0.70374	0.70401	0.70371
$^{87/86}Sr_i$	0.70515	0.70359	0.70352	0.70371	0.704157	0.70373	0.70361	0.70371
$^{143}Nd/^{144}Nd_m$	0.51288	0.51286	0.51289	0.51293	0.51287	0.51289	0.51288	0.51290
$^{143}Nd/^{144}Nd_i$	0.51286	0.51284	0.51287	0.51292	0.51286	0.51288	0.51288	0.51289
εNd_i	4.98	4.54	5.17	5.89	4.63	5.03	4.91	5.16
$^{176}Hf/^{177}Hf_m$	0.28293	0.28296	0.28294	0.28309	0.28302	0.28310	0.28304	0.28308
$^{176}Hf/^{177}Hf_i$	0.28292	0.28295	0.28294	0.28309	0.28302	0.28309	0.28303	0.28307
$^{206}Pb/^{204}Pb_m$	19.1492	19.1284	19.1496	18.8751	18.8134	18.7923	18.8252	18.8506
$^{206}Pb/^{204}Pb_i$	19.0325	19.0666	19.0790	18.8534	18.8010	18.7828	18.8105	18.8430
$^{207}Pb/^{204}Pb_m$	15.6177	15.6119	15.6065	15.5896	15.5977	15.5981	15.6026	15.5945
$^{207}Pb/^{204}Pb_i$	15.6123	15.6090	15.6032	15.5886	15.5971	15.5977	15.6019	15.5941
$^{208}Pb/^{204}Pb_m$	38.7463	38.6864	38.6714	38.4873	38.4497	38.4486	38.4721	38.4697
$^{208}Pb/^{204}Pb_i$	38.5504	38.5612	38.4650	38.4014	38.4283	38.3945	38.4538	38.1503

1. Age information from Chapter 3

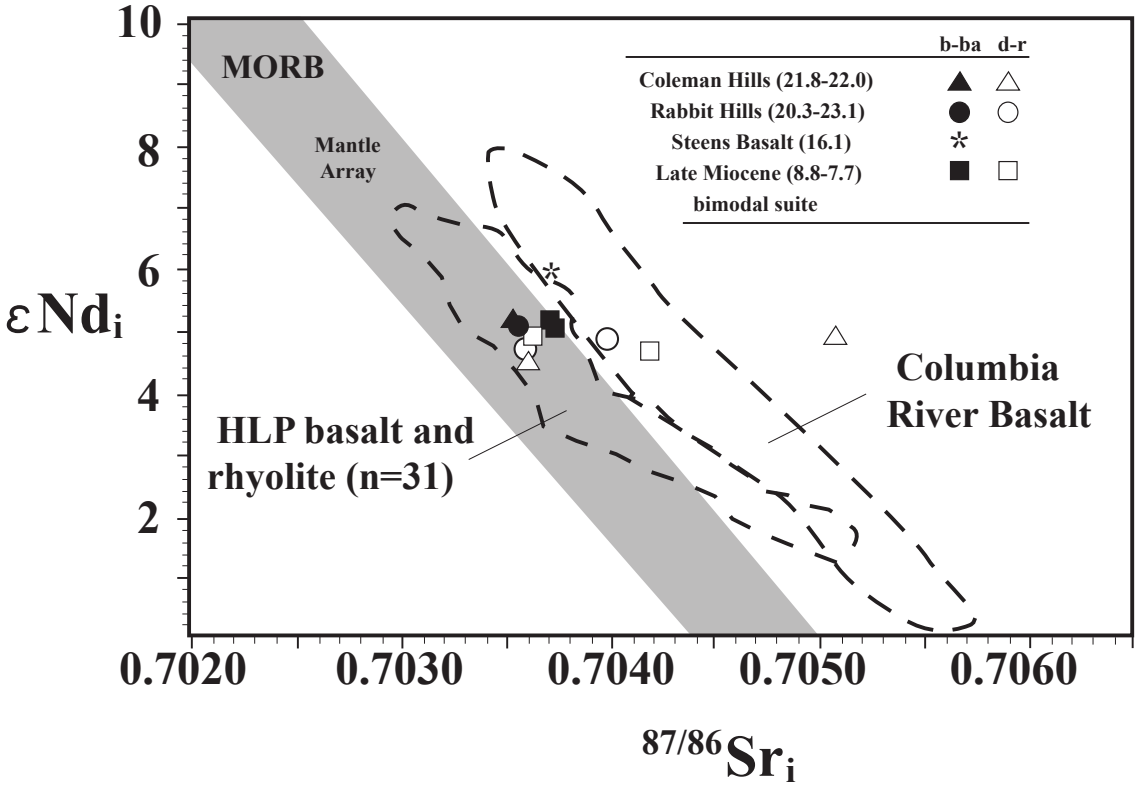

Figure 10. $^{87}Sr/^{86}Sr$ - εNd covariation diagram for bimodal volcanic rocks from the northwestern Basin and Range Province. Analyses are plotted according to composition: b-ba: basalt to basaltic andesite and d-r: dacite to rhyolite. Ages shown in parentheses in Ma. Late Cenozoic volcanics of the High Lava Plains (HLP) are from Hart (1995) and Streck and Grunder, 2006. Field of Columbia River Basalt is from Carlson et al. (1981)

evolutionary path typical of the mantle array except for a few silicic rocks that have incorporated a crustal signature (Figure 10). In terms of Pb isotopes, volcanic rocks of the northwestern Great Basin record a lower crustal and (or) enriched mantle source (Figure 11). Pb isotopes of the Coleman Hills are similar to Late Cenozoic volcanic units in eastern Oregon with respect to $^{208}Pb/^{204}Pb$ and $^{207}Pb/^{204}Pb$ ratios yet higher ratios of $^{206}Pb/^{204}Pb$ set them apart (Figure 11). An opposite pattern is displayed in Hf isotopes, as the Coleman Hills suite has substantially lower $^{176}Hf/^{177}Hf$ ratios than Late Cenozoic volcanic rocks.

DISCUSSION

Petrologic Modeling

Major, trace and isotopic data are used to test simple petrologic models of the genetic relationship between the magma compositions erupted at the Coleman Hills. Curvature in the major element data (Figure 7) and systematic changes in observed mineralogy (Figure 3) suggest that fractional crystallization was an important process in formation of at least part of the suite. However, a gap in the data between ~66 to 70% SiO_2 (Figure 7), isotopic variability (Table 1) and disequilibrium textures present in thin-section indicate that crustal anatexis, magma mixing and (or) crustal assimilation may also be an important process in the evolutionary history of the Coleman Hills.

The modeling approach is as follows: (a) Mass balance modeling of major elements using the equations of Stormer and Nichols (1978) to test whether rhyolite of the Coleman Hills can be produced from basaltic andesite via crystal fractionation and to test models of magma mixing. Mineral compositions used in mass balance modeling

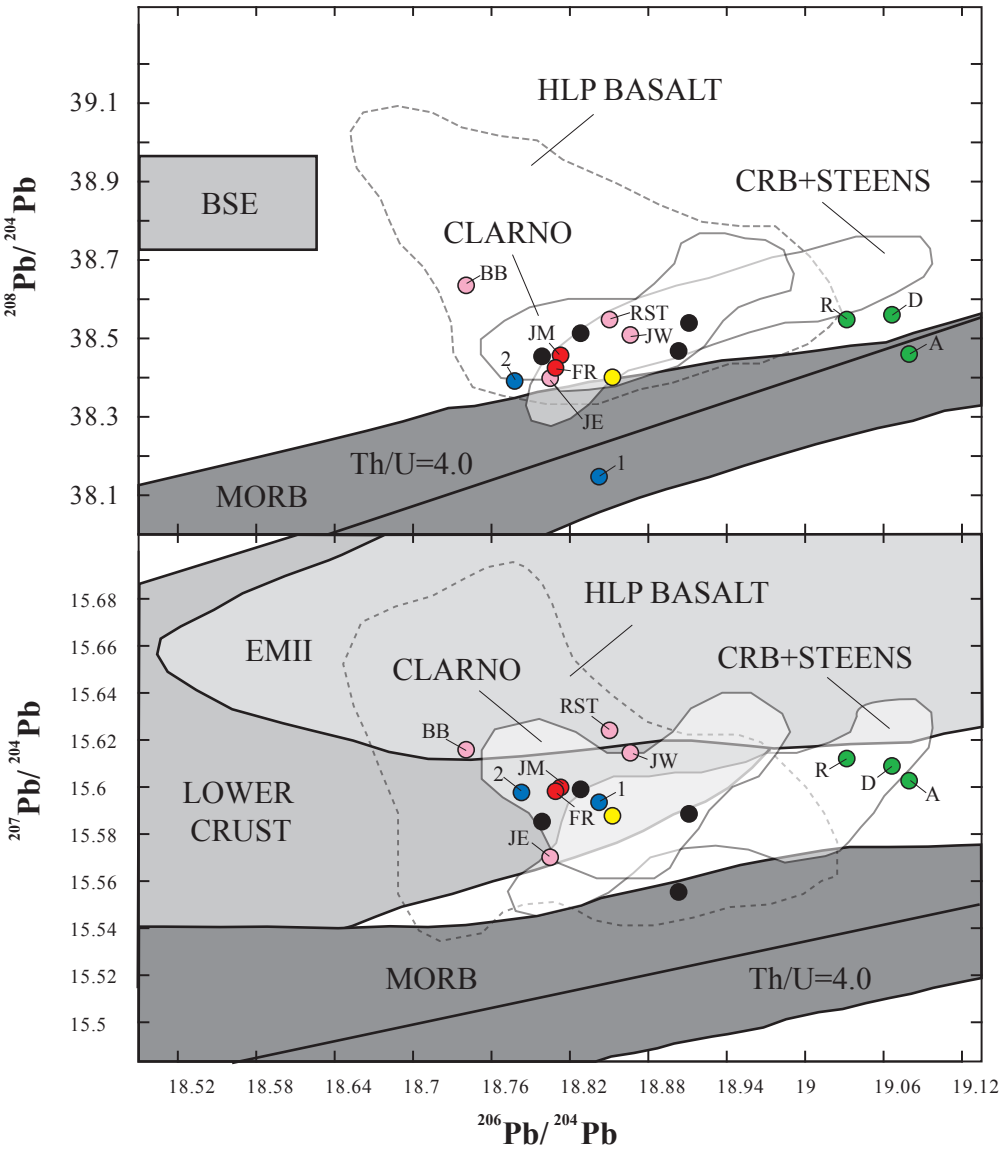

Figure 11. Pb isotope correlation diagrams show Lake Abert samples relative to mantle reservoirs and other Tertiary rocks of the northwestern Great Basin. Silica content (wt. %) listed for Lake Abert samples: basalts younger than ~16 Ma (open circles); rocks of the ~22 Ma Coleman Hills (filled circles); (1) Flint Ridge and (2) Juniper Mountain (shaded circles). Other sources of data: HLP basalt (Hart, 1985; Jordan, 2002); FB-Flood basalts of the Columbia River and Steens groups (Carlson et al., 1981; Carlson and Hart, 1987); Clarno (Urbancyzk, 1994). Bulk silicate earth (BSE) field from Allegre et al. (1988). Mantle reservoirs from Zindler and Hart (1986) with straight line representing a constant Th/U ratio of 4.0. Coleman Hills suite: R=rhyolite, D=dacite, A=andesite; basalt of Lake Abert Suite: 1=7.7 Ma HAOT, 2=8.6 Ma olivine tholeiite basalt; Late Cenozoic silicic volcanic suite: BB= 7.7 Ma Burns Butte, RST=7.1 Ma Rattlesnake Tuff, JE= 6.9 Ma Juniper Ridge east, JW=5.7 Ma Juniper Ridge west (data from Streck and Grunder, 2006); Late Cenozoic mafic volcanic suite are samples of HLP basalts (Jordan, 2001; Streck and Grunder, 2006).

(Table 3) are obtained from analyses of plagioclase crystals from Coleman Hills basaltic andsite and dacite and from existing analyses of minerals from rocks of similar age in the area (Mathis, 1993; MacLean, 1994) with an orthopyroxene from an andesite (Klemetti, 2005); (b) Testing of major element models with trace element assimilation-fractional crystilization (AFC) and mixing formulations using partition coefficients tabulated in Rollinson (1993); and (c) Further tests using isotopic data (Table 2).

Crystal fractionation

Crystal fractionation of ~37 % readily accounts for the generation of andesite and dacite compositions from basaltic andesite with acceptable r^2=0.2-0.6 (Table 3). The fractionating mode is dominated by plagioclase (42-69%) and clinopyroxene (18-46%). The major element models are not sensitive to changes in plagioclase compositions (Table 3) and the fractionating mode predicted by the models matches that observed in the rocks with the exception of amphibole. Amphibole occurs as a phenocryst phase in both andesite and dacite of the Coleman Hills but when added as a fractionating phase to the models it is precipitated rather than removed from the melt. Trace element variability from basaltic andesite to dacite can also be produced with ~20-40% fractionation (Figure 12). Enrichment of highly incompatible elements, such as La and Nb, from basaltic andesite to andesite is outside of the possible range predicted by fractionation alone and suggests that the system was affected by magma recharge during the early stages of mafic magmatism at the Coleman Hills. Sr isotopes indicate that some crustal involvement is necessary to produce dacite form basaltic andesite (Figure 12C) Isotopic compositional contrasts between rhyolite and basaltic andesite are even greater than between rhyolite

Table 3. Mineral compositions used and summary of major element fractionation models

mineral	[1] plag	[1] plag	[2] plag	[3] olivine	[2] olivine	[3] cpx	[4] opx	[2] amphibole	[2] magnetite	[2] illmenite	[5] apatite	[6] cont. crust
[A]identifyer	P1	P2	P3	Ol-1	Ol-2	CPX	OPX	A	M	I	A	C
sample	KCS-04-27	KCS-04-02	JR-92-59	AM-89-70	JR-92-15	AM-89-61	AP2-00-59	AM-89-93	JR-91-42	JR-91-42	6	
SiO_2	57.84	58.65	51.12	36.41	34.96	48.28	53.1	50.35	0.06	0.10	0.00	73.88
TiO_2	0.00	0.00	0.00	0.06	0.00	1.98	0.1	0.06	19.29	49.77	0.00	0.26
Al_2O_3	26.44	26.27	30.84	0.00	0.01	4.04	1	0.26	0.00	0.00	0.00	14.25
FeO	0.66	0.28	0.48	31.06	37.93	13.10	13.1	36.67	77.80	48.13	0.31	1.65
MnO	0.00	0.00	0.00	0.62	0.65	0.45	0.2	1.91	0.48	0.50	0.00	0.00
MgO	0.05	0.03	0.17	31.67	26.03	12.68	30.6	0.05	2.37	1.51	0.58	0.45
CaO	8.50	0.00	13.77	0.18	0.41	19.06	1.5	1.67	0.00	0.00	60.36	1.48
Na_2O	5.48	6.14	3.53	0.00	0.00	0.41	0	7.98	0.00	0.00	0.22	3.87
K_2O	1.03	0.86	0.08	0.00	0.00	0.00	0.00	1.05	0.00	0.00	0.00	4.07
P_2O_5	0.00	0.00	0.00	0.00	0.00	0.00	0.00	0.00	0.00	0.00	38.53	0.08

Summary of major element fractionation model results

model suite	parent	daughter	SiO_2 range	frac (%)	Σr^2	[A]mineral assemblage	Figure
Coleman Hills	BA	A	54.8-58.3	29-30	0.2-0.3	$P1_{42}$, CPX_{46}, M_{12}, +/- $Ol\text{-}1_{10\text{-}13}$, $I_{10\text{-}13}$	
	A	D	58.3-64.2	37	0.5-0.6	$P1_{69}$, CPX_{18}, M_{12}, +/- $Ol\text{-}1_{1\text{-}2}$, I_3	
BA=basaltic andesite	D	R	64.2-72.0	36-38	1.8-2.2	$P2_{56}$, CPX_{26}, $Ol\text{-}1_5$, M_{13}	
A=andesite	BA	D	54.8-64.2	56	0.9	$P2_{68}$, CPX_{19}, $Ol\text{-}1_3$, M_{10}	
D=dacite R=rhyolite	BA	R	54.8-72.0	68	1.4	$P1_{70}$, CPX_{13}, M_{14}, $Ol\text{-}1_3$	
	R+BA	D		mix	9.4		
Parental compositions							
	SB	BA	49.2-56.1	70	0.5	$P1_{51}$, CPX_{30}, $Ol\text{-}1_7$, M_{12}	
SB=Steens basalt	B	BA	48.6-56.1	86	0.2	$P3_{55}$, CPX_{28}, $Ol\text{-}2_{16}$, M_1	
B= HAOT	B	SB	48.6-49.2	80	0.5	$P3_{53}$, CPX_{26}, $Ol\text{-}2_{18}$, M_3	

[A]Fractionating mineral assemblage with mode removed shown in subscript.
Source of data: [1] This study; [2] MacLean, 1994; [3] Mathis, 1993; [4] Klemetti, 2005; [5] Deer, Howie and Zussman, 1992; [6] Grove et al., 1988.

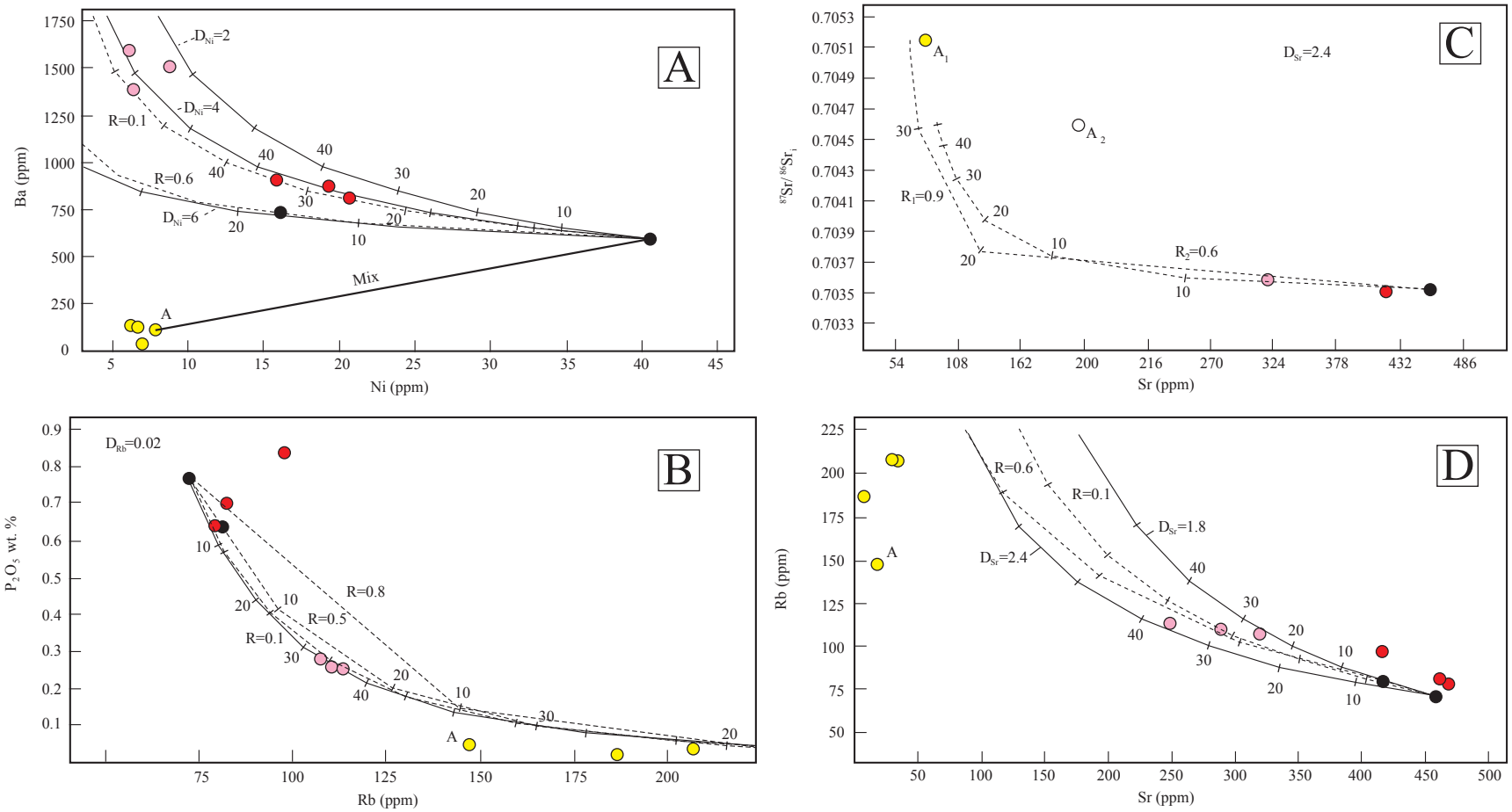

Figure 12. Trace element and isotopic AFC best-fit models for generation of rock suite observed at the Coleman Hills. Fractional crystalization (solid line) and AFC (dashed); A1 is rhyolite from the Coleman Hills. R= rate of assimilation relative to fractionation. Coleman Hills compositions: basaltic andesite (black); andesite (red); dacite (pink); rhyolite (yellow). (C) A2 is crust from Grove et al. (1988). Distribution coefficients for basaltic andesite liquids compiled in Rollinson (1993).

and dacite (Table 2). A major element model of basaltic andesite to rhyolite requires 68% and yields unacceptably high r^2=1.4 (Table 3). A range of major element models were tested to determine if the compositional range observed within the Early Miocene Coleman Hills suite could be produced by fractionation alone. These models demonstrate that fractionation alone will note generate rhyolite from dacite of the suite (Table 3) and that a crustal assimilant is required (Figure 12).

Crustal contamination and magma mixing

We consider two ways in which a crustal composition might be introduced into the petrogenetic model of the Coleman Hills: (1) as a crustal melt, represented by the rhyolite in mixing or (2) combined mixing (or assimilation) and fractional crystallization. A simple mixing model to create dacite from basaltic andesite and rhyolite fails because Ba concentrations in the dacite are higher than either of the mixing end members (Figure 12). Coupled assimilation and fractional crystallization models, in turn, illustrate that the range in compositions from the Coleman Hills may be generated by either (1) slow and steady or (2) episodic incorporation of crustal material (Figure 12). Isotopic models help to explain the role of rhyolite within the petrologic history of the Coleman Hills. Initial $^{87}Sr/^{86}Sr$ values in the rhyolite are much higher than other compositions within the Coleman Hills (Table 2) and neither of the preferred trace element models, described above, satisfactorily reproduces the isotope ratio in the rhyolite via AFC of basaltic andesite (Figure 12). However, initial $^{87}Sr/^{86}Sr$ isotopic variation among the remaining compositions in the Colman Hills suite can be adequately explained by rapid assimilation of silicic crustal rocks (Figure 12C)

Petrogenetic model

The preferred model (Figure 13) for the genesis of the Coleman Hills suite requires injection of a mafic melt into the crust, which produces pods of rhyolite via crustal anatexis. The rhyolites have characteristics of fractionation, such as low Ba, Sr, Eu) (Figures 8 and 9) indicating that while largely derived from crustal melts, as suggested by isotopic ratios (Figure 10), they subsequently were subject to differentiation (Figure 13). A range in Rb, Zr, Nb, Y, and La concentrations (Figure 7) within rhyolite of the Coleman Hills hints that more than one pod might exist within the volcano. Production of the crustal melt coincides with fractionation of the mafic parent until the system is disrupted, perhaps by faulting and/or repeated injection of mafic material, and rhyolite erupts at the surface. Textural and petrologic arguments support assimilation of pieces of the crustal rhyolite at shallow levels by basaltic andesite to form dacite of the complex. Once a pathway to the surface had been sufficiently cleared, basaltic andesite and andesite erupted and built the principal edifice of the volcano.

Textural evidence and major and trace element models of a 26 Ma, high-K section at Hart Mountain (Mathis, 1993) (Figure 1) indicate mixing within the intermediate suite and an inability to produce rhyolite via crystal fractionation from a basaltic andesite parent composition (Mathis, 1993). Johnson and Grunder (2000) attribute the existence of voluminous 10.4 Ma intermediate lavas within a bimodal suite at Duck Butte to disruption of a compositionally zoned magma system due to faulting. In their model mixing of mafic lavas and rhyolitc crustal melts form the observed suite of high-K compositions (e.g., Figure 6) during periods of tectonism. Periods of tectonic quiescence

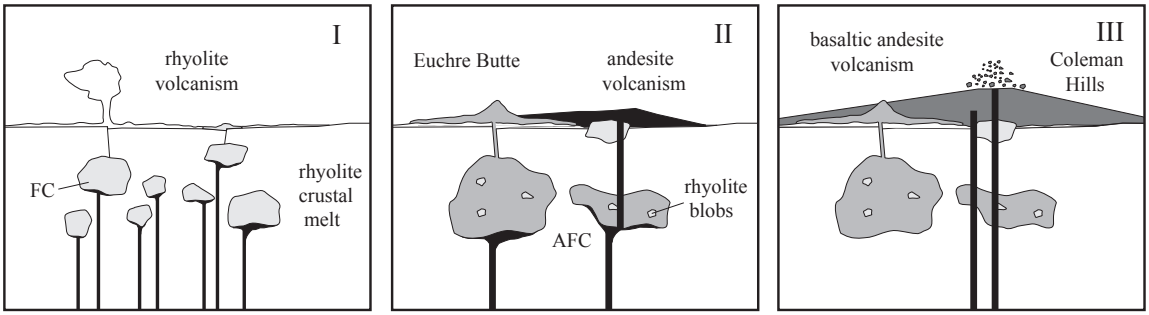

Figure 13. Cartoon illustrating a model of the three stage (I-III) petrogenesis of the Coleman Hills volcanic complex. Stage I: Crustal anetexis driven by the injection of basaltic andesite and fractionation (FC) within a diffuse zone of the crust. Eruption of rhyolite caused by dome emplacement and collapse. Stage II: Continued injection of basaltic andesite causes coallescence of pods of crustal melt fascilitating assimilation and fractional crystalization within large magma chambers. Eruption of Euchre Butte dacite and basaltic andesite tap different systems. Stage III. System is flooded by basaltic andesite due to the formation of a mature crustal pathway.

are characterized by injection and fractionation of mafic lavas and crustal anetaxis to produce rhyolite pods.

Generation of mafic parent

There are no primitive volcanic rocks associated with the Coleman Hills so the basaltic parental composition must be inferred. Primitive basalts in the area include Steens and the HAOT. Either Steens or HAOT make a suitable parent based on major element fractionation models (Table 3). Trace element concentrations in primitive HAOT show flat patterns whereas Steens Basalts show enrichments in line with those observed within the Coleman Hills suite (Figure 9). However, Steens basalts are not a suitable parent in terms of isotopic composition as the Coleman Hills suite clusters with Late Miocene mafic compositions (Figure 10). Furthermore, there are no identified sources of Steens Basalt near the study area and thus it seems unlikely that a Steens-like mantle was parental to Early Miocene magmatism. Bailey and Conrey (1992) propose that HAOT lavas that have erupted from 16 Ma to the present across the northwestern Great Basin are primitive, MORB-like, magmas that are produced by assimilation of crustal material en route to the surface. Although at odds with the interpretation of Carlson and Hart (1987), it seems likely that an enriched HAOT composition is a more likely parent to Early Miocene volcanic rocks of the Coleman Hills.

Episodes of Volcanism

Stratigraphic units in the study area (Figure 3) record three intervals of volcanism, each separated by a 6-8 m.y. period of volcanic inactivity (Figure 14): (1) formation of

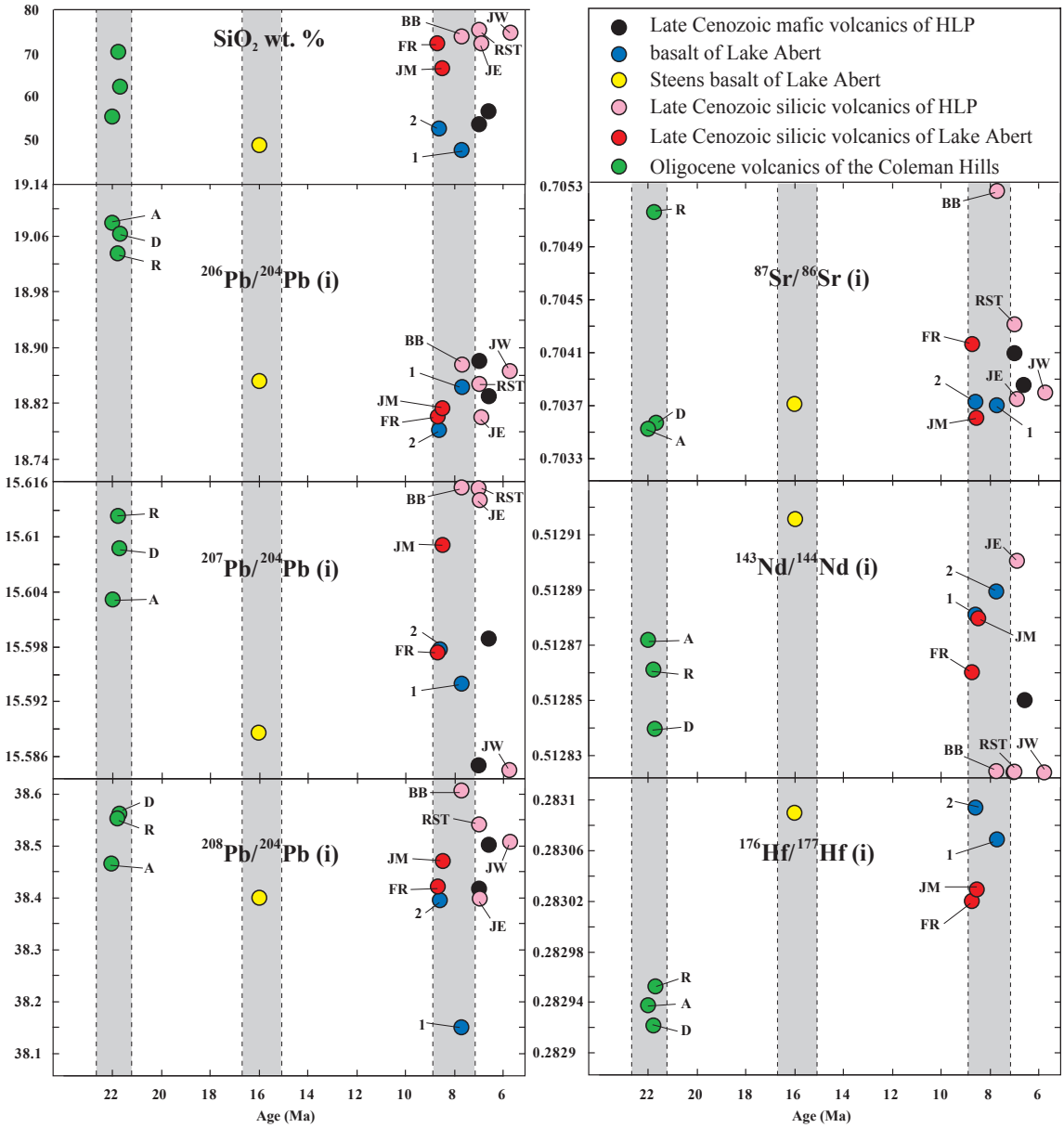

Figure 14. Isopic Pb, Sr, Nd, and Hf concentrations and SiO_2 wt. % plotted versus time for Late Cenozoic volcanic rocks of the High Lava Plains (HLP) and Lake Abert. Vertical shaded strips represent intervals of volcanism near Lake Abert based on age determinations. Interval for Steens volcanism from Hooper et al. (2002). Data sources and abbreviations are same as Figure 11.

the Coleman Hills at ~22 Ma, (2) Steens basalt volcanism at ~16 Ma, and (3) bimodal, dominantly mafic volcanism from ~9-7 Ma. However, the source of regional units such as the Steens basalt and Rattlesnake Tuff was not located in the immediate vicinity of Lake Abert but rather, significantly to the east and north, respectively (e.g., Mankinen et al., 1987; Streck and Grunder, 1997).

Early Miocene calc-alkaline intermediate volcanic units of the Coleman Hills could be lproducts of the ancestral Cascades arc because they are chemically similar to calc-alkaline suites that form in subduction zone settings. On the other hand, calc-alkaline suites occur widely in the Basin and Range Province and are related to high rates of extension (e.g., Armstrong and Ward, 1991) and the inferred HAOT parent for the suite is consistent with an extensional tectonic setting. Trace element patterns within the Coleman Hills suite (Figure 8) show enrichments in large-ion lithophile elements and to a lesser degree, in high-field strength elements, and an overall spiked pattern that is characteristic of both subduction zone and intraplate magmatic settings. A notable lack of a Nb-trough, characteristic of subduction settings, indicates that these magmas likely formed in an intraplate setting. Low $^{143}Nd/^{144}Nd_i$, $^{176}Hf/^{177}Hf_i$ and high $^{208}Pb/^{204}Pb_i$ in rocks from the Coleman Hills indicate that these magmas were either derived from a crustal source or have experienced some degree of interaction with crustal rocks.

High $^{207}Pb/^{204}Pb_i$ and $^{206}Pb/^{204}Pb_i$ within the Coleman Hills suite, relative to Late Cenozoic volcanic rocks in the area (Figure 11), indicates that Oligocene magmas sample a source that has been preferentially enriched in U. Dehydration fluids from a subducting slab are known to concentrate U in the fluid phase and transport it into the crust (e.g., Noll et al., 1996; Bourdon et al., 2003). Thus, while it is apparent that the high-K calk-

alkaline rock suite exposed in the Coleman Hills is not a subduction zone volcano, per-se, magmas that produced the suite were either generated within or contaminated by a crust that had been exposed to subduction zone processes. Furthermore, intermediate dikes within the Coleman Hills occur as NNW-trending tensional fissures, similar to those observed within the Columbia River Basalt Group (Hooper and Conrey, 1989), indicating that oblique subduction and back-arc spreading associated with the development of Basin and Range crustal extension in southern Oregon may have been ongoing by ~22 Ma, well in advance of Steens volcanism beginning at 16.6 Ma (Hooper et al., 2002).

Geochemical and isotope data provide a compelling basis for correlating 8.7 Ma and 7.7 Ma lava flows near Lake Abert (Figure 3) with volcanic vent complexes located to the north within the Alkali Lake Basin (Figures 1 and 5). For example, HAOT samples taken from Juniper Mountain, Alkali Butte and Venator Butte display similar total alkali enrichment at SiO_2 wt. % of 52-54% as the ~8.7 m.y. basaltic andesite flow near Lake Abert (Figure 6). Trace element patterns from the range of HAOT at Juniper Mountain and Venator Butte (Figure 8) suggest that these edifices (Figure 5) may be sources for both ~8.7 Ma and ~7.7 Ma HAOT in the region. Rhyolite erupted at Juniper Mountain at ~8.6 Ma and a ~8.8 Ma dacite flow forms Flint Ridge. Although rhyolite at Alkali Buttes has not been dated, Juniper Mountain is a likely source due to proximity and similar chemistry. Therefore, distinct episodes of volcanism near Lake Abert occurred at 22 Ma, ~8.8 to 8.5 Ma and at ~7.7 Ma. The age of Late Miocene volcanic products extends the distribution of ~8 Ma ryolites of the age progressive trend recognized within the HLP (e.g., Jordan et al., 2004; Walker and MacLeod, 1991),

provides a source area for widespread ~8.6 and ~7.7 Ma basaltic volcanism, and expands the distribution of HLP-style volcanism further to the south.

The periodicity of magmatism in the study area and shift from intermediate composition volcanism during the Early Miocene to the eruption of bimodal compositions during the Late Miocene can be related to changes in the tectonic configuration of plates at the western margin of North America. Reconstructions from seafloor paleomagnetic data show that forearc deformation along the western margin of North America, due to northwesterly translation of the Pacific Plate with respect to stable North America, was highly variable during the intervals of volcanism near Lake Abert: (1) at ~20 Ma the forearc was moving ~N60ºW at ~33 mm/yr and (2) at ~8 Ma the azimuth of displacement was ~N37ºW and at a rate of ~52 mm/yr (Atwater and Stock, 1998). Therefore, production of intermediate lavas that demonstrate substantial interaction with crustal material and derivation of silicic magmas from melting the crust (Figure 14) may be due to injection of mafic material into the crust during an early stage of continental rifting. The onset of bimodal, dominantly mafic, volcanism between ~9-8 Ma near Lake Abert may be due to an increase in the rate of forearc migration

CONCLUSIONS

The Early Miocene Coleman Hills volcanic complex is a dominantly intermediate composition suite that developed from rhyolite to basaltic andesite in time. Silicic magma of the Coleman Hills likely formed by melting Mesozoic crustal rocks, which acted as a contaminant in the mafic part of the suite that was dominated by fractional

crystallization. Oblique subduction and backarc rifting was ongoing in southern Oregon by ~22 Ma and the Coleman Hills suite records an early stage of continental rifting.

Late Miocene volcanism near Lake Abert consists of a dominantly bimodal, basalt-rhyolite, assemblage and rhyolitic volcanism occurred prior to basaltic volcanism. Juniper Mountain is the principal source of Late Miocene silicic volcanism and Venator Buttes is the principal source of Late Miocene mafic volcanism centered on Abert Rim. The timing and style of this interval of volcanism matches that of the HLP. The results of this study would suggest that the HLP extends further south than its geomorphic expression and into the Basin and Range Province. Bimodal volcanism of the Late Miocene suite at Lake Abert resulted from accelerated continental rifting driven by an increase in northwesterly motion of the Pacific Plate with respect to North America. The alignment of volcanic centers and progression of volcanism, from rhyolite to basalt, indicate weakening of the crust prior to (or during) formation of Abert Rim.

REFERENCES CITED

Allegre, C.J., 1988, The behavior of the Earth: continental and seafloor mobility, Harvard University Press, 272 p.

Armstrong, R.L., and Ward, P., 1991, Evolving geographic patterns of Cenozoic magmatism in the North American Cordillera: The temporal and spatial association of magmatism and metamorphic core complexes, Journal of Geophysical Research, v. 96, p. 13,201-13,224.

Atwater, T., and Stock, J., 1998, Pacific-North America plate tectonics of the Neogene southwestern United States-An update, in Ernst, W.G., ed, International Geological Review, Clarence Hall Symposium volume, v. 40, p. 375-402.

Carlson, R.W., Lugmair, G.W., and MacDougall, J.D., 1981, Columbia River volcanism: the question of mantle heterogeneity or crustal contamination, Geochemica et Cosmochimica Acta, v. 45, p. 2483-2499.

Carlson R.W. and Hart, W.K., 1987, Crustal genesis on the Oregon Plateau, Journal of Geophysical Research, v. 92, 6191-6206.

Carlson R.W., Czamanske, G. Fedorenko, V., and Ilupin, I., 2006, A comparison of Siberian meimechites and kimberlites: Implications for the source of high-Mg alkalic magmas and flood basalts: Geochemistry, Geophysics and Geosystmes, v. 7, no. 11, 22 p.

Christiansen, R.L., and McKee, E.H., 1978, Late Cenozoic volcanic and tectonic evolution of the Great Basin and Columbia Intermontane regions, Geological Society of America Memoir 152, p. 283-311.

Christiansen, R.L., Yeats, R.S., 1992, Post-Laramide geology of the U.S. Cordilleran region, in Geological Society of America Special Publication, The geology of North America: The Cordilleran Orogen; conterminous U.S., Burchfiel, B.C., Lipman, P.W., and Zoback, M.L. (eds.), p. 261-406.

Christiansen, R.L., Foulger, G.R., and Evans, J.R., 2002, Upper-mantle origin of the Yellowstone hotspot, Geological Society of America Bulletin, v. 114, p. 1,245-1,256.

Coney, P.J. and Reynolds, S.J., 1977, Cordilleran Benior zones, Nature, v. 270, p. 403-406.

Draper, D.S., 1991, Late Cenozoic bimodal magmatism in the northern Basin and Range Province of southeastern Oregon, Jounal of Volcanology and Geothermal Research, v. 47, p. 299-328.

Gerlach, D.C., 1988, Magma sources of the Cape Verdes Archipelago: isotopic and trace element constraints, Geochimica et Cosmochimica Acta, v. 52, p. 2979-2992.

Grove, T.L., Kinzler, R.J., Baker, M.B., Donnelly-Nolan, J.M., and Lesher, C.E., 1988, Assimilation of granite by basaltic magma at Burnt lava flow, Medicine Lake Volcano, northern California: decoupling of heat and mass transfer, Contributions to Mineralogy and Petrology, v. 99, p. 320-343.

Hart, S.R., and Zindler, A., 1986, In search of a bulk-Earth composition, Chemical Geology, v. 57, p. 247-267.

Hart, W.K., and Mertzman, S.A., 1982, K-Ar ages of basalts from southcentral and southeastern Oregon, Isochron-west, no. 33, p. 23-26.

Hart, W.K., Aronson, J.L., and Mertzman, S.A., 1984, Areal distribution and age of low-k, high-alumina olivine tholeitte magmatism in the northwestern Great Basin, Geological Society of America Bulletin,
v. 95, p. 186-195.

Hooper, P.R., Conrey, R.M., 1989, Volcanism and teectonism in the Columbia River flood-basalt province, GSA Special Paper v. 239, p. 293-306

Hooper, P.R., Binger, G.B., and Lees, K.R., 2002, Ages of the Steens and Columbia River flood basalts and their relationship to extension-related calc-alkalic volcanism in eastern Oregon, Geological Society of America Bulletin, v. 114, p. 43-50.

Johnson, J.A., Hawkesworth, C.J., Hooper, P.R., and Binger, G.B., 1998, Major- and trace-element analyses of Steens basalt, southeastern Oregon, U.S. Geological Survey Open-File Report 98-482, 30 p.

Johnson, D.M., Hooper, P.R., and Conrey, R.M., 1999, XRF analysis of rocks and minerals for major and trace elements on a single low dilution Li-tetraborate fused bead: Advances in X-ray analysis, v. 41, p. 843-867.

Johnson, J.A., and Grunder, A.L., 2000, The making of intermediate composition magma in a bimodalsuite: Duck Butte Eruptive Center, Oregon, USA, Journal of Volcanology and Geothermal Research, v. 95, p. 175-195.

Jordan, B.T., 2001, Basaltic volcanism and tectonics of the High Lava Plains, southeastern Oregon, [Ph.D. Thesis] Corvallis, Oregon, Oregon State University, 218 p.

Jordan, B.T., Grunder, A.L., Duncan, R.A., and Deino, A.L., 2004, Geochronology of Oregon High Lava Plains volcanism: Mirror image of the Yellowstone hotspot?, Journal of Geophysical Research, 19 pp.

LeMaitre, R.W., 1984, A proposal by the IUGS Subcommission on the Systematics of Igneous Rocks for a chemical classification of volcanic rocks based on the total alkali silica (TAS) diagram, Australian Journal of Earh Sciences, v. 31, p. 243-255.

Mankinen, E.A., Larson, E.E., Gromme, C. S., Prevot, M., and Coe, R.S., 1987, The Steens Mountain (Oregon) geomagnetic polarity transition, its regional significance, Journal of Geophysical Research, v. 92, p. 8057=8076.

Mathis, A.C., 1993, Geology and petrology of a 26-Ma trachybasalt to peralkaline rhyolite suite exposed at Hart Mountain, southern OR [M.S. thesis]: Corvallis, Oregon, Oregon State University, 141 p.

McDonough, W.F., Sun, S.S., Ringwood, A.E., Jagoutz, E., and Hofmann, A.W., 1992, Potassium, rubidium, and cesium in the Earth and Moon and the evolution of the mantle of the Earth, Geochimica et Cosmochimica Acta, v. 56, p. 1001-1012.

Pezzopane, S.K., and Weldon, R.J., 1993, Tectonic role of active faulting in central Oregon, Tectonics, v. 12, p. 1,140-1,169.

Pierce, K.L., and Morgan, L.A., 1992, The track of the Yellowstone hotspot: Volcanism, faulting, and uplift, in Link, P.K., Kuntz, M.A., and Platt, L.B., eds., Regional geology of eastern Idaho and western Wyoming: Geological Society of America Memoir 179, p. 1-53.

Rollinson, H.R., 1993, Using geochemical data: evaluation, presentation, interpretation, Harlow, UK, 352 p

Saunders, A.D., Nory, M.J., and Tarney, J., 1988, Origin of MORB and chemically depleted mantle reservoirs: trace element constraints, Journal of Petrology, v. 198, p. 415-445.

Stewart, J.H., and Carlson, J.E., 1974, Preliminary geologic map of Nevada, U.S. Geological Survey, Reston, VA.

Stille, P., Unruh, D.M., and Tatsumoto, M., 1983, Pb, Sr, and Hf isotopic evidence of multiple sources for Oahu, Hawaii basalts, Nature, v. 304, p. 25-29.

Stormer, J.C. Jr, and Nicholls, J., 1978, XLFRAC: a program for the interactive testing of magmatic differentiation models, Computers & Geosciences, v. 4, p. 143-159.

Streck, M.J., and Grunder, A.L., 1995, Crystallization and welding variations in a widespread ignimbrite sheet: The Rattlesnake Tuff, eastern Oregon: Bulletin of Volcanology, v. 57, p. 151-151-169.

Streck, M.J., and Grunder, A.L., 1997, Compositional gradients and gaps in the high-silica rhyolites of the Rattlesnake Tuff, southeastern Oregon, Journal of Petrology, v. 38, p. 133-163.

Streck, M.J., and Grunder, A.L., 2007, Phenocryst-poor rhyolites of bimodal, tholeiitic provinces: the Rattlesnake Tuff and implications for mush extraction models, Bulletin of Volcanology, DOI 10.1007/s00445-007-0144-3

Sun, S.S., and McDonough, W.F., 1989, Chemical and isotopic systematics of oceanic basalts: implications for mantle composition and processes. *In*: Saunders, A.D., and Norry, M.J. (eds.), Magmatism in ocean basins, Geological Society of London Special Publication 42, p. 313-345.

Todt, W., Cliff, R.A, Hanser, A., and Hofmann, A.W., 1996, Evaluation of a ^{202}Pb-^{205}Pb double spike for high-precision lead isotope analysis, Geophysical Monograph, v. 95, p. 429=437.

Urbancyzk, K., 1994, Geology of the eastern part of the Clarno Formation, northeast Oregon, [Ph.D. Thesis], Washington State University, Pullman, WA, 230 p.

Walker,G.W., 1963, Reconnaissance Geologic map of the eastern half of the Klamath Falls (AMS) Quadrangle, Lake and Klamath Counties, Oregon. Mineral Investigations Field Studies Map MF-260, scale 1:250,000/

Walker, G.W., Nolf, B., 1981, Roadlog for High Lava Plains, Brothers fault zone to Harney Basin, Oregon, U.S. Geological Survey Circular, p. 113-118

Walker, G.W., and MacLeod, N.S., 1991, Geologic map of Oregon, U.S. Geological Survey, Reston, VA.

Wernicke, B.P., 1992, Cenozoic extensional tectonics of the U.S. Cordillera, in Burchfiel, B.C., et al., eds., The Cordilleran orogen: Conterminous U.S.: Boulder, Colorado, Geological Society of America, Geology of North America, v. G-3, p. 553-581.

CHAPTER 3

INCEPTION AND STYLE OF FAULTING AT THE EDGE OF A PROPOGATING CONTINENTAL RIFT SYSTEM: INSIGHT FROM THE STRUCTURAL DEVELOPMENT OF THE ABERT RIM FAULT, SOUTHERN OREGON

Kaleb C. Scarberry[1]

Andrew J. Meigs[1]

[1]Department of Geosciences,
Oregon State University, Corvallis, OR 97331

For submission to Tectonics

ABSTRACT

Mapped contact relations and new ^{40}Ar-^{39}Ar ages reveal a temporal progression of faulting near Lake Abert, OR within the northwestern margin of the Basin and Range Province. Partial cross-section restorations demonstrate that the Abert Rim fault south of 42º40'N latitude had >250 m of stratigraphic separation prior to deposition of the Rattlesnake Tuff and therefore Basin and Range faulting was active in this region prior to 7 Ma. Systems of NW-striking faults formed ahead of the northward propagating Abert Rim fault between ~8.9 and 7.5 Ma, an interval of time that is coincident with widespread basaltic activity in the map region. The structural development of the Abert Rim fault is chronologically linked to the formation and northward propagation of the Walker Lane fault system and thus provides a tectonic link for along- and across-strike expansion of the margin of Basin and Range Province. A previously unrecognized episode of volcanism occurred near Lake Abert between ~21.4 and 22.3 Ma. Dike orientations within the Early Miocene volcano and evidence for the existence of as much as 500 m of paleo-topography prior to deposition of the Steens flood basalts at ~16 Ma suggests that Late Miocene faults near Lake Abert may have formed along an older structural fabric.

INTRODUCTION

Post-Laramide reorganization of the North American Plate boundary was accompanied by magmatism the development of the Basin and Range Province in western North America (e.g., Christiansen and Yeats, 1991; Armstrong and Ward, 1991; Wernicke, 1992) (Figure 1). Deformation at the western margin of the province since ~10 Ma is characterized by east-west extension and right lateral shear (Zoback, 1989).

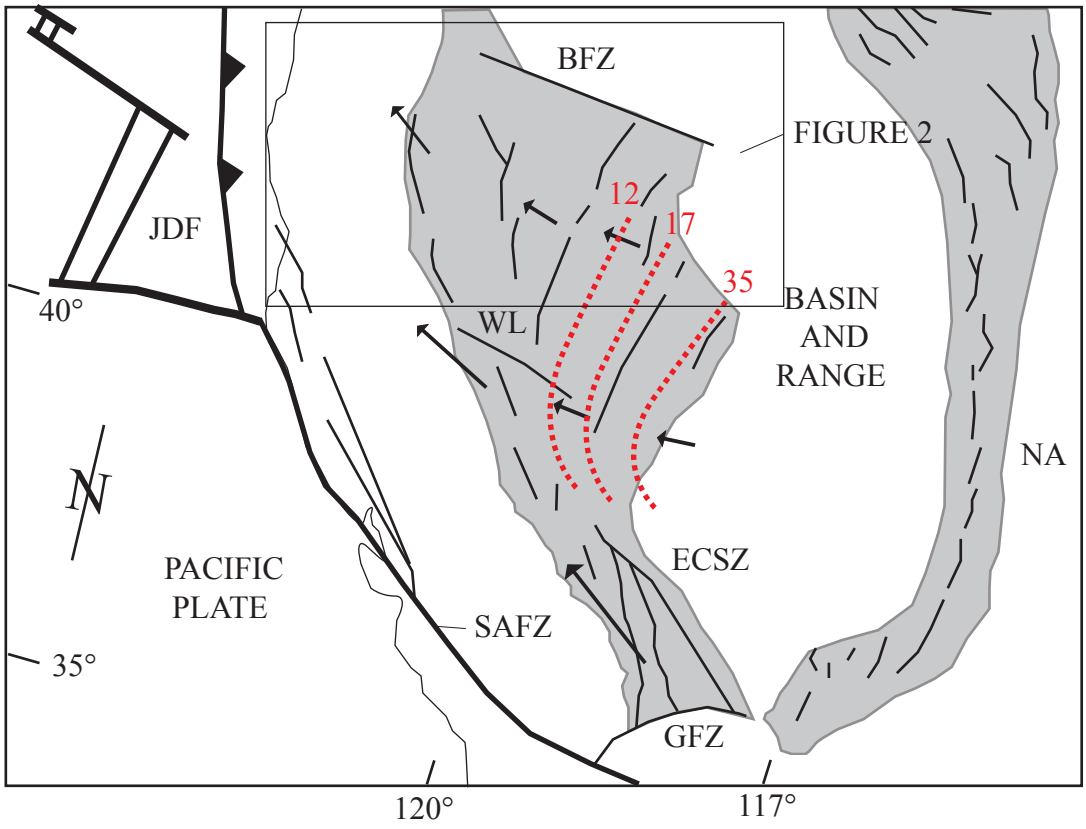

Figure 1. Tectonic setting of the Basin and Range Province of western North America. The active margins of the province are shaded and prominent faults after Pezzopane and Weldon (1993). Red stippled lines contour the age (in Ma) of onset of extensional faulting as determined by previous studies (see text). Arrows represent GPS velocity data from Miller et al. (2001) and Hammond and Thatcher (2005). These data illustrate an increase in magnitude and counterclockwise rotation of the strain field accross the western margin of the Basin and Range relative to stable North America (NA). The magnitude of strain decreases to the north, along-strike, of the province. BFZ= Brothers Fault Zone; JDF=Juan De Fuca Plate; WL= Walker Lane; ECSZ=Eastern California Shear Zone; SAFZ=San Andreas Fault Zone; GFZ=Garlock Fault Zone.

Numerous models are used to describe the forces that drive this deformation including: (1) trench pull and subduction zone rollback due to removal of the Farallon slab underneath North America (Humphreys, 1995); (2) rotation of the Cascadia forarc (e.g. Wells and Heller, 1998); (3) development and propagation of major dextral fault systems such as the San Andreas (Atwater and Stock, 1998) and Walker Lane (Wesnousky, 2005; Faulds et al., 2005); (4) collapse of the crust driven by gravitational potential energy due to thickening of the Laramide crust (Humphreys and Coblentz, 2007).

The northwest margin of the basin and Range Province in Oregon (NWBR) (Figures 2 and 3) is an ideal place to study the temporal growth and physical controls for the development of Basin and Range faults. Deformation within the NWBR is characterized by two principal fault trends (NNE-striking and NW-striking) that cut syn-rift volcanic stratigraphy (Figure 3). The temporal development of the respective fault sets across the region has not been established and it is unclear if they formed along a reactivated structural fabric or in response to the Late Miocene stress field of the region, as suggested by previous studies (Donath, 1962; Pezzopane and Weldon, 1993; Crider, 2001). This paper presents results of new $^{40}Ar/^{39}Ar$ ages and detailed geologic mapping within a ~350 km^2 area located at the northern end of Lake Abert (Figure 4). These data are used to describe the timing and style of faulting within the NWBR and to place these events in context with models of post-Larmide tectonism of western margin of the Basin and Range Province.

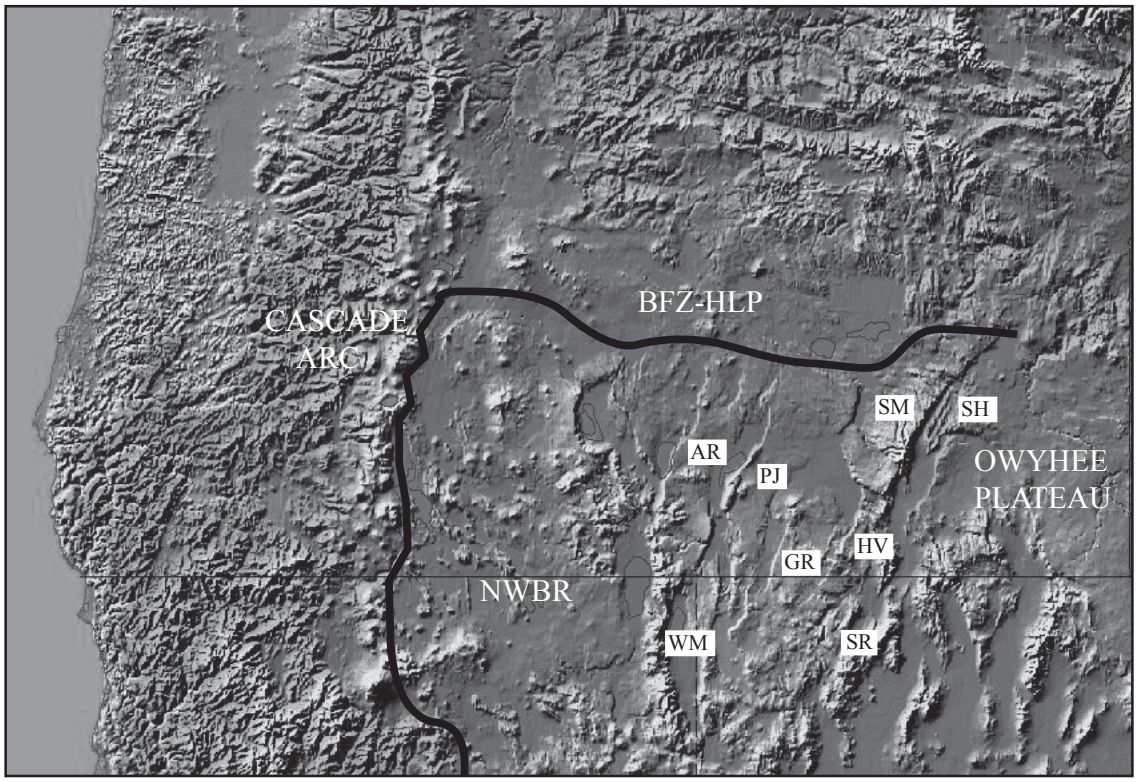

Figure 2. Digital elevation model illustrates that the structural boundary of the northwestern corner of the Basin and Range Province (NWBR) is located in southern Oregon. The NWBR is bordered to the north by the Brothers Fault Zone (BFZ) and High Lava Plains (HLP) and to the west by the Cascade Arc. Locations discussed in the text: (AR) Abert Rim; (PJ) Poker Jim Rim; (SM) Steens Mountain; (SH) Sheepshead Mountains; (HV) Hawks Valley; (GR) Guano Rim; (WM) Warner Mountains; (SR) Santa-Rosa-Pine Forrest ranges.

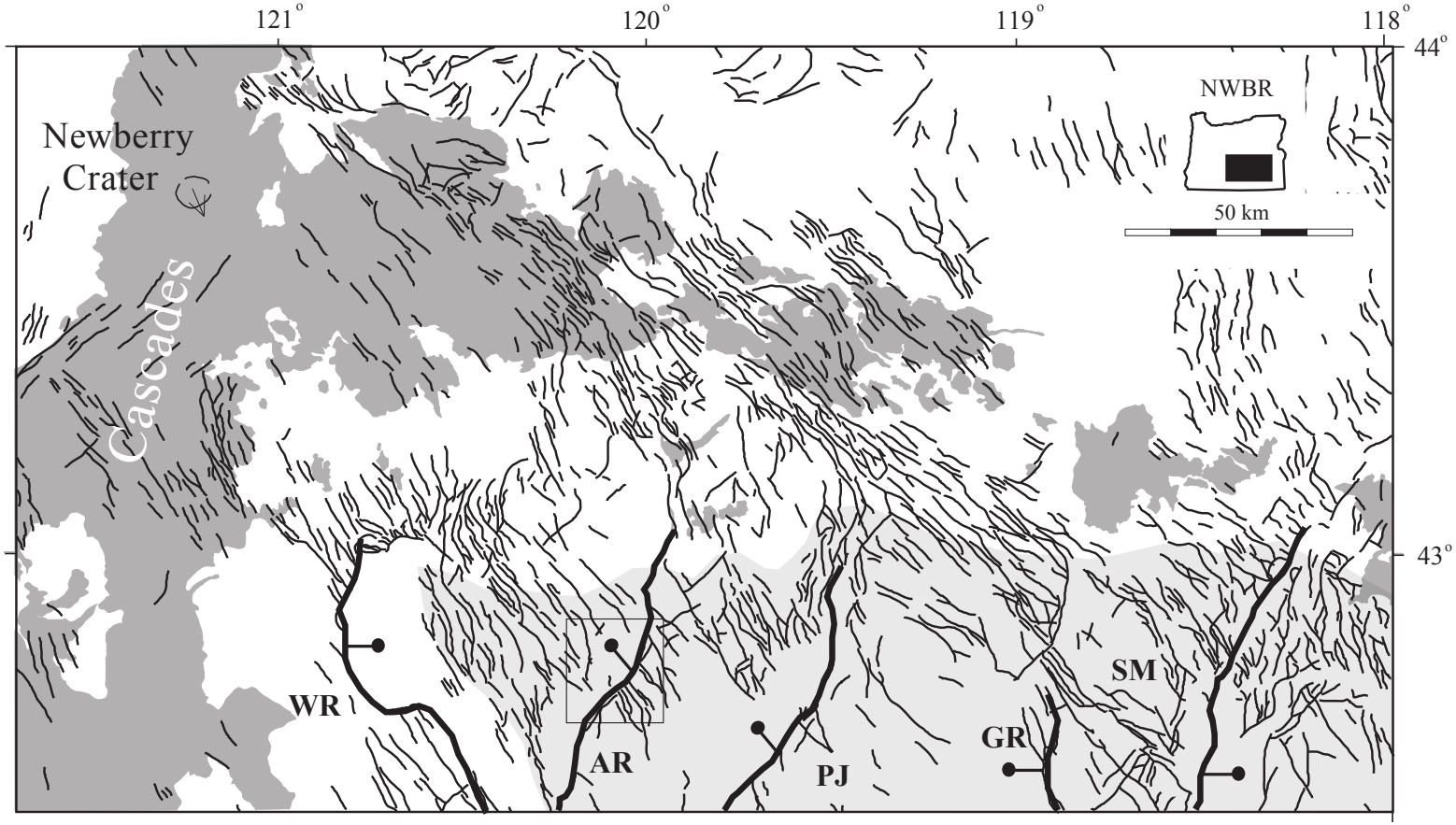

Figure 3. NNE-striking Basin and Range escarpments (thick line) and distributed systems of NW-striking faults characterize the structural fabric of the NWBR. Pliocene to Recent tracks of basalt basalt (dark shade) borders the extensional province to the west and north. The northern track defines the HLP and is coincident with the Brothers Fault Zone. Basin and Range escarpments labeled as in Figure 2. Light shade shows the approximate distribution of Steens basalts. Box denotes study location.

Regional Constraints on Basin and Range Opening

Extension was established across the NWBR sometime after 12 Ma (e.g., Colgan et al., 2004) but the exact timing of the onset of extension into this region is essentially unknown. Since ~35 Ma the onset of extensional faulting has migrated outward from the interior of the Basin and Range Province (Figure 1) and northwestward into southern Oregon (NWBR) (Figure 2) (see summaries by Seedorff, 1991 and Wernicke, 1992; Dilles and Gans, 1995; Miller et al., 1999; Surpless et al., 2002; Colgan et al., 2004). South of ~39˚ N large-magnitude extension (>100 percent) characterized the eastern (~114˚ W) part of the province between ~35-20 Ma (Miller et al., 1983, 1999). Across-strike to the west, extension was localized at ~118˚ W after 26 Ma (Dilles and Gans, 1995). Extensional deformation migrated west to the California-Nevada state line (longitude 120˚ W) after 14 Ma along the Sierra Nevada-Basin and Range transition (Dilles and Gans, 1995; Surpless et al., 2002). Thus, extension migrated westward since 35 Ma, with more than 100 km of that migration occurring after 15 Ma.

The along-strike growth of the Basin and Range extensional province is less well constrained. The Walker Lane, the western boundary of the Basin and Range north of 40˚N, propagated northward between 9 and 3 Ma (Dilles and Gans, 1995; Faulds et al., 2005). To the east, in the Santa Rosa-Pine Forrest ranges (Figure 2), extensional deformation after 10 Ma is suggested by footwall cooling ages from the Santa Rosa range-front fault (Colgan et al., 2004). Extension prior to ~10 Ma is not preserved by thermal, stratigraphic, or structural records (Colgan et al., 2004). These data imply that the locus of extension may have shifted to the NWBR between ~16 and 10 Ma

(Wernicke, 1992; Christensen and McKee, 1978), although the temporal and spatial progression is not known in detail.

OPENING OF THE OREGON BASIN AND RANGE

Net extension of the NWBR (Figure 2) is thought to be minimal (e.g., Wernicke, 1992). Wells and Heller (1988) estimate ~17 % perpendicular to a NNW-SSE extension direction since ~16 Ma based primarily on paleomagnetic data and tectonic reconstructions. Field-based estimation of net extension across a major regional escarpment, such as the Abert Rim, or across systems of NW-striking faults within the NWBR has not been undertaken.

Major Structures

The NWBR is located within a broad zone of active deformation, bordered to the west by the Cascade volcanic arc and to the north by the Brothers Fault Zone (Figure 3). Topographic and structural relief diminishes northwards towards the Brothers Fault Zone, a broad NW-striking zone of small en echelon faults that define the boundary of the northwestern Basin and Range (Lawrence, 1976). The High Lava Plains (HLP), a locus of volcanism after 10 Ma (Christiansen and McKee, 1978; Hamilton, 1989; Christiansen et al., 2002) broadly coincides with the Brothers Fault Zone. Thus, the Brothers fault zone appears to function as a 'transverse zone', that is, an extensional structure associated with magma emplacement (e.g., Rowley, 1998).

Deformation south of the HLP is accommodated by fault systems that exhibit two principal strike directions: NW and NNE (Figure 3) (Donath, 1962; Pezzopane and

Weldon, 1993; Crider, 2001). NNE-striking faults bound the major topographic escarpments, which are inferred to have the greatest stratigraphic separation. NW-striking faults, in contrast, are marked by lower topographic and, presumably, structural relief. A variety of data including analog experiments, dike orientations, cinder cone alignments, slip vectors from earthquake moment tensors, and moderate earthquakes indicate that the fault sets in the region have formed in response to right-oblique extension towards N60-70˚W (see summaries in Pezzopane and Weldon, 1993 and Crider, 2001). Geomorphic and paleoseismic observations indicate both fault sets are active (Pezzopane and Weldon, 1993). Field relationships at major escarpments, such as, Hart Mountain (Mathis, 1993) and Steens Mountain (Hemphill-Haley, 1989) demonstrate that the two fault sets have mutually cross-cutting relationships, indicating they developed coevally in some instances. Neither the age of initiation nor the duration of motion on either fault set is known regionally.

Timing of Extension

Only sparse data constrain the timing and magnitude of extension within the NWBR. Extensional faults across southeastern Oregon (Figure 2) cut and are thus younger than the ~16 Ma Steens basalt. The Steens fault appears to be a long-lived structure. An angular unconformity between the Steens Mountain basalt and underlying volcanic and volcaniclastic rocks at Steens Mountain indicate tilting of ~20˚ prior to 16.6 Ma (Minor et al., 1987; Langer, 1991; Hooper et al., 2002). The northern part of the Steens fault was active during volcanic activity at ~10 Ma (Johnson and Grunder, 2000) and the 9.8 Ma Divine Canyon Tuff is cut and ponded against a NW-striking fault

(Johnson, 1995). Well-preserved Holocene scarps at Steens Mountain indicate that the fault remains active (Hemphill-Haley, 1989). Whereas there is a ~10˚ angular discordance between Steens basalt and underlying clastic and Early Miocene volcanic units at Steens Mountain (Minor et al., 1987; Langer, 1991), there is no such discordance at Hart Mountain to the west (Mathis, 1993). Faulting along the Abert Rim has been active in the latest Pleistocene (~16 ka), where predominately normal slip of offset shoreline deposits implies a ~0.5 mm/yr extension rate (Pezzonpane and Weldon, 1993). Hart and Mertzman (1982) bracket faulting at the Abert Rim and Poker Jim Rim, the next Basin and Range escarpment to the east (Figure 2). An age of basalt flows that cap Poker Jim Rim are cut by the range-front fault were used to argue that faulting is no older than ~7 Ma. A basalt flow banked against the Abert Rim brackets movement on the fault at between 6-16 Ma. However, this relationship may be due to landsliding, thus superimposing the top of the section against the base of the section.

Insight into the spatial and temporal development of the NW and NNE fault systems is provided by location-specific studies (see Figure 2 for site locations). NW-striking structures were active between ~12 and 9 Ma within the Sheepshead Mountains prior to post ~7 Ma faulting along NE-trending structures (Sherrod et al., 1988). A prominent NW-striking graben that formed Hawks Valley developed in the ~16 Ma Lone Mountain rhyolite complex (Maloney, 1961; Legge, 1988) which channeled the flow of a younger basalt flow that is cut in turn by a NNE-striking fault. At Guano Rim, slight tilting of strata by faulting along NW-striking structures occurred between 9 and 5 Ma and preceded faulting along the NNE-striking Guano Rim Fault, which has been active

since ~5 Ma (ages reported in Sawlan et al., 1994). Thus, faulting on NW-striking structures appears to predate faulting along NE-striking structures across the NWBR.

The Abert Rim Fault

The Abert Rim fault (Figure 3) is the type of structure where questions about timing and style of Basin and Range faulting can be addressed. Topographic and presumably stratigraphic separation on the fault declines along-strike to the north until the trace of the fault yields to systems of NW-striking faults of the High Lava Plains. The Abert Rim fault is one of the major structures in Oregon (the trace is > 100 km) and systems of NW-striking faults interact with the NNE-striking Basin and Range fault at the north end of Lake Abert, a large playa that lies in the hanging wall of the fault at ~42˚ N latitude (Figure 4). Both fault sets are considered active in this region (Pezzopane and Weldon, 1993; Niewendorp, 2003). The geometry of the north end of the lake basin is controlled by the Coleman Hills and a series of 8-10 faults that are oriented N30- 40˚W (Figure 3). Langridge et al. (1996) suggest that the association of tufa mounds with a 4300 yr B.P. shoreline of Lake Chewaucan at the northern end of the lake is related to Pleistocene to Holocene fault activity along NW-striking faults. Intersection of NNE-striking and NW-striking faults at the north end of Lake Abert (Figure 3) provides an opportunity to evaluate the timing of development along the principal NWBR fault sets.

METHODS

Geologic mapping at 1:24,000 scale was conducted over a 625 km^2 area at the north end of Lake Abert over the course of three summer field seasons (Figure 4).

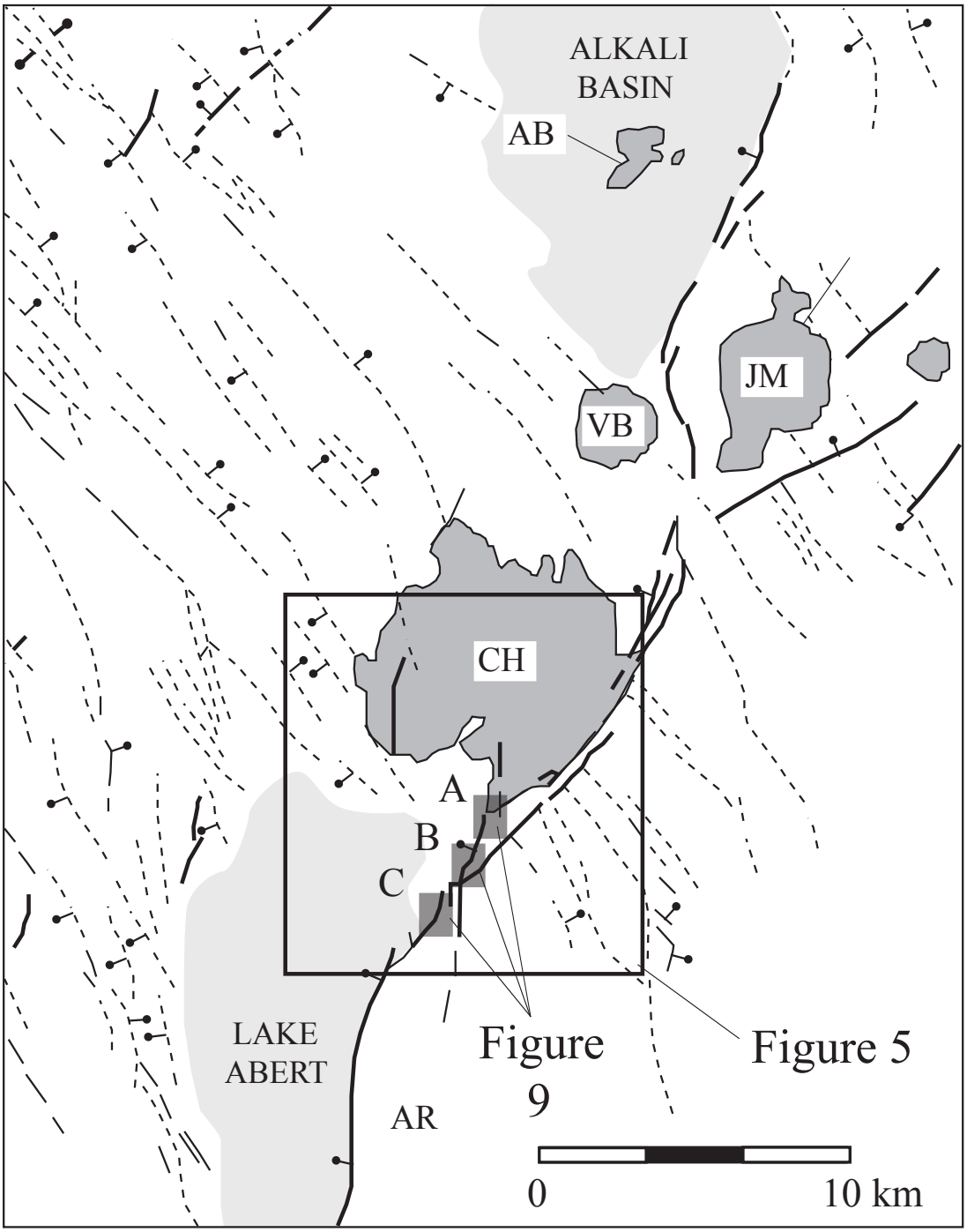

Figure 4. Map shows the association of NW-striking faults (stipple line), NNE-striking faults (solid line), volcanic centers (dark shade), and lake basins (light shade) along a segment of the Abert Rim Fault. Boxes labeled A-C are in reference to a sequence of photographs that illustrate changing fault relations along the Abert Rim (Figure 9). AB=Alkali Butte; JM=Juniper Mountain; VB=Venator Butte; CH=Coleman Hills.

Samples targeted for geochronology are located within areas of the map that purposefully complement existing stratigraphic data and maximize structural information regarding the development of the NNE-striking and NW-striking faults.

Twelve samples were analyzed by the ^{40}Ar-^{39}Ar technique in the College of Oceanic and Atmospheric Sciences at Oregon state University (Table 1; Appendix 3). The ages of only those samples collected within the map area are discussed in detail here. For discussion of the other ages please refer to Chapters 2 (Juniper Mountain and Flint Ridge) and 4 (Rabbit Hills). Samples analyzed at Oregon State University were prepared as either mineral separates (plagioclase, sanidine, and biotite) or whole-rock cores (~100 mg). Samples and standards (Fish Canyon Tuff biotite, FCT-3, 28.04 Ma) were loaded in quartz tubes and irradiated at the TRIGA reactor facility at Oregon State University. Neutron flux was determined through analysis of the standard. Samples were degassed at 400 ºC for 20 minutes prior to analysis. Samples were analyzed over a series of heating steps (experiments) that ranged from 50 to 200 ºC in order to optimize instrumental operating parameters. Sequential exposure to Zr-AL getters served to clean the furnace regularly. Analyses were done with a Mass Analyzer Products MAP-215/50 mass spectrometer operating in peak-hopping mode (Duncan and Hogan, 1994; Duncan et al., 1997). 2-σ errors are reported for all analyses.

RESULTS

Geologic Mapping and ^{40}Ar-^{39}Ar Geochronology

The map area (Figures 4 and 5) is part of a 1:250,000 scale reconnaissance map produced by Walker (1963) that includes a large portion of Lake County. Rocks exposed

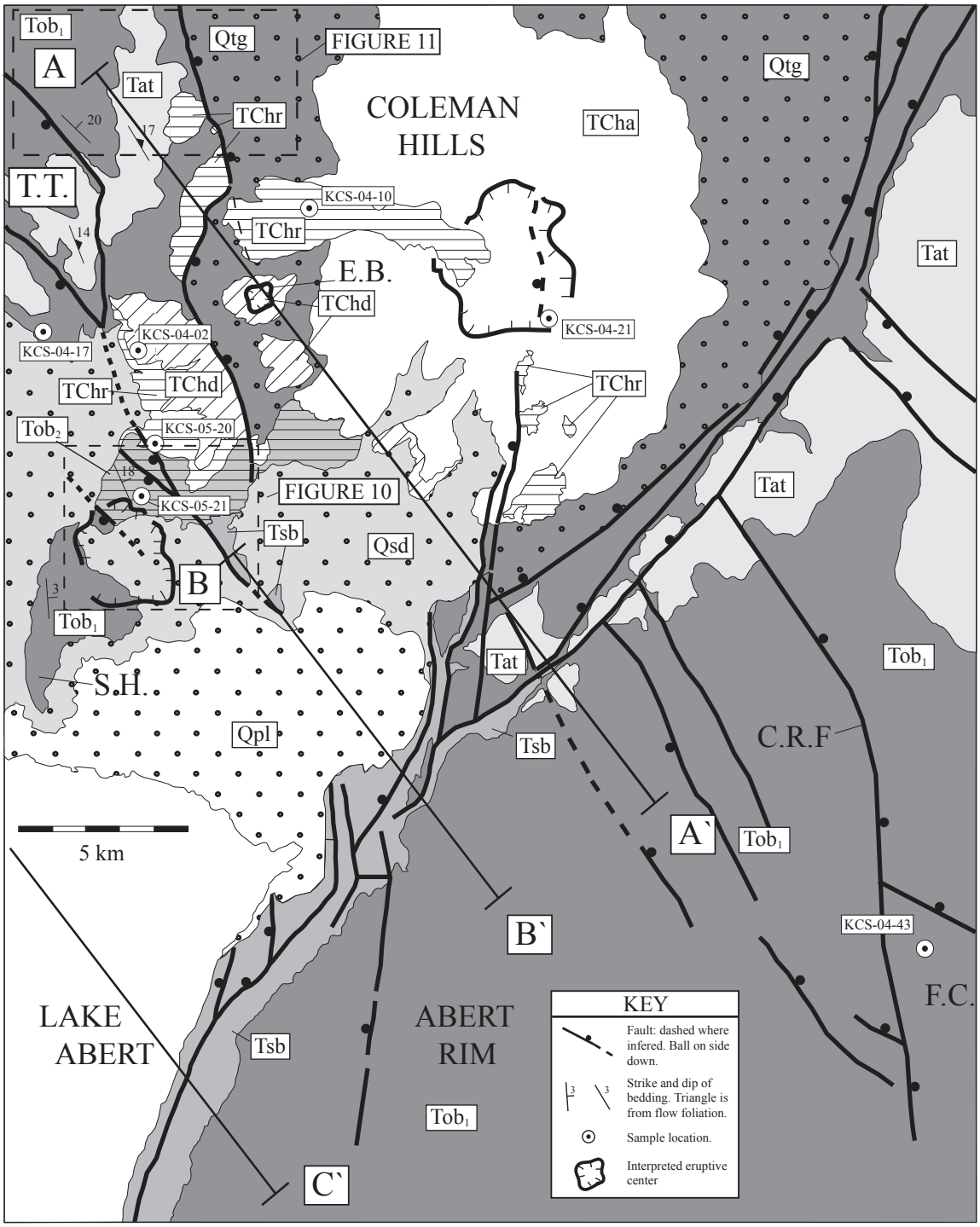

Figure 5. Sketch geologic map of the northern end of Lake Abert, OR. Description of labeled geologic units given in Figure 5 except for: Qtg=Quaternary terrace gravels; Qsd=Quaternary sand dunes; and Qpl=Quaternary playa. Figure 8 section lines (A-A` and B-B`) are shown. E.B.= Euchre Butte; S.H.= Sawed Horn; C.R.F.=Commodore Ridge Fault; F.C.=Foley Creek; T.T.=Table Top.

at the north end of Lake Abert (Figure 5) form a composite volcanic section >700 m thick (Figure 6). This section consists of two principal suites: (1) Early Miocene, dominantly intermediate composition rocks of the Coleman Hills and (2) Middle to Late Miocene, bimodal, basalt-rhyolite, lava flows and ashflow tuffs that overlie and on lap the Coleman Hills. Regionally extensive stratigraphic markers, such as the Middle Miocene Steens basalt that erupted between 16.6 and 15.3 Ma (Hooper et al., 2002), and the ~7.05 m.y. Rattlesnake Tuff (Streck and Grunder, 1995), are easy to recognize and provide stratigraphic control within the map area.

Stratigraphy of the Early Miocene Coleman Hills

The oldest units within the study area are Early Miocene intermediate to silicic volcanic and intrusive rocks that form the Coleman Hills (Figure 4). These rocks are among the oldest exposures found within southeastern Oregon. The Coleman Hills are a ~80 km^2, intermediate stratovolcano (Walker, 1963; Walker and MacLeod, 1991) that occurs in the hanging wall of the Abert Rim fault, forming a topographic barrier between the Abert and Alkali Lake basins. A field reconnaissance, geochemical and geophysical study of the area, for the purpose of mineral resource assessment, concluded that although mineralization was not obvious at the surface, rocks with gold and mercury mineralization may be located at shallow depths (Sherlock et al., 1988). Although the ages of rocks from the Coleman Hills overlap within analytical uncertainty (Table 1; Figure 7) field exposures indicate that rhyolite volcanism preceded eruption and intrusion of dacite and basaltic andesite.

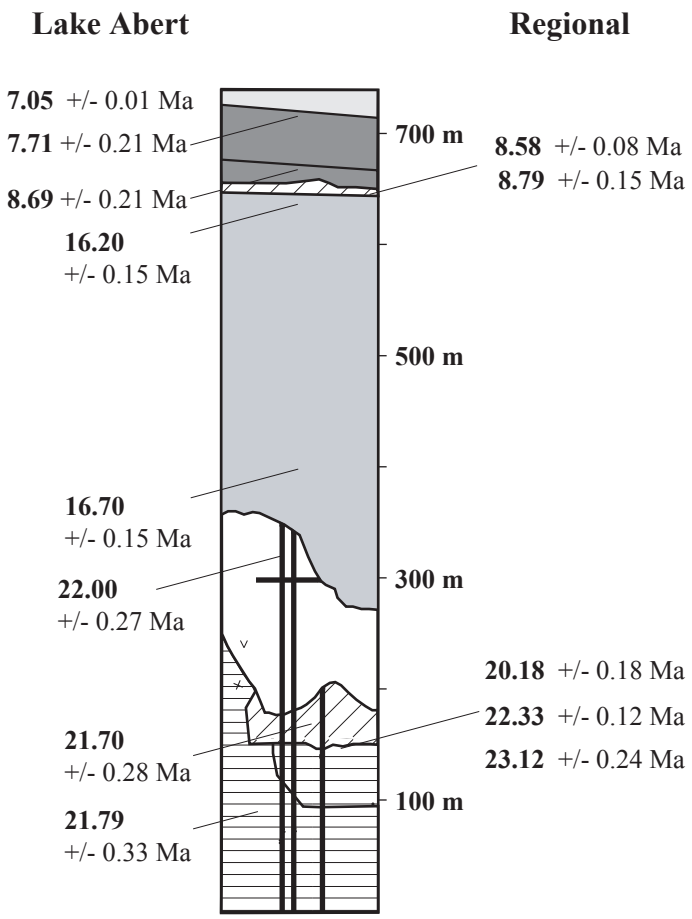

Figure 6. Composite stratigraphic section of volcanic and intrusive rocks exposed at and surrounding the north end of Lake Abert. All ages except for the Rattlesnake tuff (Tat) (Streck and Grunder, 1995) are discussed in detail in the text. Units as labeled on Figure 4: (Tchr) pyroclastic and intrusive rhyolite of the Coleman Hills; (TChd) dacite dikes and lavas; (TCha) basaltic andesite to andesite dikes, lavas and scoria tuff; (Tsb) Steens basalt; (Tob2)=basaltic lavas of crustal affinity; (Tob1) basaltic lavas of HAOT affinity.

Table 1. Summary of ^{40}Ar-^{39}Ar age results from samples collected north of Lake Abert, OR

sample	latitude	longitude	rock location/type	material dated	age analysis	steps	%^{39}Ar	K/Ca	Age (Ma)	2-σ error (Ma)
KCS-04-10	42.8108	120.1394	CH-rhyolite	sanidine	plateau	10	100.00	4.485	21.79	0.66
KCS-04-02	42.7869	120.1750	CH-dacite	plagioclase	plateau	7	88.69	0.109	21.70	0.56
KCS-04-21	42.7931	120.0847	CH-andesite	plagioclase	plateau	8	86.06	0.129	22.02	0.54
[1]KCS-06-24	42.6190	119.9096	RH-rhyolite	biotite	plateau	10	93.32	21.561	22.33	0.24
[1]KCS-06-25	42.6170	119.9152	RH-basaltic and.	plagioclase	plateau	9	95.03	0.048	23.12	0.48
[1]KCS-06-29	42.6288	119.8999	RH-rhyolite	whole-rock	plateau	7	87.89	4.345	20.34	0.36
KCS-05-20	42.7733	120.1714	LA-Steens Basalt	plagioclase	plateau	9	79.98	0.026	16.12	0.30
[2]KCS-06-16	43.0198	120.0199	FR-dacite	plagioclase	plateau	6	81.42	0.117	8.79	0.30
KCS-05-21	42.7731	120.1761	LA-basaltic and.	plagioclase	plateau	4	71.51	0.022	8.69	0.42
[2]KCS-06-37	42.9326	119.9272	JM-rhyolite	biotite	plateau	10	95.95	20.076	8.58	0.16
KCS-04-43	42.6764	120.0125	LA-basalt	whole-rock	plateau	6	83.22	0.042	7.72	0.46
KCS-04-17	42.7933	120.1967	LA-basalt	whole-rock	plateau	5	66.95	0.030	7.71	0.42

CH-Coleman Hills; RH-Rabbit Hills; LA-Lake Abert; FR-Flint Ridge; JM-Juniper Mountain.

[1]See Chapter 4 for discussion of these units; 2See Chapter [2] for discussion of these units.

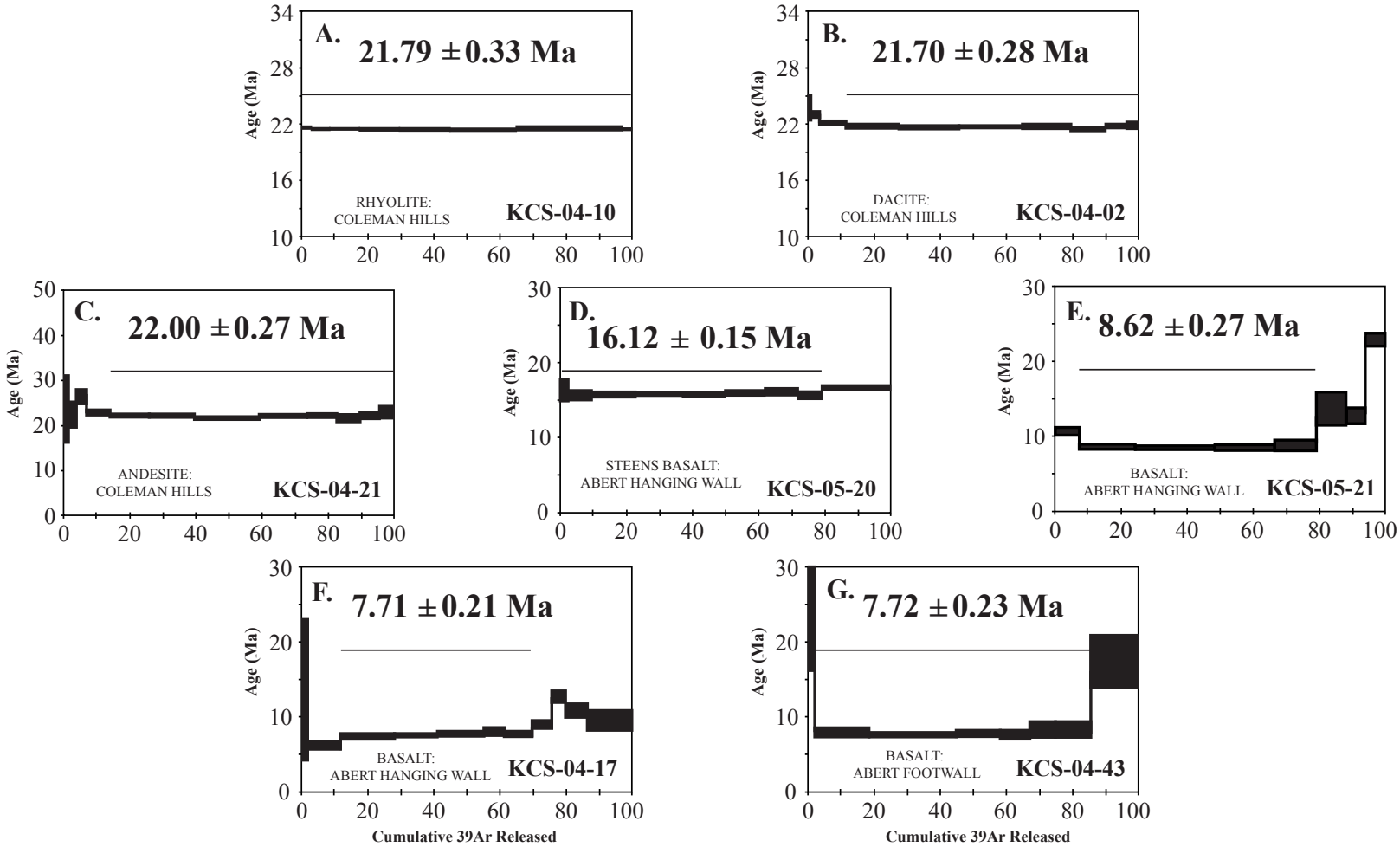

Figure 7 ^{40}Ar-^{39}Ar spectra for samples collected near the north end of Lake Abert. Bars under ages span the ^{39}Ar release steps used in the age calculation. See Table 1 for details. Rock type and general sample locations given on diagrams. Sample locations shown on Figure 4.

Rhyolite volcanism represents the initial phase of magmatism within the Coleman Hills volcanic complex (Figure 8). An explosive eruption accompanied intrusion of rhyolite domes, as evidenced by localized surge and block and ash deposits preserved around the margins of the volcano. The main rhyolite stock trends ~E-W and is located on the west side of the volcanic complex (Figure 4) where it is at least 200 m thick. A $^{40}Ar/^{39}Ar$ analysis of a sanidine separate produced a 10-step plateau age of 21.79 ± 0.66 Ma (KCS-04-10; Figure 7A, Table 1). This sample exhibits a non-complex ^{39}Ar release pattern and the plateau age is based on 100 % of the ^{39}Ar released by the sample (Figure 7B). Rhyolite pyroclastic deposits are undifferentiated from rhyolite intrusions on the map (Figure 5) and thickness in localized exposures range from 3-5 m for block and ash flows and >30 m for surge deposits.

Dacite of the Coleman Hills is thickest near its source at Euchre Butte (Figure 4) where a ~50 m section is exposed. Dacite flows, fed by dikes 3-5 m wide, cap a narrow paleochannel filled with a rhyolitic block and ash deposit on the western margin of the Coleman Hills (Figure 5). $^{40}Ar/^{39}Ar$ analysis of a plagioclase separate obtained from the top of the flow sequence produced a 7-step plateau age of 21.70 ± 0.56 Ma (KCS-04-02; Figure 7B, Table 1). The ^{39}Ar release pattern for this sample is relatively uniform with a small amount of excess argon present in the low temperature steps (Figure 7B). Excess argon in heating steps is indicative of incomplete equilibration of the magma with the atmosphere.

Andesite and basaltic andesites are the dominant compositions of the Coleman Hills. Andesite dikes 3-5 m thick cut dacite units (Figure 8) and feed flows that radiate from the center of the volcano. An extensive scoria tuff and dike swarm defines the

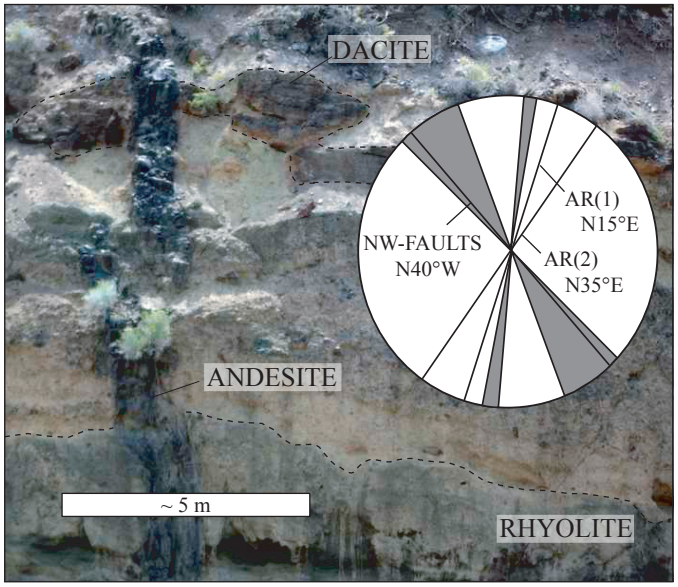

Figure 8. Andesite dike cuts rhyolite and dacite units within the Coleman Hills. Inset shows orientations of andesite and dacite dikes (shaded grey) relative to the average trends of faults in the map area. AR(1)- faults associated with Abert Rim Fault system that cut center of the Coleman Hills; AR(2)- average trend of other faults that comprise the Abert Rim Fault system.

principal vent and the volcanic edifice of the volcanic complex (Figure 5). The thickness of this unit ranges from ~75-150 m (Figure 6). $^{40}Ar/^{39}Ar$ analysis of a plagioclase separate of glass from the margin of a basaltic andesite dike produced an 8-step plateau age of 22.02 ± 0.54 Ma (KCS-04-21; Figure 7C, Table 1). ^{39}Ar release in this sample shows the effects of ^{39}Ar recoil in the early temperature steps (Figure 7C).

Stratigraphy of Middle to Late Miocene rock units

The Middle to Late Miocene section in the field area consists of a bimodal, dominantly mafic, basalt-rhyolite suite that was deposited between ~16 and 7 Ma (Figure 6). This section is typical of Late Cenozoic volcanism across a broad region east of the Cascades volcanic arc in Oregon.

Middle Miocene Steens basalt is easily recognized by its coarseness; it contains plagioclase laths that are up to ~5 cm in length and is exposed in most of the escarpments across southeastern Oregon (Figure 2). Steens basalt was erupted across the region between 16.6 and 15.3 Ma (Hooper et al., 2002) and correlation of sections exposed in escarpments on the basis of age, chemical and paleomagnetic data suggests that the unit is ~450 m thick within the Abert Rim (Mankinen et al., 1987). Within the map area (Figure 5) the exposed thickness of the Steens basalt decreases from ~365 m to ~150 m to the north over a distance of ~10 km, along-strike of the Abert Rim fault. $^{40}Ar/^{39}Ar$ analysis of a plagioclase separate from the top of the section exposed in the hanging wall of the Abert Rim fault system produced an 8-step plateau age of 16.12 ± 0.30 Ma (KCS-05-20; Figure 7D, Table 1). ^{39}Ar release in this sample shows slight effects of ^{39}Ar recoil in the early temperature steps (Figure 7D).

Late Miocene basalt overlies the Steens section in the field area and is chemically similar to compositions that have erupted on the HLP (Figure 3) during the past ~10 Ma (e.g., Jordan, 2001; Jordan et al., 2004). The base of this section consists of at least 40 m of lavas that exhibit chemical and radiogenic isotopic characteristics, such as higher SiO_2 and $^{87}Sr/^{86}Sr$ and lower $^{143}Nd/^{144}Nd$ (see Chapter 2), which indicate a larger degree of interaction with crustal rocks, relative to the remainder of the basalt section. This sequence consists of 2-3 basalt flows that are exclusively exposed southwest of the Coleman Hills where they are cut by a system of NW-striking faults (Figures 5). $^{40}Ar/^{39}Ar$ analysis of a plagioclase separate from the top flow produced a 4-step plateau age of 8.69 ± 0.42 Ma (KCS-05-21; Figure 7E Table 1). This sample exhibits an excess argon release pattern (Figure 7E), particularly in the high temperature heating steps. The remaining lavas are compositionally similar to mantle melts, high-alumina olivine tholeiite (HAOT) of Hart (1984), and achieve a maximum thickness of 50-60 m. The thickest exposure of this unit occurs in Foley Creek, located within the southeastern corner of the map area (Figure 4), where the basalt section consists of 4 flows that are each ~10-15 m thick. The top ~25 m of this unit is exposed in the hanging wall of the Abert Rim Fault system.

$^{40}Ar/^{39}Ar$ analyses of whole-rock cores from the top flow of sections exposed on either side of the Abert Rim Fault system (Figure 4) yield a 5-step plateau age of 7.71 ± 0.42 Ma for basalt in the hanging wall (KCS-04-17; Figure 7F, Table 1) and a 6-step plateau age of 7.72 ± 0.23 Ma for basalt in the footwall (KCS-04-43; Figure 7G Table 1). The former sample displays a complex ^{39}Ar release pattern (Figure 7F) and exhibits excess argon in the low temperature steps and displays the effects of minor ^{39}Ar recoil in

the high-temperature steps. A U-shaped ^{39}Ar release pattern exhibited by the latter sample (Figure 7G) reflects excess argon in the early and late heating steps.

HAOT lavas are capped by the 7.05 Ma Rattlesnake Tuff (Streck and Grunder, 1995) across the study area. The Rattlesnake Tuff is only exposed in half of the map area, extending to just south of the Coleman Hills on both flanks of the volcanic complex (Figure 4). Exposures of Rattlesnake Tuff near Lake Abert likely represent the southern limit of the tuff in the region.

STRUCTURAL GEOLOGY

Faults that cut volcanic strata in the study area (Figure 6) are grouped into three systems: (1) NW-striking faults, (2) south segment of Abert Rim fault, and (3) north segment of Abert Rim fault. NW-striking faults display an average trend of ~N40°W and occur within a ~5-10 km wide zone that crosses the Abert Rim (Figure 5). The Abert Rim fault is subdivided into two segments for two principal reasons: (1) the trend of the Abert Rim fault abruptly changes by ~20°, from a strike of ~ N15°E to ~ N35°E, where the fault splays into multiple strands (Figure 5), and (2) interactions between the principal NNE- and NW-striking fault sets change along-strike of the Abert rim fault, where from south to north: (a) NNE faults cut NW faults, (b) the fault sets are mutually cross-cut, and (c) NW faults cut NNE faults (Figure 9).

NW-striking faults

The footwall of the Abert Rim (Figure 4) consists of a conformable Late Cenozoic section (Figure 5) that is tilted ~2-5° to the east. The section is cut by 9-10

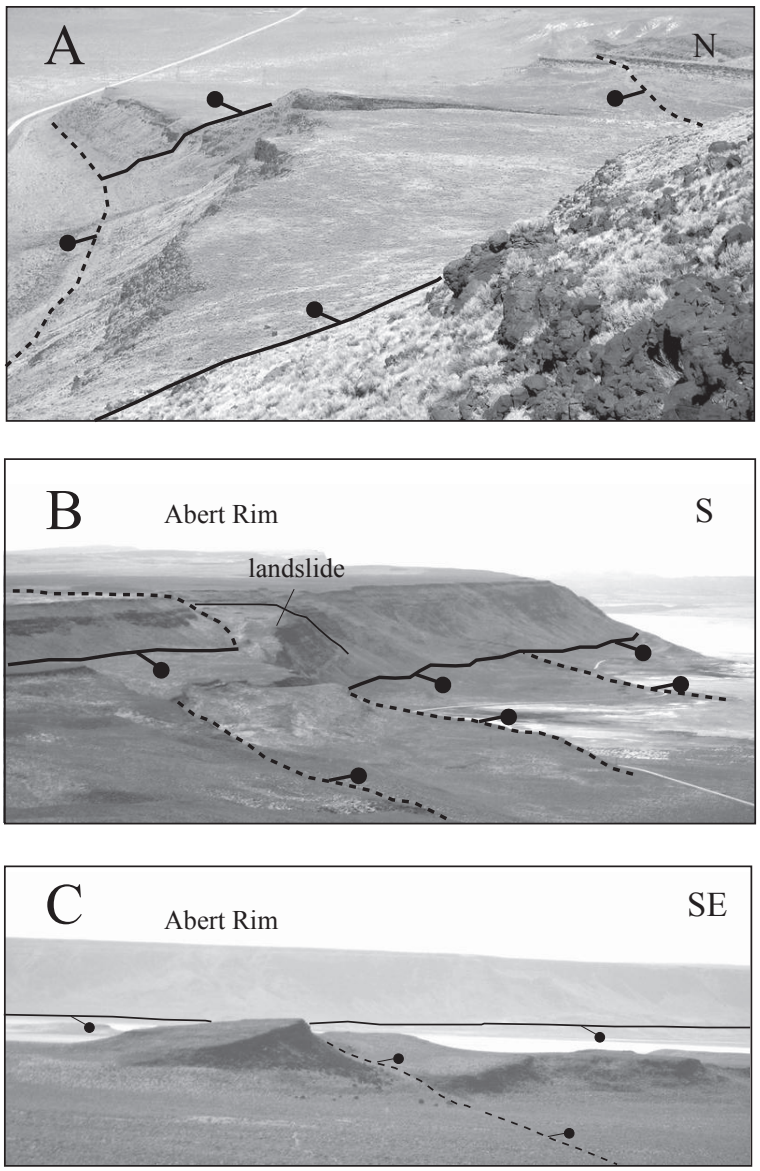

Figure 9. Photographs illustrate along-strike morphology of the principal NW- and NNE-striking faults, dashed and solid lines, respectively. From south to north along the escarpment (see Figure 4 for position of photographs): (A) NW-striking faults cut NNE-striking faults, (B) the fault sets are mutaully cross-cut, (C) NNE-striking faults cut NW-striking faults.

predominantly NW-striking faults that have an average length of ~7 km and an average strike of ~N40°W. These faults produce a series of NW-SE-trending low-relief horst and graben structures within the footwall block of the Abert Rim. Displacement along any of these faults is minor but difficult to gauge because they cut only Rattlesnake Tuff and basalt (Tob1) without exposing any older units (Figure 5). The Commodore Ridge fault, which is ~13 km long, east dipping, ~N-S striking fault that bends NW along-strike to the north, exhibits the most pronounced scarp and offsets basalt (Tob_1) by a maximum of ~60 m.

NW-striking faults within the hanging wall of the Abert Rim are curved and have a north component to their strike, relative to NW-striking faults in the footwall block, and are more complex because they record differential tilt as a function of age (Figures 10 and 11). A set of two west-dipping faults located north of the Sawed Horn (Figure 5) strike ~N40°W and create a ~10-15° angular unconformity between 7.7 Ma and 8.6 Ma basalt units (Figure 10). The larger of these two faults can be traced for ~3 km before it splays and bends to the north. Just north of this zone a pair of ~N-S trending, east-dipping, ~3 km long faults cut dacite of the Coleman Hills before converging into a single east-dipping fault zone that strikes ~N25°E (Figure 5). To the north, this fault intersects an east-dipping fault that trends ~N15°W and together they form the western margin of a ~N-S-trending sedimentary basin in which the Middle to Late Miocene volcanic units have been buried by Quaternary sediments. The northern end of this fault system, near Table Top (Figure 5) is of particular interest because the footwall block preserves a depositional contact between Oligocene and Miocene units and contains units that exhibit differential tilt (Figure 11). An angular unconformity of

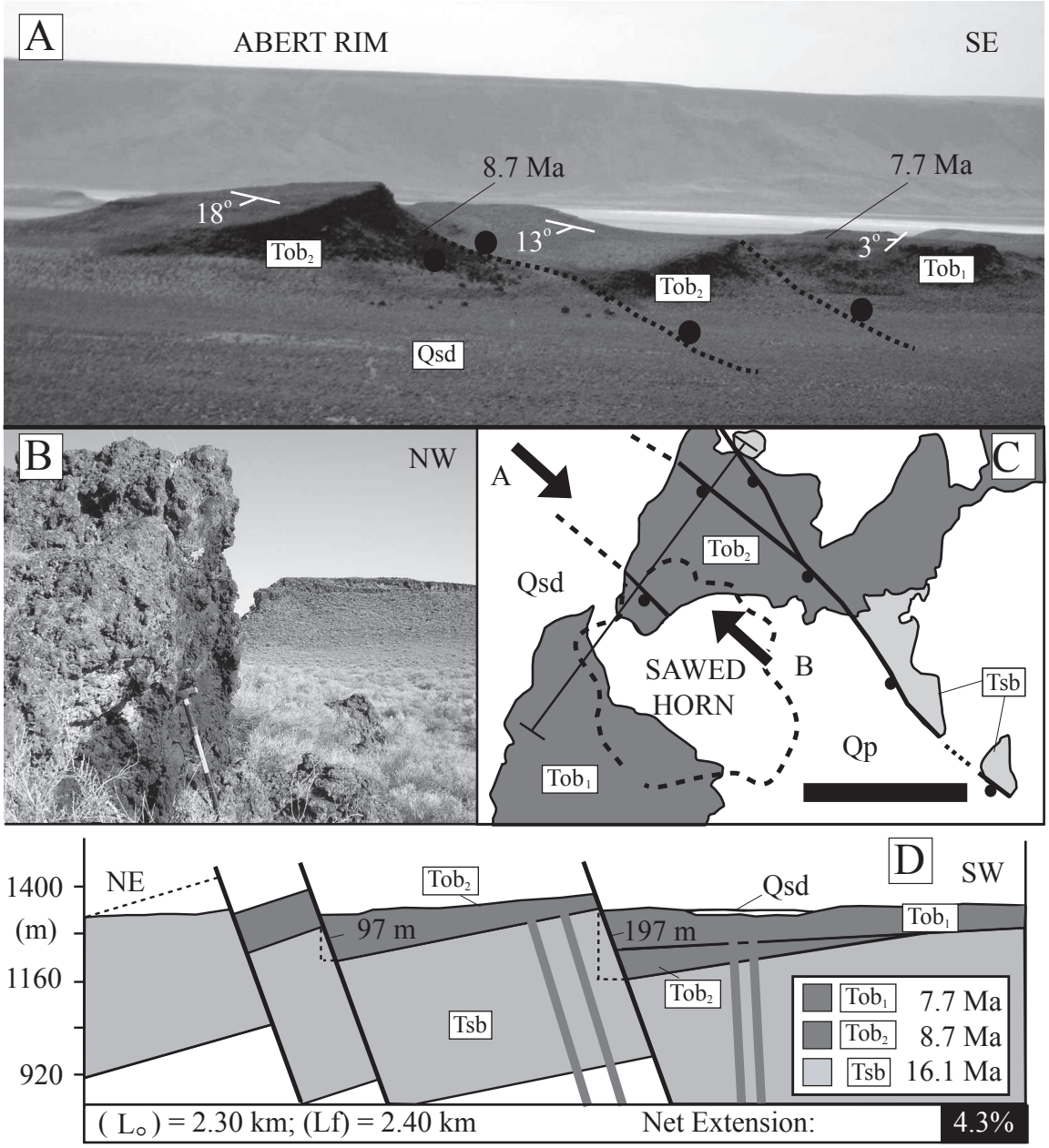

Figure 10. (A) Oblique view of younger lavas banked onto NW-striking faults cut into older lavas near Sawed Horn with the Abert Rim fault in the backdrop. See figure 5 for description of map units. (B) Scoria and cinders from thick lavas. (C) Map view of the unconformable relationship between the lavas. Perspective of photographs A and B given by arrows; (D) Cross-section interpretation of unconformable relationship showing dikes feeding lava flows.

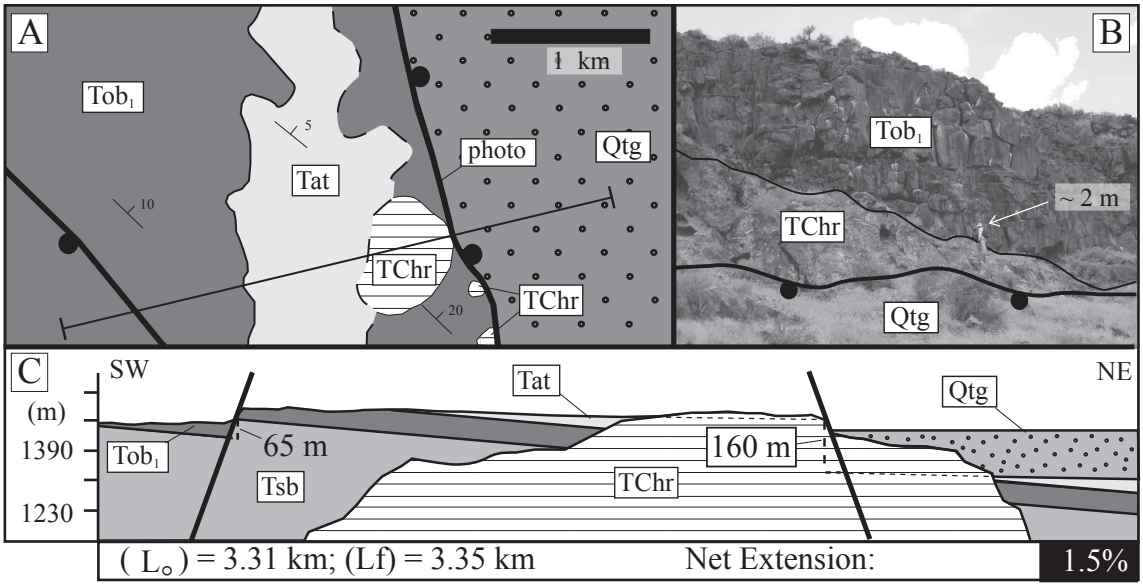

Figure 11. (A) Map view of NW-striking faults in the northwestern corner of the map area (see Figure 4). Unit labels are same as previous figures. (B) Depositional cantact between Tob_1 and TChr exposed in a fault scarp. (C) cross-section illustrating differences in tilt between Tob_1 and Tat. Line of section shown on panel A.

~5° is preserved between 7.05 Ma Rattlesnake Tuff (Streck and Grunder, 1995) and 7.7 Ma (Tob_1; Figure 5). Deposition of 7.7 Ma lavas directly on top of Oligocene rhyolite of the Coleman Hills is not seen elsewhere in the study area.

Southern segment: Abert Rim fault

The southern segment of the Abert Rim Fault system is defined by a group of faults that occur along a strike line of ~N15°E from Lake Abert extending northward into the center of the Coleman Hills (Figure 4). This segment of the Abert Rim controls the eastern extent of the Lake Abert basin and truncates Quaternary colluvium (gravels?) that surrounds the Coleman Hills. West-dipping faults of this segment strike ~N15°-20°E, collectively, and define the topographic escarpment commonly referred to as the Abert Rim (Figure 8; section B-B`). Fault splays that strike between N10°W and N10°E are common and act in concert with the more easterly striking faults to produce a zig-zag fault trace. The ~N-S trending faults occur as shorter ~1 to 3 km segments that join the NE-trending structures and project into the Lake Abert basin. Two of these faults extend 6-9 km northward into the Coleman Hills.

Northern segment: Abert Rim fault

Just north of the Coleman Hills, at the latitude of the Sawed Horn, the Abert Rim fault system is a fault zone characterized by a number of strands (Figure 5). Faults of the northern segment follow a more easterly strike line of ~N35°E relative to the southern segment. This transition marks the boundary of the northern segment of the Abert Rim, which trends ~N45°E and extends northward through the map area. The northern

segments of the fault system are also characterized by lower topographic relief, from ~400 m to ~225 m, over an along-strike distance of ~3 km (Figure 8). An apparent decline in structural relief from the southern to northern segments of the fault coincides with a decrease in topographic relief, from ~400 m to the south to ~225 m to the north (Figure 9B). The decline in topographic relief likely reflects a decline in stratigraphic separation as a ~300 m thick exposures of the Steens basalt in the southern segment gradually thins to the north before it is not exposed at all (Figure 5).

TIMING OF DEFORMATION

Previous work in the NWBR (Dilles and Gans, 1995; Johnson and Grunder, 2000; Colgan et al., 2004; Faulds et al., 2005;) suggests that the onset of Basin and Range extension in southern Oregon occurred sometime after 12 Ma (Figure 1) with the earliest deformation recognized at Steens Mountain (Figure 2) by 10 Ma. Sparse data exist in southern Oregon that would suggest tilting of stratigraphic units due to tectonic uplift prior to ~16 Ma. Three intervals of structural development are recognized at Lake Abert that can be used to evaluate the timing of extensional deformation in southern Oregon.

Oligocene magmatism

Structural elements of Early Miocene magamtism, such as dikes and dome alignments, exhibit similar orientations to faults that developed within Middle and Late Miocene volcanic strata in the field area (Figures 4 and 7). Andesite and dacite dikes (Figure 8) occur along N5°-10°E or N20°-45°W fractures and map patterns (Figure 5) suggest that rhyolite domes of the Coleman Hills were emplaced along ~N-S and ~E-W

trending structures. Thus, the tectonic fabric produced by Early Miocene magmatism is mimicked in younger episodes of faulting in the field area (Figure 5), particularly within NW-striking faults and the southern segment of the Abert Rim Fault. Onlapping contact relations between Steens basalt and rhyolite of the Coleman Hills suggests ~500 m of paleo-relief, likely volcanic, existed prior to ~16 Ma (Figure 12). Deposition of ~7.7 Ma basalt directly against ~22 Ma rhyolite of the Coleman Hills (Figure 11) provides further support for the existence of significant, pre-16 Ma paleo-relief near Lake Abert. Correlated exposures of Steens basalt by Mankinen et al. (1987) show that pre-Steens topography was irregular and that local relief of ~ 1000 m may have existed in places.

Late Cenozoic faulting: 16-7 Ma

Partial restorations across the southern segment of the Abert Rim fault (Figure 13) and differences in tilt of volcanic units cut by NW-striking faults suggest that NNE-striking and NW-striking faults were both active in the region prior to ~7Ma. Restoration of measured vertical offset of the ~16 Ma Steens basalt shows that nearly half of the present-day structural relief on the southern segment of the Abert Rim fault existed prior to deposition of the Rattlesnake tuff at ~7 Ma (Figure 13). NW-striking faults were active in the hanging wall of the Abert Rim fault between ~8.6 and 7 Ma. South of the Coleman Hills, near the Sawed Horn (Figure 5), 8.6 Ma lavas were tilted 10-15º along a pair of west-dipping, NW-striking normal faults prior to deposition of

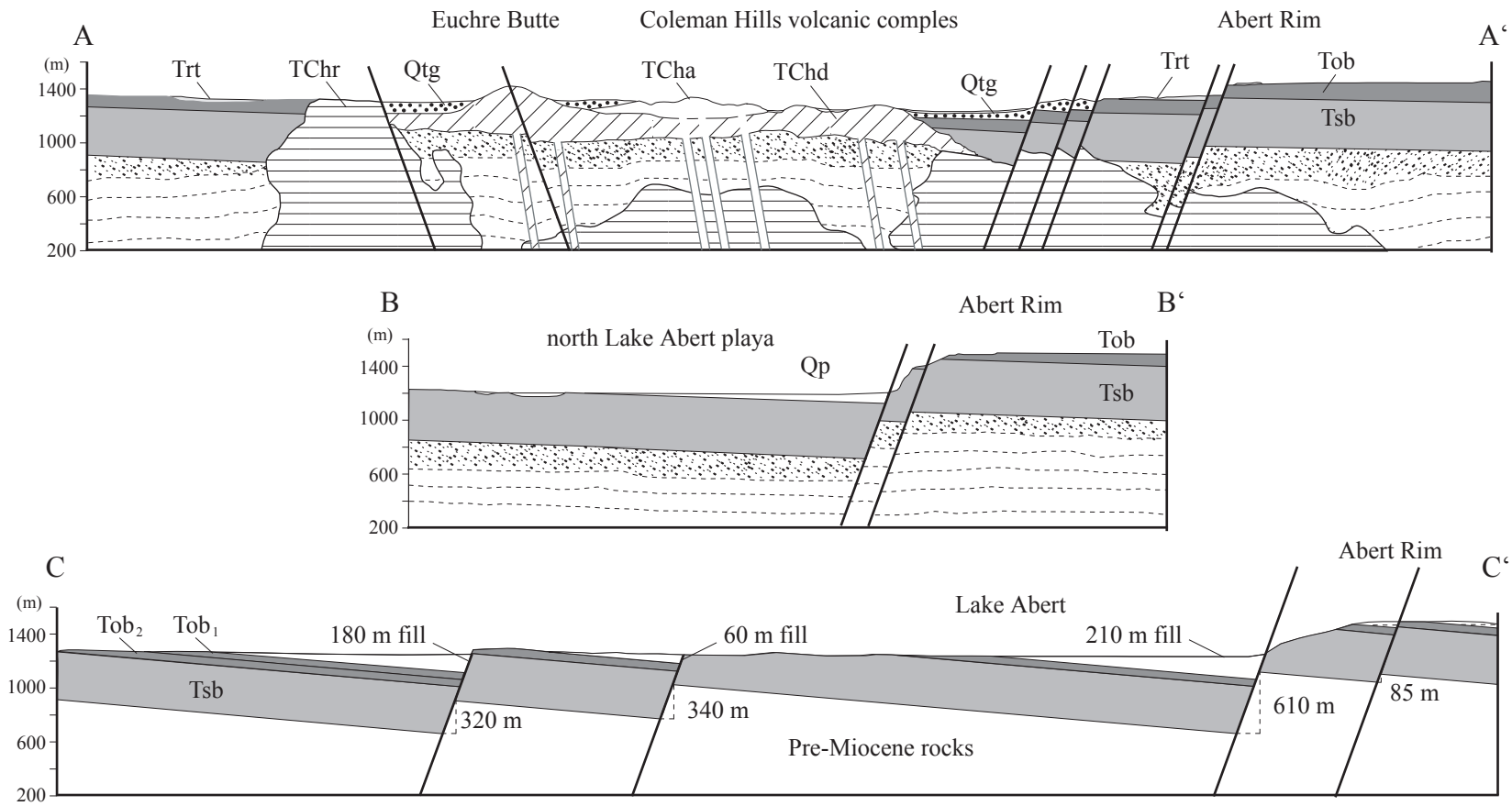

Figure 12. Cross-sections through the Abert Rim and Coleman Hills. Line of sections shown on figure 5 (section line C-C’ only shown partially).Tertiary basement rocks older than the Coleman Hills are not exposed (shown here by dashed lines and dot pattern). Qtg=Terrace gravels; Qp=Playa; Trt=Rattlesnake Tuff; Tob=7.7 Ma olivine basalt; Tsb=Steens Basalt; TCha=Coleman Hills andesite; TChd=Coleman Hills dacite; TChr=Coleman Hills rhyolite. Horizontal length of sections: (A-A’): 10.75 km; (B-B’): 5.80 km; (C-C’): 13.40 km. No vertical exaggeration. Dip of strata 2° (A-A’; B-B’), 5° (C-C’). Faults dip 70°.

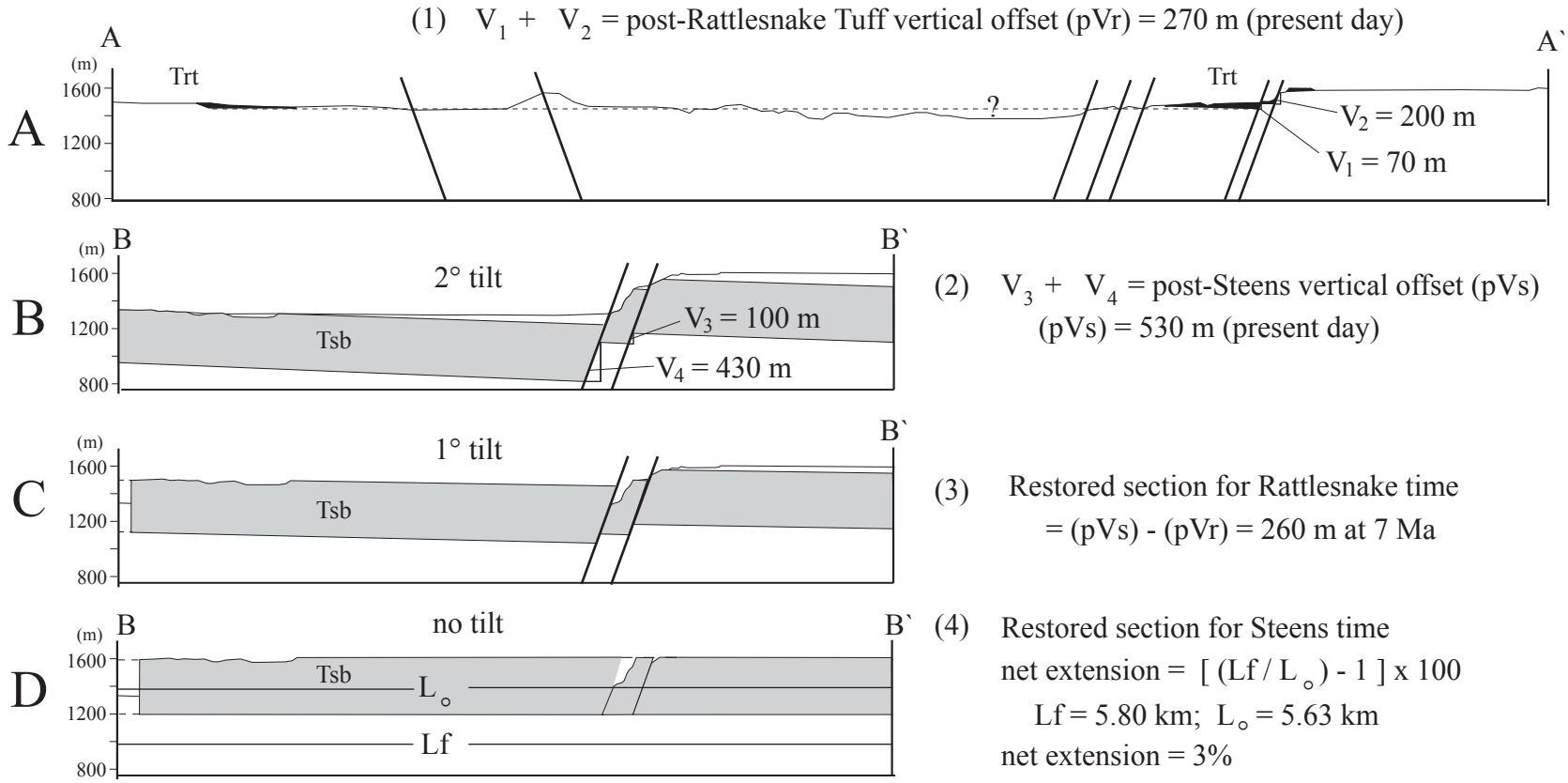

Figure 13. Calculation of separation and net extension along a portion of the Abert Rim Fault system from restored cross-sections. Panels A and B show are simplified from Figure 12 (A-A' and B-B' respectively). Panels C and D show partial restorations for Rattlesnake and Steens time. Faults dip 70° and the thickness of Steens basalt is assumed constant at 450 m (e.g., Maniken et al., 1987). Steens basalt does not outcrop in panel A, as shown on Figure 12. No vertical exaggeration.

7.7 Ma basalt flows (Figure 10). In the northwestern corner of the map area, near Table Top (Figure 5), footwall uplift on a west-dipping NW-striking normal fault between ~7.7 and 7.0 Ma is recorded by a 5º angular discordance between the Rattlesnake Tuff and the basalt flows that underlie it (Figure 11).

Late Cenozoic faulting: post-7 Ma

Structural development near Lake Abert continued after 7 Ma as many of the faults, both NNE-striking and NW-striking, cut the Rattlesnake Tuff. Dislocation along the northern segment of the Abert Rim fault (Figure 13) post-dates 7 Ma.

MAGNITUDE OF DEFORMATION

In general, Miocene volcanic units exhibit very small amounts of tilt (2-5º) and are cut by steeply dipping (assumed ~70º) faults, which suggests that the magnitude of extension within the map area is small. The magnitude of extension across NW-striking faults in the field area (Figure 4) is derived by integrating extension estimates from individual faults from cross-sections within the hanging wall of the Abert Rim (Figures 10 and 11). The degree of extension across a ~6 km wide zone of 4-5 faults that strike ~N40°W decreases from south to north and a net value of ~3% is calculated. Net extension since ~16 Ma across the southern segment of the Abert Rim (Figure 12; B-B') is estimated at ~3 % (Figure 13). Next extension along the northern segment of the Abert Rim (Figure 12; B-B') is not estimated but is even less. A maximum of ~15% extension across the Abert Rim and Lake Abert Basin in the southern extreme of the map area (Figure 5) is calculated by assuming larger tilts (5º) and the presence of buried faults

underneath the Lake Abert basin (Figure 12; C-C'). This model predicts structural control of sedimentation and segmentation of the Lake Abert basin into multiple sub-basins that are filled with modest thicknesses, 60 m to >200 m, amounts of Quaternary sediments.

GEOLOGIC RATES OF DEFORMATION

Active deformation measured via GPS shows that strain decreases systematically with latitude (Figure 1) from ~14 mm/yr near 35˚ N to as little as ~2 mm/yr at 41˚ N (Figure 1) (Bennett et al., 1998; Thatcher et al., 1999, Miller et al., 2001; Oldow, 2003). A slip rate of ~0.5 mm/yr is calculated for displacement along a portion of the NE-striking Abert Rim since ~16 K.y. (Pezzonpane and Weldon, 1993). Long-term rates of deformation for any of the major fault systems in southern Oregon (Figure 2), or NW-striking fault systems, have not been estimated.

Rates of extension for NW-striking faults are documented at three locations within a 5-10 km wide zone in the study area (Figure 4): (1) southwest corner of the Abert Rim hanging wall (Figure 10), (2) northwest corner of the Abert Rim hanging wall (Figure 11) and, (3) the Commodore Ridge fault within the Abert Rim footwall (Figure 5). Individual faults within this zone began to form prior to 7.7 Ma and produced normal offset at a rate ranging from ~0.30 to 0.01 mm/yr. An extension rate of 0.3 mm/yr is calculated for a set of three faults located at the southern end of the NW-striking fault system (Figure 10) where faults were active between 8.7 and 7.7 Ma. This deformation records the earliest phase of extension documented in the field site. Across-strike of the NW-striking fault system, to the north (Figure 11), the extension rate decreases significantly. A rate of 0.1 mm/yr is calculated for displacement of Tob1 during footwall

uplift between 7.7 and 7.0 Ma. A rate of ~0.01 mm/yr since 7.7 Ma is calculated for the Commodore Ridge fault within the Abert Rim footwall block. Thus, the greatest rates of extension along NW-striking structures occurred within the hanging wall of the Abert Rim at the southern end of the system (Figure 5) and during the earliest stages of deformation. The rate of extension declines to the north and through time, suggesting that following an initial burst of deformation beginning after 8.7 Ma strain was gradually transferred northward and then to another fault system, perhaps NE-striking, by 7.0 Ma.

Long-term rates of extension for the NE-striking Abert Rim fault are calculated for southern and northern segments of the fault system at intervals of 7.7 to 7 Ma and post 7 Ma, respectively. These fault segments are interpreted to overlap and join just south of the Coleman Hills (Figure 5). Extension on the southern segment of the fault occurred at a rate of ~0.4 mm/yr following deposition of the 7.7 Ma HAOT (Tob1) and prior to eruption of the 7.05 Ma Rattlesnake Tuff. Extension along the northern segment of the fault occurred after eruption of the Rattlesnake Tuff and at a rate of ~0.04 mm/yr. The latter estimate is an order of magnitude lower than that for the southern segment of the Abert Rim as well as the latest Pleistocene estimate of 0.5 mm/yr (Pezzopanne and Weldon, 1993). This might suggest that the rate of extension on the northern segment of the Abert Rim Fault system has increased significantly since the Quaternary.

DISCUSSION

The intermeshed fabric of NW-striking and NNE-striking faults, characteristic of the margin of the Basin and Range Province in southern Oregon (Figure 3) are interpreted to form in response to the modern stress field in the region (Donath, 1962; Pezzopane and

Weldon, 1993; Crider, 2001). The occurrence of Early Miocene dikes that mimmick Late Miocene fault trends (Figure 8) is evidence for extensional faulting near Lake Abert prior to Steens volcanism and suggests that Late Miocene faulting may have reactivated a pre-existing regional structural fabric.

Regional studies (Maloney, 1961; Legge, 1988; Sherrod et al., 1988; Sawlan et al., 1994) suggest that NW-striking faults form prior to or, coeval with, the development of NE-striking faults in any particular area of the NWBR in Oregon. At Lake Abert it is clear that NW-striking faults formed within a narrow zone (~5 km) at the latitude of the Coleman Hills (Figure 5) prior to the appearance of a through-going Abert Rim fault.

Regional Model for NW-Propagation of the Basin and Range

Development and northward propagation of the Walker Lane, the western boundary of the Basin and Range north of 40°N lat. (Figure 1) provides the most obvious tectonic explanation for the progression of faulting observed in southern Oregon. The structural development of the Abert Rim can be linked to regional tectonic events (Figure 14). Arc volcanism was active inboard of a subduction zone along the entire west coast ~22 Ma (e.g., Christiansen and Yeats, 1992). The Coleman Hills, a dominantly andesitic stratovolcano was a component of this arc. Dikes associated with emplacement of the Coleman Hills occurred along a set of conjugate shear fractures, consistent with a transtensional arc setting (Nakamura and Uyeda, 1980). By ~15 Ma The Walker Lane had formed (Faulds et al., 2005) within the continental interior and began to propagate northward as it accommodated plate motion. Basin and Range faulting occurred throughout Nevada (e.g., Colgan et al., 2004) and into Oregon at Steens Mountain by

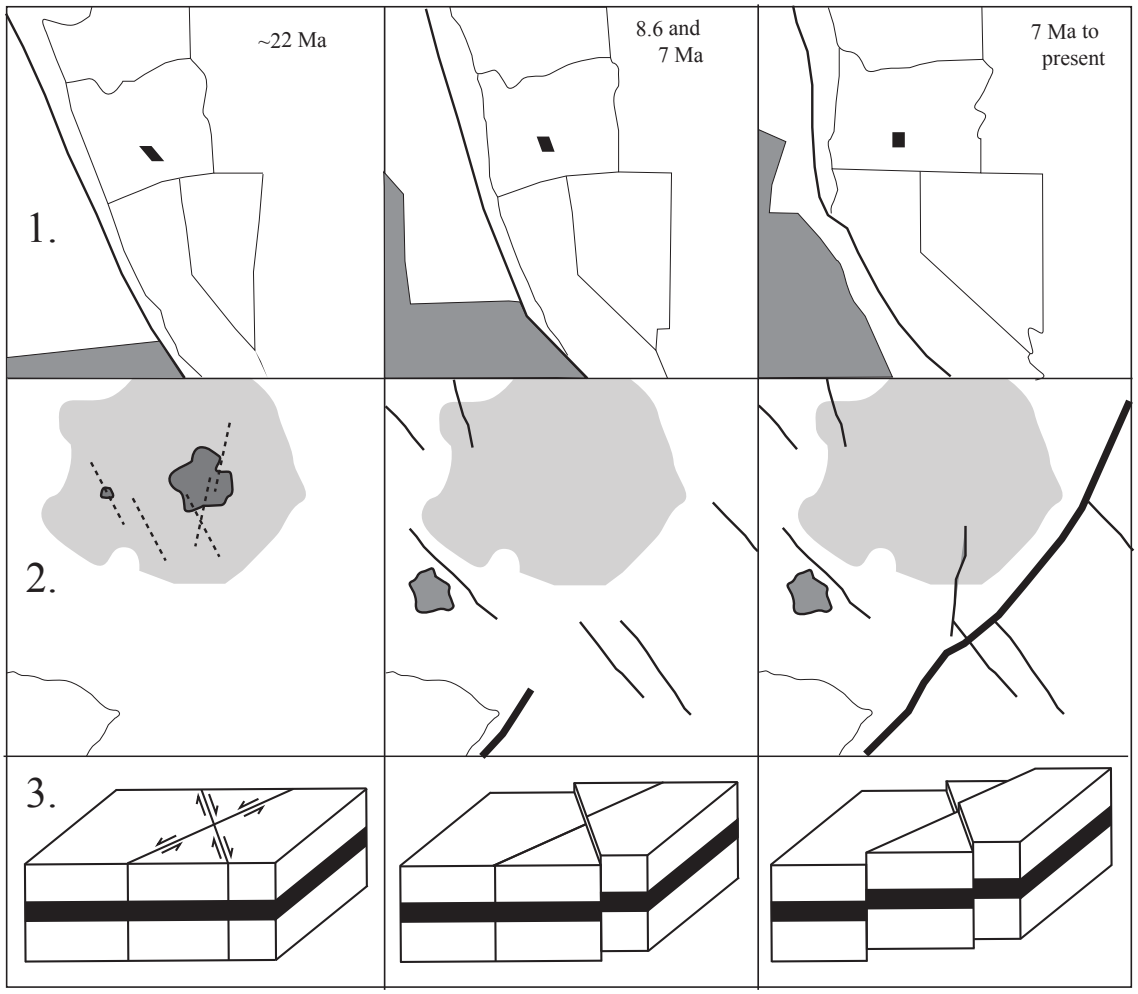

Figure 14. Summary of clonclusions regarding the tectonic development of the study area. Panel (1) shows evolution of the western margin of North America since ~22 Ma. Panel (2) shows structural development of faults in the study area. Abert Rim is shown by heavy line. Panel (3) a simplified block diagram relating 2D deformation along the primary NW- and NE-striking fault sets.

10 Ma (Johnson and Grunder, 2000). At 8 Ma, to the west, volcanism and deformation along NW-striking features near Lake Abert may reflect dilatational fracturing ahead of a northward propagation NNE-striking Basin and Range fault formed at the tip of the Walker Lane (e.g. Faulds et al, 2005). Dilatational fracturing ahead of propagating normal faults is observed elsewhere within the Basin and Range Province (e.g., Murphy et al., 2004; Rowley, 1998) and within propagating rift systems around the world (e.g., Khodayar, 1999; Tentler and Mazzoli, 2005).

Implications for the Kinematic Nature of the Brothers Fault Zone

A lack of measurable extensional strain (Thatcher et al., 1999) within a region proposed to accommodate as much as 6 mm/yr (Pezzopanne and Weldon) suggests that strain is accommodated by magmatic addition rather than extensional faulting within the NWBR. If NE-striking regional escarpments are in fact propagating northward with time, than the alignment of fissures and faults within the Brothers Fault Zone (BFZ) suggests that NW-diking occurs at the tips of propagating NE-trending Basin and Range faults (Figs. 2b and 3). Perhaps dike emplacement within the Coleman Hills near Lake Abert (Fig. 3a) reflects this process. Dilatational fracturing ahead of propagating normal faults is observed elsewhere within the Basin and Range Province (e.g., Murphy et al., 2004: Rowley, 1998) and within propagating rift systems around the world (e.g., Khodayar, 1999; Tentler and Mazzoli, 2005). In this model, Basin and Range faults that extend up to the High Lava Plains (Figure 2b) will eventually cut, and perhaps link via, NW-striking faults over million year time scales. The Brothers Fault Zone will either be abandoned in favor of a newly formed transverse zone to the north, or develop into a

lithosphere-scale transfer fault that accommodates significant plate motion like the Walker Lane and San Andreas.

CONCLUSIONS

We report new ^{40}Ar-^{39}Ar ages for twelve Miocene volcanic rocks. These analyses are complimented with detailed geologic mapping of volcanic units and their relation to NW- and NNE-striking extensional structures near Abert Rim, one of the primary Basin and Range faults in southern Oregon. The ages indicate that volcanic activity was centered near Abert Rim between ~21-23 Ma and ~9-7 Ma. Early Miocene magmatism is related to arc volcanism and/or transtensional rifting whereas Late Miocene magmatism is related to the structural development of the Abert Rim.

Early Miocene dikes mimic the strike of Late Miocene faults although it is not clear whether or not extensional faulting occurred during this time. Extensional deformation was ongoing near Lake Abert by 7 Ma. At roughly the latitude of the study area, the onset of extension within the High Cascade graben to the west occurred at ~4.5 Ma (Hughes and Taylor, 1986) and extensional faulting at Steens Mountain, to the east, was ongoing by ~10 Ma (Johnson and Grunder, 2000). Within the study area, partial restoration of cross-sections illustrates that the southern segment of the Abert Rim fault was active prior to the northern segment. Thus, the onset of extensional faulting within the NWBR shows both along- and across-strike migration since the last ~10 Ma. Furthermore, the NW- and NNE-striking faults associated with this deformation are likely reactivating an older structural fabric.

Angular unconformities of ~5-15º, related to stratigraphic separation due to faulting, are identified between ~8.7, ~7.7 and 7.0 Ma volcanic units. While both NW- and NNE-striking faults cut Late Miocene volcanic units, it is demonstrated through field documentation and partial restorations of cross-sections that NW-striking faults formed ahead of NNE-striking faults at the latitude of the Coleman Hills. In this way, the ~9-7 Ma volcano-tectonic setting of this part of Abert Rim is similar to the modern configuration of volcanism of the HLP at the northern tip of Abert Rim.

REFERENCES CITED

Armstrong, R.L., and Ward, P., 1991, Evolving geographic patterns of Cenozoic magmatism in the North American Cordillera: The temporal and spatial association of magmatism and metamorphic core complexes, Journal of Geophysical Research, v. 96, p. 13,201-13,224.

Atwater, T., and Stock, J., 1998, Pacific-North America plate tectonics of the Neogene southwestern United States-An update, in Ernst, W.G., ed, International Geological Review, Clarence Hall Symposium volume, v. 40, p. 375-402.

Bennett, R.A., Davis, J.L., Meertens, C.M., Smith, R.B., Wernicke, B.P., and Sheehan, A.F., 1998, Integration of the northern Basin and Range (NBAR) and Wasatch Front GPS networks for crustal deformation in and around the southern Intermouuntain seismic belt, in, Seismological Society of America 93rd annual meeting, Boulder, Colorado, p. 159.

Christiansen, R.L., and McKee, E.H., 1978, Late Cenozoic volcanic and tectonic evolution of the Great Basin and Columbia Intermontane regions, Geological Society of America Memoir 152, p. 283-311.

Christiansen, R.L., Foulger, G.R., and Evans, J.R., 2002, Upper-mantle origin of the Yellowstone hotspot, Geological Society of America Bulletin, v. 114, p. 1,245-1,256.

Colgan, J.P., Dumitru, T.A., and Miller, E.L., 2004, Diachroneity of Basin and Range extension and Yellowstone hotspot volcanism in northwestern Nevada, Geological Society of America Bulletin, v. 32, p. 121-124.

Crider, J.G., 2001, Oblique slip and the geometry of normal-fault linkage: mechanics and a case study from the Basin and Range in Oregon, Journal of Structural Geology, v. 23, p. 1,997-2,009.

Dilles, J.H., and Gans, P.B., 1995, The chronology of Cenozoic volcanism and deformation in the Yerringtion area, western Basin and Range and Walker Lane, Geological Society of America Bulletin, v. 107, p. 474-486.

Donath, F.A., 1962, Analysis of Basin-Range structure, south-central Oregon, Geological Society of America Bulletin, v. 73, p. 1-16.

Duncan, R.A., and Hogan, L.G., 1994, Radiometric dating of young MORB using the ^{40}Ar-^{39}Ar incremental heating method, Geophysical Research Letters, v. 21, p. 1927-1930.

Duncan, R.A., Hooper, P.R., Rehacek, J., Marsh, J.S., and Duncan, A.R., 1997, The timing and duration of the Karoo igneous event, southern Gondwana, Journal of Geophysical Research, v. 102, p. 18127-18138.

Faulds, J.E., Henry, C.D., and Hinz, N.H., 2005, Kinematics of the northern Walker Lane: An incipient transform fault along the Pacific-North American plate boundary, Geology, v. 33, p. 505-508.

Hamilton, W.B., 1989, Crustal geologic processes of the United States, in Pakiser, L.C., and Mooney, W.D., Geological Society of America Memoir, v. 172, 743-781.

Hart, W.K., Aronson, J.L., and Mertzman, S.A., 1984, Areal distribution and age of low-k, high-alumina olivine tholeitte magmatism in the northwestern Great Basin, Geological Society of America Bulletin,v. 95, p. 186-195.

Hart, W.K., and Mertzman, S.A., 1982, K-Ar ages of basalts from southcentral and southeastern Oregon, Isochron-west, no. 33, p. 23-26.

Hemphill-Haley, M.A., Page, W.D., Burke, R., and Carver, G.A., 1989, Holocene activity of the Alvord fault, Steens Mountain, southeastern Oregon: Rinal Report to the U.S. Geological Survey under Grant No. 14-08-001-61333, 45 p.

Hooper, P.R., Binger, G.B., and Lees, K.R., 2002, Ages of the Steens and Columbia River flood basalts and their relationship to extension-related calc-alkalic volcanism in eastern Oregon, Geological Society of America Bulletin, v. 114, p. 43-50.

Hughes, S.S., and Taylor, E.M., 1986, Geochemistry, petrogenesis, and tectonic implications of central High Cascade mafic platform lavas, Geological Society of America Bulletin, v. 97, p. 1024-1036.

Humphreys, E.D., 1994, post-Laramide removal of the Farallon slab, western United States, Geology, v. 23, p. 987-990.

Humphreys, E.D., and Coblentz, D.D., 2007, North American dynamics and western U.S. tectonics, Reviews of Geophysics, v. 45, 30 p.

Jordan, B.T., 2001, Basaltic volcanism and tectonics of the High Lava Plains, southeastern Oregon, [Ph.D. Thesis] Corvallis, Oregon, Oregon State University, 218 p.

Jordan, B.T., Grunder, A.L., Duncan, R.A., and Deino, A.L., 2004, Geochronology of Oregon High Lava Plains volcanism: Mirror image of the Yellowstone hotspot?, Journal of Geophysical Research, 19 pp.

Khodayar, M., 1999, On the pattern of faults and dykes in Borgarfjordur, W-Iceland, Jokull, v. 47, p. 21-44.

Langer, V.W., 1991, Geology and petrologic evolution of silicic and intermediate volcanic rocks underneath Steens Mountain basalt, SE Oregon: Queen's University (CAN) M.S. thesis, 109 pp.

Langridge, R.M., Weldon, R.J., Pezzopane, S.K., and Jellinek, A. M., 1996, Active faulting and tufa formation at Sawed Horn, central Oregon: a possible kinematic link between the Abert Rim and Viewpoint faults, Geological Society of America Abstracts with Programs, v. 28, no. 5, p. 84.

Lawrence, R.D., 1976, Strike-slip faulting terminates the Basin and Range province in Oregon, Geologic Society of America Bulletin, v. 87, p. 846-850.

Legge, P.W., 1988, The bimodal basalt-rhyolite association west of and adjacent to the Pueblo Mountains, southeastern Oregon [M.S. Thesis] Miami University of Ohio, Oxford, Ohio

Maloney, N.J., 1961, Geology of the Eastern Part Beaty Butte Four Quadrangle, Oregon, [M.S. Thesis], Oregon State University, Corvallis, Oregon, 88 p.

Mankinen, E.A., Larson, E.E., Gromme, C. S., Prevot, M., and Coe, R.S., 1987, The Steens Mountain (Oregon) geomagnetic polarity transition, its regional significance, Journal of Geophysical Research, v. 92, p. 8057=8076.

Mathis, A.C., 1993, Geology and petrology of a 26-Ma trachybasalt to peralkaline rhyolite suite exposed at Hart Mountain, southern OR [M.S. thesis]: Corvallis, Oregon, Oregon State University, 141 p.

Miller, E.L, Gans P.B., and Garing, J.,1983, the Snake Range decollement, an exhumed mid-Tertiary ductile-brittle transition, Tectonics, v. 2, p. 239-263.

Miller, E.L., Dumitru, T., Brown, R., and Gans P.B., 1999, Rapid Miocene slip on the Snake Range decollement, Geol. Soc Am . Bull, v. 111, p. 886-905.

Miller, M. M., Johnson, D.J., Dixon, T.H., and Dokka, R.K., 2001, Refined kinematics of the Eastern California shear zone from GPS observations, 1993-1998, Journal of Geophysical Research, v. 106, p. 2245-2263.

Minor, S.A., Plouff, D., Esparza, L.E., and Peters, T.J., 1987, Geologic map of the High Steens and Little Blitzen Gorge wilderness study areas, Harney County, Oregon: U.S. Geological Survey Miscellaneous Field Studies Map MF-1976, scale 1:24,000.

Murphy, R.T., Faulds, J.E., and Hillemeyer, F.L., 2004, Evolution of Miocene extensional fault and fold systems and influence of magmatism in the northern Colorado River extensional corridor, Union Passarea, northwest Arizonea, Geological Society of America Abstracts with Programs, v. 36, no. 4, p. 21.

Nakamura, K., and Uyeda, S., 1980, Stress gradient in arc-back arc regions and plate subduction, Journal of Geophysical Research, v. 85, p. 6419-6428.

Niewendorp, C.A., and Neuhaus, M.E., 2003, Map of selected earthquakes for Oregon, 1841 through 2002, State of Oregon Department of Geology and Mineral Industries Open-File Report 03-02.

Oldow, J.S., 2003, Active transtensional boundary zone between the western Great Basin and Sierra Nevada block, Western U.S. Cordillera, Geology, v. 31, p. 1033-1036.

Pezzopane, S.K., and Weldon, R.J., 1993, Tectonic role of active faulting in central Oregon, Tectonics, v. 12, p. 1,140-1,169.

Rowley, P.D., 1998, Cenozoic transverse zones and igneous belts in the Great Basin, western United States: their tectonic and economic implications, *in* Faulds, J.E., and Stewart, J.H., eds., Accommodation zones and Transfer Zones: The regional segmentation of the Basin and Range Province: Boulder, Colorado, Geological Society of America Special Paper 323.

Sawlan, M.G., King, H.D., Plouff, D., and Miller, M.S., 1995, Mineral resources of the Spaulding Wilderness study area, Lake and Harney Counties, Oregon, USGS Bulletin Report no. B1738-E, 18 p.

Seedorff, E., 1991, Magmatism, extension, and ore deposits of Eocene to Holocene age in the Great Basin; mutual effects and preliminary proposed genetic relationships, *in* G.L., Raines, R.E. Lisle, R.W. Schafer and W.H. Wilkinson, eds., Geology and ore deposits of the Great Basin, Symposium Proceedings, p. 133-178.

Sherlock, M.G., Gettings, M.E., King, H.D., and Neumann, T.R., 1988, Mineral resources of the Abert Rim Wilderness Study Area, Lake County, Oregon, U.S. Geolgical Survey Bulletin, p. C1-C6.

Sherrod, D.R., Griscom, A., Turner, R.L., Minor, S.A., Graham, D.E., and Buehler, A.R., 1988, Mineral resources of the Sheepshead montains, Wildcat Canyon, and Table Mouuntain Wilderness Study Areas, Malheur and Harney counties, Oregon, U.S. Geological Survey Bulletin, p. A1-A16,

Streck, M.J., and Grunder, 1995, Crystallization and welding variations in a widespread ignimbrite sheet: The Rattlesnake Tuff, eastern Oregon: Bulletin of Volcanology, v. 57, p. 151-151-169.

Surpless, B.E., Stockli, D.F., Dumitru, T.A., Miller, E.L., and Farley, K.A., 2002, Progressive westward encroachment of Basin and Range extension into the stable northern Sierra Nevada block, Tectonics, v. 21, no. 1, 2-1 – 2-13.

Tentler, T., and Mazzoli, S., 2005, Architecture of normal faults in the rift zone of central north Iceland, Journal of Structural Geology, v. 27, p. 1721-1739.

Thatcher,W., Foulger, G.R., Julian, B.R, Svar, J.L, Quilty, E., and Bawden, G.W., 1999, Present-day deformation across the Basin and Range Province, Western United States, Science, v. 283, p. 1714-1718.

Walker,G.W., 1963, Reconnaissance Geologic map of the eastern half of the Klamath Falls (AMS) Quadrangle, Lake and Klamath Counties, Oregon. Mineral Investigations Field Studies Map MF-260, scale 1:250,000/

Walker, G.W., and MacLeod, N.S., 1991, Geologic map of Oregon, U.S. Geological Survey, Reston, VA.

Wells, R.E., and Heller, P.H., 1988, The relative contribution of accretion, shear, and extension to Cenozoic tectonic rotation in the Pacific Northwest, Geological Society of America Bulletin, v. 100, p. 325-338.

Wernicke, B.P., and Axen, G.J., 1988, On the role of isostacy in the evolution of normal fault systems, Geology, v. 16, p. 848-851.

Wernicke, B.P., 1992, Cenozoic extensional tectonics of the U.S. Cordillera, in Burchfiel, B.C., et al., eds., The Cordilleran orogen: Conterminous U.S.: Boulder, Colorado, Geological Society of America, Geology of North America, v. G-3, p. 553-581.

Zoback, M.L., 1989, State of Stress and Modern Deformation of the Northern Basin and Range Province, Journal of Geophysical Research, v. 94, p. 7105-7128.

CHAPTER 4

EARLY MIOCENE VOLCANOES IN SOUTHERN OREGON: LONG-TERM EXTENSION IN AN EVOLVING BACKARC

Kaleb C. Scarberry[1]

[1]Department of Geosciences,
Oregon State University, Corvallis OR 97331

For submission to Geological Society of America Bulletin

ABSTRACT

New ^{40}Ar-^{39}Ar ages indicate that intermediate volcanism was active near Beatys Butte prior to ~21 Ma and that intermediate and rhyolitic volcanism was active between 21-23 Ma at the Rabbit Hills. Chemical and isotopic data from Beatys Butte and the Rabbit Hills exhibit similar total-alkali enrichment to other Early Miocene volcanic centers in southern Oregon. Trace element enrichment within individual suites of Early Miocene volcanic rocks in southern Oregon are highly variable.

INTROCUCTION

Early Miocene intermediate to silicic magmatism prior to Late Miocene bimodal volcanism in Oregon is often associated with John Day volcanism where most exposures are found in the John Day basin in north-central Oregon (Figure 1) and consist largely of ash tuffs (e.g., Bestland et al., 1993). Intermediate volcanism was widespread across Nevada during the Eocene through Oligocene (e.g., John et al., 1999; Seedorff, 1990) and these volcanic centers are often associated with ore deposits (e.g., Seedorff, 1990). High-K intermediate volcanism occurred in southern Oregon between 37-17 Ma (e.g., Christiansen and Yeats, 1992) but only a few centers have been identified (Figure 1). This paper present new geologic mapping, ^{40}Ar-^{39}Ar ages, major and trace element chemical data and isotopic concentrations from Beatys Butte and the Rabbit Hills.

PRE-STEENS VOLCANOES OF SOUTHERN OREGON

Maniken et al. (1987) noted that in the vicinity of Abert Rim, Poker Jim Ridge, and Steens Mtn, that the base of the Steens basalt section covered a hilly terrane

composed mostly of Oligocene to Early Miocene volcanic and volcaniclastic rocks. Early Miocene volcanic centers within the Oregon Basin and Range (Figure 1) are exposed by or in close proximity to major Basin and Range escarpments. The Rabbit and Coyote Hills, located in the footwall block of the Abert Rim, are the only volcanic centers not directly linked to prominent regional fault escarpments. The Paisley Hills are located along the southern extension of the Winter Rim fault and the Guano Rim terminates into Beatys Butte. The 22 Ma Coleman Hills are situated adjacent to the Abert Rim fault and the 26 Ma Hart Mountain volcanic complex (Mathis, 1993) and a 23-25 Ma intermediate to rhyolitic suite (Langer, 1991) are exposed by the Poker Jim Rim and Steens faults, respectively. A striking feature of pre-Steens volcanic centers is that they appear aligned along a NW-striking trend across the southern part of Oregon, somewhat parallel to the axis of the High Lava Plains (Figure 1).

METHODS

Reconnaissance geologic mapping and sample collection was conducted at Beatys Butte and the Rabbit Hills during two summer field seasons. Geochemical analysis was performed by the Geoanalytical Laboratory at Washington State University. Isotope dilutions were done at the Carnegie Institution of Washington (See Chapter 2 for detailed methods). ^{40}Ar-^{39}Ar age analyses were conducted at Oregon State University in the College of Oceanic and Atmospheric Sciences (See Chapter 3 for detailed methods; Appendix 3 for detailed results). ^{40}Ar-^{39}Ar ages discussed her are presented with 2-σ errors unless otherwise noted.

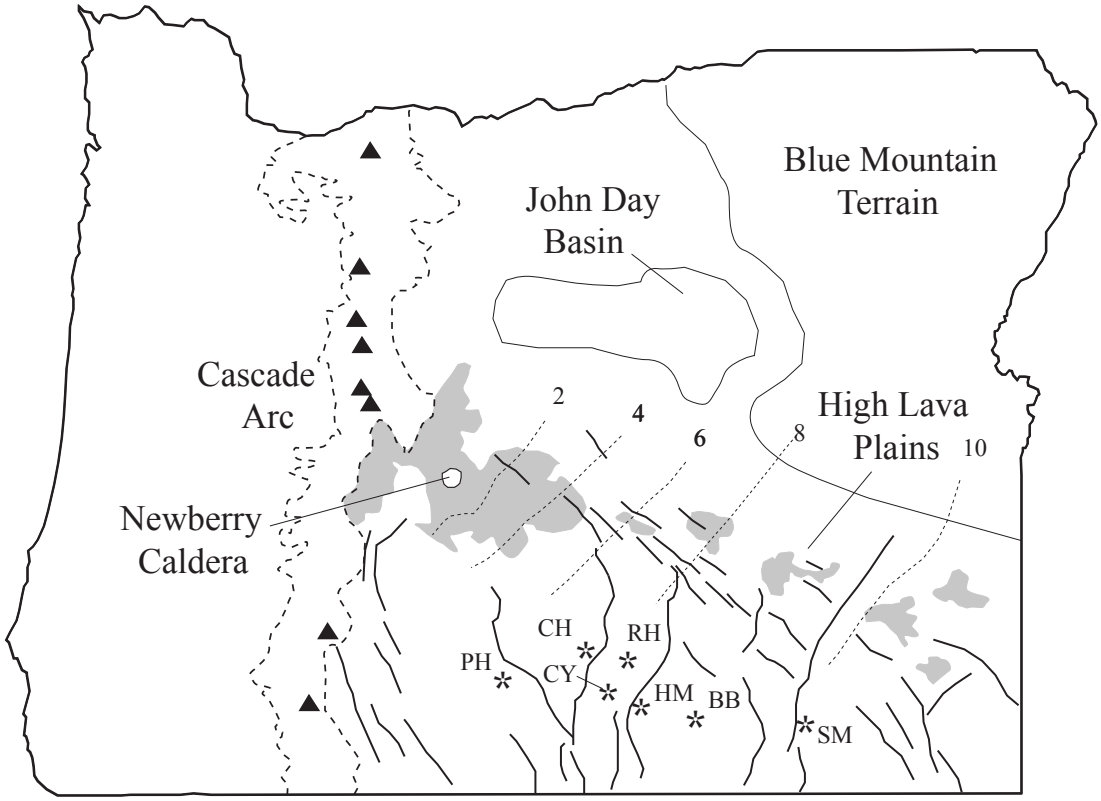

Figure 1. Map of Oregon showing the location of Oligocen-Early Miocene intermediate volcanic center within the margin of the Basin and Range Province. Frow west to east: PH=Paisley Hills, CH=Coleman Hills, CY=Coyote Hills, R.H.=Rabbit Hills, HM=Hart Mountain, BB=Beatys Butte, SM=Steens Mountain. A track of Quaternary basalts (shade); westward younging trend of the High Lava Plains (HLP) silicic volcanism (thin stippled line; age of onset in Ma) after Jordan et al., (2004).

RESULTS

Beatys Butte

Beatys Butte is a volcanic complex located at the northern termination of the Gauno Rim in southern Oregon (Figure 2). Within the complex, rhyolite (Tvs) appears to intrude into an existing mafic center (Tvm). Prominent structural features of the complex include: (1) ~N-S alignment of rhyolite domes; (2) NW- and NNE-striking trends of intermediate-mafic dikes; (3) onlapping of andesite lavas that tilt ~20° to the north on the north side of the butte; (4) ~E-W-striking dikes associated with the vent for the andesites (Tal; Figure 2); and (5) biotite-rich ashflow tuff banked against the west side of the butte. ^{40}Ar-^{39}Ar analyses of volcanic rocks from Beatys Butte include some spotty, yet not worthless ages. Analysis of a plagioclase separates from an andesite dike (KCS-05-12; Figure 2) yielded an age of 25.27 +/- 4.11 Ma (1-σ error) and from an andesite dike northwest of the complex (KCS-05-44; Figure 2) an age of 25.24 +/- 12.49 (1-σ error) Although the ages are poor it confirms that the andesite units are, at the very least, older than ~21 and ~12 m.y, respectively (See Appendix for data). Field relationships indicate that Tal (KCS-05-44) is younger than Tvm (KCS-05-12) because the former is banked against the latter (Figure 2). Analysis of the main rhyolite stock at Beatys Butte (KCS-05-15; Figure 2) produced a three-step error-plateau age of 12.05 +/- 0.66 Ma (Figure 3) and an isochron age of 11.82 +/- 1.26 Ma. A sanidine separate from the biotite tuff banked against the complex (KCS-05-15; Figure 2) yielded an acceptable, 6-step plateau age of 9.75 +/- 0.36 Ma.

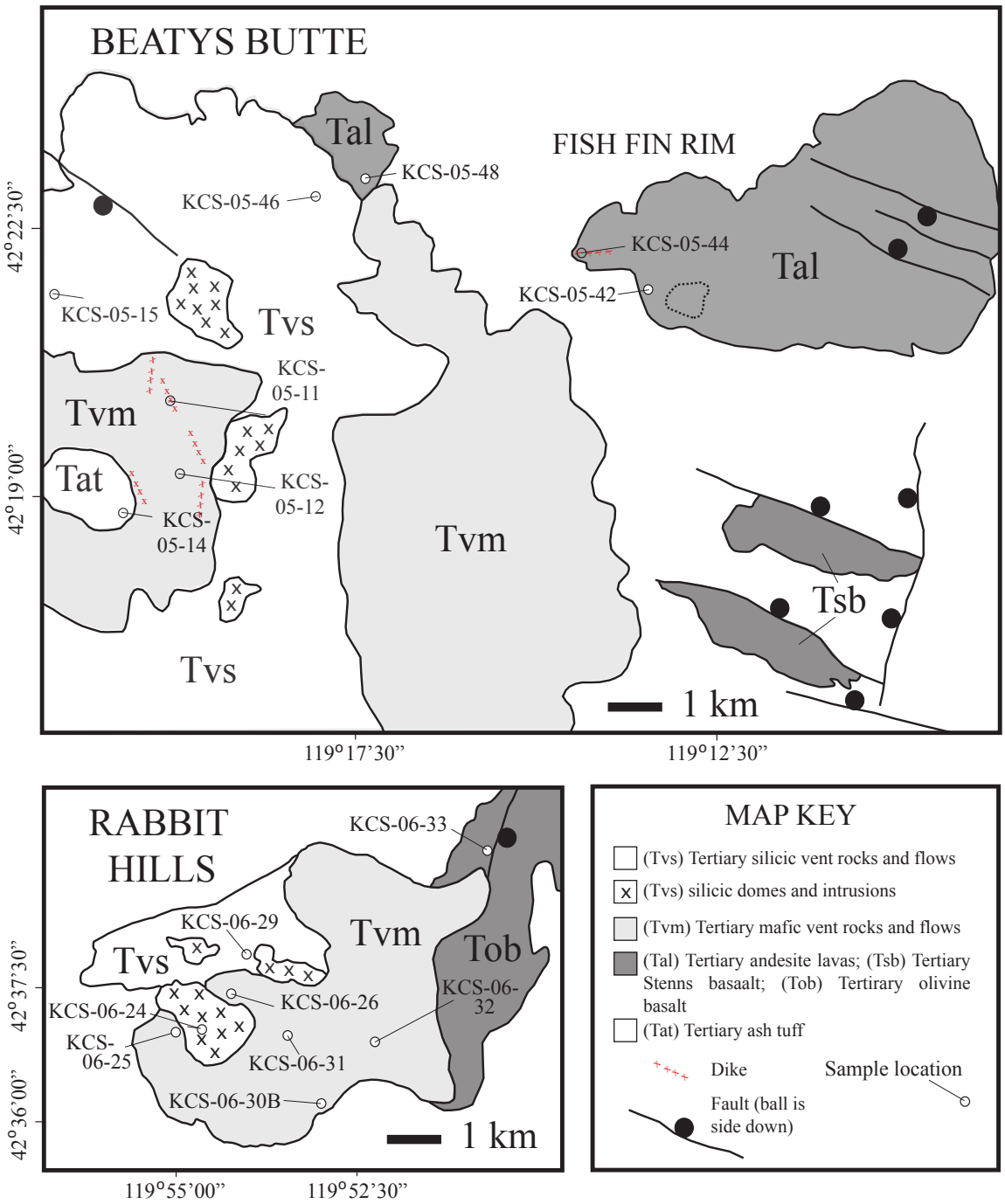

Figure 2. Sketch geologic maps showing sampled portions of Beatys Butte and the Rabbit Hills.

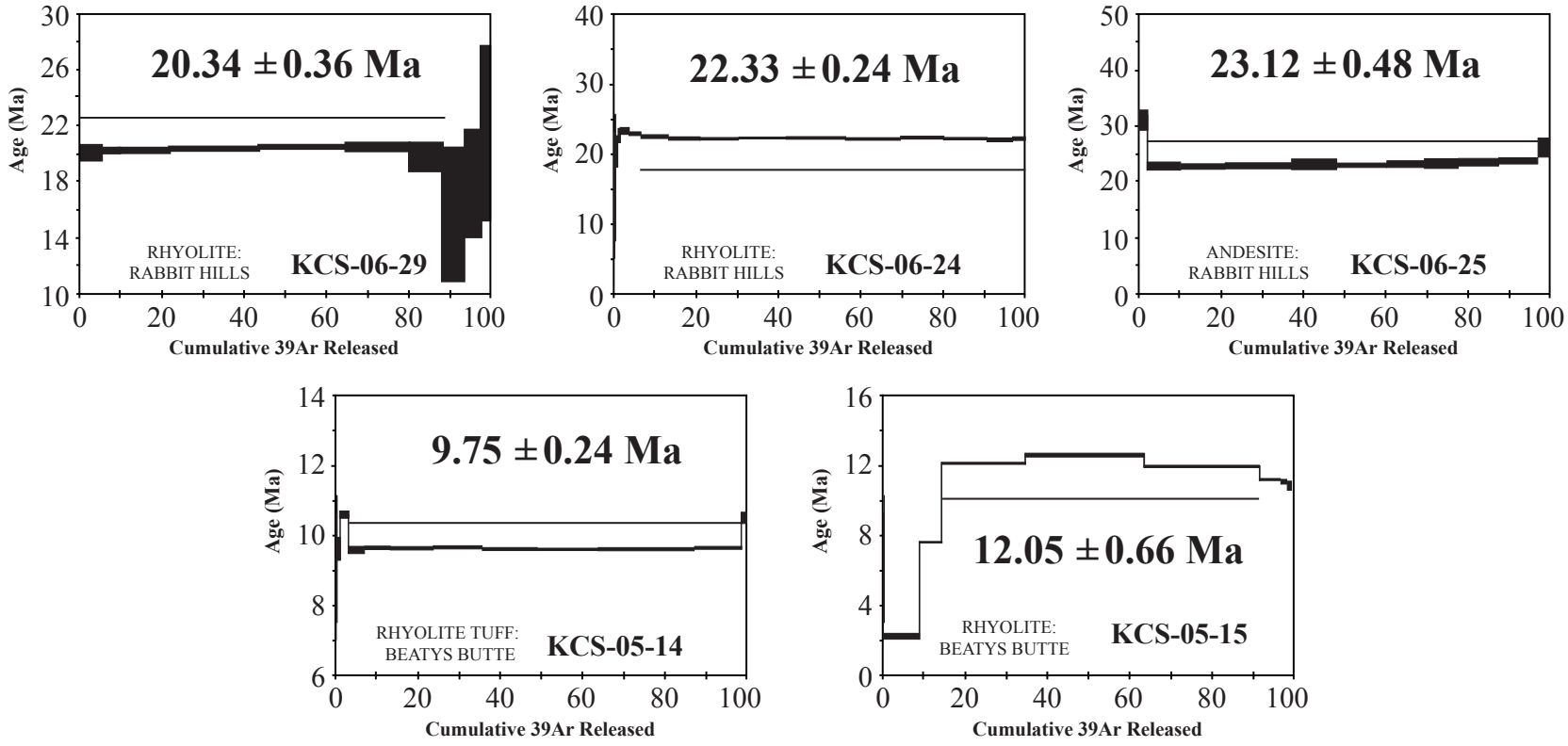

Figure 3. ^{40}Ar-^{39}Ar spectra for samples of the Rabbit Hills and Beatys Butte. Bars under ages span the ^{39}Ar release steps used in the age calculation. See Table 2 for more detail and the Appendix for all data. Rock type and general sample locations given on diagrams. Sample locations shown on Figure 4.

The Rabbit Hills

The Rabbit Hills are a volcanic complex located ~20 km east of the Coleman Hills within the footwall block of the Abert Rim fault (Figure 1). Like Beatys Butte, the Rabbit Hills consist of silicic and mafic vent rocks that are onlapped by younger lavas (Figure 2). Prominent features of the Rabbit Hills include: (1) a linear E-W set of 4-5, nearly aphyric, rhyolite domes on the northwest side of the comlex; (2) a large, porphorytic (biotite, sanidine and hornblende) intrusion on the west side of the complex; (3) a loose NNE trend of the axis of intermediate-mafic volcanism; and tilting of ~10º to the north of basalts that lap onto the northeast corner of the complex. ^{40}Ar-^{39}Ar analyses of a whole-rock core from the fine-grained rhyolite (KCS-06-29; Figure 2) yielded a 6-step plateau age of 20.34 +/- 0.36 Ma (Figure 3). Analysis of a biotite separate from the porphorytic biotite hornblende rhyolite on the west side of the complex (KCS-06-24; Figure 2) yielded a 9-step plateau age of 22.33 +/- 0.24 Ma (Figure 3). Analysis of a plagioclase separate from the intemediate-mafic unit of the Rabbit Hills yielded an 8-step plateau age of 23.12 +/-0.48 Ma.

CHEMICAL COMPOSITION

Chemical data for the Rabbit Hills and Beatys Butte is presented in Table 1. These rock suites are compared to other rock suites from Oligocene-Late Miocene volcanic centers in southern Oregon (Figure 4). Although rhyolite from Beatys Butte is does not conform to this age-range, the association with intermediate volcanism > 21 m.y. is significant for the purpose of this analysis. Oligocene-Late Miocene volcanic complexes consist of high-K, intermediate compositions and rhyolite (Figure 4). The

Table 1. Chemical composition of volcanic rocks from the Rabbit hills and Beatys Butte normalized to 100% volatile free.

sample ID	**KCS-06-33**	**KCS-06-26**	**KCS-06-31**	**KCS-06-32**	**KCS-06-25**	**KCS-06-30B**	**KCS-06-24**	**KCS-06-29**	**KCS-06-20**
location	Rabbit Hills	Rabbit Hills	Rabbit Hills	Rabbit Hills	Rabbit Hills	Rabbit Hills	Rabbit Hills	Rabbit Hills	Coyote Hills
rock type	basalt-flow	bas-ands-flow	bas-ands-flow	bas-ands-flow	bas-ands	rhyolite-intrus.	rhyolite-intrus.	rhyolite-intrus	andesite
lat. (N)	42.61375	42.5908	42.61483	42.61375	42.617	42.6015	42.61903	42.62884	42.56165
long. (W)	119.88803	119.99987	119.8905	119.88803	119.91518	119.881	119.90955	119.89993	119.99244
XRF (wt. %)									
SiO_2	48.10	57.14	58.22	61.36	61.37	72.06	72.32	75.49	55.57
TiO_2	0.83	1.59	1.58	1.30	1.25	0.31	0.31	0.06	1.57
Al_2O_3	17.65	16.91	16.47	16.36	16.10	14.47	14.35	14.01	17.51
FeO*	9.39	8.59	7.76	6.38	6.29	2.29	2.21	0.60	8.52
MnO	0.18	0.12	0.13	0.11	0.10	0.05	0.04	0.06	0.35
MgO	9.23	2.23	2.86	2.14	2.47	0.44	0.49	0.19	3.03
CaO	11.75	6.21	5.47	4.43	4.68	1.40	1.32	0.99	7.56
Na_2O	2.45	4.16	3.90	4.16	3.81	3.73	4.04	3.69	3.94
K_2O	0.30	2.50	3.16	3.39	3.59	5.18	4.84	4.90	1.63
P_2O_5	0.12	0.55	0.44	0.38	0.33	0.08	0.08	0.01	0.32
a.t.	98.74	96.49	97.36	96.33	97.95	96.12	97.87	96.01	95.99
Trace elements (ppm)									
Ni	164	32	28	17	26	5	4	1	19
Cr	167	32	13	7	11	2	1	1	26
Sc	42	13	15	11	11	3	3	3	21
V	256	108	122	95	109	14	19	4	211
Ba	118	713	928	901	878	924	962	183	828
Rb	3	38	51	61	63	110	102	137	27
Sr	301	469	436	395	396	160	155	59	621
Zr	39	293	304	325	300	242	243	71	146
Y	22	34	31	31	28	22	20	38	23
Nb	2	22	20	22	17	16	17	55	13
Ga	16	23	22	21	22	17	17	23	19
Cu	126	27	36	12	34	8	17	4	70
Zn	66	107	97	86	81	46	41	34	86
Pb	2	6	8	8	8	13	12	12	8
La	1	28	29	34	30	29	32	6	20
Ce	5	63	54	64	57	52	47	15	40
Th	0	4	5	6	5	11	11	12	3
Nd	8	36	32	34	30	23	23	9	21

Table 1. Continued.

	KCS-06-33	KCS-06-26	KCS-06-31	KCS-06-32	KCS-06-25	KCS-06-30B	KCS-06-24	KCS-06-29	KCS-06-20
Trace elements (ppm) (ICP-MS)									
La	3.1	28.7	29.9	35.3	32.5	31.6	34.0	8.6	20.3
Ce	8.3	59.4	59.4	65.8	54.5	50.3	50.3	16.6	40.8
Pr	1.4	7.9	7.8	8.5	7.4	5.9	6.8	2.1	5.1
Nd	7.1	33.5	32.5	33.8	29.5	21.3	24.5	8.3	21.2
Sm	2.3	7.8	7.7	7.3	6.6	4.2	4.9	3.1	4.8
Eu	1.0	2.4	2.2	2.1	1.8	1.0	1.1	0.3	1.7
Gd	2.9	7.6	7.2	6.7	6.1	3.9	4.1	4.1	4.5
Tb	0.6	1.2	1.1	1.0	0.9	0.6	0.6	0.9	0.7
Dy	3.8	6.7	6.3	6.0	5.3	3.7	3.7	6.1	4.3
Ho	0.8	1.3	1.2	1.1	1.0	0.8	0.7	1.3	0.9
Er	2.4	3.2	3.1	3.0	2.7	2.2	1.9	3.6	2.3
Tm	0.3	0.5	0.4	0.4	0.4	0.3	0.3	0.5	0.3
Yb	2.3	2.7	2.7	2.6	2.3	2.1	1.8	3.4	2.0
Lu	0.4	0.4	0.4	0.4	0.4	0.3	0.3	0.5	0.3
Ba	114.1	706.1	917.9	903.2	872.4	938.9	979.2	186.3	815.5
Th	0.3	3.6	4.0	5.2	4.8	8.3	8.4	8.5	3.4
Nb	2.1	21.8	20.5	22.9	17.2	16.2	16.2	54.7	13.5
Y	21.2	33.8	31.2	30.5	27.5	21.6	18.8	36.8	22.6
Hf	1.2	6.9	7.2	7.8	7.0	6.4	6.3	4.3	3.6
Ta	0.1	1.5	1.4	1.7	1.3	1.5	1.6	6.0	0.9
U	0.1	1.2	1.4	1.7	1.7	2.9	2.9	4.9	1.1
Pb	0.9	5.1	6.2	7.6	7.6	11.6	11.6	9.6	7.4
Rb	3.1	37.9	49.3	59.3	60.7	105.4	97.1	130.3	26.0
Cs	0.0	0.6	0.8	1.0	1.1	2.1	2.1	4.6	3.0
Sr	299.7	473.1	435.0	391.5	391.4	157.8	153.1	58.1	632.5
Sc	46.2	15.2	15.6	12.2	13.1	3.5	4.1	2.3	23.0
Zr	36.8	278.2	292.0	314.0	288.3	234.6	229.6	69.9	139.9

Table 1. Continued.

sample ID	**KCS-06-19**	**KCS-05-48**	**KCS-05-44**	**KCS-05-42**	**KCS-05-15**	**KCS-05-46**	**KCS-05-14**	**KCS-05-12**	**KCS-05-11**
location	Coyote Hills	N side of butte	Fish Fin Rim	Fish Fin Rim	Beatys Butte	Beatys Butte	Shirks Look	Beatys Butte	Beatys Butte
rock type	andesite	andesite	andesite	andesite	rhyolite	rhyolite	rhyolite (tuff)	andesite dike	andesite dike
lat. (N)	42.5908	42.40889		42.39583	42.39944	42.40722	42.34778	41.35889	41.36500
long. (W)	119.99987	119.29583		119.23944	119.37667	119.29972	119.35083	119.32944	119.34806
XRF (wt. %)									
SiO_2	67.85	62.46	61.55	61.44	74.88	74.86	75.87	62.61	62.60
TiO_2	0.57	1.11	1.17	1.16	0.16	0.16	0.15	1.55	1.58
Al_2O_3	15.40	16.13	16.19	16.07	13.88	13.98	13.15	16.56	16.65
FeO*	4.06	6.01	6.28	6.39	1.09	1.07	1.11	5.37	5.70
MnO	0.12	0.12	0.14	0.14	0.02	0.03	0.07	0.15	0.11
MgO	0.34	1.74	2.15	2.10	0.06	0.03	0.15	0.97	0.65
CaO	1.17	4.27	4.59	4.66	1.16	1.11	1.01	2.92	2.67
Na_2O	5.61	4.20	3.98	3.98	3.60	3.58	3.67	5.20	5.25
K_2O	4.79	3.49	3.50	3.56	5.10	5.13	4.79	4.17	4.24
P_2O_5	0.10	0.47	0.46	0.50	0.04	0.05	0.02	0.50	0.55
a.t.	96.91	98.50	98.48	98.24	98.62	98.49	98.76	97.45	97.18
Trace elements (ppm)									
Ni	3	10	9	9	6	6	6	7	7
Cr	2	4	4	4	0	1	3	3	2
Sc	8	13	14	15	3	3	3	15	16
V	4	116	135	132	8	7	10	40	38
Ba	1011	1086	977	975	963	951	622	1370	1352
Rb	94	83	77	77	122	125	121	81	81
Sr	108	401	406	404	175	169	113	368	369
Zr	568	172	171	171	150	149	116	302	299
Y	51	29	26	25	12	12	17	40	44
Nb	55	16	16	15	9	9	9	20	18
Ga	25	19	19	19	16	15	15	21	23
Cu	6	34	36	34	7	8	7	16	9
Zn	116	81	83	79	20	22	25	96	103
Pb	12	12	13	13	20	20	21	16	14
La	56	26	24	26	25	29	21	34	32
Ce	110	49	50	51	35	39	36	72	83
Th	14	4	4	2	7	8	7	6	5
Nd	51	28	25	26	13	19	15	38	44

Table 1. Continued.

	KCS-06-19	KCS-05-48	KCS-05-44	KCS-05-42	KCS-05-15	KCS-05-46	KCS-05-14	KCS-05-12	KCS-05-11
Trace element: Trace elements (ppm) (ICP-MS)									
La	57.8	29.7	25.3	26.7	26.1	29.4	22.1	34.7	
Ce	111.5	48.4	46.5	49.5	35.0	34.2	34.8	68.3	
Pr	13.6	6.5	5.4	5.8	4.0	4.8	3.7	8.5	
Nd	51.5	27.4	22.8	24.3	14.1	17.0	13.7	36.4	
Sm	11.0	6.4	5.4	5.8	2.7	3.3	3.0	8.9	
Eu	2.1	1.8	1.7	1.8	0.6	0.7	0.5	2.9	
Gd	9.6	6.1	5.2	5.5	2.3	2.6	2.8	8.5	
Tb	1.6	1.0	0.8	0.9	0.4	0.4	0.5	1.4	
Dy	10.1	5.9	5.0	5.3	2.2	2.4	3.0	8.0	
Ho	2.0	1.2	1.0	1.1	0.5	0.5	0.6	1.6	
Er	5.5	3.2	2.9	3.0	1.3	1.3	1.9	4.5	
Tm	0.8	0.5	0.4	0.4	0.2	0.2	0.3	0.6	
Yb	5.1	3.0	2.7	2.7	1.4	1.4	2.0	3.9	
Lu	0.8	0.5	0.4	0.4	0.2	0.2	0.3	0.6	
Ba	1021.6	1080.8	981.8	981.9	979.5	956.9	618.3	1364.7	
Th	11.8	4.4	4.2	4.3	7.1	7.0	6.6	6.2	
Nb	54.2	16.4	16.3	16.3	9.1	9.1	10.1	18.0	
Y	50.6	31.4	28.7	29.3	13.4	13.5	19.2	43.9	
Hf	14.0	4.5	4.5	4.5	4.2	4.2	3.7	7.7	
Ta	3.6	1.2	1.2	1.2	1.0	1.0	1.1	1.2	
U	3.7	1.8	1.6	1.7	2.5	2.5	2.7	2.1	
Pb	11.4	12.7	12.2	12.4	18.4	18.6	19.6	14.8	
Rb	88.8	78.1	73.7	74.5	115.7	118.3	115.8	77.5	
Cs	2.3	1.7	1.7	1.7	1.9	2.1	3.1	1.4	
Sr	105.2	388.4	399.0	399.8	165.2	157.4	106.2	358.5	
Sc	8.6	13.6	14.7	14.5	2.2	2.3	2.8	18.0	
Zr	550.8	163.1	164.6	165.2	144.6	143.6	107.7	290.4	

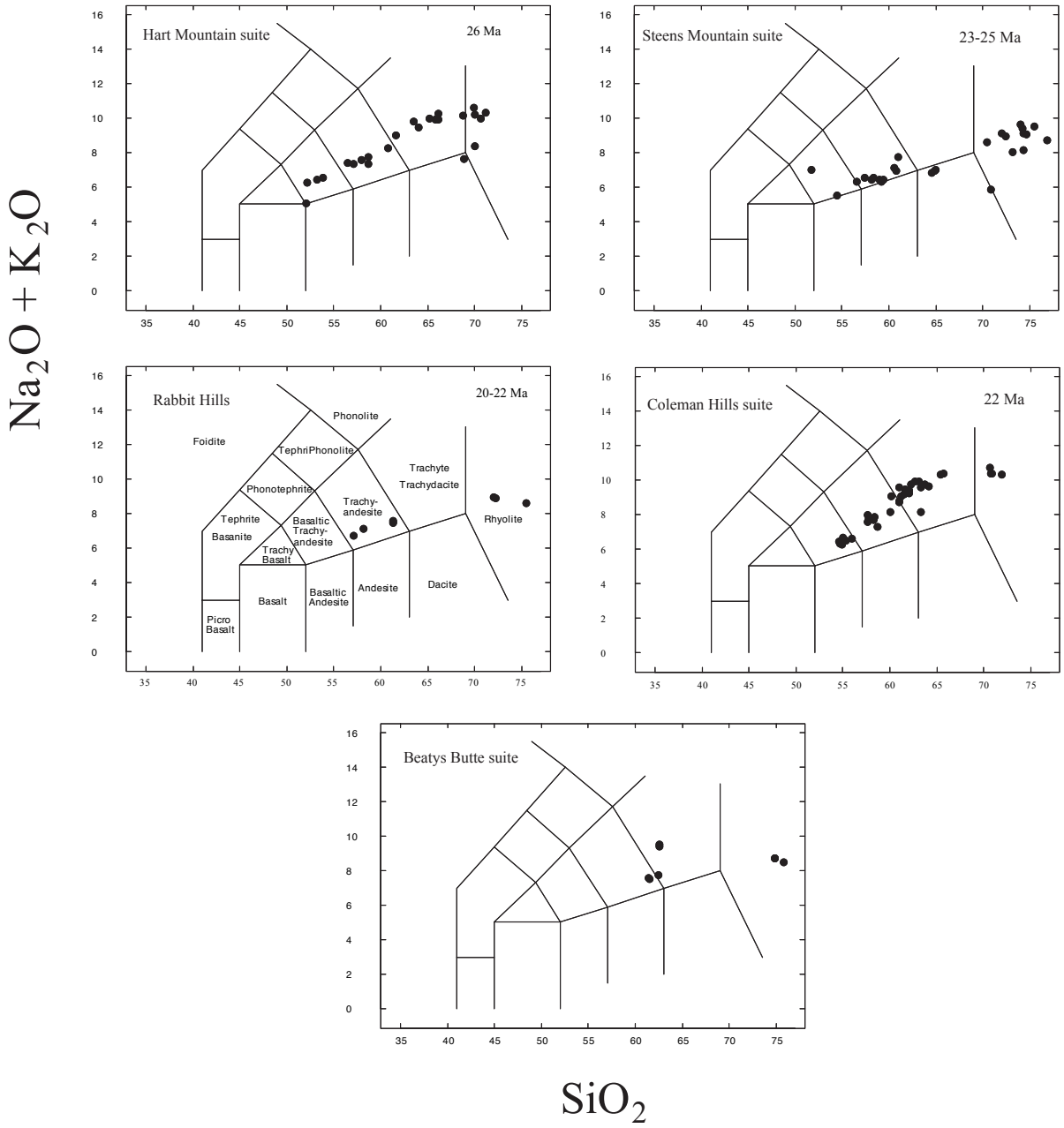

Figure 4. Total Alkalis vs. Silica classification diagram (after Lebas et al., 1986) for Oligocene to Late Miocene volcanic rocks of the NWBR. Data sources: Hart Mountain. suite (Mathis, 1993); Steens Mountain. suite (Langer, 1991); Coleman Hills suite (see Chapter 2 this thesis); Rabbit Hills and Beatys Butte suite (this study).

Hart Mountain and Coleman Hills suites exhibit the highest enrichment in total-alkalis while the Steens Mountain suite displays the lowest. The respective suites show variable chondrite-normalized trace-element enrichments (Figure 5). All of the suites exhibit Ti-troughs and modest K-spikes.

Isotopic Composition

New Sr, Nd, Pb, and Hf isotope ratios from rhyolite and intermediate compositions from the Rabbit Hills are presented in Table 2. ^{87}Sr-$^{86}Sr_i$ and ^{143}Nd-$^{144}Nd_i$ ratios range from 0.70356 to 0.70400 and 0.51285 to 0.51286, respectively and overlap with reported values for the region (Figure 6). Regional values exhibit two principal trends: (1) those that closely follow the mantle array, and (2) those that have acquired a crustal signature. Analyses from the Rabbit Hills fall into the former category.

DISCUSSION

Based on available data, Oligocene-Late Miocene volcanic centers within the Oregon Basin and Range Province are in general older within the eastern half of the state (Figure 7). Trace element patterns and ages of rocks from the Coleman Hills (see Chapter 2 of this thesis) are quite similar to those of the Rabbit Hills and the fact that they are located ~20 km from one another suggests that they may be part of the same ~20-22 Ma volcanic system in the region.

The orientations of Oligocene-Late Miocene dike swarms within the western portion of the Basin and Range Province suggests that either a subduction zone trench or a back-arc extensional region related to a southwesterly retreating subduction system

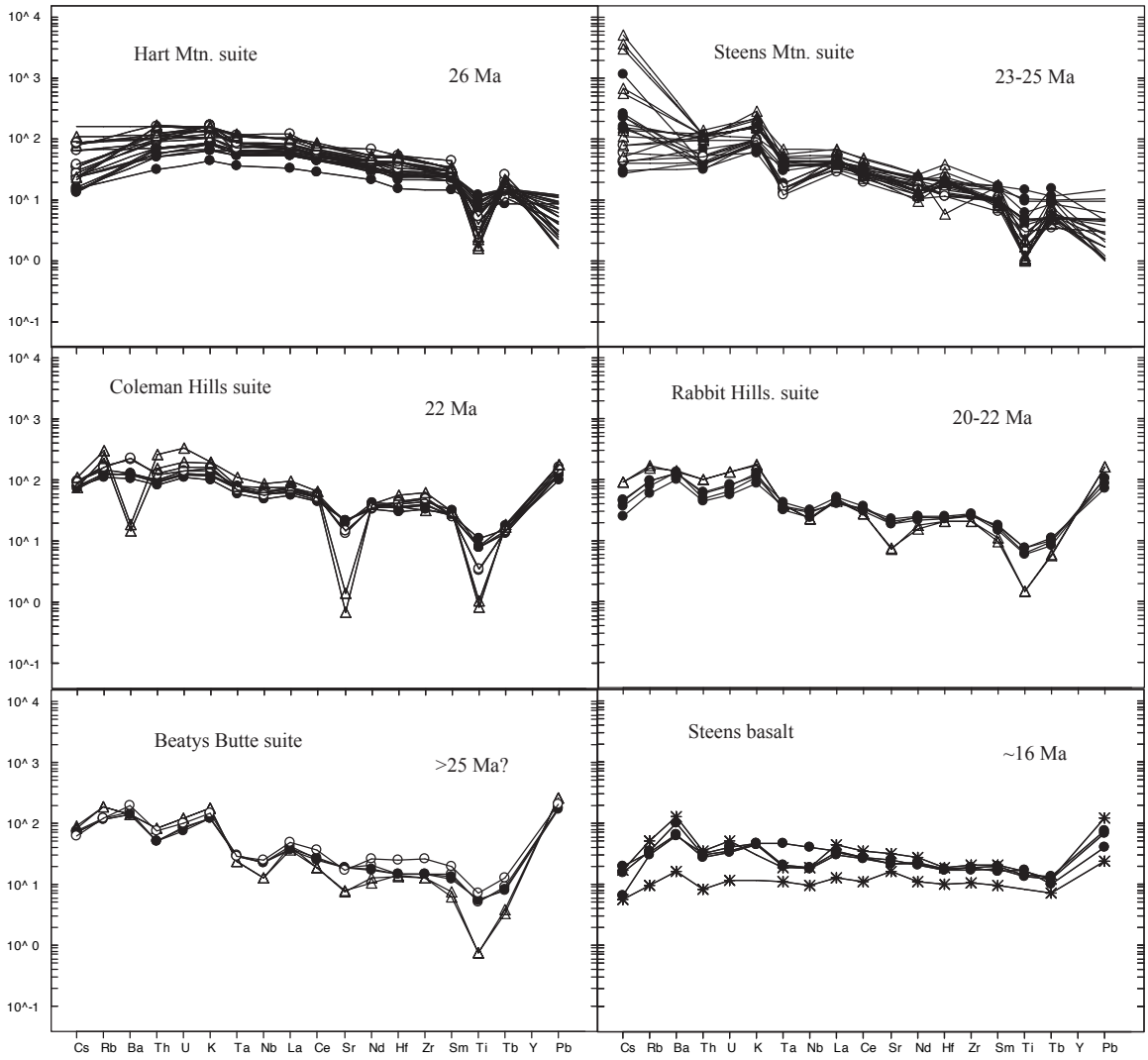

Figure 5. Chondrite-normalized spider plots using normalization values from McDonough et al., 1992. Rhyolie (triangles), dacite (open circles), andesite-basaltic andesite (closed circles). The Steens basalts are shown for comparission: 16.1 Ma samples from Lake Abert (closed circles) and range of complete section at Steens Mountain (asterisks) from Johnson et al., 1998.

Table 2. Isotopic composition of rocks from the Rabbit Hills

Sample	**KCS-06-24**	**KCS-06-25**	**KCS-06-29**
Age	**22.33**	**22.12**	**20.34**
location	**Rabbit Hills**	**Rabbit Hills**	**Rabbit Hills**
rock type	**rhyolite**	**and-dacite**	**rhyolite**
SiO_2 (wt. %)	72.34	61.37	75.49
$^{87/86}Sr_m$	0.704178	0.703708	0.705869
$^{87/86}Sr_i$	0.703597	0.703561	0.703997
$^{143}Nd/^{144}Nd_m$	0.5128677	0.51288435	0.5128877
$^{143}Nd/^{144}Nd_i$	0.512850	0.512864	0.512858
εNd_i	4.74	5.02	4.84
$^{176}Hf/^{177}Hf_m$	0.28294	0.28295	0.28294
$^{176}Hf/^{177}Hf_i$	0.28294	0.28295	0.28294
$^{206}Pb/^{204}Pb_m$	18.9449	18.9047	19.0040
$^{206}Pb/^{204}Pb_i$	18.8908	18.8552	18.9026
$^{207}Pb/^{204}Pb_m$	15.6035	15.6036	15.6163
$^{207}Pb/^{204}Pb_i$	15.6010	15.6013	15.6116
$^{208}Pb/^{204}Pb_m$	38.5425	38.5376	38.5762
$^{208}Pb/^{204}Pb_i$	38.4444	38.4006	38.3536

Sample procedure described in Carlson et al. (2006)
Reference standards and corrections: Sr (NBSA987, 0.710250); Nd (La Jolla, 0.511860);
Hf (JMC475, 0.282160). Pb isotopes corrected for mass fractionation using current NBS 981 average to . calculate bias factors. Todt et al. (1996) measurement of standard NBS 981. Run on Axiom with spray chamber and Tl-spiking.

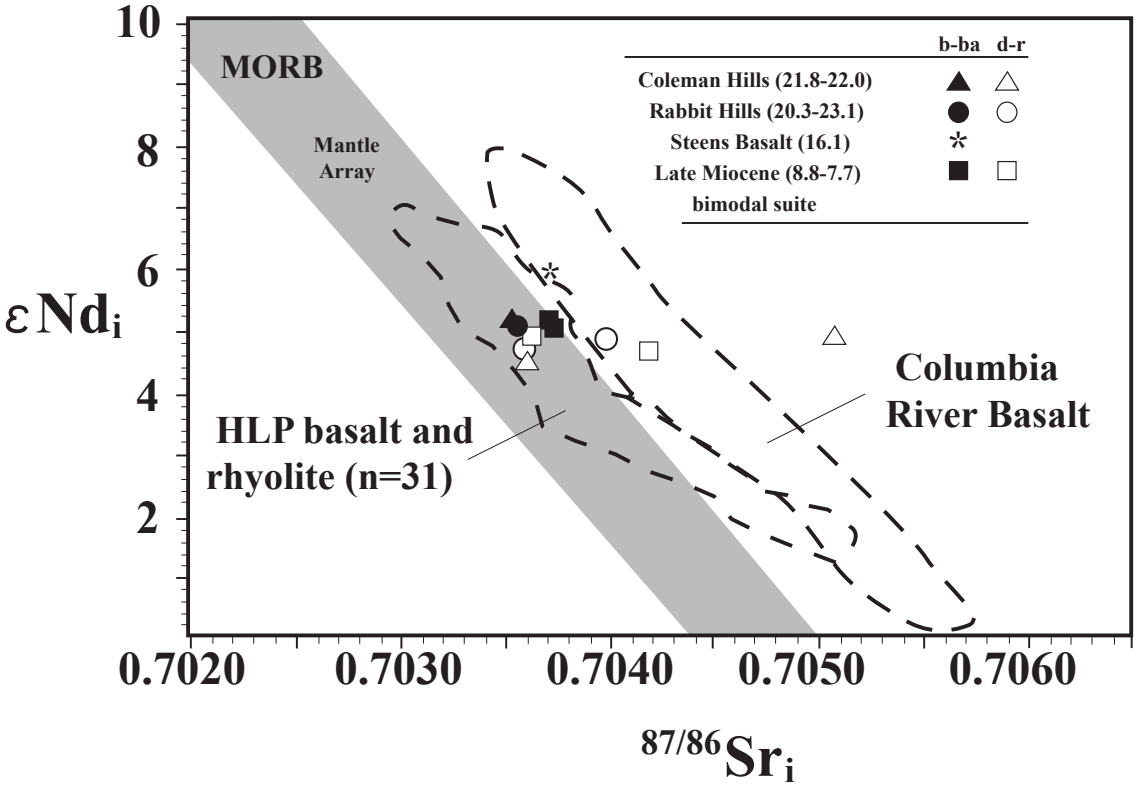

Figure 6. $^{87}Sr/^{86}Sr$ - εNd covariation diagram for bimodal volcanic rocks from the northwestern Basin and Range Province. Analyses are plotted according to composition: b-ba: basalt to basaltic andesite and d-r: dacite to rhyolite. Ages shown in parentheses in Ma. Late Cenozoic volcanics of the High Lava Plains (HLP) are from Hart (1995) and Streck and Grunder, 2006. Field of Columbia River Basalt is from Carlson et al. (1981)

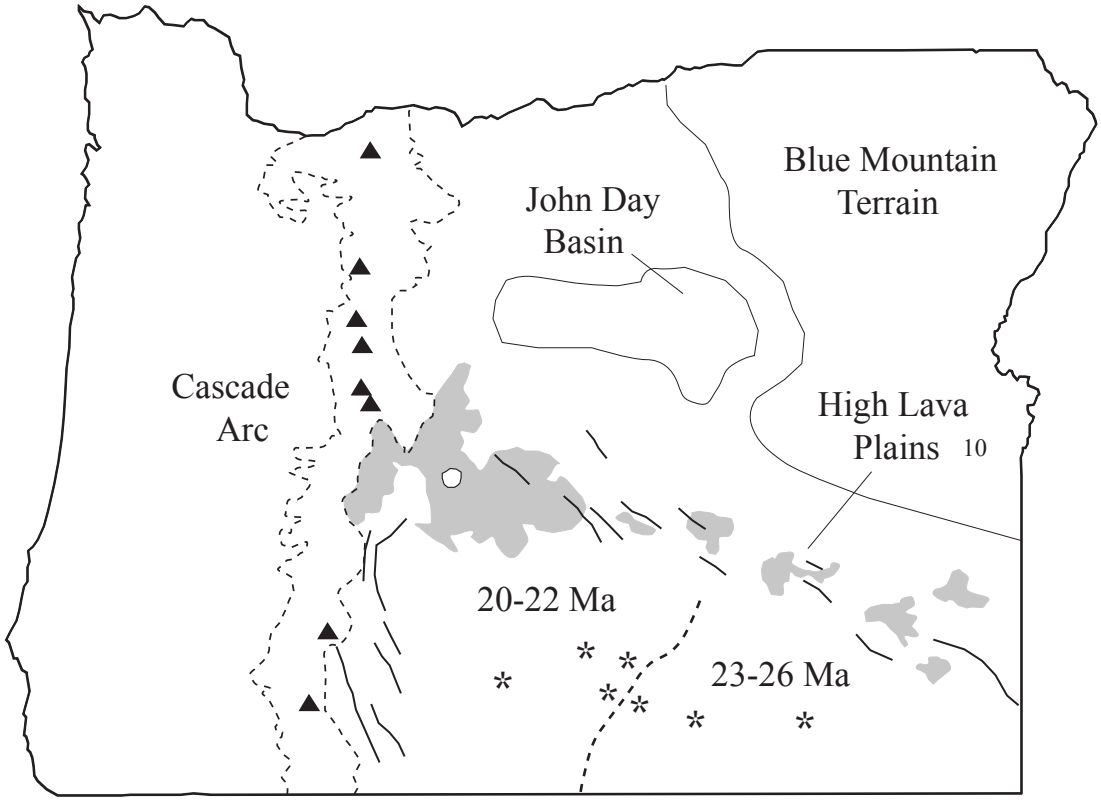

Figure 7. Map of Oregon showing the location of Oligocene-Early Miocene intermediate volcanic center within the margin of the Basin and Range Province. A track of Quaternary basalts (shade); westward younging trend of the High Lava Plains (HLP) silicic volcanism (thin stippled line; age of onset in Ma) after Jordan et al., 2004.

existed in the region between ~35 and 20 Ma (Best, 1988; Price and Henry, 1984). Tectonic reconstructions suggest that ~500-900 km of right-lateral offset was accommodated since Cretaceous time along structures that are now buried by Tertiary and Late Cenozoic volcanic rocks in Oregon (Wyld et al., 2006).

Rhyolite domes of Beatys Butte complex were likely emplaced along fractures assocated with the Basin and Range fault in the area (Guano Rim) at ~12.5 Ma. Faulting and tectonic tilting of units occurred near Beatys Butte sometime after ~12 Ma. NW-strking faults are younger than ~12 Ma as they cut Tal (Figure 2). Tilting of Tal (~20º) to the north was likely related to subsidence of the region following emplacement of the rhyolite at ~12 Ma.

CONCLUSIONS

Volcanic rocks exposed at Beatys Butte and the Rabbit Hills belong to an episode of Early Miocene, intermediate composition, magmatism within the Oregon Basin and Range Province. Like the Coleman Hills (Chapter 2), these rocks were part of an ancestral Cascade arc or a back-arc extensional system that formed soon after arc volcanism. Correlating younger ages with the western part of the province and older ages with the eastern part of the province is tenuous, at best.

REFERENCES CITED

Best, M, G., 1988, Early Miocene change in direction of least principal stress, southwestern Unived States: conflicting inferences from dikes and metamorphic core-detachment fault terranes, Tectonics, v. 7, p. 249-259.

Carlson, R.W., Lugmair, G.W., and MacDougall, J.D., 1981, Columbia River volcanism: the question of mantle heterogeneity or crustal contamination, Geochemica et Cosmochimica Acta, v. 45, p. 2483-2499.

Carlson R.W. and Hart, W.K., 1987, Crustal genesis on the Oregon Plateau, Journal of Geophysical Research, v. 92, 6191-6206.

Gerlach, D.C., 1988, Magma sources of the Cape Verdes Archipelago: isotopic and trace element constraints, Geochimica et Cosmochimica Acta, v. 52, p. 2979-2992.

John, D.A., Garside, L.J., and Wallace, A.R., 1999, Magmatic and tectonic setting of Late Cenozoic epithermal gold-silver deposits in northern Nevada, with an emphasis on the Pah Rah and Virginia Ranges and the Northern Nevada Rift, Geological Society of Nevada spring 1999 field trip guidebood, Special Publication #29, p. 65-110.

Johnson, J.A., Hawkesworth, C.J., Hooper, P.R., and Binger, G.B., 1998, Major- and trace-element analyses of Steens basalt, southeastern Oregon, U.S. Geological Survey Open-File Report 98-482, 30 p.

Jordan, B.T., 2001, Basaltic volcanism and tectonics of the High Lava Plains, southeastern Oregon, [Ph.D. Thesis] Corvallis, Oregon, Oregon State University, 218 p.

Langer, V.W., 1991, Geology and petrologic evolution of silicic and intermediate volcanic rocks underneath Steens Mountain basalt, SE Oregon [M.S. Thesis] Oregon State University, Corvallis, OR, 109 p.

LeBas, M.J., LeMaitre, R.W, Streckeisen, A., and Zanettin, B., 1986, A chemical classification of volcanic rocks based on the total alkali-silica diagram, Journal of Petrology, v. 27, p. 745-750.

Mathis, A.C., 1993, Geology and petrology of a 26-Ma trachybasalt to peralkaline rhyolite suite exposed at Hart Mountain, southern OR [M.S. thesis]: Corvallis, Oregon, Oregon State University, 141 p.

McDonough, W.F., Sun, S.S., Ringwood, A.E., Jagoutz, E., and Hofmann, A.W., 1992, Potassium, rubidium, and cesium in the Earth and Moon and the evolution of the mantle of the Earth, Geochimica et Cosmochimica Acta, v. 56, p. 1001-1012.

Price, J.G., and Henry, C.D., 1984, Stress orientations during Oligocene volcanism in Trans-Pecos Texas: Timing the transition from Laramide compression to Basin and Range tension, Geology, v. 12, p. 238-241.

Saunders, A.D., Nory, M.J., and Tarney, J., 1988, Origin of MORB and chemically depleted mantle reservoirs: trace element constraints, Journal of Petrology, v. 198, p. 415-445.

Seedorff, E., 1991, Magmatism, extension, and ore deposits of Eocene to Holocene age in the Great Basin; mutual effects and preliminary proposed genetic relationships, *in* G.L., Raines, R.E. Lisle, R.W. Schafer and W.H. Wilkinson, eds., Geology and ore deposits of the Great Basin, Symposium Proceedings, p. 133-178.

Stille, P., Unruh, D.M., and Tatsumoto, M., 1983, Pb, Sr, and Hf isotopic evidence of multiple sources for Oahu, Hawaii basalts, Nature, v. 304, p. 25-29.

Streck, M.J., and Grunder, A.L., 2007, Phenocryst-poor rhyolites of bimodal, tholeiitic provinces: the Rattlesnake Tuff and implications for mush extraction models, Bulletin of Volcanology, DOI 10.1007/s00445-007-0144-3

Wyld, S., J., Umhoefer, P.J., and Wright, J.E., 2006, Reconstructing northern Cordilleran terranes along known Cretaceous and Cenozoic strike-slip faults: Implications for the Baja British Columbia hypothesis and other models, *in* Haggart, J.W., Enkin, R.J., and Monger, J.W.H., *eds.*, Paleogeography of the North American Cordillera: Evidence For and Against Large-Scale Displacements: Geological Association of Canada, Special Paper 46, p. 277-298.

CHAPTER 5: SUMMARY

CONCLUSIONS

I report 58 new major and trace element analyses, 12 new ^{40}Ar-^{39}Ar ages and 11 new Sr, Nd, Pb, and Hf isotopic ratios from Miocene volcanic rocks. These analyses are complimented with detailed geologic mapping of volcanic units and their relation to NW- and NNE-striking extensional structures near Abert Rim, one of the primary Basin and Range faults in the northwestern Basin and Range Province (NWBR). Below I outline the principal findings of my work and present them in line with the research questions posted at the beginning of this thesis.

RE-VISIT RESEARCH QUESTIONS

1. ***What are causes for a change form calc-alkaline to mafic/bimodal magmatism within the NWBR?***

The change from Early Miocene calc-alkaline to mafic/bimodal magmatism within the NWBR records a change in the tectonic setting of the region. Early Miocene magmas were formed within a subduction zone setting or, an immature transtensional setting, which had recently been metasomatized by subduction zone processes. In contrast, Late Miocene magmatism reflects maturation of an extensional regime and ongoing continental rifting.

2. ***Are intermediate Early Miocene volcanoes within the NWBR part of the ancestral Cascades volcanic arc?***

Early Miocene volcanic rocks of the NWBR are intermediate calc-alkaline rock suites that have chemical attributes similar to arc magmas. However, their formation in a tensional setting cannot be ruled out, particularly due to the fact that a composition similar to a Late Miocene HAOT is the best-fit for a parental composition of basaltic andesites of the Coleman Hills suite.

3. ***When did extension arrive in southern Oregon, and what were the tectonic controls on its arrival?***

Extensional faulting arrived in southern Oregon, near Lake Abert, between 8.8 and 7 Ma. The alignment of volcanic centers and progression of volcanism, from rhyolite to basalt, indicate weakening of the crust prior to (or during) formation of Abert Rim. Bimodal volcanism of the Late Miocene suite resulted from accelerated continental rifting driven by an increase in northwesterly motion of the Pacific Plate with respect to North America.

4. ***How did extension expand into the NWBR? Along-strike propagation from the south? Across-strike propagation from the east? Both?***

Extensional structures within the NWBR propagated both along-strike, from south to north, and across-strike, from east to west. At roughly the latitude of the study area, the onset of extension within the High Cascade graben to the west occurred at ~4.5 Ma and extensional faulting at Steens Mountain, to the east, was ongoing by ~10 Ma. Within the study area, partial restoration of cross-sections illustrates that the southern segment of the Abert Rim fault was active prior to the northern segment. Thus, the onset of extensional faulting within the NWBR shows both along- and across-strike migration since the last ~10 Ma.

5. ***What is the relative temporal development of NW- vs. NNE-striking faults of the NWBR?***

Near Lake Abert, NW-striking faults formed prior to NNE-striking faults. Angular unconformities of ~5-15º, related to stratigraphic separation due to faulting, are identified between ~8.7, ~7.7 and 7.0 Ma volcanic units. While both NW- and NNE-striking faults cut Late Miocene volcanic units, it is demonstrated through field documentation and partial restorations of cross-sections that NW-striking faults formed ahead of NNE-striking faults at the latitude of the Coleman Hills. In this way, the ~9-7 Ma volcano-tectonic setting of this part of Abert Rim is similar to the modern configuration of volcanism of the HLP at the northern tip of Abert Rim.

6. ***Are the patterns of Late Miocene faults of the NWBR formed solely in response to regional stress or are their orientations affected by an older tectonic fabric?***

Early Miocene dikes mimic the strike of Late Miocene faults at both Abert Rim and Guano Rim although it is not clear whether or not extensional faulting occurred during this time. NW- and NNE-striking faults associated with Late Miocene extensional deformation are likely reactivating an older structural fabric.

BIBLIOGRAPHY

Allegre, C.J., 1988, The behavior of the Earth: continental and seafloor mobility, Harvard University Press, 272 p.

Allmendinger, R.W., Hauge, T.A., Huaser, E.C., Potter, C.J., Klemperer, S.L., Nelson, K.D., Knuepfer, P., and Oliver, J., 1987, Overview of the COCORP 40˚ N transect, western United States: The fabric of an orogenic belt, Geological Society of America Bulletin, v. 98, p. 308-319

Armstrong, R.L., and Ward, P., 1991, Evolving geographic patterns of Cenozoic magmatism in the North American Cordillera: The temporal and spatial association of magmatism and metamorphic core complexes, Journal of Geophysical Research, v. 96, p. 13,201-13,224.

Atwater, T., and Stock, J., 1998, Pacific-North America plate tectonics of the Neogene southwestern United States-An update, in Ernst, W.G., ed, International Geological Review, Clarence Hall Symposium volume, v. 40, p. 375-402.

Bennett, R.A., Davis, J.L., Meertens, C.M., Smith, R.B., Wernicke, B.P., and Sheehan, A.F., 1998, Integration of the northern Basin and Range (NBAR) and Wasatch Front GPS networks for crustal deformation in and around the southern Intermouuntain seismic belt, in, Seismological Society of America 93rd annual meeting, Boulder, Colorado, p. 159.

Best, M, G., 1988, Early Miocene change in direction of least principal stress, southwestern Unived States: conflicting inferences from dikes and metamorphic core-detachment fault terranes, Tectonics, v. 7, p. 249-259.

Blackwell, D.D., 1978, Heat flow and energy loss in the Western United States, Geological Society of America Memoir 152, p. 175-208.

Carlson, R.W., Lugmair, G.W., and MacDougall, J.D., 1981, Columbia River volcanism: the question of mantle heterogeneity or crustal contamination, Geochemica et Cosmochimica Acta, v. 45, p. 2483-2499.

Carlson R.W. and Hart, W.K., 1987, Crustal genesis on the Oregon Plateau, Journal of Geophysical Research, v. 92, 6191-6206.

Carlson R.W., Czamanske, G. Fedorenko, V., and Ilupin, I., 2006, A comparison of Siberian meimechites and kimberlites: Implications for the source of high-Mg alkalic magmas and flood basalts: Geochemistry, Geophysics and Geosystmes, v. 7, no. 11, 22 p.

Catchings, R.D., and Mooney, W.D., 1988, Crustal structure of east central Oregon: Relation between Newberry volcano and regional crustal structure, Journal of Geophsical Research, v. 93, p. 10,081-10,094.

Christiansen, R.L., and McKee, E.H., 1978, Late Cenozoic volcanic and tectonic evolution of the Great Basin and Columbia Intermontane regions, Geological Society of America Memoir 152, p. 283-311.

Christiansen, R.L., Yeats, R.S., 1992, Post-Laramide geology of the U.S. Cordilleran region, in Geological Society of America Special Publication, The geology of North America: The Cordilleran Orogen; conterminous U.S., Burchfiel, B.C., Lipman, P.W., and Zoback, M.L. (eds.), p. 261-406.

Christiansen, R.L., Foulger, G.R., and Evans, J.R., 2002, Upper-mantle origin of the Yellowstone hotspot, Geological Society of America Bulletin, v. 114, p. 1,245-1,256.

Colgan, J.P., Dumitru, T.A., and Miller, E.L., 2004, Diachroneity of Basin and Range extension and Yellowstone hotspot volcanism in northwestern Nevada, Geological Society of America Bulletin, v. 32, p. 121-124.

Coney, P.J. and Reynolds, S.J., 1977, Cordilleran Benior zones, Nature, v. 270, p. 403-406.

Crider, J.G., 2001, Oblique slip and the geometry of normal-fault linkage: mechanics and a case study from the Basin and Range in Oregon, Journal of Structural Geology, v. 23, p. 1,997-2,009.

Dilles, J.H., and Gans, P.B., 1995, The chronology of Cenozoic volcanism and deformation in the Yerringtion area, western Basin and Range and Walker Lane, Geological Society of America Bulletin, v. 107, p. 474-486.

Donath, F.A., 1962, Analysis of Basin-Range structure, south-central Oregon, Geological Society of America Bulletin, v. 73, p. 1-16.

Draper, D.S., 1991, Late Cenozoic bimodal magmatism in the northern Basin and Range Province of southeastern Oregon, Jounal of Volcanology and Geothermal Research, v. 47, p. 299-328.

Duncan, R.A., and Hogan, L.G., 1994, Radiometric dating of young MORB using the ^{40}Ar-^{39}Ar incremental heating method, Geophysical Research Letters, v. 21, p. 1927-1930.

Duncan, R.A., Hooper, P.R., Rehacek, J., Marsh, J.S., and Duncan, A.R., 1997, The timing and duration of the Karoo igneous event, southern Gondwana, Journal of Geophysical Research, v. 102, p. 18127-18138.

Faulds, J.E., Henry, C.D., and Hinz, N.H., 2005, Kinematics of the northern Walker Lane: An incipient transform fault along the Pacific-North American plate boundary, Geology, v. 33, p. 505-508.

Geological Society of America, 1987, Gravity Anomaly Map of North America, GSA Decade of North American Geology, scale: 1:5,000,000.

Gerlach, D.C., 1988, Magma sources of the Cape Verdes Archipelago: isotopic and trace element constraints, Geochimica et Cosmochimica Acta, v. 52, p. 2979-2992.

Grove, T.L., Kinzler, R.J., Baker, M.B., Donnelly-Nolan, J.M., and Lesher, C.E., 1988, Assimilation of granite by basaltic magma at Burnt lava flow, Medicine Lake Volcano, northern California: decoupling of heat and mass transfer, Contributions to Mineralogy and Petrology, v. 99, p. 320-343.

Hamilton, W.B., 1989, Crustal geologic processes of the United States, in Pakiser, L.C., and Mooney, W.D., Geological Society of America Memoir, v. 172, 743-781.

Hart, S.R., and Zindler, A., 1986, In search of a bulk-Earth composition, Chemical Geology, v. 57, p. 247-267.

Hart, W.K., and Mertzman, S.A., 1982, K-Ar ages of basalts from southcentral and southeastern Oregon, Isochron-west, no. 33, p. 23-26.

Hart, W.K., Aronson, J.L., and Mertzman, S.A., 1984, Areal distribution and age of low-k, high-alumina olivine tholeitte magmatism in the northwestern Great Basin, Geological Society of America Bulletin,
v. 95, p. 186-195.

Hemphill-Haley, M.A., Page, W.D., Burke, R., and Carver, G.A., 1989, Holocene activity of the Alvord fault, Steens Mountain, southeastern Oregon: Rinal Report to the U.S. Geological Survey under Grant No. 14-08-001-61333, 45 p.

Hearn, T., Beghoul, N., and Barazangi, M., 1991, Tomography of the Western UnitedStates from regional arrival times, Journal of Geophysical Research, v. 96, p. 16,369-16,381.

Hooper, P.R., Conrey, R.M., 1989, Volcanism and teectonism in the Columbia River flood-basalt province, GSA Special Paper v. 239, p. 293-306

Hooper, P.R., Binger, G.B., and Lees, K.R., 2002, Ages of the Steens and Columbia River flood basalts and their relationship to extension-related calc-alkalic volcanism in eastern Oregon, Geological Society of America Bulletin, v. 114, p. 43-50.

Hughes, S.S., and Taylor, E.M., 1986, Geochemistry, petrogenesis, and tectonic implications of central High Cascade mafic platform lavas, Geological Society of America Bulletin, v. 97, p. 1024-1036.

Humphreys, E.D., 1994, post-Laramide removal of the Farallon slab, western United States, Geology, v. 23, p. 987-990.

Humphreys, E.D., and Coblentz, D.D., 2007, North American dynamics and western U.S. tectonics, Reviews of Geophysics, v. 45, 30 p.

John, D.A., Garside, L.J., and Wallace, A.R., 1999, Magmatic and tectonic setting of Late Cenozoic epithermal gold-silver deposits in northern Nevada, with an emphasis on the Pah Rah and Virginia Ranges and the Northern Nevada Rift, Geological Society of Nevada spring 1999 field trip guidebood, Special Publication #29, p. 65-110.

Johnson, J.A., Hawkesworth, C.J., Hooper, P.R., and Binger, G.B., 1998, Major- and trace-element analyses of Steens basalt, southeastern Oregon, U.S. Geological Survey Open-File Report 98-482, 30 p.

Johnson, J.A., and Grunder, A.L., 2000, The making of intermediate composition magma in a bimodalsuite: Duck Butte Eruptive Center, Oregon, USA, Journal of Volcanology and Geothermal Research, v. 95, p. 175-195.

Johnson, D.M., Hooper, P.R., and Conrey, R.M., 1999, XRF analysis of rocks and minerals for major and trace elements on a single low dilution Li-tetraborate fused bead: Advances in X-ray analysis, v. 41, p. 843-867.

Jordan, B.T., 2001, Basaltic volcanism and tectonics of the High Lava Plains, southeastern Oregon, [Ph.D. Thesis] Corvallis, Oregon, Oregon State University, 218 p.

Jordan, B.T., Grunder, A.L., Duncan, R.A., and Deino, A.L., 2004, Geochronology of Oregon High Lava Plains volcanism: Mirror image of the Yellowstone hotspot?, Journal of Geophysical Research, 19 pp.

Khodayar, M., 1999, On the pattern of faults and dykes in Borgarfjordur, W-Iceland, Jokull, v. 47, p. 21-44.

Langer, V.W., 1991, Geology and petrologic evolution of silicic and intermediate volcanic rocks underneath Steens Mountain basalt, SE Oregon: Queen's University (CAN) M.S. thesis, 109 pp.

Langridge, R.M., Weldon, R.J., Pezzopane, S.K., and Jellinek, A. M., 1996, Active faulting and tufa formation at Sawed Horn, central Oregon: a possible kinematic link between the Abert Rim and Viewpoint faults, Geological Society of America Abstracts with Programs, v. 28, no. 5, p. 84.

Lawrence, R.D., 1976, Strike-slip faulting terminates the Basin and Range province in Oregon, Geologic Society of America Bulletin, v. 87, p. 846-850.

Legge, P.W., 1988, The bimodal basalt-rhyolite association west of and adjacent to the Pueblo Mountains, southeastern Oregon [M.S. Thesis] Miami University of Ohio, Oxford, Ohio

LeBas, M.J., LeMaitre, R.W, Streckeisen, A., and Zanettin, B., 1986, A chemical classification of volcanic rocks based on the total alkali-silica diagram, Journal of Petrology, v. 27, p. 745-750.

LeMaitre, R.W., 1984, A proposal by the IUGS Subcommission on the Systematics of Igneous Rocks for a chemical classification of volcanic rocks based on the total alkali silica (TAS) diagram, Australian Journal of Earh Sciences, v. 31, p. 243-255.

Maloney, N.J., 1961, Geology of the Eastern Part Beaty Butte Four Quadrangle, Oregon, [M.S. Thesis], Oregon State University, Corvallis, Oregon, 88 p.

Mankinen, E.A., Larson, E.E., Gromme, C. S., Prevot, M., and Coe, R.S., 1987, The Steens Mountain (Oregon) geomagnetic polarity transition, its regional significance, Journal of Geophysical Research, v. 92, p. 8057=8076.

Mathis, A.C., 1993, Geology and petrology of a 26-Ma trachybasalt to peralkaline rhyolite suite exposed at Hart Mountain, southern OR [M.S. thesis]: Corvallis, Oregon, Oregon State University, 141 p.

McDonough, W.F., Sun, S.S., Ringwood, A.E., Jagoutz, E., and Hofmann, A.W., 1992, Potassium, rubidium, and cesium in the Earth and Moon and the evolution of the mantle of the Earth, Geochimica et Cosmochimica Acta, v. 56, p. 1001-1012.

Miller, E.L, Gans P.B., and Garing, J.,1983, the Snake Range decollement, an exhumed mid-Tertiary ductile-brittle transition, Tectonics, v. 2, p. 239-263.

Miller, E.L., Dumitru, T., Brown, R., and Gans P.B., 1999, Rapid Miocene slip on the Snake Range decollement, Geol. Soc Am . Bull, v. 111, p. 886-905.

Miller, M. M., Johnson, D.J., Dixon, T.H., and Dokka, R.K., 2001, Refined kinematics of the Eastern California shear zone from GPS observations, 1993-1998, Journal of Geophysical Research, v. 106, p. 2245-2263.

Minor, S.A., Plouff, D., Esparza, L.E., and Peters, T.J., 1987, Geologic map of the High Steens and Little Blitzen Gorge wilderness study areas, Harney County, Oregon: U.S. Geological Survey Miscellaneous Field Studies Map MF-1976, scale 1:24,000.

Mooney, W.D., and Braile, L.W., 1989, The seismic structure of the continental crust and upper mantle of North America, *in* The geology of North America-An overview, Bally, A.W., and Palmer, A.R. *eds.*, Boulder, Colorado: Geological Society of America, Decade of North American Geology, v. 1 p. 437-462.

Murphy, R.T., Faulds, J.E., and Hillemeyer, F.L., 2004, Evolution of Miocene extensional fault and fold systems and influence of magmatism in the northern Colorado River extensional corridor, Union Passarea, northwest Arizonea, Geological Society of America Abstracts with Programs, v. 36, no. 4, p. 21.

Nakamura, K., and Uyeda, S., 1980, Stress gradient in arc-back arc regions and plate subduction, Journal of Geophysical Research, v. 85, p. 6419-6428.

Niewendorp, C.A., and Neuhaus, M.E., 2003, Map of selected earthquakes for Oregon, 1841 through 2002, State of Oregon Department of Geology and Mineral Industries Open-File Report 03-02.

Oldow, J.S., 2003, Active transtensional boundary zone between the western Great Basin and Sierra Nevada block, Western U.S. Cordillera, Geology, v. 31, p. 1033-1036.

Pezzopane, S.K., and Weldon, R.J., 1993, Tectonic role of active faulting in central Oregon, Tectonics, v. 12, p. 1,140-1,169.

Pierce, K.L., and Morgan, L.A., 1992, The track of the Yellowstone hotspot: Volcanism, faulting, and uplift, in Link, P.K., Kuntz, M.A., and Platt, L.B., eds., Regional geology of eastern Idaho and western Wyoming: Geological Society of America Memoir 179, p. 1-53.

Price, J.G., and Henry, C.D., 1984, Stress orientations during Oligocene volcanism in Trans-Pecos Texas: Timing the transition from Laramide compression to Basin and Range tension, Geology, v. 12, p. 238-241.

Qamar, A., and Meagher, K.L., 1993, Precisely locating the Klamath Falls, Oregon, earthquakes, Earthquakes and Volcanoes, v. 24, p. 129-139.

Rollinson, H.R., 1993, Using geochemical data: evaluation, presentation, interpretation, Harlow, UK, 352 p

Rowley, P.D., 1998, Cenozoic transverse zones and igneous belts in the Great Basin, western United States: their tectonic and economic implications, *in* Faulds, J.E., and Stewart, J.H., eds., Accommodation zones and Transfer Zones: The regional segmentation of the Basin and Range Province: Boulder, Colorado, Geological Society of America Special Paper 323.

Saunders, A.D., Nory, M.J., and Tarney, J., 1988, Origin of MORB and chemically depleted mantle reservoirs: trace element constraints, Journal of Petrology, v. 198, p. 415-445.

Sawlan, M.G., King, H.D., Plouff, D., and Miller, M.S., 1995, Mineral resources of the Spaulding Wilderness study area, Lake and Harney Counties, Oregon, USGS Bulletin Report no. B1738-E, 18 p.

Seedorff, E., 1991, Magmatism, extension, and ore deposits of Eocene to Holocene age in the Great Basin; mutual effects and preliminary proposed genetic relationships, *in* G.L., Raines, R.E. Lisle, R.W. Schafer and W.H. Wilkinson, eds., Geology and ore deposits of the Great Basin, Symposium Proceedings, p. 133-178.

Sherlock, M.G., Gettings, M.E., King, H.D., and Neumann, T.R., 1988, Mineral resources of the Abert Rim Wilderness Study Area, Lake County, Oregon, U.S. Geolgical Survey Bulletin, p. C1-C6.

Sherrod, D.R., Griscom, A., Turner, R.L., Minor, S.A., Graham, D.E., and Buehler, A.R., 1988, Mineral resources of the Sheepshead montains, Wildcat Canyon, and Table Mouuntain Wilderness Study Areas, Malheur and Harney counties, Oregon, U.S. Geological Survey Bulletin, p. A1-A16,

Stewart, J.H., and Carlson, J.E., 1974, Preliminary geologic map of Nevada, U.S. Geological Survey, Reston, VA.

Stille, P., Unruh, D.M., and Tatsumoto, M., 1983, Pb, Sr, and Hf isotopic evidence of multiple sources for Oahu, Hawaii basalts, Nature, v. 304, p. 25-29.

Stormer, J.C. Jr, and Nicholls, J., 1978, XLFRAC: a program for the interactive testing of magmatic differentiation models, Computers & Geosciences, v. 4, p. 143-159.

Streck, M.J., and Grunder, A.L., 1995, Crystallization and welding variations in a widespread ignimbrite sheet: The Rattlesnake Tuff, eastern Oregon: Bulletin of Volcanology, v. 57, p. 151-151-169.

Streck, M.J., and Grunder, A.L., 1997, Compositional gradients and gaps in the high-silica rhyolites of the Rattlesnake Tuff, southeastern Oregon, Journal of Petrology, v. 38, p. 133-163.

Streck, M.J., and Grunder, A.L., 2007, Phenocryst-poor rhyolites of bimodal, tholeiitic provinces: the Rattlesnake Tuff and implications for mush extraction models, Bulletin of Volcanology, DOI 10.1007/s00445-007-0144-3

Sun, S.S., and McDonough, W.F., 1989, Chemical and isotopic systematics of oceanic basalts: implications for mantle composition and processes. *In*: Saunders, A.D., and Norry, M.J. (eds.), Magmatism in ocean basins, Geological Society of London Special Publication 42, p. 313-345.

Surpless, B.E., Stockli, D.F., Dumitru, T.A., Miller, E.L., and Farley, K.A., 2002, Progressive westward encroachment of Basin and Range extension into the stable northern Sierra Nevada block, Tectonics, v. 21, no. 1, 2-1 – 2-13.

Tentler, T., and Mazzoli, S., 2005, Architecture of normal faults in the rift zone of central north Iceland, Journal of Structural Geology, v. 27, p. 1721-1739.

Thatcher,W., Foulger, G.R., Julian, B.R, Svar, J.L, Quilty, E., and Bawden, G.W., 1999, Present-day deformation across the Basin and Range Province, Western United States, Science, v. 283, p. 1714-1718.

Thomas, T.H., 1981, Geology and Mineral Deposits of the Coyote Hills Mining District, Lake County, Oregon, [M.S. Thesis] Oregon State University, Corvallis, OR 137 p.

Todt, W., Cliff, R.A, Hanser, A., and Hofmann, A.W., 1996, Evaluation of a ^{202}Pb-^{205}Pb double spike for high-precision lead isotope analysis, Geophysical Monograph, v. 95, p. 429=437.

Urbancyzk, K., 1994, Geology of the eastern part of the Clarno Formation, northeast Oregon, [Ph.D. Thesis], Washington State University, Pullman, WA, 230 p.

Walker,G.W., 1963, Reconnaissance Geologic map of the eastern half of the Klamath Falls (AMS) Quadrangle, Lake and Klamath Counties, Oregon. Mineral Investigations Field Studies Map MF-260, scale 1:250,000/

Walker, G.W., Nolf, B., 1981, Roadlog for High Lava Plains, Brothers fault zone to Harney Basin, Oregon, U.S. Geological Survey Circular, p. 113-118

Walker, G.W., and MacLeod, N.S., 1991, Geologic map of Oregon, U.S. Geological Survey, Reston, VA.

Wells, R.E., and Heller, P.H., 1988, The relative contribution of accretion, shear, and extension to Cenozoic tectonic rotation in the Pacific Northwest, Geological Society of America Bulletin, v. 100, p. 325-338.

Wernicke, B.P., and Axen, G.J., 1988, On the role of isostacy in the evolution of normal fault systems, Geology, v. 16, p. 848-851.

Wernicke, B.P., 1992, Cenozoic extensional tectonics of the U.S. Cordillera, in Burchfiel, B.C., et al., eds., The Cordilleran orogen: Conterminous U.S.: Boulder, Colorado, Geological Society of America, Geology of North America, v. G-3, p. 553-581.

Wyld, S., J., Umhoefer, P.J., and Wright, J.E., 2006, Reconstructing northern Cordilleran terranes along known Cretaceous and Cenozoic strike-slip faults: Implications for the Baja British Columbia hypothesis and other models, *in* Haggart, J.W., Enkin, R.J., and Monger, J.W.H., *eds.*, Paleogeography of the North American Cordillera: Evidence For and Against Large-Scale Displacements: Geological Association of Canada, Special Paper 46, p. 277-298.

Zoback, M.L., 1989, State of Stress and Modern Deformation of the Northern Basin and Range Province, Journal of Geophysical Research, v. 94, p. 7105-7128.

APPENDIX I: COMPARISSON OF XRF AND ICP-MS ANAYTICAL TOTALS

Comparrison made for primary compositions of samples collected from Lake Abert: HAOT basalt, Steens basalt, and Coleman Hills andesite, dacite and rhyolite. Samples with the highest analytical totals were chosen. Difference error measered: (XRF-ICP-MS)/ICP-MS

	Sc	Ba	Rb	Sr	Zr	Y	Nb	Pb	La	Ce	Th	Nd
						HAOT-basalt						
KCS-04-43												
XRF	41.80	144.50	2.10	280.30	43.70	21.50	1.00	2.80	5.00	11.60	0.00	8.50
ICP-MS	42.19	139.27	2.30	284.53	39.77	23.02	1.29	0.67	3.62	8.82	0.19	7.41
differen(	-0.39	5.23	-0.20	-4.23	3.93	-1.52	-0.29	2.13	1.38	2.78	-0.19	1.09
error %	-0.01	0.04	-0.09	-0.01	0.10	-0.07	-0.23	3.18	0.38	0.32	-1.00	0.15
						Steens-basalt						
KCS-05-20												
XRF	34.10	711.20	21.90	452.20	210.80	38.40	13.00	7.80	19.80	49.80	2.00	31.90
ICP-MS	36.88	686.71	22.32	459.96	207.39	43.58	13.47	5.31	22.93	50.44	2.49	31.41
	-2.78	24.49	-0.42	-7.76	3.41	-5.18	-0.47	2.49	-3.13	-0.64	-0.49	0.49
	-0.08	0.04	-0.02	-0.02	0.02	-0.12	-0.04	0.47	-0.14	-0.01	-0.20	0.02
						C.H. andesite						
KCS-04-23												
XRF	12.50	819.80	82.40	462.40	448.70	40.10	39.50	8.40	42.70	91.10	6.30	50.80
ICP-MS	13.16	832.80	79.30	463.36	433.66	45.32	41.21	8.67	46.39	93.49	7.75	49.11
	-0.66	-13.00	3.10	-0.96	15.04	-5.22	-1.71	-0.27	-3.69	-2.39	-1.45	1.69
	-0.05	-0.02	0.04	0.00	0.03	-0.12	-0.04	-0.03	-0.08	-0.03	-0.19	0.03
						C.H. dacite						
KCS-04-02												
XRF	15.10	1586.70	107.70	318.90	560.50	38.00	39.00	11.30	47.40	100.00	10.20	49.20
ICP-MS	16.36	1584.74	103.29	313.53	543.26	43.01	40.83	10.45	47.73	94.63	10.03	47.37
	-1.26	1.96	4.41	5.37	17.24	-5.01	-1.83	0.85	-0.33	5.37	0.17	1.83
	-0.08	0.00	0.04	0.02	0.03	-0.12	-0.04	0.08	-0.01	0.06	0.02	0.04
						C.H. rhyolite						
KCS-05-19												
XRF	5.50	128.10	206.80	30.00	367.10	70.40	57.30	13.30	68.00	122.60	21.70	58.20
ICP-MS	6.29	129.09	195.75	29.85	347.13	80.34	60.31	12.63	68.55	120.86	22.35	55.73
	-0.79	-0.99	11.05	0.15	19.97	-9.94	-3.01	0.67	-0.55	1.74	-0.65	2.47
	-0.13	-0.01	0.06	0.01	0.06	-0.12	-0.05	0.05	-0.01	0.01	-0.03	0.04

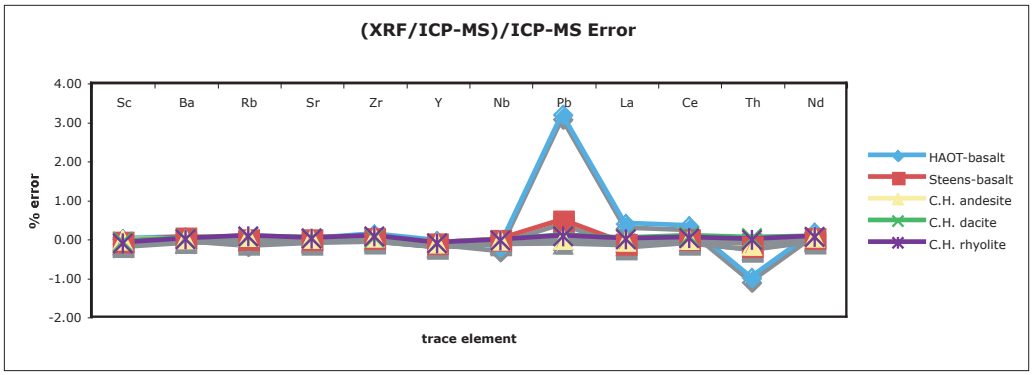

APPENDIX 2: CIPW NORMATIVE MINERAL COMPOSITIONS FOR ROCK ANALYSES

LAKE ABERT: MIOCENE VOLCANIC ROCKS

	KCS-04-22	*KCS-04-21	KCS-04-28	KCS-04-23	KCS-04-27
	Coleman Hills	Coleman Hills	Coleman Hills	Coleman Hills	Coleman Hills
	bas-ands-dike	bas-ands-dike	andesite-flow	andesite-flow	andesite-dike
wt %					
Quartz	1.36	4.18	4.83	3.61	3.44
Plagioclase	49.79	50.52	53.28	52.08	48.6
Orthoclase	16.07	17.14	20.33	20.03	23.64
Nepheline	0	0	0	0	0
Corundum	0	0	0	0	0
Diopside	8.11	4.68	1.42	3.98	4.32
Hypersthene	19.1	17.28	15.43	15.4	14.72
Olivine	0	0	0	0	0
Ilmenite	4.08	4.43	3.23	3.27	3.34
Apatite	1.48	1.78	1.48	1.62	1.95

	KCS-04-14	*KCS-04-02	KCS-04-15	KCS-04-01	*KCS-04-10
	Coleman Hills	Coleman Hills	Coleman Hills	Coleman Hills	Coleman Hills
	dacite-dike	dacite flow	dacite-scoria	rhy-block/ash	rhy-dome
wt %					
Quartz	8.08	6.86	8.37	16.89	18.28
Plagioclase	49.94	51.1	43.6	42.12	42.7
Orthoclase	27.6	26.89	33.15	35.28	33.92
Nepheline	0	0	0	0	0
Corundum	0	0	0	0	0.1
Diopside	1.49	1.2	2.23	1.68	0
Hypersthene	10.96	11.93	10.73	3.73	4.59
Olivine	0	0	0	0	0
Ilmenite	1.33	1.39	1.35	0.27	0.34
Apatite	0.6	0.65	0.58	0.05	0.07

	KCS-05-19	KCS-04-33	*KCS-05-20	KCS-04-38	KCS-04-07
	Coleman Hills	Coleman Hills	Steens	Steens	Steens
	rhy-flow	rhy-dome	basalt	basalt	basalt
wt %					
Quartz	18.45	19.95	0	0	0
Plagioclase	42.62	43.75	50.87	51.66	53.16
Orthoclase	33.92	31.79	7.86	7.45	7.92
Nepheline	0	0	0	0.27	0
Corundum	0.07	0	0	0	0
Diopside	0	0.06	15.02	15.83	13.23
Hypersthene	4.51	3.92	1.41	0	0.19
Olivine	0	0	18.03	18.36	17.4
Ilmenite	0.34	0.42	5.58	5.3	6.86
Apatite	0.09	0.12	1.23	1.14	1.25

APPENDIX II: CONTINUED

LAKE ABERT: MIOCENE VOLCANIC ROCKS

	*KCS-05-21	KCS-04-40	KCS-04-41	KCS-04-42	KCS-04-43
	HAOT	HAOT	HAOT	HAOT	HAOT
	bas-andesite	basalt	basalt	basalt	basalt
wt %					
Quartz	0	0	0	0	0
Plagioclase	58.04	56.4	57.65	56.45	55.99
Orthoclase	8.33	1.36	1.6	1.71	1.6
Nepheline	0	0.58	0.31	0.37	0.36
Corundum	0	0	0	0	0
Diopside	10.57	17.7	17.91	18.57	17.96
Hypersthene	9.23	0	0	0	0
Olivine	11.47	21.85	20.35	20.56	22.06
Ilmenite	1.82	1.82	1.88	1.99	1.71
Apatite	0.53	0.3	0.3	0.32	0.32

	KCS-04-19	KCS-04-04	KCS-04-08	*KCS-04-17	KCS-04-34
	HAOT	HAOT	HAOT	HAOT	HAOT
	basalt	basalt	basalt	basalt	basalt
wt %					
Quartz	0	0	0	0	0
Plagioclase	55.09	55.46	56.92	55.64	57.2
Orthoclase	1.42	1.54	1.3	1.24	1.77
Nepheline	0.76	0.46	0	0.46	0.33
Corundum	0	0	0	0	0
Diopside	17.57	16.92	16.97	17.59	18.53
Hypersthene	0	0	4.39	0	0
Olivine	23.09	23.55	18.97	23.11	19.81
Ilmenite	1.8	1.8	1.29	1.69	1.96
Apatite	0.25	0.25	0.16	0.28	0.39

REGIONAL VOLCANIC CENTERS: LATE MIOCENE VOLCANIC ROCKS

	KCS-06-34	KCS-06-36	KCS-06-18	KCS-06-38	KCS-06-35B
	Juniper Mtn.	Juniper Mtn.	Juniper Mtn.	Juniper Mtn.	Juniper Mtn.
	basalt	basalt	basalt	basaalt	rhyolite
wt %					
Quartz	0	0	0	0	24.14
Plagioclase	54.28	55.02	60.17	54.94	41.31
Orthoclase	3.6	3.55	1.36	7.15	28.6
Nepheline	1.39	1.05	0.36	0	0
Corundum	0	0	0	0	0.8
Diopside	14.57	14.66	14.69	14.08	0
Hypersthene	0	0	0	12.48	4.66
Olivine	22.38	21.9	21.65	7.97	0
Ilmenite	3.25	3.27	1.48	2.66	0.4
Apatite	0.53	0.56	0.3	0.72	0.09

APPENDIX II: CONTINUED

REGIONAL VOLCANIC CENTERS: LATE MIOCENE VOLCANIC ROCKS

	KCS-06-35A Juniper Mtn. rhyolite	KCS-06-37 Juniper Mtn. rhyolite	KCS-06-09 Venator Butte basalt	KCS-06-11 Venator Butte basalt	KCS-06-10 Venator Butte basalt
wt %					
Quartz	25.78	25.77	0	0	0
Plagioclase	37.95	40.39	56.87	57.54	57.18
Orthoclase	31.03	29.37	1.06	5.08	5.26
Nepheline	0	0	0.57	0	0
Corundum	0.51	0.2	0	0	0
Diopside	0	0	17.08	12.93	12.9
Hypersthene	4.28	3.88	0	5.27	3.01
Olivine	0	0	22.61	15.68	18.19
Ilmenite	0.36	0.32	1.63	2.83	2.75
Apatite	0.09	0.07	0.16	0.67	0.72

	KCS-06-16 Flint Ridge obsidian
wt %	
Quartz	16.16
Plagioclase	50.57
Orthoclase	23.99
Nepheline	0
Corundum	0.3
Diopside	0
Hypersthene	7.54
Olivine	0
Ilmenite	0.97
Apatite	0.46

RABBIT HILLS AND BEATYS BUTTE: EARLY AND LATE MIOCENE VOLCANIC ROCKS

	KCS-06-33 Rabbit Hills basalt	KCS-06-26 Rabbit Hills bas-ands	KCS-06-31 Rabbit Hills bas-ands	KCS-06-32 Rabbit Hills bas-ands	KCS-06-25 Rabbit Hills bas-ands
wt %					
Quartz	0	3.75	4.63	8.89	9.32
Plagioclase	56.1	55.28	51.1	51.15	48.46
Orthoclase	1.77	14.77	18.67	20.03	21.22
Nepheline	0.49	0	0	0	0
Corundum	0	0	0	0	0
Diopside	17.37	6.07	5.19	2.99	4.06
Hypersthene	0	15.83	16.39	13.59	13.8
Olivine	22.42	0	0	0	0
Ilmenite	1.58	3.02	3	2.47	2.37
Apatite	0.28	1.27	1.02	0.88	0.76

APPENDIX II: CONTINUED

RABBIT HILLS AND BEATYS BUTTE: EARLY AND LATE MIOCENE VOLCANIC ROCKS

	KCS-06-30B Rabbit Hills *rhyolite-subcrop	KCS-06-24 Rabbit Hills rhyolite	KCS-06-29 Rabbit Hills rhyolite	KCS-06-20 Coyote Hills andesite	KCS-06-19 Coyote Hills andesite
wt %					
Quartz	25.37	25.33	32.39	2.55	11.62
Plagioclase	37.98	40.21	36.07	58.62	50.16
Orthoclase	30.61	28.6	28.96	9.63	28.31
Nepheline	0	0	0	0	0
Corundum	0.37	0.26	0.86	0	0
Diopside	0	0	0	8.56	2.15
Hypersthene	4.88	4.84	1.59	16.93	6.46
Olivine	0	0	0	0	0
Ilmenite	0.59	0.59	0.11	2.98	1.08
Apatite	0.19	0.19	0.02	0.74	0.23

	KCS-05-48 N side of butte andesite	KCS-05-44 Fish Fin Rim andesite	KCS-05-42 Fish Fin Rim andesite	KCS-05-15 Beatys Butte rhyolite	KCS-05-46 Beatys Butte rhyolite
wt %					
Quartz	10.67	9.58	9.32	31.16	31.32
Plagioclase	50.39	49.65	49.15	35.96	35.47
Orthoclase	20.62	20.68	21.04	30.14	30.32
Nepheline	0	0	0	0	0
Corundum	0	0	0	0.42	0.64
Diopside	2.77	3.2	3.71	0	0
Hypersthene	12.35	13.6	13.43	1.92	1.83
Olivine	0	0	0	0	0
Ilmenite	2.11	2.22	2.2	0.3	0.3
Apatite	1.09	1.07	1.16	0.09	0.12

	*KCS-05-14 Shirks Look rhyolite (tuff)	KCS-05-12 Beatys Butte andesite dike	KCS-05-11 Beatys Butte andesite dike
wt %			
Quartz	32.99	7.03	7.09
Plagioclase	35.93	53.53	53.77
Orthoclase	28.31	24.64	25.06
Nepheline	0	0	0
Corundum	0.14	0	0
Diopside	0	1.45	0.27
Hypersthene	2.29	9.25	9.54
Olivine	0	0	0
Ilmenite	0.28	2.94	3
Apatite	0.05	1.16	1.27

APPENDIX 3: DETAILED DATA FOR $^{40}Ar/^{39}Ar$ ANALYSES CONDUCTED AT OREGON STATE UNIVERSITY

Shown here are detailed data, plateaus plots and inverse isochron plots for all $^{40}Ar/^{39}Ar$ age determinations discussed in the body of the thesis. Lines plotted on inverse isochron plots represent best fits through selected data and the best fir with respect to an atmospheric intercept ($^{36}Ar/^{40}Ar$ = 1/295.5 = .003384).

KCS-04-10: COLEMAN HILLS RHYOLITE

Incremental Heating			36Ar(a)	37Ar(ca)	38Ar(cl)	39Ar(k)	40Ar(r)	Age ± 2σ (Ma)	40Ar(r) (%)	39Ar(k) (%)	K/Ca ± 2σ
06C1943	600 °C	✓	0.00061	0.00336	0.00011	0.02978	0.19738	21.79 ± 1.01	52.18	0.19	3.809 ± 0.237
06C1944	700 °C	✓	0.00000	0.00073	0.00002	0.01021	0.06811	21.94 ± 0.20	99.98	0.07	6.041 ± 1.665
06C1945	800 °C	✓	0.00028	0.04055	0.00032	0.39585	2.64040	21.94 ± 0.13	96.91	2.59	4.198 ± 0.175
06C1946	900 °C	✓	0.00039	0.09078	0.00075	0.85527	5.65999	21.76 ± 0.11	98.01	5.59	4.051 ± 0.169
06C1947	975 °C	✓	0.00037	0.10505	0.00123	1.37197	9.08831	21.79 ± 0.09	98.79	8.97	5.616 ± 0.237
06C1948	1050 °C	✓	0.00093	0.12188	0.00147	1.84791	12.22404	21.76 ± 0.17	97.79	12.08	6.520 ± 0.306
06C1949	1125 °C	✓	0.00081	0.12936	0.00269	2.31553	15.30642	21.74 ± 0.16	98.45	15.13	7.697 ± 0.403
06C1950	1200 °C	✓	0.00219	0.16018	0.00458	3.06848	20.25587	21.71 ± 0.14	96.89	20.05	8.238 ± 0.411
06C1951	1300 °C	✓	0.00630	0.27518	0.00550	4.91506	32.62827	21.83 ± 0.27	94.59	32.12	7.680 ± 0.336
06C1952	1400 °C	✓	0.00081	0.06708	0.00048	0.49031	3.24314	21.75 ± 0.17	93.10	3.20	3.143 ± 0.133
		Σ	0.01269	0.99414	0.01715	15.30039	101.31193				

Information on Analysis	
Sample	KCS-04-10
Material	plagioclase
Location	OR
Analyst	jh
Project	HLP
Irradiation	OSU1E06
J-value	0.001834
Standard	28.03

Results	40(r)/39(k) ± 2σ	Age ± 2σ (Ma)	MSWD	39Ar(k) (%,n)	K/Ca ± 2σ
Weighted Plateau	6.6268 ± 0.0147 ± 0.22%	21.79 ± 0.33 ± 1.53%	1.08	100.00 10	4.485 ± 0.992
		External Error ± 0.48	2.26	Statistical T ratio	
		Analytical Error ± 0.05	1.0413	Error Magnification	
Total Fusion Age	6.6215 ± 0.0297 ± 0.45%	21.78 ± 0.34 ± 1.58%		10	6.618 ± 0.122
		External Error ± 0.49			
		Analytical Error ± 0.10			

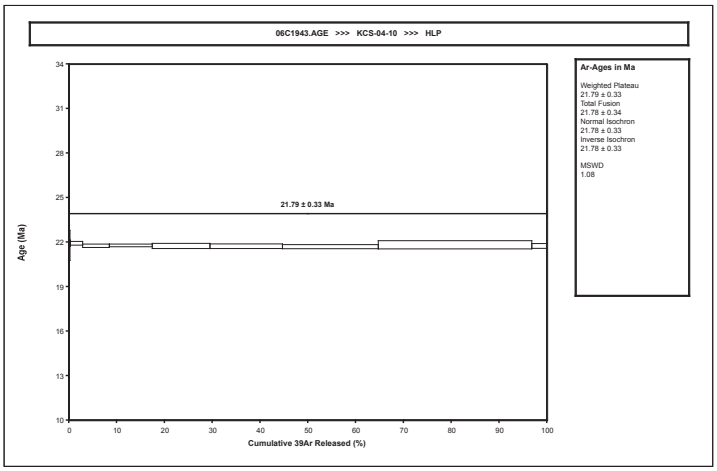

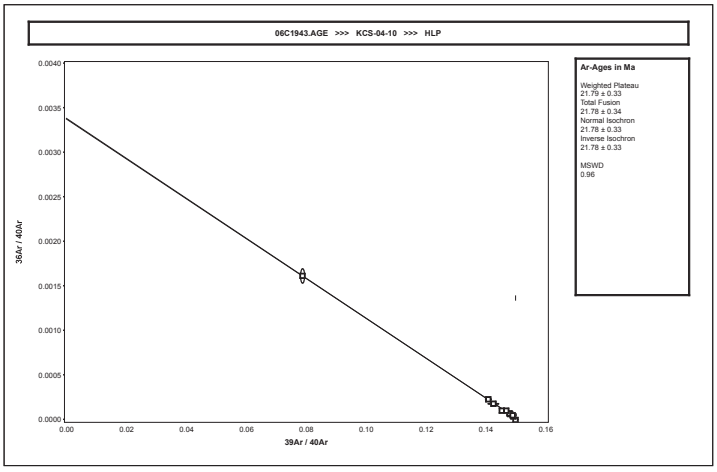

KCS-04-02: COLEMAN HILLS DACITE

Incremental Heating			36Ar(a)	37Ar(ca)	38Ar(cl)	39Ar(k)	40Ar(r)	Age ± 2σ (Ma)	40Ar(r) (%)	39Ar(k) (%)	K/Ca ± 2σ
06C1933	600 °C		0.00019	0.05376	0.00012	0.01797	0.12605	23.74 ± 1.32	68.94	0.89	0.144 ± 0.006
06C1934	700 °C		0.00004	0.16490	0.00004	0.05273	0.35891	23.04 ± 0.31	97.10	2.60	0.137 ± 0.006
06C1935	800 °C		0.00005	0.51511	0.00008	0.15860	1.03733	22.14 ± 0.16	98.57	7.82	0.132 ± 0.006
06C1936	900 °C	✓	0.00009	1.10041	0.00016	0.32280	2.07282	21.74 ± 0.15	98.67	15.93	0.126 ± 0.005
06C1937	975 °C	✓	0.00010	1.37639	0.00015	0.37250	2.38681	21.69 ± 0.16	98.73	18.38	0.116 ± 0.005
06C1938	1050 °C	✓	0.00010	1.49992	0.00017	0.38630	2.48224	21.75 ± 0.15	98.85	19.06	0.111 ± 0.005
06C1939	1125 °C	✓	0.00022	1.18483	0.00025	0.29704	1.90824	21.75 ± 0.24	96.71	14.65	0.108 ± 0.005
06C1940	1200 °C	✓	0.00026	0.86948	0.00018	0.21348	1.35381	21.47 ± 0.18	94.62	10.53	0.106 ± 0.004
06C1941	1300 °C	✓	0.00023	0.52987	0.00022	0.12862	0.82706	21.77 ± 0.20	92.42	6.35	0.104 ± 0.004
06C1942	1400 °C	✓	0.00011	0.32602	0.00009	0.07689	0.49667	21.87 ± 0.36	93.65	3.79	0.101 ± 0.004
		Σ	0.00139	7.62068	0.00146	2.02693	13.04993				

Information on Analysis	
Sample	KCS-04-02
Material	plagioclase
Location	OR
Analyst	jh
Project	HLP
Irradiation	OSU1E06
J-value	0.001888
Standard	28.03

Results	40(r)/39(k) ± 2σ		Age ± 2σ (Ma)		MSWD	39Ar(k) (%,n)	K/Ca ± 2σ
Weighted Plateau	6.4101	± 0.0250 ± 0.39%	21.70	± 0.28 ± 1.31%	1.47	88.69 7	0.109 ± 0.006
			External Error	± 0.45	2.45	Statistical T ratio	
			Analytical Error	± 0.08	1.2126	Error Magnification	
Total Fusion Age	6.4383	± 0.0201 ± 0.31%	21.80	± 0.28 ± 1.29%		10	0.114 ± 0.002
			External Error	± 0.45			
			Analytical Error	± 0.07			

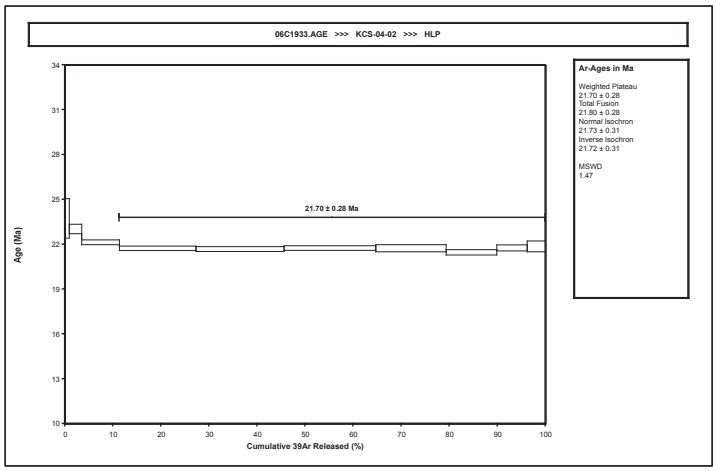

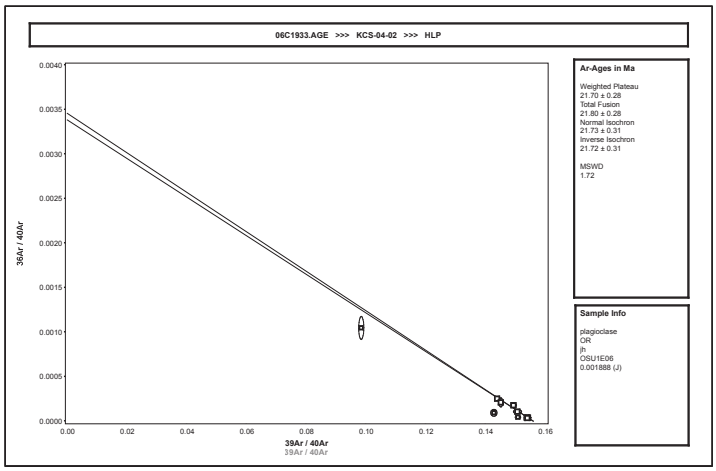

KCS-04-21: COLEMAN HILLS ANDESITE

Incremental Heating			36Ar(a)	37Ar(ca)	38Ar(cl)	39Ar(k)	40Ar(r)	Age ± 2σ (Ma)	40Ar(r) (%)	39Ar(k) (%)	K/Ca ± 2σ
06C1874	400 °C		0.00184	0.00169	0.00005	0.00161	0.02047	45.80 ± 41.92	3.62	0.19	0.410 ± 0.061
06C1875	500 °C		0.00170	0.00569	0.00004	0.00443	0.04739	38.60 ± 12.41	8.63	0.54	0.335 ± 0.020
06C1876	600 °C		0.00154	0.01303	0.00002	0.00781	0.05132	23.84 ± 7.32	10.16	0.94	0.258 ± 0.011
06C1877	700 °C		0.00130	0.04014	0.00013	0.01853	0.11440	22.39 ± 2.84	22.96	2.24	0.198 ± 0.008
06C1879	800 °C		0.00064	0.06388	0.00010	0.02524	0.18390	26.40 ± 1.60	49.21	3.05	0.170 ± 0.007
06C1880	900 °C		0.00047	0.16706	0.00010	0.05785	0.36560	22.92 ± 0.55	72.66	6.99	0.149 ± 0.006
06C1881	975 °C	✓	0.00050	0.31050	0.00015	0.09935	0.60904	22.24 ± 0.40	80.36	12.00	0.138 ± 0.006
06C1883	1050 °C	✓	0.00049	0.36281	0.00014	0.11214	0.68608	22.19 ± 0.41	82.64	13.54	0.133 ± 0.005
06C1884	1125 °C	✓	0.00074	0.53373	0.00009	0.16238	0.97022	21.68 ± 0.25	81.55	19.61	0.131 ± 0.005
06C1885	1200 °C	✓	0.00069	0.39988	0.00005	0.12009	0.73307	22.14 ± 0.36	78.26	14.50	0.129 ± 0.005
06C1887	1250 °C	✓	0.00039	0.25355	0.00001	0.07365	0.45075	22.20 ± 0.42	79.64	8.89	0.125 ± 0.005
06C1888	1300 °C	✓	0.00051	0.19952	0.00001	0.05800	0.34572	21.63 ± 0.83	69.65	7.00	0.125 ± 0.005
06C1890	1350 °C	✓	0.00041	0.16463	0.00000	0.04847	0.29608	22.16 ± 0.62	70.87	5.85	0.127 ± 0.005
06C1891	1400 °C	✓	0.00070	0.13159	0.00000	0.03852	0.24398	22.97 ± 1.34	54.17	4.65	0.126 ± 0.005
		Σ	0.01191	2.64771	0.00091	0.82807	5.11799				

Information on Analysis	
Sample	KCS-04-21
Material	feldspar
Location	OR
Analyst	kcs
Project	HLP
Irradiation	OSU1F06
J-value	0.002023
Standard	28.03

Results	40(r)/39(k) ± 2σ		Age ± 2σ (Ma)		MSWD	39Ar(k) (%,n)	K/Ca ± 2σ
Weighted Plateau	6.0663	± 0.0568 ± 0.94%	22.00	± 0.27 ± 1.22%	1.93	86.06 8	0.129 ± 0.003
			External Error	± 0.44	2.36	Statistical T ratio	
			Analytical Error	± 0.20	1.3891	Error Magnification	
Total Fusion Age	6.1806	± 0.0585 ± 0.95%	22.42	± 0.28 ± 1.23%		14	0.134 ± 0.002
			External Error	± 0.45			
			Analytical Error	± 0.21			

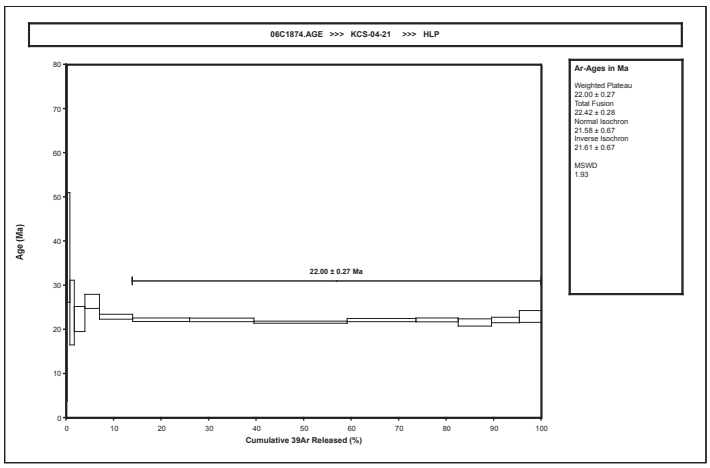

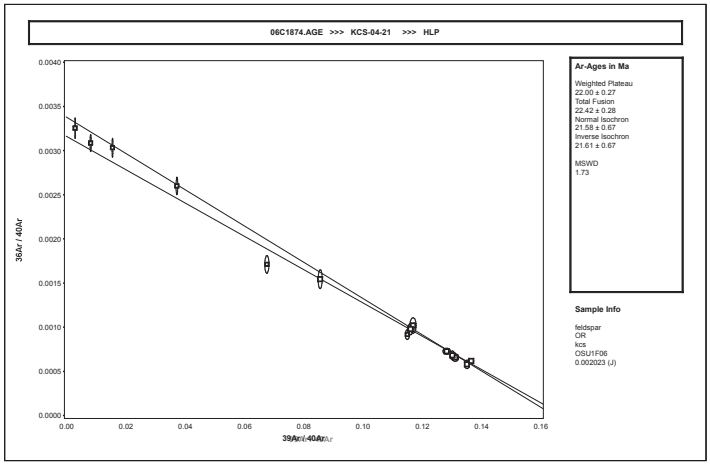

KCS-06-24: RABBIT HILLS RHYOLITE

Incremental Heating			36Ar(a)	37Ar(ca)	38Ar(cl)	39Ar(k)	40Ar(r)	Age ± 2σ (Ma)	40Ar(r) (%)	39Ar(k) (%)	K/Ca ± 2σ
07C2235	400 °C		0.001297	0.001636	0.000016	0.003723	0.018583	14.23 ± 9.00	4.63	0.18	0.979 ± 0.264
07C2236	500 °C		0.001149	0.001793	0.000024	0.004480	0.031930	20.28 ± 5.45	8.59	0.22	1.075 ± 0.203
07C2237	600 °C		0.001218	0.002514	0.000033	0.010027	0.072296	20.51 ± 2.25	16.73	0.49	1.715 ± 0.265
07C2238	700 °C		0.000546	0.001596	0.000020	0.013708	0.109765	22.77 ± 1.02	40.45	0.67	3.693 ± 0.693
07C2240	800 °C		0.000760	0.002154	0.000108	0.044309	0.364724	23.40 ± 0.46	61.85	2.16	8.846 ± 1.468
07C2241	875 °C		0.000638	0.002243	0.000142	0.060874	0.491998	22.98 ± 0.28	72.22	2.97	11.672 ± 2.384
07C2242	950 °C	✓	0.001293	0.003901	0.000324	0.134963	1.073743	22.62 ± 0.28	73.69	6.58	14.878 ± 2.002
07C2243	1000 °C	✓	0.001330	0.002970	0.000334	0.156777	1.228944	22.29 ± 0.22	75.70	7.64	22.698 ± 4.370
07C2245	1050 °C	✓	0.001484	0.003747	0.000471	0.193612	1.517899	22.30 ± 0.19	77.51	9.43	22.217 ± 2.777
07C2246	1100 °C	✓	0.001813	0.004408	0.000569	0.238681	1.876170	22.35 ± 0.14	77.71	11.63	23.284 ± 2.423
07C2247	1150 °C	✓	0.002257	0.005768	0.000755	0.294436	2.318199	22.39 ± 0.18	77.58	14.34	21.950 ± 2.242
07C2248	1200 °C	✓	0.002019	0.004738	0.000665	0.273085	2.135225	22.24 ± 0.19	78.08	13.30	24.784 ± 3.023
07C2250	1250 °C	✓	0.001586	0.003588	0.000514	0.217196	1.713637	22.44 ± 0.20	78.45	10.58	26.029 ± 3.862
07C2251	1300 °C	✓	0.001735	0.003456	0.000499	0.214528	1.680379	22.28 ± 0.15	76.55	10.45	26.695 ± 3.540
07C2252	1350 °C	✓	0.001031	0.002465	0.000304	0.127241	0.989144	22.11 ± 0.29	76.38	6.20	22.196 ± 4.007
07C2253	1400 °C	✓	0.000508	0.000805	0.000148	0.064977	0.509371	22.29 ± 0.27	77.16	3.17	34.709 ± 15.963
		Σ	0.020662	0.047781	0.004926	2.052617	16.132008				

Information on Analysis	Results	40(r)/39(k) ± 2σ		Age ± 2σ (Ma)		MSWD	39Ar(k) (%,n)	K/Ca ± 2σ	
KCS-06-24 bio HLP 4F2-06 biotite Rabbit Hills ks	Weighted Plateau	7.8514	± 0.0232 ± 0.29%	22.33	± 0.12 ± 0.53%	1.14	93.32 10	21.561	± 2.600
				External Error	± 0.37	2.26	Statistical T Ratio		
				Analytical Error	± 0.07	1.0662	Error Magnification		
Project = HLP Irradiation = OSU4F06 J = 0.0015861 ± 0.0000035 FCT-3 = 28.030 ± 0.003 Ma	Total Fusion Age	7.8592	± 0.0233 ± 0.30%	22.35	± 0.12 ± 0.53%		16	0.489	± 0.019
				External Error	± 0.37				
				Analytical Error	± 0.07				

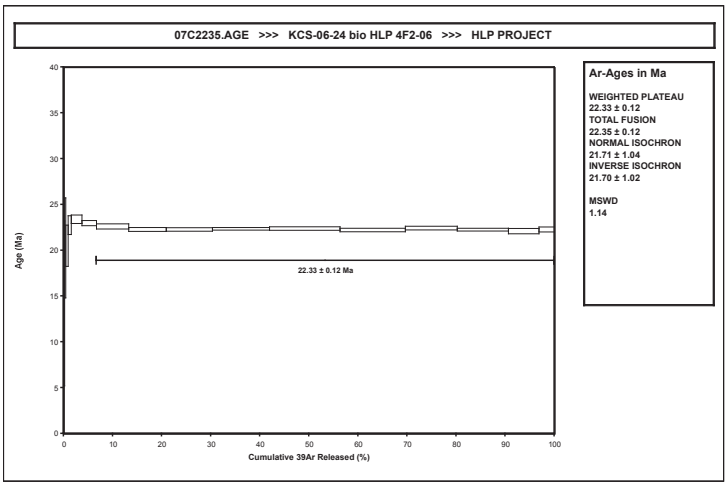

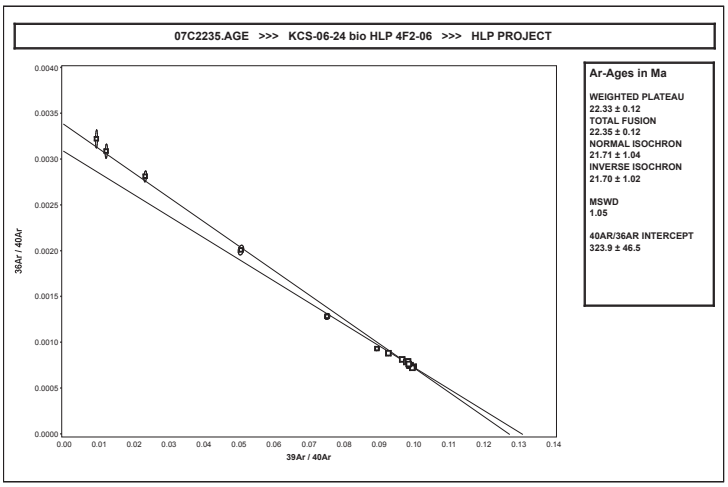

KCS-06-25: RABBIT HILS: BASALTIC ANDESITE

Incremental Heating			36Ar(a)	37Ar(ca)	38Ar(cl)	39Ar(k)	40Ar(r)	Age ± 2σ (Ma)	40Ar(r) (%)	39Ar(k) (%)	K/Ca ± 2σ
07C2181	500 °C		0.000128	0.009541	0.000019	0.005047	0.055525	31.16 ± 1.83	59.47	2.29	0.227 ± 0.016
07C2182	600 °C	✓	0.000047	0.072903	0.000012	0.017708	0.142837	22.90 ± 0.70	90.96	8.03	0.104 ± 0.008
07C2184	700 °C	✓	0.000031	0.153178	0.000018	0.023758	0.190576	22.77 ± 0.49	95.35	10.77	0.067 ± 0.004
07C2185	800 °C	✓	0.000063	0.271260	0.000008	0.035667	0.287978	22.92 ± 0.58	93.85	16.17	0.057 ± 0.004
07C2186	875 °C	✓	0.000083	0.209532	0.000002	0.024490	0.199987	23.18 ± 0.99	89.02	11.11	0.050 ± 0.003
07C2187	950 °C	✓	0.000101	0.237831	0.000013	0.026819	0.217535	23.03 ± 0.38	87.83	12.16	0.048 ± 0.003
07C2189	1025 °C	✓	0.000065	0.194678	0.000000	0.020194	0.165208	23.22 ± 0.61	89.44	9.16	0.045 ± 0.003
07C2190	1100 °C	✓	0.000061	0.177255	0.000000	0.018196	0.149003	23.24 ± 0.88	89.08	8.25	0.044 ± 0.003
07C2192	1200 °C	✓	0.000091	0.215405	0.000020	0.021832	0.180977	23.53 ± 0.70	86.97	9.90	0.044 ± 0.003
07C2193	1300 °C	✓	0.000090	0.215044	0.000000	0.020908	0.175297	23.80 ± 0.59	86.79	9.48	0.042 ± 0.003
07C2195	1400 °C		0.000006	0.061003	0.000000	0.005903	0.054558	26.21 ± 1.68	96.99	2.68	0.042 ± 0.003
		Σ	0.000765	1.817631	0.000093	0.220523	1.819482				

Information on Analysis	Results	40(r)/39(k) ± 2σ		Age ± 2σ (Ma)		MSWD	39Ar(k) (%,n)	K/Ca ± 2σ
KCS-06-25 plag HLP 4F4-06 plagioclase OR jh	Weighted Plateau	8.1461	± 0.0772 ± 0.95%	23.12	± 0.24 ± 1.04%	1.24	95.03 9	0.048 ± 0.007
				External Error	± 0.44	2.31	Statistical T Ratio	
				Analytical Error	± 0.22	1.1119	Error Magnification	
Project = HLP Irradiation = OSU4F06 J = 0.0015836 ± 0.0000035 FCT-3 = 28.030 ± 0.003 Ma	Total Fusion Age	8.2508	± 0.0785 ± 0.95%	23.42	± 0.24 ± 1.04%		11	0.001 ± 0.000
				External Error	± 0.44			
				Analytical Error	± 0.22			

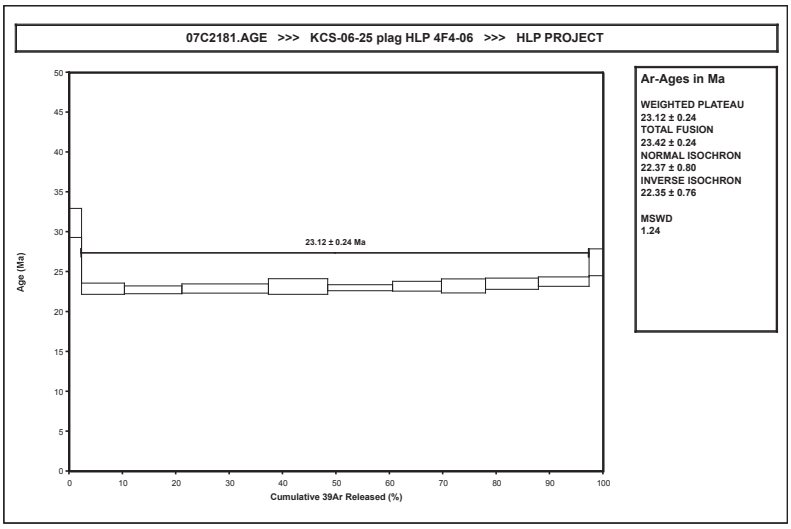

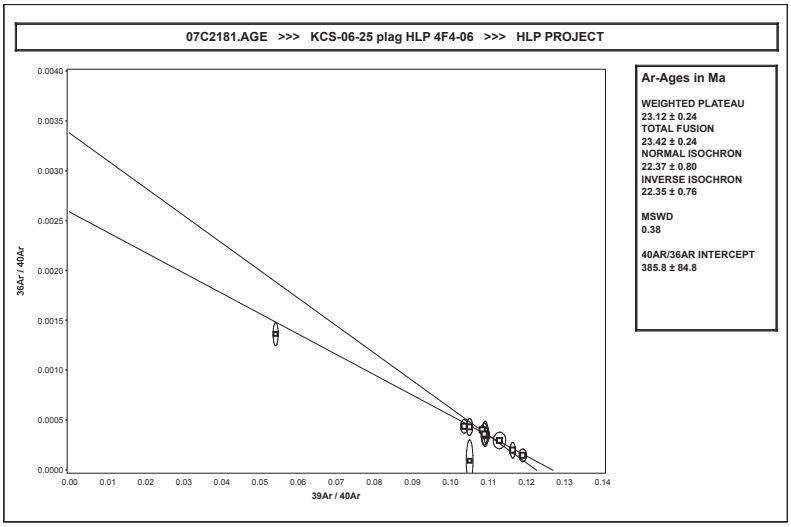

KCS-06-29: RABBIT HILLS RHYOLITE

Incremental Heating			36Ar(a)	37Ar(ca)	38Ar(cl)	39Ar(k)	40Ar(r)	Age ± 2σ (Ma)	40Ar(r) (%)	39Ar(k) (%)	K/Ca ± 2σ
07C1347	400 °C	✓	0.009215	0.018554	0.000176	0.360390	2.688642	20.02 ± 0.50	49.68	5.23	8.352 ± 0.387
07C1348	500 °C	✓	0.001052	0.014778	0.000179	0.304737	2.293764	20.20 ± 0.17	88.05	4.42	8.867 ± 0.394
07C1349	600 °C	✓	0.001790	0.041371	0.000411	0.828959	6.249572	20.23 ± 0.18	92.19	12.04	8.616 ± 0.413
07C1350	700 °C	✓	0.004582	0.097911	0.001198	1.493367	11.314439	20.33 ± 0.12	89.30	21.68	6.559 ± 0.277
07C1351	775 °C	✓	0.008695	0.142031	0.001403	1.454410	11.087200	20.46 ± 0.11	81.18	21.12	4.403 ± 0.185
07C1352	850 °C	✓	0.015860	0.135416	0.001275	1.061056	8.087102	20.45 ± 0.28	63.31	15.41	3.369 ± 0.144
07C1353	925 °C	✓	0.033495	0.076259	0.000461	0.550718	4.057167	19.77 ± 1.01	29.07	8.00	3.105 ± 0.138
07C1354	1000 °C		0.082142	0.043542	0.000274	0.380362	2.218677	15.67 ± 4.71	8.37	5.52	3.756 ± 0.200
07C1355	1075 °C		0.089434	0.024944	0.000532	0.262927	1.749381	17.87 ± 3.79	6.21	3.82	4.532 ± 0.319
07C1356	1175 °C		0.070556	0.017026	0.000638	0.171938	1.373273	21.43 ± 6.17	6.18	2.50	4.342 ± 0.349
07C1357	1300 °C		0.009580	0.006411	0.000078	0.018651	0.189087	27.16 ± 6.06	6.26	0.27	1.251 ± 0.067
		Σ	0.326402	0.618243	0.006626	6.887515	51.308304				

Information on Analysis	Results	40(r)/39(k) ± 2σ		Age ± 2σ (Ma)		MSWD	39Ar(k) (%,n)	K/Ca ± 2σ
KCS-06-29 wr 4C17-06 whole rock Rabbit Hills ks	Weighted Plateau	7.5801	± 0.0347 ± 0.46%	20.34	± 0.18 ± 0.87%	2.06	87.89 7	4.345 ± 1.488
				External Error	± 0.37	2.45	Statistical T Ratio	
				Analytical Error	± 0.09	1.4345	Error Magnification	
Project = HLP Irradiation = OSU4C06 J = 0.0014960 ± 0.0000055 FCT-3 = 28.030 ± 0.003 Ma	Total Fusion Age	7.4495	± 0.1313 ± 1.76%	19.99	± 0.38 ± 1.90%		11	0.127 ± 0.002
				External Error	± 0.50			
				Analytical Error	± 0.35			

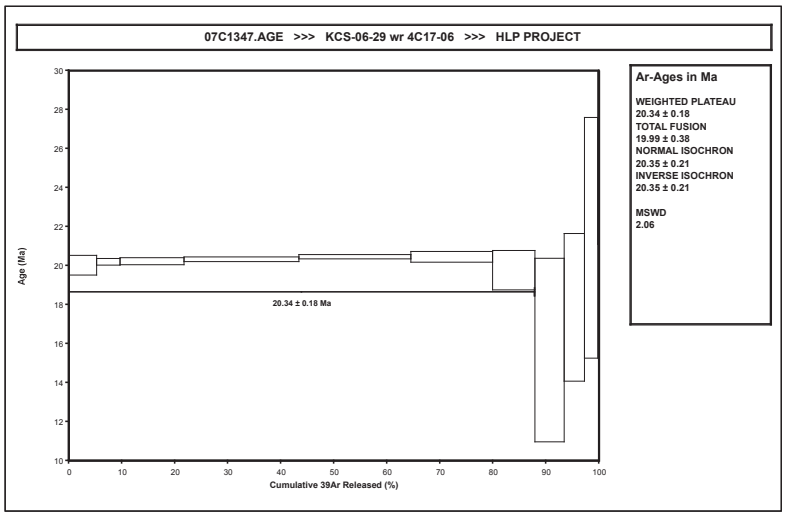

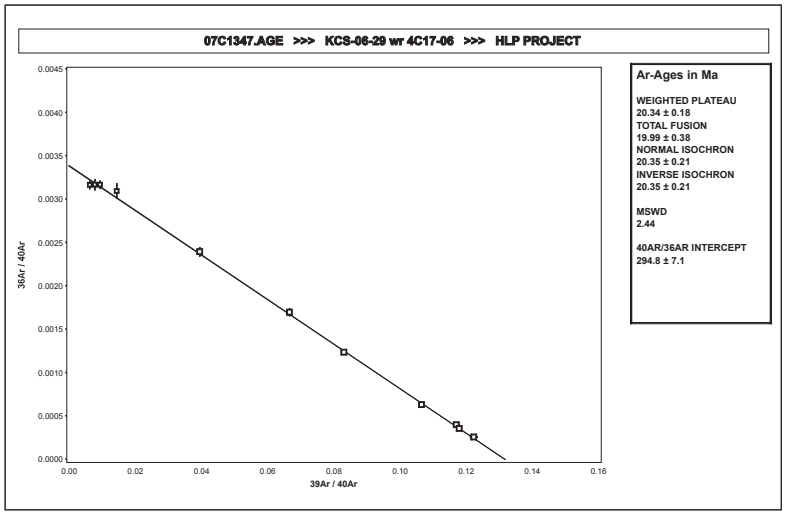

KCS-05-20: LAKE ABERT STEENS BASALT

Incremental Heating			36Ar(a)	37Ar(ca)	38Ar(cl)	39Ar(k)	40Ar(r)	Age ± 2σ (Ma)	40Ar(r) (%)	39Ar(k) (%)	K/Ca ± 2σ
07C1359	600 ℃	✓	0.000120	0.021706	0.000006	0.001635	0.008732	15.10 ± 7.30	19.76	0.54	0.032 ± 0.002
07C1360	700 ℃	✓	0.000003	0.108446	0.000001	0.006979	0.041098	16.64 ± 1.49	98.11	2.29	0.028 ± 0.001
07C1361	800 ℃	✓	0.000034	0.365414	0.000000	0.021824	0.123326	15.97 ± 0.64	92.46	7.17	0.026 ± 0.001
07C1362	900 ℃	✓	0.000036	0.686114	0.000000	0.040576	0.230069	16.03 ± 0.36	95.61	13.32	0.025 ± 0.001
07C1363	975 ℃	✓	0.000009	0.734911	0.000000	0.043475	0.248423	16.15 ± 0.23	98.87	14.28	0.025 ± 0.001
07C1364	1050 ℃	✓	0.000031	0.657055	0.000000	0.039358	0.223312	16.04 ± 0.29	96.07	12.92	0.026 ± 0.001
07C1365	1125 ℃	✓	0.000154	0.610972	0.000000	0.036926	0.211801	16.21 ± 0.29	82.32	12.13	0.026 ± 0.001
07C1366	1200 ℃	✓	0.000094	0.518060	0.000000	0.030883	0.179239	16.40 ± 0.48	86.56	10.14	0.026 ± 0.001
07C1367	1300 ℃	✓	0.000369	0.350393	0.000000	0.021910	0.123667	15.95 ± 0.52	53.16	7.19	0.027 ± 0.001
07C1368	1400 ℃		0.000509	0.985159	0.000000	0.060959	0.365777	16.95 ± 0.31	70.87	20.02	0.027 ± 0.001
		Σ	0.001358	5.038230	0.000007	0.304524	1.755444				

Information on Analysis	Results	40(r)/39(k) ± 2σ		Age ± 2σ (Ma)		MSWD	39Ar(k) (%,n)	K/Ca ± 2σ
KCS-05-20 plag 4F7-06 plag Lake Abert MF	Weighted Plateau	5.7053	± 0.0456 ± 0.80%	16.12	± 0.15 ± 0.92%	0.45	79.98 9	0.026 ± 0.001
				External Error	± 0.30	2.31	Statistical T Ratio	
				Analytical Error	± 0.13	1.0000	Error Magnification	
Project = HLP Irradiation = OSU4F06 J = 0.0015736 ± 0.0000036 FCT-3 = 28.030 ± 0.003 Ma	Total Fusion Age	5.7645	± 0.0483 ± 0.84%	16.29	± 0.15 ± 0.95%		10	0.001 ± 0.000
				External Error	± 0.30			
				Analytical Error	± 0.14			

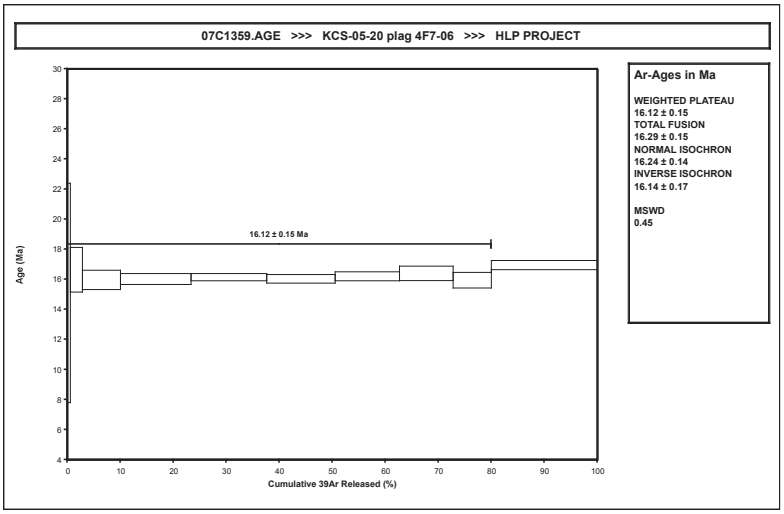

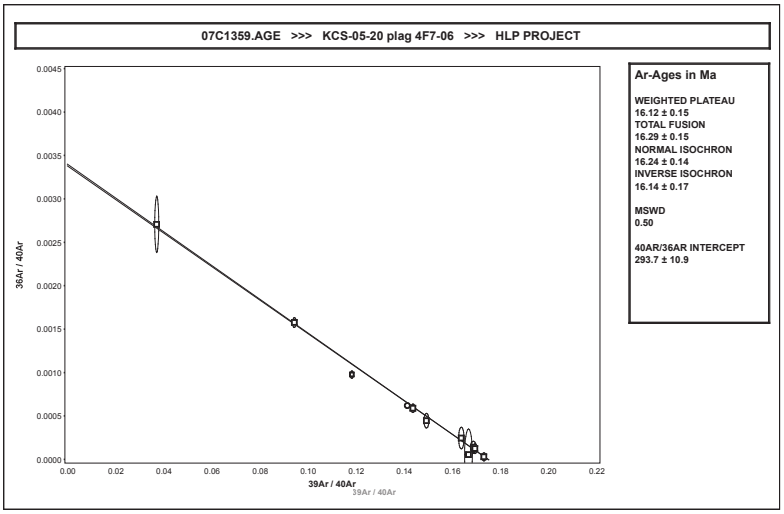

KCS-05-16: FLINT RIDGE DACITE

Incremental Heating			36Ar(a)	37Ar(ca)	38Ar(cl)	39Ar(k)	40Ar(r)	Age ± 2σ (Ma)	40Ar(r) (%)	39Ar(k) (%)	K/Ca ± 2σ
07C2203	500 °C		0.000041	0.005770	0.000001	0.003240	0.008044	7.07 ± 3.81	40.04	0.98	0.241 ± 0.024
07C2204	600 °C		0.000319	0.036950	0.000020	0.014823	0.052257	10.03 ± 1.18	35.59	4.49	0.173 ± 0.011
07C2205	700 °C	✓	0.000079	0.081346	0.000029	0.028718	0.087529	8.68 ± 0.63	78.82	8.70	0.152 ± 0.010
07C2206	800 °C	✓	0.000044	0.166284	0.000037	0.051389	0.153648	8.51 ± 0.26	91.97	15.56	0.133 ± 0.009
07C2208	900 °C	✓	0.000074	0.192941	0.000020	0.054684	0.170484	8.87 ± 0.20	88.37	16.56	0.122 ± 0.008
07C2209	1000 °C	✓	0.000055	0.195168	0.000008	0.051596	0.158546	8.75 ± 0.22	90.41	15.63	0.114 ± 0.007
07C2210	1100 °C	✓	0.000048	0.160286	0.000025	0.039672	0.121195	8.70 ± 0.24	89.18	12.01	0.106 ± 0.007
07C2211	1200 °C	✓	0.000037	0.180736	0.000029	0.042794	0.135846	9.04 ± 0.23	92.32	12.96	0.102 ± 0.007
07C2213	1300 °C		0.000040	0.122936	0.000018	0.028881	0.095748	9.44 ± 0.36	88.89	8.75	0.101 ± 0.007
07C2214	1400 °C		0.000070	0.061403	0.000001	0.014401	0.047241	9.34 ± 0.81	69.49	4.36	0.101 ± 0.007
		Σ	0.000806	1.203820	0.000188	0.330198	1.030538				

Information on Analysis	Results	40(r)/39(k) ± 2σ		Age ± 2σ (Ma)		MSWD	39Ar(k) (%,n)	K/Ca ± 2σ
KCS-06-16 plag HLP 4F5-06 whole rock Flint Ridge ks	Weighted Plateau	3.0870	± 0.0517 ± 1.67%	8.79	± 0.15 ± 1.73%	2.14	81.42 6	0.117 ± 0.014
				External Error	± 0.21	2.57	Statistical T Ratio	
				Analytical Error	± 0.15	1.4612	Error Magnification	
Project = HLP Irradiation = OSU4F06 J = 0.0015817 ± 0.0000035 FCT-3 = 28.030 ± 0.003 Ma	Total Fusion Age	3.1210	± 0.0433 ± 1.39%	8.88	± 0.13 ± 1.45%		10	0.003 ± 0.000
				External Error	± 0.19			
				Analytical Error	± 0.12			

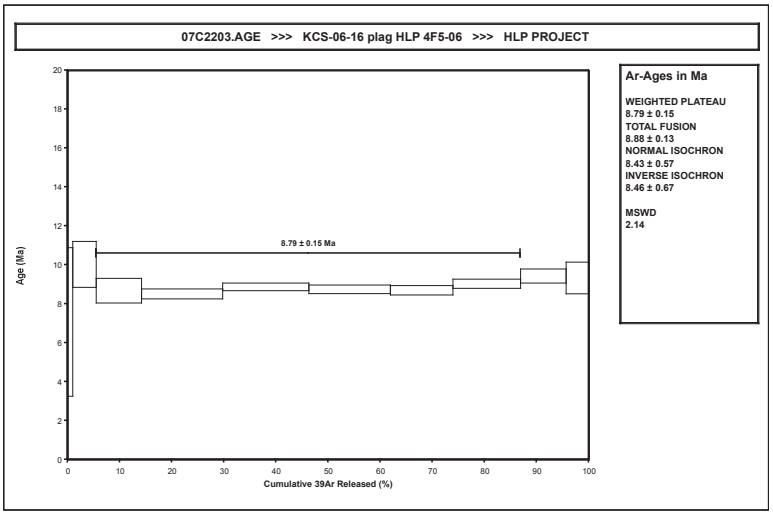

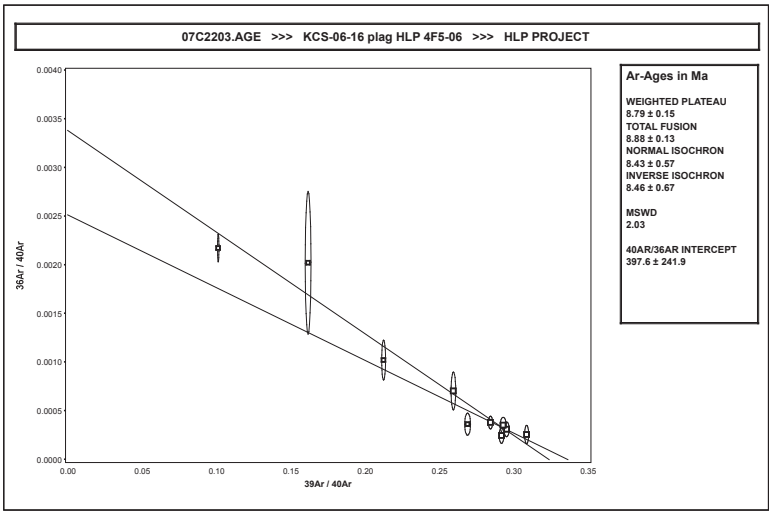

KCS-05-21: LAKE ABERT BASALTIC ANDESITE

Incremental Heating			36Ar(a)	37Ar(ca)	38Ar(cl)	39Ar(k)	40Ar(r)	Age ± 2σ (Ma)	40Ar(r) (%)	39Ar(k) (%)	K/Ca ± 2σ
06C1924	600 °C		0.00029	0.01036	0.00006	0.00191	0.01557	27.23 ± 11.49	15.57	0.28	0.079 ± 0.005
06C1925	700 °C		0.00067	0.67163	0.00018	0.04942	0.15997	10.84 ± 0.53	44.50	7.24	0.032 ± 0.001
06C1926	800 °C	✓	0.00044	1.89662	0.00000	0.11510	0.30162	8.78 ± 0.37	69.95	16.87	0.026 ± 0.001
06C1927	900 °C	✓	0.00017	2.89265	0.00000	0.16421	0.42353	8.64 ± 0.25	89.21	24.07	0.024 ± 0.001
06C1928	1000 °C	✓	0.00018	2.69640	0.00000	0.12324	0.31823	8.65 ± 0.37	85.90	18.07	0.020 ± 0.001
06C1929	1100 °C	✓	0.00107	1.74984	0.00008	0.08525	0.22800	8.96 ± 0.74	41.93	12.50	0.021 ± 0.001
06C1930	1200 °C		0.00508	1.04009	0.00033	0.06083	0.25233	13.87 ± 2.19	14.39	8.92	0.025 ± 0.001
06C1931	1300 °C		0.00188	0.63385	0.00018	0.04007	0.15497	12.94 ± 1.07	21.84	5.87	0.027 ± 0.001
06C1932	1400 °C		0.00110	0.50943	0.00020	0.04209	0.29110	23.07 ± 0.86	47.29	6.17	0.036 ± 0.001
		Σ	0.01087	12.10086	0.00103	0.68212	2.14530				

Information on Analysis	
Sample	KCS-05-21
Material	plagioclase
Location	OR
Analyst	jh
Project	HLP
Irradiation	OSU1E06
J-value	0.001861
Standard	28.03

Results	40(r)/39(k) ± 2σ	Age ± 2σ (Ma)	MSWD	39Ar(k) (%,n)	K/Ca ± 2σ
Weighted Plateau	2.5946 ± 0.0526 ± 2.03%	8.69 ± 0.21 ± 2.45%	0.32	71.51 4	0.022 ± 0.003
		External Error ± 0.25	3.18	Statistical T ratio	
		Analytical Error ± 0.18	1.0000	Error Magnification	
Total Fusion Age	3.1451 ± 0.0783 ± 2.49%	10.53 ± 0.30 ± 2.84%		9	0.024 ± 0.000
		External Error ± 0.34			
		Analytical Error ± 0.26			

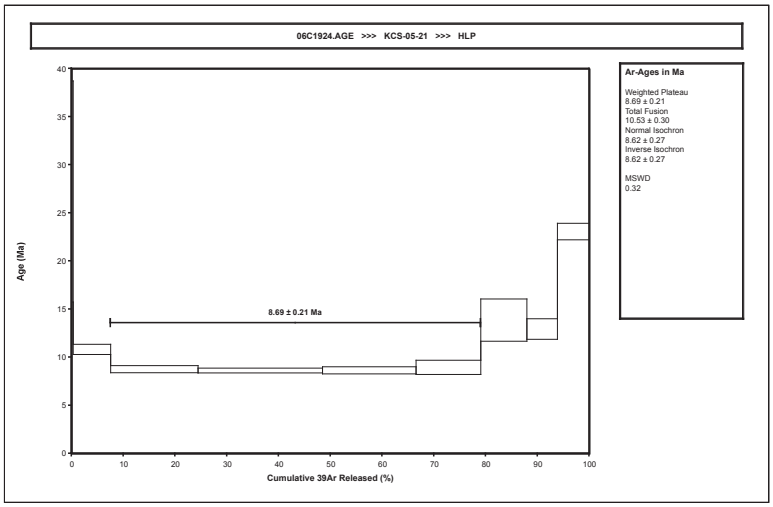

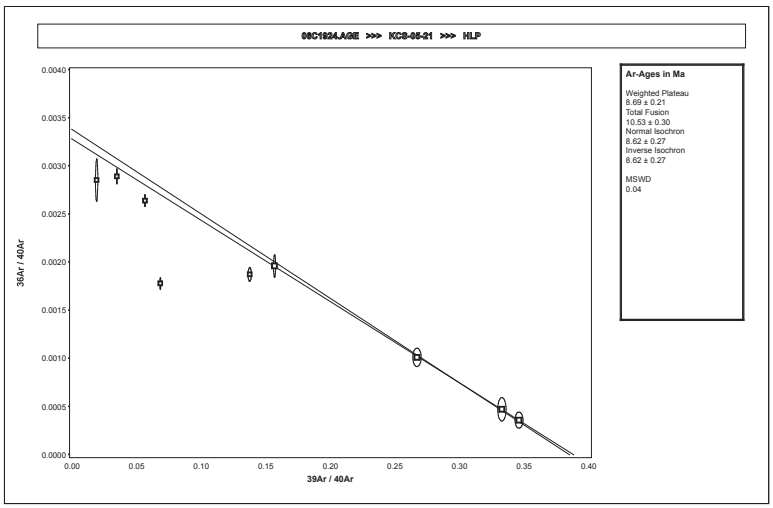

KCS-06-37: JUNIPER MOUNTAIN RHYOLITE

Incremental Heating			36Ar(a)	37Ar(ca)	38Ar(cl)	39Ar(k)	40Ar(r)	Age ± 2σ (Ma)	40Ar(r) (%)	39Ar(k) (%)	K/Ca ± 2σ
07C2215	300 °C		0.000925	0.000745	0.000023	0.001654	0.016323	28.03 ± 24.40	5.63	0.07	0.955 ± 0.491
07C2216	400 °C		0.001574	0.000912	0.000029	0.006608	0.029575	12.77 ± 5.58	5.98	0.30	3.114 ± 1.127
07C2218	500 °C		0.001636	0.002134	0.000044	0.011035	0.025485	6.60 ± 2.10	5.01	0.50	2.224 ± 0.262
07C2219	600 °C		0.001911	0.002818	0.000093	0.024036	0.099754	11.84 ± 1.94	15.01	1.08	3.668 ± 0.472
07C2220	700 °C		0.001444	0.003359	0.000137	0.046587	0.164471	10.08 ± 0.49	27.79	2.10	5.963 ± 0.725
07C2221	800 °C	✓	0.002458	0.006059	0.000638	0.229617	0.702043	8.73 ± 0.24	49.07	10.35	16.295 ± 1.530
07C2223	875 °C	✓	0.001987	0.006159	0.000702	0.257927	0.770114	8.53 ± 0.15	56.64	11.63	18.007 ± 1.416
07C2224	950 °C	✓	0.002505	0.006904	0.001105	0.397790	1.188376	8.53 ± 0.17	61.49	17.93	24.776 ± 1.941
07C2225	1025 °C	✓	0.002170	0.007286	0.001010	0.374213	1.117010	8.53 ± 0.16	63.39	16.87	22.085 ± 2.046
07C2226	1100 °C	✓	0.001460	0.005398	0.000709	0.256542	0.772689	8.60 ± 0.17	64.03	11.56	20.435 ± 1.971
07C2228	1150 °C	✓	0.001189	0.003643	0.000519	0.189514	0.573870	8.65 ± 0.13	61.89	8.54	22.372 ± 3.584
07C2229	1200 °C	✓	0.000825	0.002378	0.000341	0.126820	0.372215	8.38 ± 0.20	60.31	5.72	22.929 ± 3.997
07C2230	1250 °C	✓	0.000679	0.001880	0.000280	0.111139	0.329600	8.47 ± 0.27	62.02	5.01	25.423 ± 4.828
07C2231	1325 °C	✓	0.000603	0.001990	0.000299	0.115110	0.348003	8.63 ± 0.21	65.99	5.19	24.869 ± 5.749
07C2233	1400 °C	✓	0.000376	0.001098	0.000208	0.069970	0.215473	8.80 ± 0.22	65.83	3.15	27.398 ± 8.776
		Σ	0.021744	0.052764	0.006136	2.218562	6.725002				

Information on Analysis	Results	40(r)/39(k) ± 2σ		Age ± 2σ (Ma)		MSWD	39Ar(k) (%,n)	K/Ca ± 2σ
KCS-06-37 bio HLP 4F1-06 biotite Juniper Mtn ks	Weighted Plateau	3.0053	± 0.0235 ± 0.78%	8.58	± 0.08 ± 0.90% External Error ± 0.16 Analytical Error ± 0.07	1.39 2.26 1.1798	95.95 10 Statistical T Ratio Error Magnification	20.076 ± 2.080
Project = HLP Irradiation = OSU4F06 J = 0.0015870 ± 0.0000035 FCT-3 = 28.030 ± 0.003 Ma	Total Fusion Age	3.0312	± 0.0246 ± 0.81%	8.66	± 0.08 ± 0.92% External Error ± 0.16 Analytical Error ± 0.07		15	0.478 ± 0.016

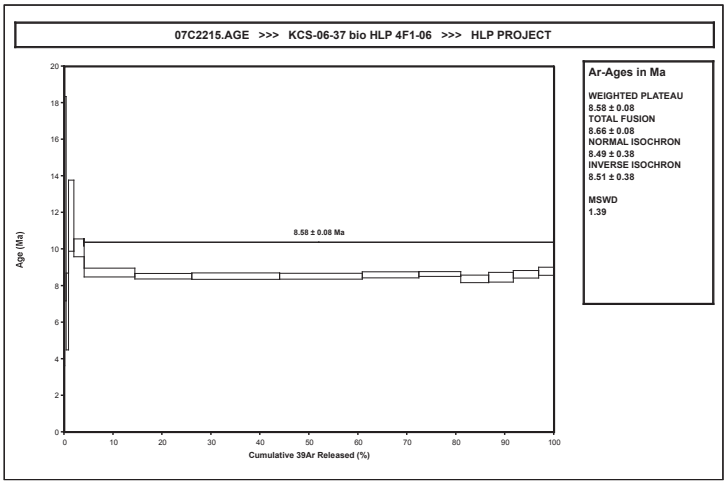

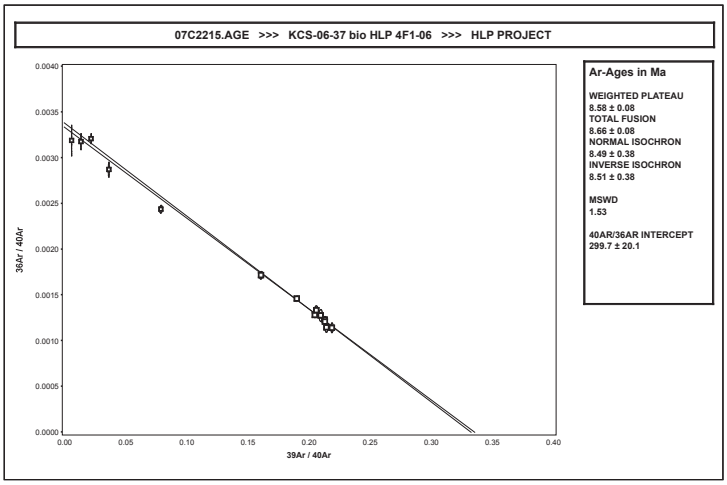

KCS-04-43: LAKE ABERT HAOT

Incremental Heating			36Ar(a)	37Ar(ca)	38Ar(cl)	39Ar(k)	40Ar(r)	Age ± 2σ (Ma)	40Ar(r) (%)	39Ar(k) (%)	K/Ca ± 2σ
06C1649	500 °C		0.01748	0.10491	0.00050	0.00658	0.15105	73.44 ± 42.25	2.84	0.66	0.027 ± 0.001
06C1650	600 °C		0.01044	0.21009	0.00040	0.01507	0.13499	29.01 ± 12.80	4.19	1.50	0.031 ± 0.001
06C1651	750 °C	✓	0.00664	2.05818	0.00045	0.16278	0.39538	7.91 ± 0.60	16.77	16.24	0.034 ± 0.001
06C1652	850 °C	✓	0.00290	2.43330	0.00039	0.26576	0.61964	7.60 ± 0.27	41.95	26.51	0.047 ± 0.001
06C1653	925 °C	✓	0.00191	1.03150	0.00029	0.13310	0.31740	7.77 ± 0.37	35.99	13.27	0.055 ± 0.002
06C1654	1000 °C	✓	0.00166	0.90001	0.00033	0.08978	0.20920	7.59 ± 0.59	29.90	8.95	0.043 ± 0.001
06C1655	1075 °C	✓	0.00156	0.78848	0.00050	0.07603	0.19379	8.30 ± 1.03	29.65	7.58	0.041 ± 0.001
06C1656	1175 °C	✓	0.00434	0.98897	0.00165	0.10690	0.27125	8.27 ± 0.99	17.44	10.66	0.046 ± 0.001
06C1657	1275 °C		0.02772	9.57641	0.00090	0.12689	0.67980	17.41 ± 3.43	7.66	12.66	0.006 ± 0.000
06C1658	1400 °C		0.01471	1.60258	0.00011	0.01973	0.22453	36.78 ± 10.70	4.91	1.97	0.005 ± 0.000
		Σ	0.08935	19.69442	0.00553	1.00262	3.19703				

Information on Analysis	
Sample	KCS-04-43
Material	whole rock
Location	Lake Abert
Analyst	kcs
Project	HLP
Irradiation	OSU1A06
J-value	0.00181
Standard	28.03

Results	40(r)/39(k) ± 2σ		Age ± 2σ (Ma)		MSWD	39Ar(k) (%,n)	K/Ca ± 2σ
Weighted Plateau	2.3695	± 0.0577 ± 2.43%	7.72	± 0.23 ± 2.93%	0.80	83.22 6	0.042 ± 0.006
			External Error	± 0.26	2.57	Statistical T ratio	
			Analytical Error	± 0.19	1.0000	Error Magnification	
Total Fusion Age	3.1887	± 0.1931 ± 6.05%	10.38	± 0.65 ± 6.25%		10	0.022 ± 0.000
			External Error	± 0.67			
			Analytical Error	± 0.63			

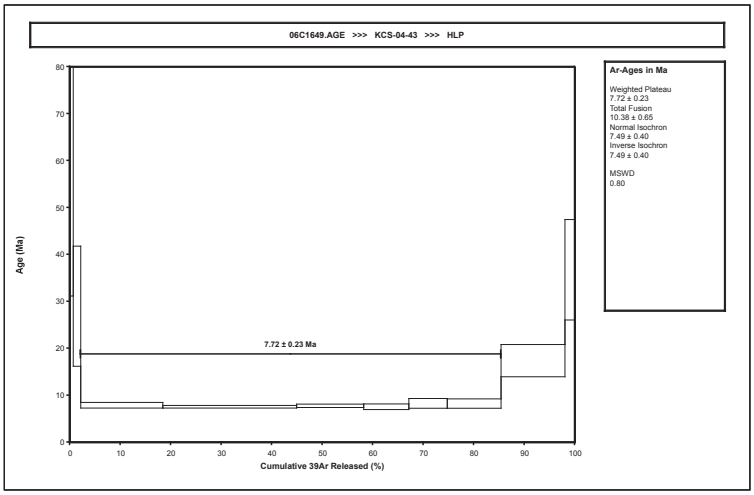

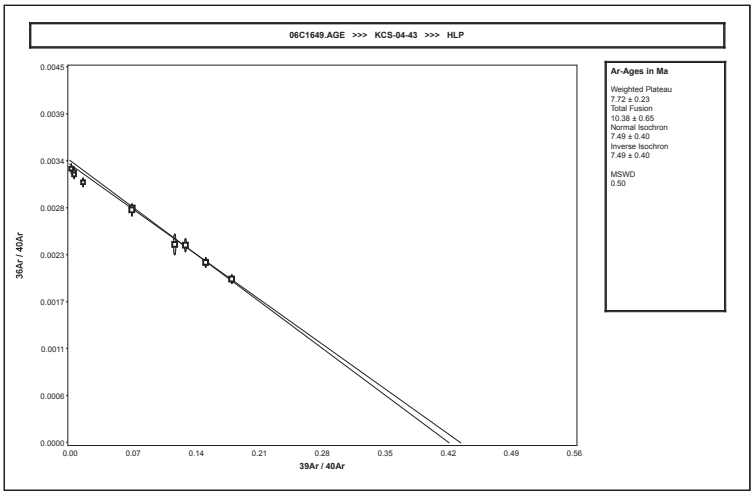

KCS-04-43: LAKE ABERT HAOT

Incremental Heating			36Ar(a)	37Ar(ca)	38Ar(cl)	39Ar(k)	40Ar(r)	Age ± 2σ (Ma)	40Ar(r) (%)	39Ar(k) (%)	K/Ca ± 2σ
06C1649	500 °C		0.01748	0.10491	0.00050	0.00658	0.15105	73.44 ± 42.25	2.84	0.66	0.027 ± 0.001
06C1650	600 °C		0.01044	0.21009	0.00040	0.01507	0.13499	29.01 ± 12.80	4.19	1.50	0.031 ± 0.001
06C1651	750 °C	✓	0.00664	2.05818	0.00045	0.16278	0.39538	7.91 ± 0.60	16.77	16.24	0.034 ± 0.001
06C1652	850 °C	✓	0.00290	2.43330	0.00039	0.26576	0.61964	7.60 ± 0.27	41.95	26.51	0.047 ± 0.001
06C1653	925 °C	✓	0.00191	1.03150	0.00029	0.13310	0.31740	7.77 ± 0.37	35.99	13.27	0.055 ± 0.002
06C1654	1000 °C	✓	0.00166	0.90001	0.00033	0.08978	0.20920	7.59 ± 0.59	29.90	8.95	0.043 ± 0.001
06C1655	1075 °C	✓	0.00156	0.78848	0.00050	0.07603	0.19379	8.30 ± 1.03	29.65	7.58	0.041 ± 0.001
06C1656	1175 °C	✓	0.00434	0.98897	0.00165	0.10690	0.27125	8.27 ± 0.99	17.44	10.66	0.046 ± 0.001
06C1657	1275 °C		0.02772	9.57641	0.00090	0.12689	0.67980	17.41 ± 3.43	7.66	12.66	0.006 ± 0.000
06C1658	1400 °C		0.01471	1.60258	0.00011	0.01973	0.22453	36.78 ± 10.70	4.91	1.97	0.005 ± 0.000
		Σ	0.08935	19.69442	0.00553	1.00262	3.19703				

Information on Analysis	
Sample	KCS-04-43
Material	whole rock
Location	Lake Abert
Analyst	kcs
Project	HLP
Irradiation	OSU1A06
J-value	0.00181
Standard	28.03

Results	40(r)/39(k) ± 2σ	Age ± 2σ (Ma)	MSWD	39Ar(k) (%,n)	K/Ca ± 2σ
Weighted Plateau	2.3695 ± 0.0577 ± 2.43%	7.72 ± 0.23 ± 2.93%	0.80	83.22 6	0.042 ± 0.006
		External Error ± 0.26	2.57	Statistical T ratio	
		Analytical Error ± 0.19	1.0000	Error Magnification	
Total Fusion Age	3.1887 ± 0.1931 ± 6.05%	10.38 ± 0.65 ± 6.25%		10	0.022 ± 0.000
		External Error ± 0.67			
		Analytical Error ± 0.63			

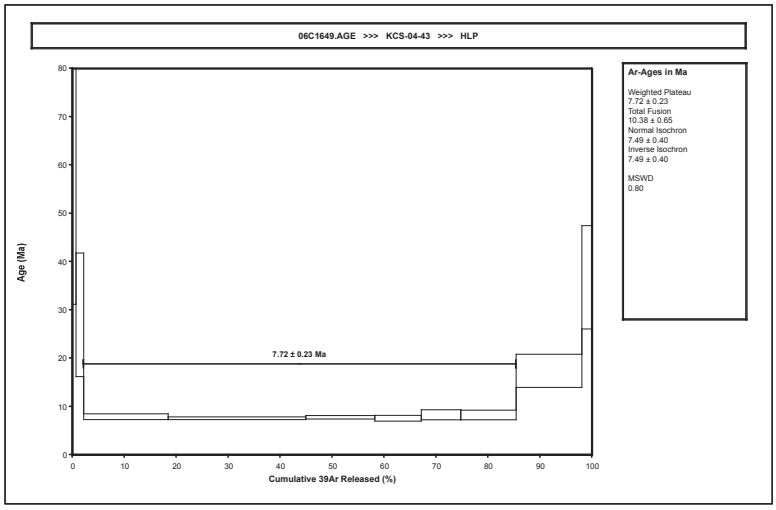

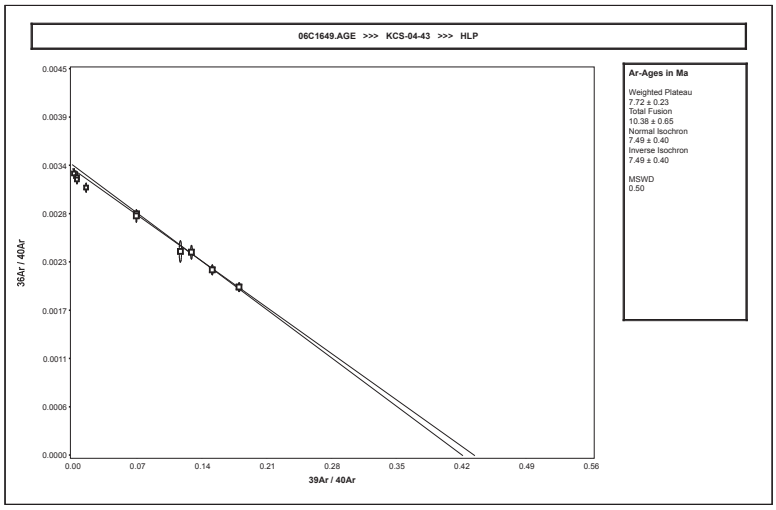

KCS-05-12: BEATYS BUTTE ANDESITE

Incremental Heating			36Ar(a)	37Ar(ca)	38Ar(cl)	39Ar(k)	40Ar(r)	Age ± 2σ (Ma)	40Ar(r) (%)	39Ar(k) (%)	K/Ca ± 2σ
06C1812	600 °C	✓	0.00240	0.00948	0.00004	0.00222	0.02391	34.71 ± 43.37	3.27	0.14	0.101 ± 0.006
06C1814	800 °C	✓	0.12607	0.59601	0.00045	0.15983	1.38783	28.09 ± 16.36	3.59	9.77	0.115 ± 0.005
06C1815	900 °C	✓	0.10071	0.90919	0.00022	0.21587	1.15920	17.42 ± 14.83	3.75	13.20	0.102 ± 0.004
06C1816	1000 °C	✓	0.19156	2.21071	0.00107	0.41837	2.39958	18.60 ± 8.71	4.07	25.58	0.081 ± 0.003
06C1817	1100 °C	✓	0.26164	2.32847	0.00168	0.40309	2.65560	21.35 ± 15.12	3.32	24.65	0.074 ± 0.003
06C1818	1175 °C	✓	0.17376	1.20903	0.00107	0.20520	2.18609	34.40 ± 17.56	4.08	12.55	0.073 ± 0.003
06C1819	1250 °C	✓	0.09085	0.50647	0.00002	0.10158	1.03496	32.91 ± 14.43	3.71	6.21	0.086 ± 0.003
06C1820	1400 °C	✓	0.03295	0.76983	0.00018	0.12921	1.10460	27.66 ± 6.29	10.19	7.90	0.072 ± 0.003
		Σ	0.97993	8.53921	0.00473	1.63539	11.95176				

Information on Analysis	
Sample	KCS-05-12
Material	plg
Location	Beatys Butte
Analyst	kcs
Project	HLP
Irradiation	OSU1E06
J-value	0.001807
Standard	28.03

Results	40(r)/39(k) ± 2σ		Age ± 2σ (Ma)		MSWD	39Ar(k) (%,n)	K/Ca ± 2σ
Weighted Plateau	7.8060	± 1.2732 ± 16.31%	25.27	± 4.11 ± 16.28%	0.97	100.00 8	0.083 ± 0.010
			External Error	± 4.13	2.36	Statistical T ratio	
			Analytical Error	± 4.09	1.0000	Error Magnification	
Total Fusion Age	7.3082	± 1.7346 ± 23.73%	23.67	± 5.59 ± 23.64%		8	0.082 ± 0.001
			External Error	± 5.61			
			Analytical Error	± 5.58			

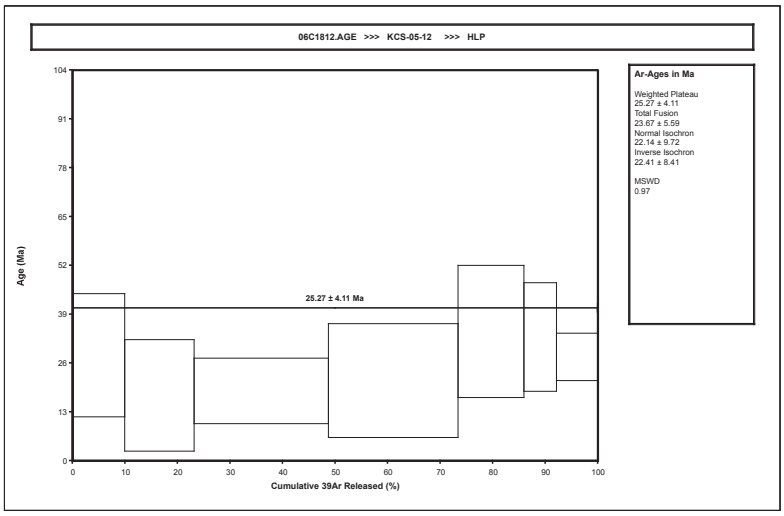

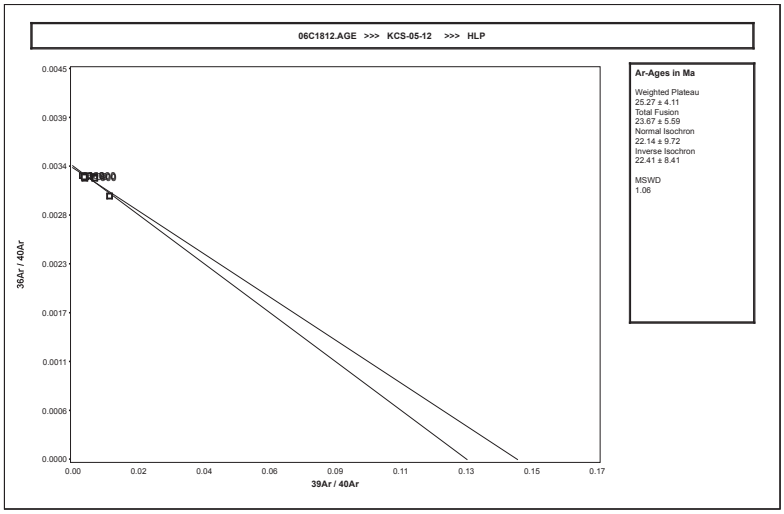

KCS-05-44: BEATYS BUTTE ANDESITE

Incremental Heating			36Ar(a)	37Ar(ca)	38Ar(cl)	39Ar(k)	40Ar(r)	Age ± 2σ (Ma)	40Ar(r) (%)	39Ar(k) (%)	K/Ca ± 2σ
06C1864	600 °C	✓	0.21020	0.15210	0.00169	0.15800	1.05168	23.06 ± 29.89	1.66	11.33	0.447 ± 0.020
06C1865	700 °C	✓	0.14375	0.30493	0.00085	0.05163	0.93193	61.87 ± 40.78	2.15	3.70	0.073 ± 0.003
06C1866	800 °C	✓	0.19380	1.18678	0.00079	0.16061	0.83121	17.96 ± 25.22	1.43	11.52	0.058 ± 0.002
06C1867	900 °C	✓	0.21430	2.37730	0.00109	0.29078	2.50403	29.78 ± 12.49	3.80	20.85	0.053 ± 0.002
06C1868	1000 °C	✓	0.34703	3.11590	0.00107	0.25298	0.30059	4.14 ± 24.28	0.29	18.14	0.035 ± 0.001
06C1869	1100 °C		0.42252	2.62980	0.00395	0.20039	5.05229	85.85 ± 47.78	3.89	14.37	0.033 ± 0.001
06C1870	1200 °C		0.33334	1.30912	0.00309	0.10942	4.18350	128.64 ± 59.85	4.07	7.85	0.036 ± 0.002
06C1871	1400 °C		0.11727	0.87870	0.00127	0.17051	2.96773	59.70 ± 12.88	7.89	12.23	0.083 ± 0.004
		Σ	1.98222	11.95463	0.01380	1.39432	17.82295				

Information on Analysis	
Sample	KCS-05-44
Material	feldspar
Location	OR
Analyst	kcs
Project	HLP
Irradiation	OSU1E06
J-value	0.001933
Standard	28.03

Results	40(r)/39(k) ± 2σ		Age ± 2σ (Ma)		MSWD	39Ar(k) (%,n)	K/Ca ± 2σ
Weighted Plateau	7.2878	± 3.6299 ± 49.81%	25.24	± 12.49 ± 49.47%	1.78	65.55 5	0.048 ± 0.025
			External Error	± 12.49	2.78	Statistical T ratio	
			Analytical Error	± 12.48	1.3326	Error Magnification	
Total Fusion Age	12.7825	± 3.2601 ± 25.50%	44.03	± 11.10 ± 25.22%		8	0.050 ± 0.001
			External Error	± 11.13			
			Analytical Error	± 11.09			

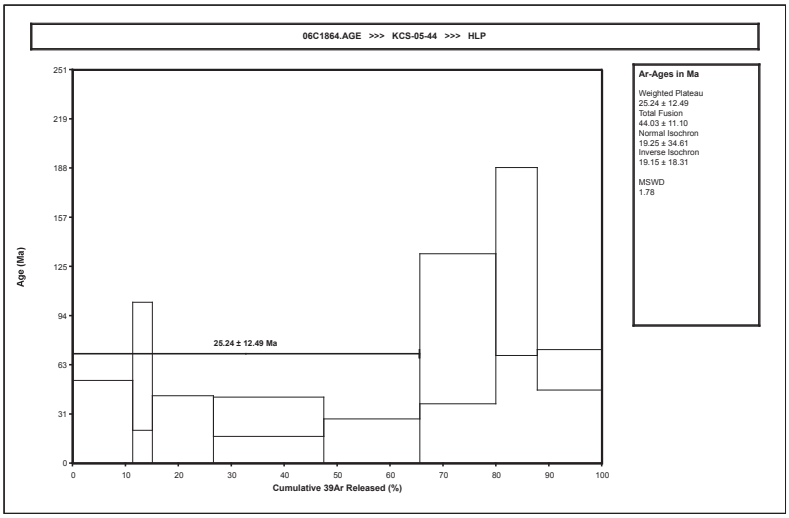

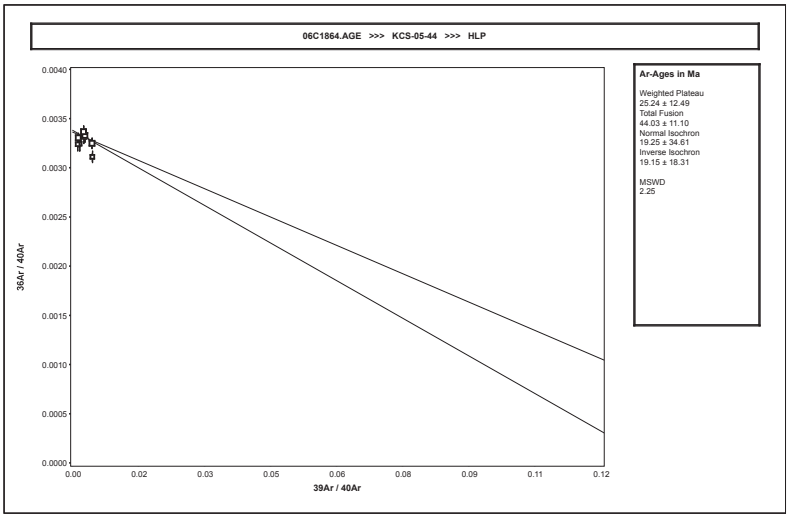

KCS-05-15: BEATYS BUTTE RHYOLITE

Incremental Heating			36Ar(a)	37Ar(ca)	38Ar(cl)	39Ar(k)	40Ar(r)	Age ± 2σ (Ma)	40Ar(r) (%)	39Ar(k) (%)	K/Ca ± 2σ
06C1638	500 °C		0.00841	0.08001	0.00745	1.19834	0.76656	2.10 ± 0.18	23.57	9.14	6.440 ± 0.216
06C1639	600 °C		0.00045	0.03915	0.00253	0.71644	1.64384	7.54 ± 0.06	92.42	5.47	7.869 ± 0.258
06C1640	700 °C	✓	0.00022	0.17390	0.00152	2.67613	9.85374	12.08 ± 0.06	99.33	20.42	6.617 ± 0.207
06C1641	775 °C	✓	0.00012	0.26078	0.00000	3.77396	14.42508	12.54 ± 0.11	99.73	28.79	6.223 ± 0.200
06C1642	850 °C	✓	0.00007	0.36471	0.00000	3.69363	13.40155	11.91 ± 0.05	99.83	28.18	4.355 ± 0.135
06C1643	900 °C		0.00004	0.12217	0.00070	0.68433	2.32589	11.16 ± 0.07	99.48	5.22	2.409 ± 0.076
06C1644	950 °C		0.00004	0.05267	0.00075	0.19615	0.65898	11.03 ± 0.14	98.11	1.50	1.601 ± 0.051
06C1645	1050 °C		0.00016	0.03469	0.00073	0.11559	0.38032	10.80 ± 0.27	89.05	0.88	1.433 ± 0.050
06C1646	1150 °C		0.00002	0.00936	0.00007	0.01795	0.05478	10.02 ± 1.34	88.81	0.14	0.825 ± 0.029
06C1647	1400 °C		0.00019	0.12727	0.00014	0.03589	0.09177	8.40 ± 0.65	61.68	0.27	0.121 ± 0.004
		Σ	0.00972	1.26473	0.01389	13.10842	43.60251				

Information on Analysis	
Sample	KCS-05-15
Material	whole rock
Location	Beatys Butte
Analyst	kcs
Project	HLP
Irradiation	OSU1A06
J-value	0.001825
Standard	28.03

Results	40(r)/39(k) ± 2σ	Age ± 2σ (Ma)	MSWD	39Ar(k) (%,n)	K/Ca ± 2σ
Error Plateau	3.6723 ± 0.0825 ± 2.25%	12.05 ± 0.33 ± 2.73%	54.02	77.38 3	5.323 ± 1.466
		External Error ± 0.38	4.30	Statistical T ratio	
		Analytical Error ± 0.27	7.3501	Error Magnification	
Total Fusion Age	3.3263 ± 0.0116 ± 0.35%	10.92 ± 0.17 ± 1.59%		10	4.457 ± 0.059
		External Error ± 0.25			
		Analytical Error ± 0.04			

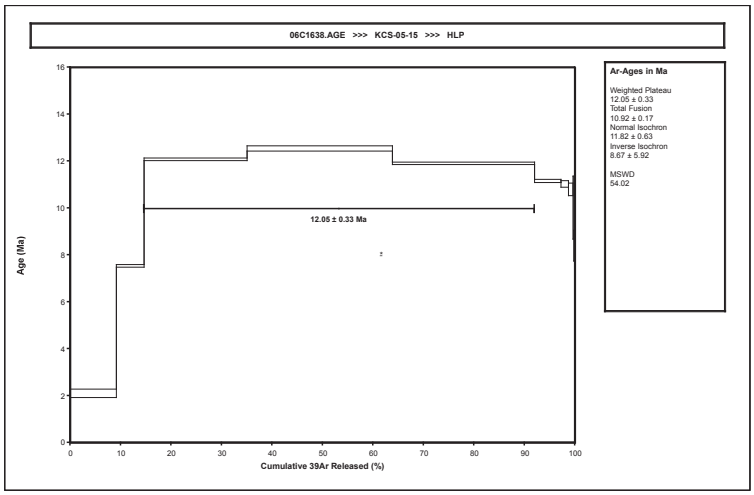

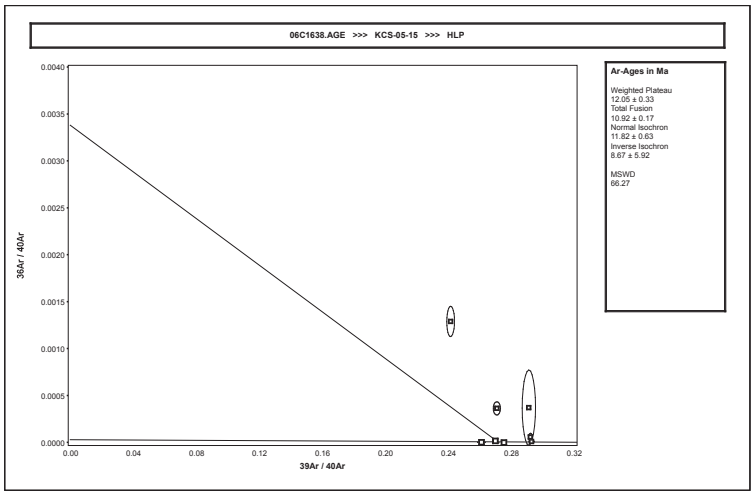

KCS-05-14: BEATYS BUTTE ASHFLOW TUFF

Incremental Heating			36Ar(a)	37Ar(ca)	38Ar(cl)	39Ar(k)	40Ar(r)	Age ± 2σ (Ma)	40Ar(r) (%)	39Ar(k) (%)	K/Ca ± 2σ
06C1750	600 °C		0.00333	0.00863	0.00032	0.02823	0.07494	9.12 ± 2.61	7.07	0.19	1.406 ± 0.058
06C1751	700 °C		0.00100	0.01512	0.00008	0.05912	0.16773	9.75 ± 0.43	36.26	0.40	1.681 ± 0.067
06C1752	800 °C		0.00083	0.08822	0.00017	0.31998	1.02981	11.06 ± 0.14	80.79	2.17	1.560 ± 0.057
06C1753	900 °C	✓	0.00072	0.18941	0.00052	0.57243	1.61527	9.70 ± 0.14	88.32	3.89	1.300 ± 0.046
06C1754	975 °C	✓	0.00061	0.25699	0.00069	0.91439	2.60237	9.78 ± 0.06	93.45	6.21	1.530 ± 0.054
06C1755	1050 °C	✓	0.00103	0.35296	0.00116	1.55443	4.41769	9.77 ± 0.06	93.50	10.56	1.894 ± 0.067
06C1756	1100 °C	✓	0.00176	0.34298	0.00149	1.76274	5.02611	9.80 ± 0.06	90.62	11.97	2.210 ± 0.077
06C1757	1150 °C	✓	0.00243	0.32395	0.00150	1.98646	5.62447	9.73 ± 0.05	88.65	13.49	2.637 ± 0.093
06C1758	1200 °C	✓	0.00178	0.26593	0.00145	2.18305	6.17414	9.72 ± 0.04	92.11	14.83	3.530 ± 0.124
06C1759	1250 °C	✓	0.00100	0.21368	0.00263	3.46434	9.80785	9.73 ± 0.07	97.04	23.53	6.971 ± 0.247
06C1760	1300 °C	✓	0.00071	0.19965	0.00108	1.67295	4.76197	9.78 ± 0.06	95.74	11.36	3.603 ± 0.126
06C1761	1400 °C		0.00025	0.09662	0.00009	0.20211	0.64323	10.93 ± 0.22	89.75	1.37	0.900 ± 0.033
		Σ	0.01546	2.35414	0.01117	14.72024	41.94557				

Information on Analysis	
Sample	KCS-05-14
Material	feldspar
Location	OR
Analyst	jh
Project	HLP
Irradiation	OSU1E06
J-value	0.00191
Standard	28.03
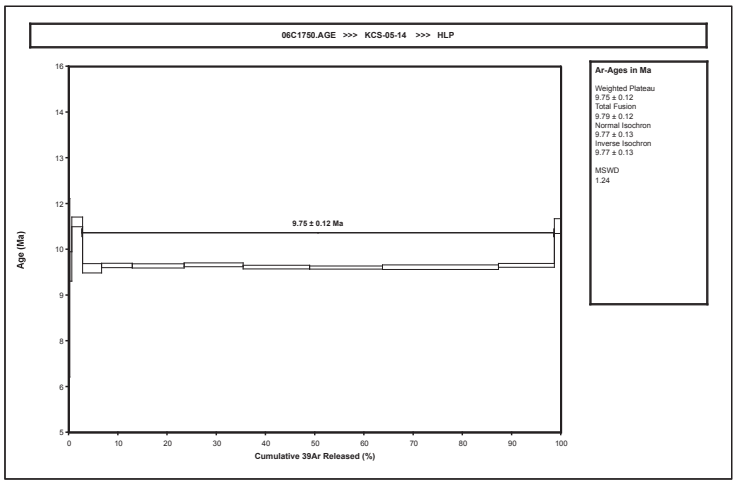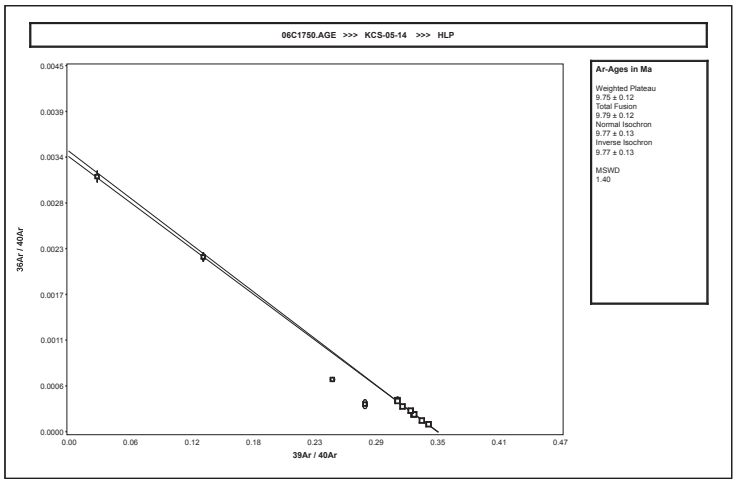
Results	40(r)/39(k) ± 2σ	Age ± 2σ (Ma)	MSWD	39Ar(k) (%,n)	K/Ca ± 2σ
Weighted Plateau	2.8382 ± 0.0069 ± 0.24%	9.75 ± 0.12 ± 1.18%	1.24	95.86 8	1.910 ± 0.644
		External Error ± 0.19	2.36	Statistical T ratio	
		Analytical Error ± 0.02	1.1136	Error Magnification	
Total Fusion Age	2.8495 ± 0.0070 ± 0.25%	9.79 ± 0.12 ± 1.18%		12	2.689 ± 0.032
		External Error ± 0.19			
		Analytical Error ± 0.02